WILLIAN AS A NOVEL 4.1 EZRIN RADIXIN MOESIN (FERM) DOMAIN PROTEIN IN THE MAMMALIAN HIPPO SIGNALLING PATHWAY

Liselotte Angus

A Thesis Submitted for the Degree of PhD
at the
University of St. Andrews

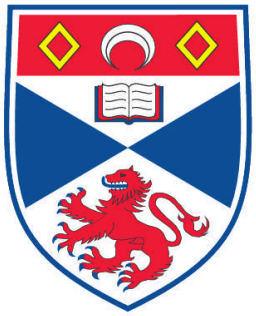

2011

THE UNIVERSITY OF ST. ANDREWS

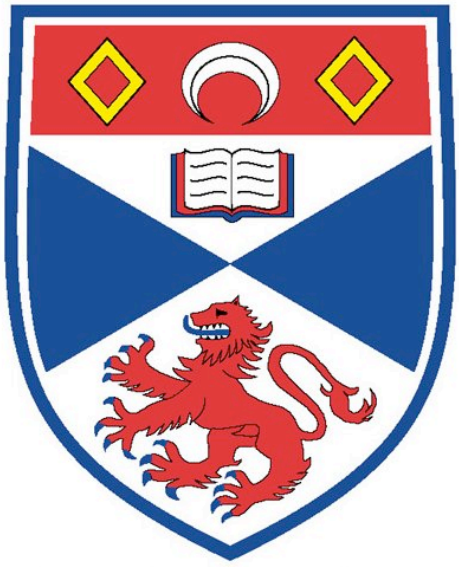

Willin as a Novel 4.1 Ezrin Radixin Moesin (FERM) Domain Protein in the Mammalian Hippo Signalling Pathway

Liselotte Angus, B.Sc

Submitted for the degree of Ph.D

2011

Abstract

The Salvador/Warts/Hippo (Hippo) pathway defines a novel signalling cascade regulating cell contact inhibition, organ size control, cell growth, proliferation, apoptosis and cancer development in mammals. The Hippo pathway was initially utilised in *D. melanogaster*, where the Expanded protein acts in the Hippo signalling cascade to control organ size. Willin is the proposed human orthologue of Expanded and the aim of this thesis is to investigate whether willin can activate the mammalian Hippo signalling pathway.

Ectopic willin expression causes an increase in phosphorylation of the core Hippo signalling pathway components MST1/2, LATS1 and YAP, an effect which can be antagonised by ezrin. In MCF10A cells, willin over-expression antagonises a YAP-induced epithelial-to-mesenchymal transition via the N-terminal FERM (Four-point-one Ezrin Radixin Moesin) domain of willin. Preliminary results show that willin is expressed within the sciatic nerve of rat and mice, and within the neuromast cells in the zebrafish; suggesting that willin and the Hippo pathway may play a vital role in the developmental regulation within the peripheral nervous system. To conclude, willin influences Hippo signalling activity by activating the core Hippo pathway kinase cassette in mammalian cells.

Science never solves a problem without creating ten more . . .

George Bernard Shaw

Contents

List of Figures

List of Tables

Acknowledgements

Firstly I would like to thank my Ph.D. supervisor Prof. Frank Gunn-Moore for his support, feedback and lab meeting discussions. I am grateful for the research freedom he has given me to let me investigate the role of willin in whichever direction I wanted to take.

A very specials thanks also goes to Dr. Elaine Campbell. Who has not only been a great friend but also found time to act as a post-doc in our lab. I am truly grateful for her patience, positive attitude, knowledge of laboratory techniques, help and support. I would also like to thank Dr Paul Reynolds for becoming interested in the Hippo pathway after hearing one of my 'work in progress' talks in the department. His assistance with retroviral work and providing cell lines and reagents are very much appreciated.

I would like to thank all the researchers in Prof. Frank Gunn-Moore's lab. Especially Eva Borger who could always be counted upon for great science discussions and company during the weekends. Susana Moleirinho, who has taken over the important job of further investigating willin and Lani Torres for finding another good use for the inducible cell line that I created.

I would like to thank the following people for their help in providing me with materials. Dr. Chris Tate (University of Cambridge, UK) for kindly providing me with the TRex HEK-293 cell line; Prof. Sue Barnett and Dr. Jennifer R. Higginson (University of Glasgow, UK) for kindly providing primary fibroblast and Schwann cells; Dr. D. Haber (Harvard University, USA) for providing the FLAG-YAP construct and Stuart Fleming (University of Edinburgh, UK) who kindly provided mouse sciatic nerve RNA samples.

Dr. Ian Sheppard (Emory University, USA), Ian Armitt and Dr. Daniel J MacQueen (University of St Andrews, UK) assistance with zebrafish collection, preparation and cryo-sectioning is greatly appreciated. The zebrafish in-situ hybridisations would never have been possible without their help.

I would like to thank my whole family for encouraging me to follow my interests. Finally I would like to thank my husband, Garry Angus, for his endless support.

Declaration

I, Liselotte Angus, hereby certify that this thesis, which is approximately 50,000 words in length, has been written by me, that it is the record of work carried out by me and that it has not been submitted in any previous application for a higher degree.

I was admitted as a research student in October 2007 and as a candidate for the degree of PhD in October 2007; the higher study for which this is a record was carried out in the University of St Andrews between 2007 and 2011.

Date: September 21, 2011 Signature of Candidate:

I hereby certify that the candidate has fulfilled the conditions of the Resolution and Regulations appropriate for the degree of PhD in the University of St Andrews and that the candidate is qualified to submit this thesis in application for that degree.

Date: September 21, 2011 Signature of Supervisor:

The following is an agreed request by candidate and supervisor regarding the electronic publication of this thesis:

Access to printed copy and electronic publication of thesis through the University of St Andrews.

Date: September 21, 2011 Signature of Candidate:

Date: September 21, 2011 Signature of Supervisor:

Copyright Declaration

Abbreviations

BCIP	5- Bromo-4-Chloro-Indolyl-Phosphatase
bp	Base pair
BMP2	Bone morphogenetic protein 2
BSA	Bovine serum albumin
C-terminus	Carboxy terminus
CD44	Cluster of differentiation
cDNA	Complementary DNA
CTD	C-terminal domain
DAPI	4',6-diamidino-2-phenylindole
DEPC	Diethyl pyrocarbonate
DMEM	Dulbecco's modied Eagle's medium
DMF	Dimethylformamide
DMSO	Dimethyl sulfoxide
DNA	Deoxyribonucleic acid
dNTP	Deoxynucleotide Triphosphate
DTT	Dithiothreitol
EBP50	ERM binding phosphoprotein 50
E. Coli	*Escherichia coli*
EDTA	Ethylenediaminetetraacetic acid
EGF	Epidermal growth factor
ERM	Ezrin radixin moesin
FACS	Fluorescence Activated Cell Sorting
FCS	Foetal calf serum
FERM	4.1 ezrin radixin moesin
G_1	Gap 1 of cell cycle
G_2	Gap 2 of cell cycle
GFP	Green fluorescent protein
HB	Hybridization buffer
HEK-293	Human embryonic kidney cell line
Hpo	Hippo protein
HRP	Horseradish peroxidase
IGFBP3	Insulin growth factor-binding protein 3
kb	kilobase
LATS	Large tumour suppressor homologue
LB	Luria-Bertani broth
Mts	Mats homologue
MCF10A	Human mammary epithelial cell line
MDA-231	Human breast adenocarcinoma cell line
MEM	Minimum Essential Medium
MQ	Milli-Q purified water

MST	Mammalian STE20 Kinase
MTT	3-(4,5-Dimethylthiazol-2-yl)-2,5-diphenyltetrazolium bromide
N-terminus	Amino terminus
NBF	Neutral buffered formalin
NBT	Nitro blue tetrazolium
NF2	Neurofibromatosis type 2
NSCLC	Non small cell lung carcinoma
P	Proline
P13K	Phosphatidylinositol 3 kinase
PBS	Phosphate buffered saline
PCR	Polymerase chain reaction
PDGF	Platelet derived growth factor
PDZ	Postsynaptic density 95, discs large, ZO-1
PFA	Paraformaldehyde
pH	Potential for hydrogen ion concentration
PH	Pleckstrin homology
PI	Propidium iodine
PMSF	Phenylmethylsulfonyl fluoride
PONs	phosphorothioate oligonucleotides
PRL	Prolactin
PSB	Protein sample buffer
qPCR	Quantitative PCR
RASSF8	Ras association domain family 8
RNA	Ribonucleic acid
S	Synthesis phase of the cell cycle
Sav	Salvador homologue
SDS	Sodium dodecyl sulfate
SDS PAGE	Sodium dodecyl sulfate polyacrylamide gel electrophoresis
siRNA	Small interference RNA
SOC	Super optimal catabolite repression broth
TAZ	Tafazzin
TBE	Tris-borate- EDTA
TBS	Tris buffered saline
TBS-T	Tris buffered saline with Tween-20
TEAD	TEA domain family member
tet	Tetracycline
TNFα	Tumour necrosis factor α
Tris	Tris(hydroxymethyl)aminomethane
Triton-X100	Octylphenolpoly(ethyleneglycolether)
Tween 20	Polyoxyethylenesorbitan monolaurate
UV	Ultraviolet
Wts	Warts homologue
X-gal	5-bromo-4-chloro-3-indolyl-galactopyranoside
Y	Tyrosine
YAP	Yes-associated protein

Chapter 1

Introduction

1.1 FERM domain proteins modulation on cell growth in mammals

1.1.1 FERM domain family of proteins

The band 4.1 superfamily of proteins consists of a group of proteins that contain a highly conserved Four point one Ezrin Radixin Moesin (FERM) domain. FERM domains occur in numerous membrane associated signalling and cytoskeletal proteins, in which they act as multifunctional proteins. The FERM superfamily of proteins can be classified into FERM domain families based on sequence analysis. Many FERM domain containing protein family members exist and include: merlin, ERM proteins (Ezrin, Radixin, Moesin), Band 4.1, talin related proteins, expanded, protein tyrosine phosphatases (PTP) and myosin (Bretscher et al., 2002; Sun et al., 2002) (Figure 1.1). For the purpose of this thesis, the focus will be on expanded, merlin, ERM proteins and a novel FERM domain containing protein called willin.

1.1.2 A closer look at the FERM domain

The FERM domain is usually found within the N-terminus of the 4.1 superfamily of proteins, with the exception of myosin: where the FERM domain is located within the C-terminus (Chishti et al., 1998) (Figure 1.1). The FERM domain is a cysteine rich hydrophobic protein module of around 300 amino acids in length that is able to bind to various plasma membrane receptors (Conboy, 1986). Structural studies of the FERM domain have revealed three distinct

subdomains termed F1, F2 and F3 (Edwards and Keep, 2001), which interact together to form a globular clover-leaf-shaped structure (Hamada et al., 2000; Pearson et al., 2000) (Figure 1.1). F1 has a ubiquitin-like structure containing a Ras-binding domain; F2 has an acyl-CoA binding protein-like structure; and F3 contains a phosphotyrosine binding (PTB), a pleckstrin homology (PH) and an Enabled/VASP Homology 1 (EVH1) domain (Hamada et al., 2000; Pearson et al., 2000).

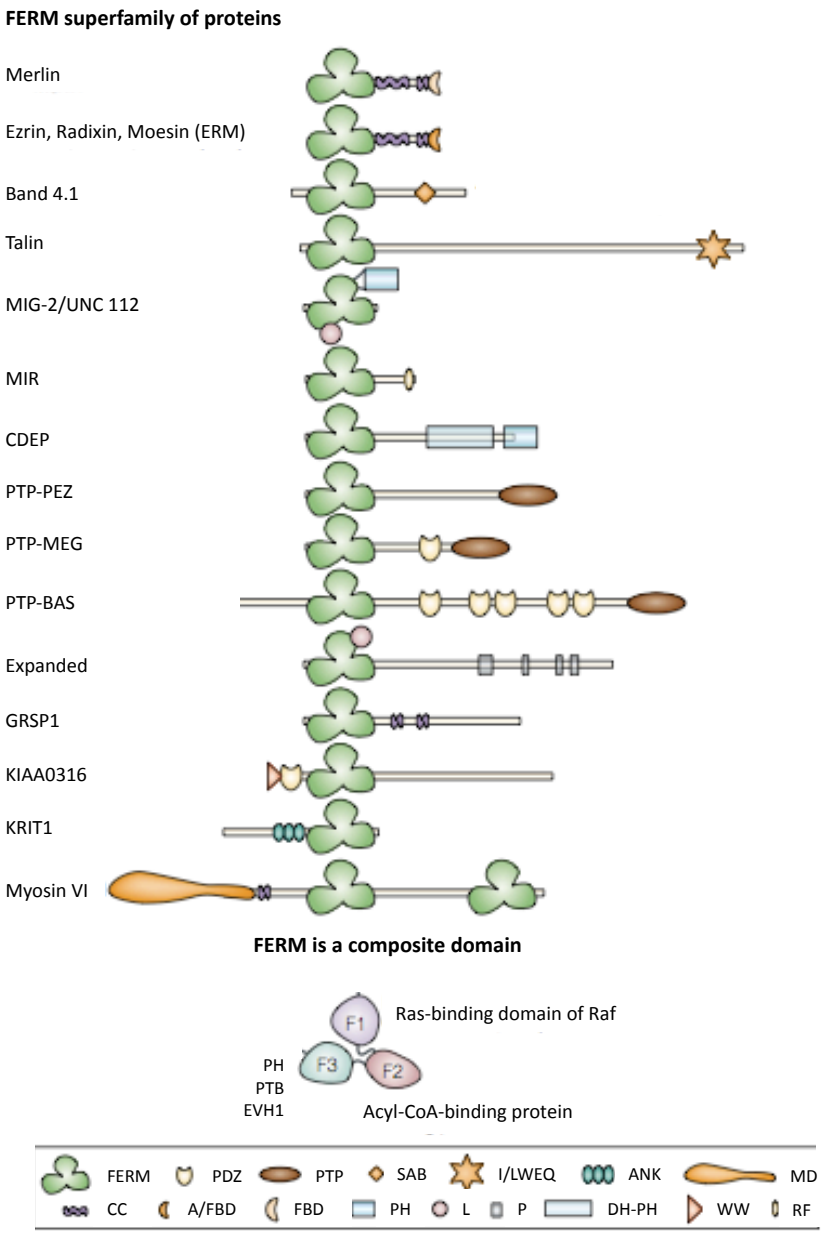

Figure 1.1: Schematic representation of FERM domain containing superfamily of proteins. Image taken from Bretscher et al. (2002).

The FERM domain of the 4.1 superfamily of proteins has been shown to bind to a diverse range of molecules such as phosphoinositols (Martel et al., 2001), glycophorins (Kusunoki and Kohno, 2009), CD44 (Tsukita et al., 1994; Morrison et al., 2001; Bretscher et al., 2002; Morrison et al., 2007), ICAM-2 (Ramesh, 2004), actin (Tsukita et al., 1994; Lee et al., 2004), neurofascin (Gunn-Moore et al., 2006) and the C-terminal domain of FERM containing proteins (Chishti et al., 1998). It has been proposed that the FERM domain of the 4.1 superfamily of proteins is responsible for correct protein localisation to the cell cytoskeleton (Section 1.1.4.2).

1.1.3 ERM protein conformation and regulation

ERM proteins contain highly conserved protein domains: where the N-terminal FERM domain is followed by an α-helix spectrin binding domain, which in turn is followed by a C-terminal domain (Figure 1.1). All three conserved domains (FERM, α-helix and the C-terminal domains) are also identified in merlin.

ERM proteins can be isolated as monomers, homo- and heterodimers that are able to bind to themselves or associate with other ERM family proteins respectively (Gary and Bretscher, 1995). ERM proteins can be found in an open 'active' conformation or closed 'inactive' conformation (Figure 1.2). The globular FERM domain can interact with the C-terminal domain (CTD) of the ERM protein (Chishti et al., 1998). Inter- and intra-molecular interaction between ERM protein's FERM and CTD result in a closed inactive head-to-tail ERM conformation, in which binding sites of the ERM protein, such as the actin and plasma membrane receptor binding motifs, are masked. ERM proteins may bind to themselves or other ERM proteins in a monometric, dimetric or oligometric conformation (Figure 1.2). The strong binding between the FERM and CTD of ERM proteins explains why most interacting partners cannot bind to purified full-length ERM proteins *in-vitro* (Mangeat et al., 1999).

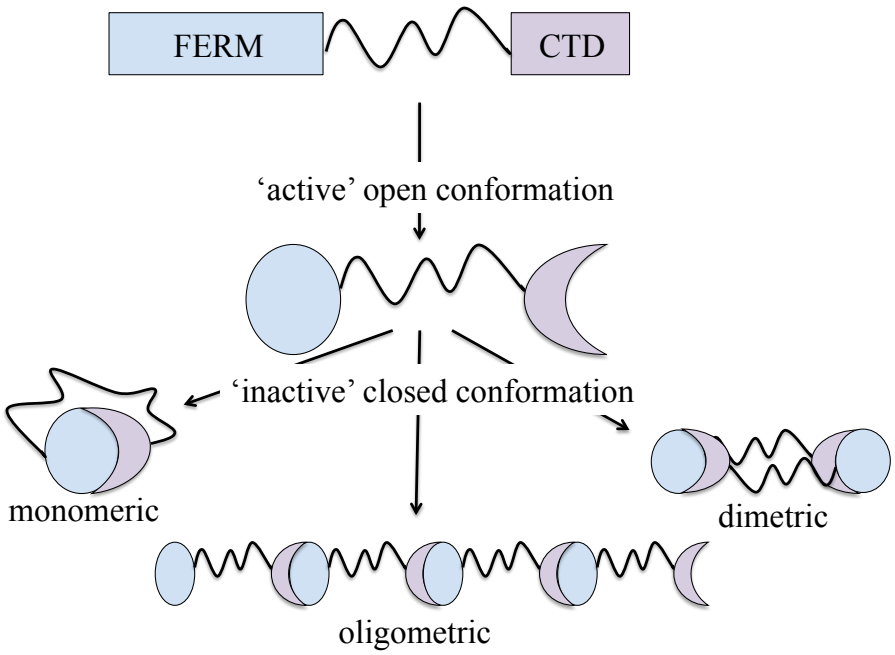

Figure 1.2: Schematic diagram showing different conformational states that ERM proteins may form. ERM proteins bind through a head-to-tail interaction, where the N-terminal FERM domain of the ERM protein can bind to the C-terminal domain (CTD). ERM proteins can be in an open or a closed conformation. ERM proteins may bind to themselves or other ERM proteins in a monometric, dimetric or oligometric conformation.

Modifications that reduce and weaken the head-to-tail conformation of the FERM domain binding to the C-terminal domain are expected to result in the unfolding and activation of the ERM protein (Pearson et al., 2000). Binding of phosphatidylinositol biphosphate (PIP2) to the FERM domain and Rho kinase phosphorylation of a conserved theonine in the F-actin binding site (T567 in ezrin, T564 in radixin and T558 in moesin) stimulates the weakening of the FERM domain binding to the CTD, resulting in the unfolding and unmasking of essential binding sites within ERM proteins (Gary and Bretscher, 1995; Bretscher et al., 2000; Hamada et al., 2000; Pearson et al., 2000). Dephosphorylation triggers the reversion of ERM proteins from an active open to an inactive closed conformation (Kondo et al., 1997). ERM proteins are thereby regulated by conformational changes, in which unphosphorylated ERM proteins are in an inactive closed conformational state and active in a phosphorylated open conformation. Conversely, merlin is active in its unphosphorylated closed state (Xu and Gutmann, 1998).

1.1.4 Functions of merlin and ERM proteins

ERM proteins share approximately 78% amino acid identity and therefore cover overlapping functions that include: cell adhesion, regulation of cell shape, formation of microvilli, motility, membrane trafficking and signal transduction (Bretscher et al., 2000, 2002). The scaffolding and signal transduction functions of merlin and ERM proteins are discussed in more detail below.

1.1.4.1 Cellular scaffolding function of ERM proteins

ERM proteins were first identified as scaffolding linker molecules, located underneath the plasma membrane, connecting several plasma membrane receptors to the actin cytoskeleton. ERM proteins are mostly located in actin-rich protrusion areas just underneath the plasma membrane, including microvilli, filopodia and membrane ruffles (Franck et al., 1993; Amieva and Furthmayr, 1995).

The N-terminal FERM domain and extreme 30 residues of the carboxyl-terminal are necessary for the maintenance of ERM proteins' scaffolding linker role (Turunen et al., 1994; Matsui et al., 1998). The FERM domain is essential for ERM and related proteins to bind, either directly or indirectly, to various plasma membrane receptors. FERM binding motifs are present in transmembrane receptors including the hyaluronate receptors CD44, CD43 and intracellular adhesion molecules 1, 2 and 3 (ICAM-1,2,3) (Tsukita et al., 1994; Bretscher et al., 2002; Ramesh, 2004). Indirect linkage of the FERM domain containing proteins to the plasma membrane receptors is conducted by adapter proteins, such as the ERM binding phosphoprotein-50 (EBP50) and a sodium-hydrogen exchanger regulatory factor (NHERF) via their PDZ domains (Bretscher et al., 2000) (Figure 1.3). The N-terminal domain of ERM proteins are able to bind to the F-actin cytoskeleton (Matsui et al., 1998; Turunen et al., 1994) (Figure 1.3).

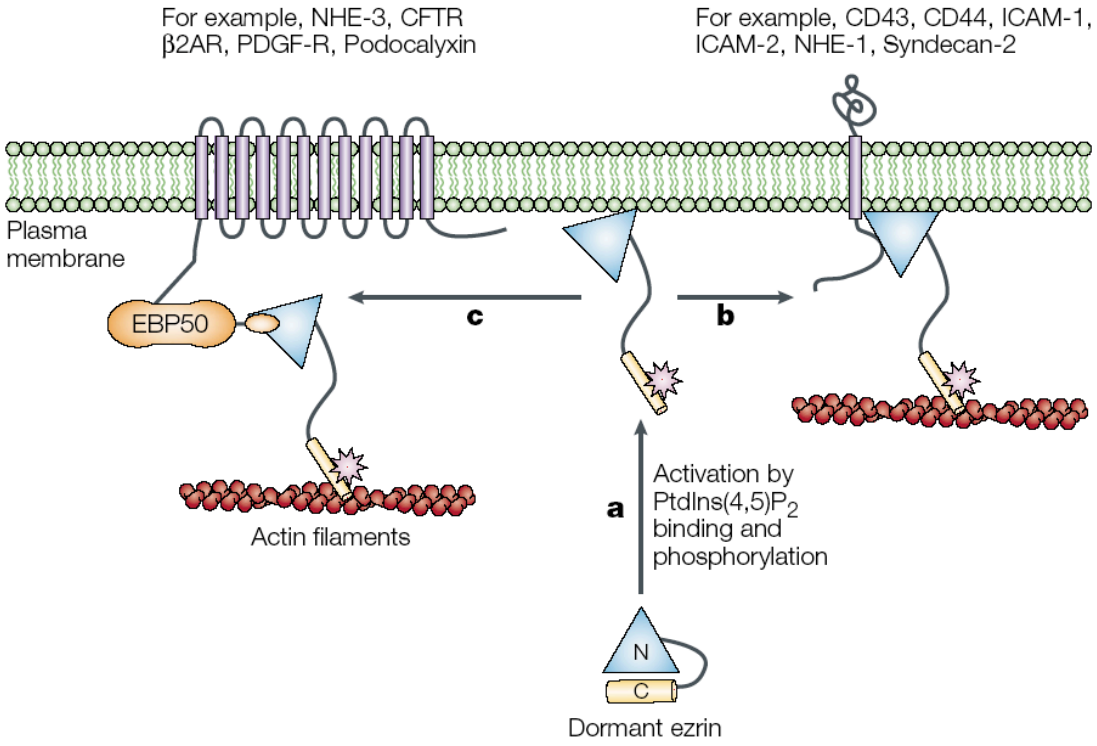

Figure 1.3: Schematic representation of ERM proteins acting as scaffolding linkage protein. ERM proteins are dormant when the N-terminal FERM domain (N) binds to the C-terminal domain (C); forming a closed conformation. Upon activation (a), ERM proteins form an open conformation where the FERM domain is able to bind to other proteins. The FERM domain can bind to various upstream membrane receptors either directly (b) or indirectly (c) using adaptor proteins such as EBP50. The C-terminus binds to actin cytoskeleton. Image taken from Bretscher et al. (2002).

Takeuchi et al. (1994) elegantly demonstrated the importance of ERM proteins as cellular scaffolding molecules by showing that the microvilli on thymoma cells completely disappear in the presence of a mixture of ezrin, radixin and moesin anti-sense phosphorothioate oligonucleotides (PONs; Figure 1.4). Depletion of individual ERM proteins by anti-sense oligonucleotides results in no significant phenotypic changes (Takeuchi et al., 1994). Cellular phenotypic changes are only observed when the synthesis of all ERM proteins are suppressed (Tsukita et al., 1994; Takeuchi et al., 1994). Functional redundancy within the ERM protein family may potentially explain observations of ERM protein compensation when another ERM protein is lost.

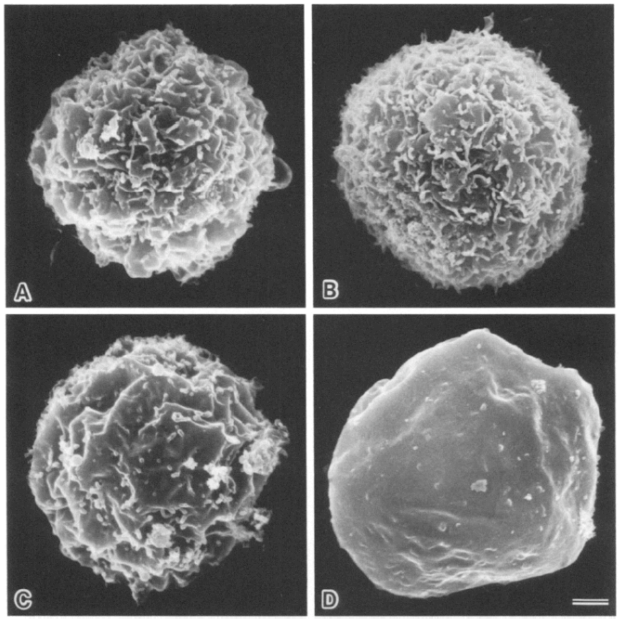

Figure 1.4: Effects of ERM family member antisense PONs on the microvilli structure of thymoma cells. Thymoma cells were cultured in the presence of ezrin (A), radixin (B), or moesin (C) antisense PONs, or in the presence of the ezrin/radixin/moesin antisense PONs mixture (D). In the presence of the mixture of antisense PONs, microvilli completely disappeared, leaving a smooth cell surface (D). Image taken from Takeuchi et al. (1994).

1.1.4.2 ERM proteins and merlin regulate growth signalling pathways

ERM proteins have not only been found to be important in assembling membrane cytoskeletal associated protein complexes, but are also involved in membrane trafficking, cell adhesion, formation of microvilli, motility and signal transduction. ERM proteins can act both upstream and downstream of signalling pathways (Bretscher et al., 2002). As ERM proteins contain the ability to bind to membrane receptors, they are placed at a crucial juncture for the integration of the extracellular environment and intracellular signalling pathways. ERM proteins have been predominantly studied in their ability to transduce growth signals essential for cell proliferation and survival (Gautreau et al., 2002).

Phosphorylated ERM proteins bind to the hyaluronate CD44 receptor to induce downstream signalling pathways that are involved in cell cycle proliferation, endorsing a growth promoting cellular state (Morrison et al., 2001; Bai et al., 2007). ERM proteins interact with NHE1 to mediate phosphatidyli-

nositol 3-kinase (PI3K) and Akt cell survival signals (Wu et al., 2004). Ezrin has been identified as a component in tumour metastasis through binding to the CD44 receptor, activating signalling pathways Rho-GTPase and interacting with the Akt-mediated cell apoptotic pathway (Hunter, 2004). Hypophosphorylated, active, merlin may compete with, and therefore inhibit ezrin and other ERM proteins in binding to the CD44 receptor (Morrison et al., 2001; Bai et al., 2007). Hypophosphorylated merlin is able to interfere with JNK activation and platelet derived growth factor (PDGF) dependent activation of Erk and PI3K (Morrison et al., 2001, 2007; Hilton et al., 2009). This results in a growth inhibitory cellular state, opposing ERM metastasis cell growth (Figure 1.5). Through this pathway, merlin may act as a tumour suppressor. The expression of merlin and ERM proteins therefore have opposing effects on growth signalling cascades, where merlin is growth inhibitory though binding to CD44 and ERM proteins promote cell growth though CD44 binding. Previous results by Alfthan et al. (2004) show that merlin binds with a strong affinity to ezrin, suggesting that merlin can directly inhibit the downstream effects of ezrin.

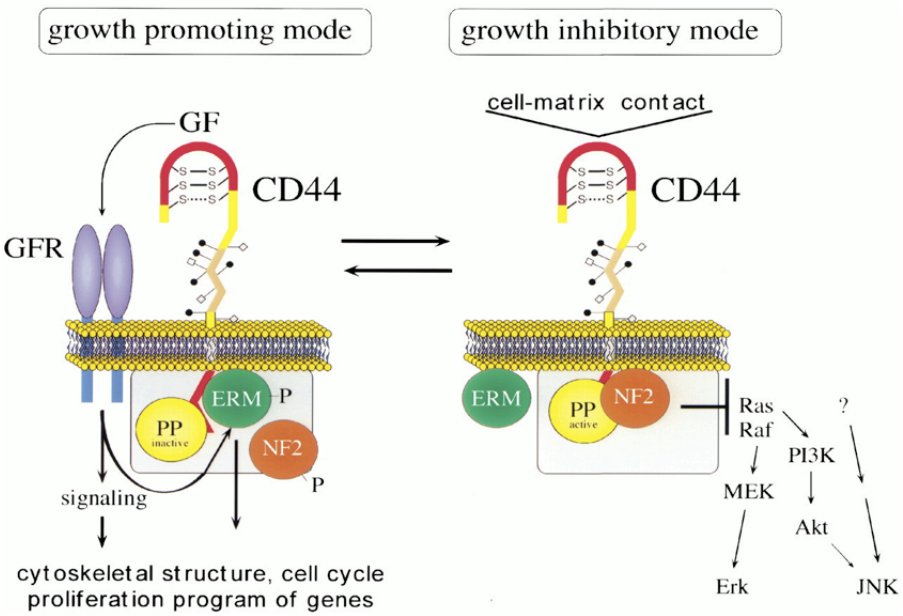

Figure 1.5: Schematic representation of growth promoting and inhibitory role of ERM and merlin (NF2) through binding to the hyaluronate CD44 plasma membrane receptor. In the growth promoting mode, phosphorylated ERM protein binds to CD44 and results in downstream proliferative growth. In the growth inhibitory mode, unphosphorylated merlin binds to CD44 and inhibits downstream MEK and Akt signalling pathways resulting in inhibition of cell proliferation. Image taken from Morrison et al. (2001).

Translocation of ERM and related proteins between the cytoplasm and the plasma membrane could therefore be seen as a homeostatic balance between active and inactive proteins to regulate growth signalling intensity. The active, phosphorylated and open conformation of ERM proteins can bind to CD44 and therefore localise to the plasma membrane. Whereas, the inactive, dephosphorylated and closed ERM conformations are observed within the cytoplasm of the cell. Merlin, in contrast, is believed to be in an inactive open conformation state in the cytoplasm, whereas the closed hypo-phosphorylated form of merlin is believed to be active in its tumour suppressive role at the apical plasma membrane (Xu and Gutmann, 1998).

1.1.5 Willin: a novel FERM protein

Using a yeast two-hybrid screen of a rat sciatic nerve library, Gunn-Moore et al. (2005) found a novel protein that binds to the carboxyl terminal of neurofascin, which is a receptor essential for the formation of the node of Ranvier and myelination in the nervous system (Charles et al., 2002). The novel intracellular binding partner of neurofascin was sequenced and named 'willin' (also termed FRMD6; FERM domain-containing 6). Willin (see Appendix A for sequence) was identified as a 614 amino acid protein with a predicted molecular weight of approximately 71kDa (Gunn-Moore et al., 2005). Complete sequencing showed that willin contains an amino-terminal FERM domain, that is structurally most closely related to ERM proteins (Gunn-Moore et al., 2005) (Figure 1.6).

Willin shares high sequence similarity to merlin and ERM proteins within the highly conserved N-terminal FERM domain (Figure 1.7). Willin, however, comprises little homology with other FERM domain containing proteins outside the FERM domain (Gunn-Moore et al., 2005; Madan et al., 2006). The FERM domain of willin shares 43% protein similarity with the FERM domain of ezrin, 47% with that of radixin, 45% with moesin and 46% with merlin (Figure 1.7). To date, the only identified and confirmed domain in willin is the FERM domain. No proline-rich and actin binding domains are identified in willin (Figure 1.7).

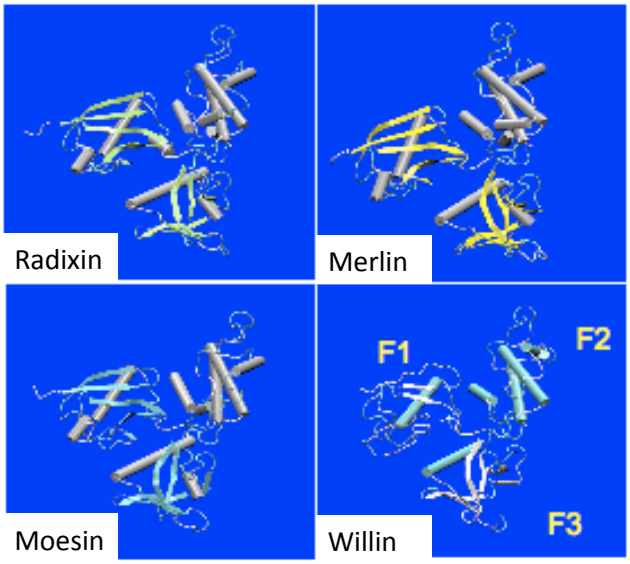

Figure 1.6: Predicted 3D structure of the FERM domain of willin, compared to the crystal structures of the FERM domain of ezrin, radixin and moesin. The structural prediction was performed by V. Zaitsev (University of St. Andrews, UK). F1= ubiquitin-like subdomain, F2= acyl-CoA binding-like subdomain and F3= phosphotyrosine binding (PTB)/pleckstrin homology (PH)-like subdomain.

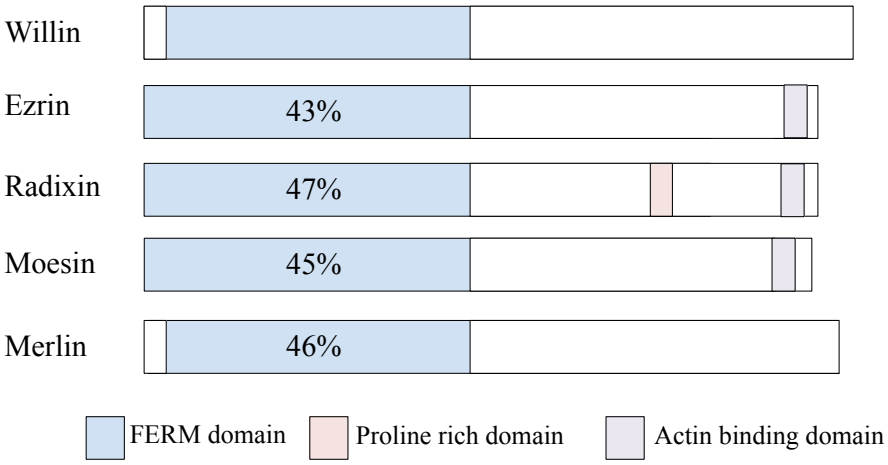

Figure 1.7: Willin shares high sequence homology to ERM (ezrin, radixin and moesin) proteins and merlin within the N-terminal FERM domain. Willin, merlin and ERM proteins contain a highly conserved FERM domain within the N-terminus. The FERM domain of willin shares 43% protein similarity with the FERM domain of ezrin, 47% with that of radixin, 45% with moesin and 46% with merlin. No proline-rich and actin binding domains are identified in willin.

Willin, like other ERM proteins, is expressed in neuronal as well as non-neuronal tissues. Willin has previously been identified in sciatic nerves (Gunn-Moore et al., 2005), as well as being widely expressed in non-neuronal epithelial cells (Madan et al., 2006). cDNA of willin has been identified in the human uterus, placenta and cervix (Madan et al., 2006). Willin appears to have a very similar cellular localisation to merlin and all three ERM proteins (Sun et al., 2002; Gunn-Moore et al., 2005), presumably due to the conserved and essential FERM domain shared by these proteins. Immunohistochemistry studies have shown that willin, like ERM proteins, are found within different cellular sites including intracellular sites such as the cytoplasm and nucleus but the most pronounced staining was found at the apical plasma membrane (Gunn-Moore et al., 2005; Herron et al., 2007; Stickney et al., 2004).

Willin has been shown to co-localise with actin (Gunn-Moore et al., 2005) but precise binding interactions are unknown. The presence of the actin cytoskeleton is, however, not required for the plasma membrane localisation of willin as cytochalasin-D induced actin disruption does not affect the localisation of willin expression at the plasma membrane (Gunn-Moore et al., 2005). The FERM domain of willin may bind strongly to phospholipids in the lipid rafts and cell surface glycoprotein, resulting in the localisation of willin near the plasma membrane independent of the presence of actin (Herron et al., 2007).

Previous investigation into the intracellular distribution of willin under epidermal growth factor (EGF) treatment has shed light on willin's potential, as with the closely related merlin and ERM proteins, to be involved in growth signalling pathways. In PC12 cells, a cytoplasmic pool of willin-GFP is seen to translocate to the plasma membrane when the cells are treated with growth factors (Gunn-Moore et al., 2005). Cytoplasmic to plasma membrane translocation of willin under the influence of epidermal growth factor is not blocked by wortmannin (Gunn-Moore et al., 2005), indicating that phosphatidylinositol 3-kinase (PI3K) activity is not required to translocate willin. It is plausible that EGF is causing tyrosine phosphorylation of willin, as EGF is a known activator of Ras (Marshall, 1995), Rho and Rac (Maddala et al., 2003); which in turn interacts with and regulates the activation of ERM proteins (Section 1.1.3).

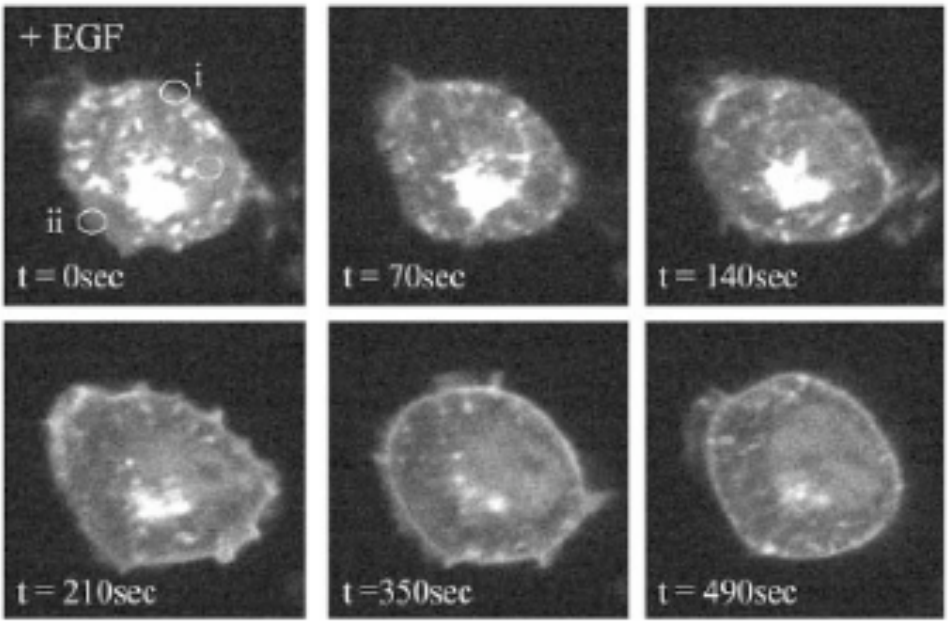

Figure 1.8: Willin translocates to the plasma membrane after epidermal growth factor (EGF) treatment. Before addition of EGF (t=0), willin-GFP expression was mostly observed within the cytoplasm of a PC-12 cell. Upon addition of 100ng/ml EGF, willin-GFP expression translocated to the plasma membrane in under 10 minutes. t= time of addition of EGF. Images were taken from Gunn-Moore et al. (2005).

1.1.6 ERM proteins and associations with disease

FERM domain containing proteins are multifunctional proteins regulating the architecture of the cell as well as being involved in tightly regulating cell growth signals within the cell. Deregulation of ERM proteins have therefore been implicated in disease, especially in tumours where an imbalance between growth promoting and growth inhibitory signals has occurred.

Table 1.1 summarises disease states associated with FERM domain containing proteins; 4.1 Band, merlin, ezrin, radixin, moesin and willin. For the purpose of this thesis, further focus on FERM domain containing proteins and their associated disease states will be on merlin, ezrin and willin.

Protein	Tissue Expression	Disease associations	Reference
4.1R	Erythrocytes, brain	Hereditary elliptocytosis	Conboy (1993)
4.1B	Brain, heart, lung, kidney, adrenal gland, intestine testis	NSCLC	Gutmann et al. (2000)
Merlin	Brain, lens, sciatic nerve, adrenal gland, Schwann cells, peripheral nerve, gonads, blood vessels	Neurofibromatosis Schwannomas Meningiomas	McClatchey et al. (1997) Hanemann (2008) Trofatter et al. (1993)
Ezrin	Brain, kidney, intestine, peripheral nerve, Schwann cells, lung	Tumour metastasis Osteocarcinoma Breast cancer Prostate cancer	Hunter (2004) Wang et al. (2010) Elliott et al. (2005) Pang et al. (2004)
Radixin	Brain, kidney, liver, lung, peripheral nerve, Schwann cells, thymus, gonads, skin	Lung adenocarcinomas Deafness	Tokunou et al. (2000) Kitajiri et al. (2004)
Moesin	Brain, endothelial cells, heart, muscle, lung, liver, peripheral nerve, Schwann cells, kidney, spleen	Lung adenocarcinomas	Tokunou et al. (2000)
FRMD3	Brain, kidney, liver, lung heart, pancreas, prostate	NSCLC	Haase et al. (2007)
Willin	Brain, thymus, heart, muscle, kidney, lung, liver, prostate, breast, placenta, testis	Unknown	

Table 1.1: Adult expression of FERM domain containing proteins and their association with diseases. NSCLC= Non-Small-Cell Lung Carcinoma.

1.1.6.1 Merlin's associations with disease

Merlin is one of the most well studied FERM domain containing proteins in relation to disease states as the gene responsible for schwannomas formation is NF2 (neurofibromatosis type 2), the gene encoding the merlin protein (Rouleau et al., 1993; Trofatter et al., 1993). Universal absence of merlin, but not of other ERM protein family member, results in schwannoma formation (Stemmer-Rachamimov et al., 1997).

Schwannomas are encapsulated tumours of pure Schwann cells which proliferate next to, rather than ensheath nerve cells (Evans et al., 2000) (Figure 1.9). Schwannomas are benign, usually bilaterally growing, lesions that commonly occur on the 8th cranial nerve but can arise anywhere within the peripheral nervous system (PNS) (Coons, 2001). Schwannoma formation is a dominant inherited autosomal disease, where tumour formation follows the two-hit model (Knudson, 1993). Transmission of a mutant gene through the germline predisposes the patient to tumour formation, after which schwannomas are initiated by somatic mutation of the remaining copy in Schwann cells.

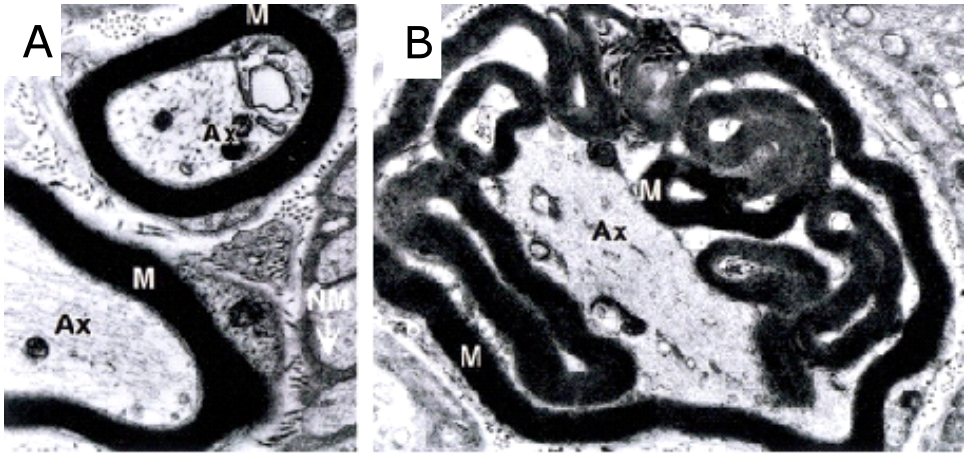

Figure 1.9: Loss of merlin results in schwannoma hyper-proliferation. **A)** Normal myelinating Schwann cells ensheathing axons. **B)** Loss of merlin, by biallelic inactivation, results in abnormal myelination and axon-glia interaction, where the Schwann cells no longer tightly ensheath axons. M= myelin and Ax= axon of the neuron. Image taken from Giovannini et al. (2000).

Schwann cell tumours, lacking axon interactions, have pronounced effects on myelination. Abnormal myelination results in the loss of saltatory conduction but may also result in neuropathy of adjacent nerve cells that become compressed. A few suggestions explaining the impaired axon-glia interactions

have been proposed so far. Loss of merlin in Schwann cells may lead to the inability of cells to adhere to and ensheath axons due to abnormal adhesive, motility and/or polarity properties of Schwann cells (Gutmann et al., 1999; Giovannini et al., 2000).

Merlin is a tumour suppressor gene, although the precise mechanisms by which its mutations result in schwannomas are unknown. One major setback to further understanding human schwannomas is that no successful model has yet been developed in mice. Homozygous NF2 mutants in mice results in embryonic lethality (McClatchey et al., 1997), whereas murine NF2 heterozygosity effects proliferation of other tissues not observed in human schwannomas, such as osteoblasts, ondotoblasts and renal tubular cells (Giovannini et al., 2000). Giovannini et al. (2000) have shown that biallelic inactivation of merlin leads to Schwann cell hyperplasia and disruption of the axon-glial interaction (Figure 1.9.B). Schwann cell hyperplasia is believed to be an early symptom of human schwannomas, although Schwann cell hyperplasia in mice does not progress to tumour formation (Giovannini et al., 2000). The loss of merlin in human schwannoma tissues has supported merlin's tumour suppressive role. Additionally, over-expression of wild type merlin in schwannoma cells leads to a significant reduction in proliferation and results in apoptosis (Lutchman and Rouleau, 1995; Sherman et al., 1997).

1.1.6.2 Ezrin's associations to disease

Ezrin has been identified as a component in tumour metastasis through binding to the CD44 receptor, thereby activating signalling pathways Rho-GTPase and interacting with the Akt-mediated cell apoptotic pathway (Harrison et al., 2002; Hunter, 2004). Ezrin expression has been proposed to play a key role in cell motility, adhesion and tumour metastasis, and over-expression of ezrin expression has been found in osteocarcinoma (Wang et al., 2010), breast (Elliott et al., 2005) and prostate cancer (Pang et al., 2004). Increased expression of ezrin in some cancer types has been shown to correlate well with both metastasis and poor cancer prognosis (Saotome et al., 2004).

Ezrin is able to activate MAPK and Akt signalling pathways for cell survival (Section 1.1.4.2), which further supports that ezrin is a tumour promoting protein which may allow metastatic cells to survive in what may otherwise be a hostile environment (Saotome et al., 2004). Further evidence for ezrin as a tumour promoting protein is observed in gliomas, where ezrin expression

promotes tumour motility and invasion by mediating the hepatocyte growth factor signalling cascade (Wick et al., 2001).

In addition to an increased expression of ezrin found in numerous tumours, the distribution of ezrin has also been shown to correlate with severity and prognosis of certain cancers. For example, in head and neck cancers, a significant correlation is found between cytoplasmic ezrin and poor prognosis (Madan et al., 2006), implying that the distribution of ezrin is critical for its ability to affect cellular proliferation.

1.1.6.3 Associated diseases related to willin

Diseases related to loss or over-expression of willin remain, to date, unknown. However, the closely related FERM domain containing protein 3 (FRMD3) has been shown to be a novel tumour suppressor in non-small-cell lung carcinoma (Haase et al., 2007).

A closer look at the location of the willin gene implies that, like FRMD3, the willin gene may be implicated in human cancers. The human willin gene is located on chromosome 14, open reading frame 31. Interestingly, the 14q region of the chromosome is found to be implicated in numerous cancers such as: uterine leiomyoma and leiomyosarcoma (Levy et al., 2000), meningiomas (Tse et al., 1997), gastro-intestinal stromal tumours (Fukasawa et al., 2000), neuroblastomas (Theobald et al., 1999) and gliomas (Dichamp et al., 2004).

14q mutations and loss of heterozygosity have also been linked with mutations and loss of heterozygosity on chromosome 22q12 - the location of the merlin gene (Leone et al., 1999; Fukasawa et al., 2000). This raises the possibility that willin, like merlin, may act as a tumour suppressor. This possibility is further supported by suggestions that willin is the human homologue of the *Drosophila* protein called expanded: a protein that acts as a tumour suppressor in the Hippo pathway in *Drosophila* (Section 1.2).

1.2 FERM domain proteins modulation of cell growth in *Drosophila*

Drosophila Melanogaster genetics has given insight into how a tumour suppressor signalling complex, termed the Hippo pathway, could modulate cell growth by regulating cell proliferation and apoptosis. Two FERM domain containing proteins, merlin and expanded, have been found to act upstream of the *Drosophila* Hippo pathway, and have therefore provided another avenue on which FERM domain containing proteins may act as tumour suppressors to regulate cell proliferation.

1.2.1 Hippo pathway regulates organ size and cell proliferation

The Hippo pathway is composed of several signalling proteins and cascades, and is essential for the modulation of cell growth, proliferation, apoptosis and cell adhesion. The control of cell growth via the Hippo pathway is of particular importance during development and tissue size control and has to be tightly regulated as cell over-proliferation may result in tumourigenesis (Edgar, 2006; Harvey and Tapon, 2007; Pan, 2007). The ultimate downstream effect of the Hippo pathway is to inhibit cell growth and promote apoptosis, thereby acting as a tumour suppressor signalling cascade.

The core Hippo pathway complex consists of Hippo/Salvador, Mats/Warts and Yorkie and a schematic summary of the pathway is represented in Figure 1.10. The Hippo kinase interacts with and phosphorylates a scaffolding protein called Salvador (Wu et al., 2003). Hippo and Salvador together phosphorylate and activate Warts kinase and its associated protein Mats (Lai et al., 2005). Phosphorylated Warts then phosphorylates a transcriptional co-activator, Yorkie, on three sites (Oh and Irvine, 2009). Phosphorylation of Yorkie on site S168 induces 14-3-3 binding, further resulting in Yorkie cytoplasmic retention (Dong et al., 2007). When Yorkie is relieved from the inhibition by the Hippo pathway, Yorkie positively regulates cell growth and survival by binding to and activating a transcription factor, Sd, to induce cyclin E, DIAP1 and *ex* expression (Goulev et al., 2008; Wu et al., 2009; Zhang et al., 2008b). Inhibition of Yorkie, through cytoplasmic retention, therefore results in cell cycle arrest and apoptosis.

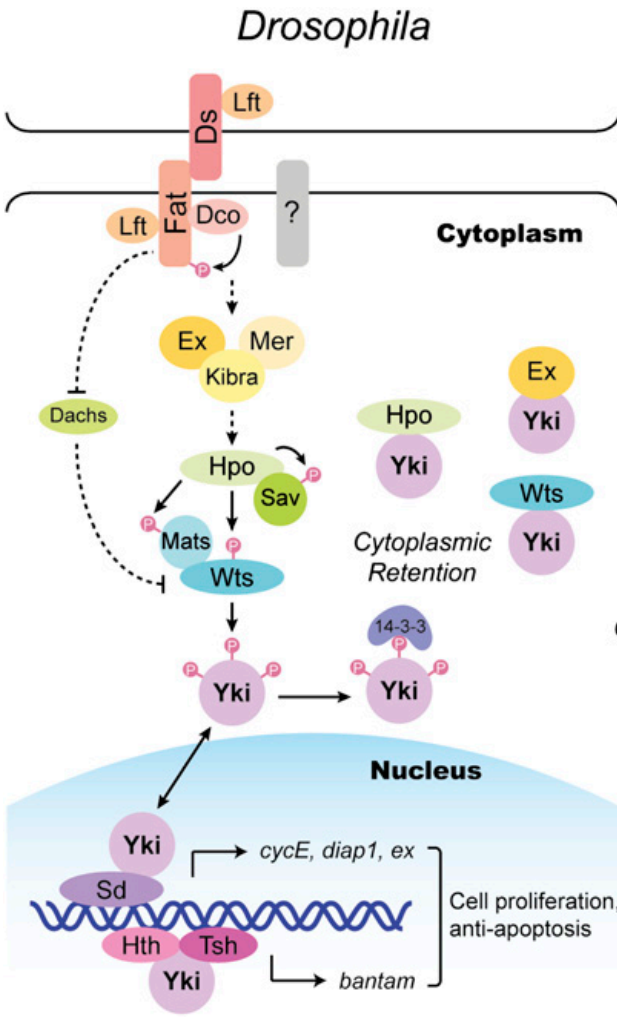

Figure 1.10: Schematic diagram of the Hippo pathway in *Drosophila*. Dashed arrows indicate unknown biochemical mechanisms. Image taken from Zhao et al. (2010a).

Signalling proteins involved in the Hippo cascade were identified using *Drosophila* mutants. Deregulation of the Hippo pathway results in significant apical hypertrophy of epithelial structures such as the wings, legs and eyes in adult *Drosophila* (Boedigheimer and Laughon, 1993; Boedigheimer et al., 1997; McCartney et al., 2000; Hamaratoglu et al., 2006) (Figure 1.11). Loss of Hippo, Salvador or Warts caused abnormal proliferation and survival of non-neuronal epithelial cells which failed to die but instead proliferated further, resulting in the expansion of adult *Drosophila* wings and eye tissue. Hippo, Salvador, Warts or Mats mutants all resulted in a significant increase in the cell cycle regulator cyclin E and DIAP-1, a *Drosophila* inhibitor of apoptosis

gene product (Tapon et al., 2002; Harvey et al., 2003; Pantalacci et al., 2003; Wu et al., 2003; Udan et al., 2003). Huang et al. (2005) identified a downstream transcriptional co-activator, Yorkie, involved in increasing cyclin E and DIAP-1 expression. Suppression of Yorkie downstream of the Hippo cascade was supported by observations that over-expression of Yorkie recapitulates Warts and Hippo mutant phenotypes: such as tissue atrophy and significant increase in DIAP-1 transcription (Huang et al., 2005).

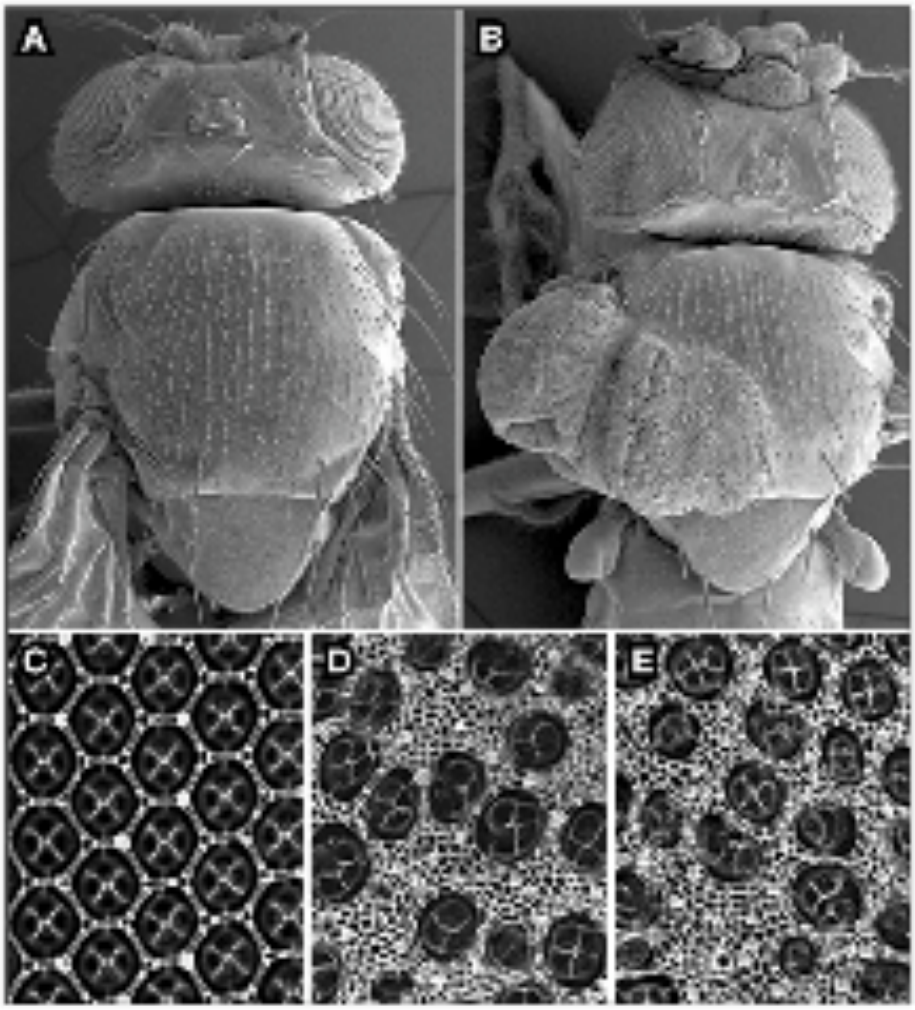

Figure 1.11: Overgrowth phenotypes are observed when Hippo pathway components are mutated in *D. Melanogaster*. **A)** Normal fly thorax. **B)** A tumour outgrowth of the thorax as a result of clonal deletion of both expanded and merlin. **C-E)** The crystalline arrangement of cells in the pupal retina of the fly as observed through a scanning electron microscope. **C)** Normal retina cell arrangement. The retina arrangement of cells is disrupted by over-proliferation and inappropriate survival of cells in hippo **(D)** and merlin and expanded **(E)** mutant retinas. Image taken from Edgar (2006).

1.2.2 Merlin and expanded modulate the Hippo pathway

Genetic epistasis experiments have positioned the FERM domain containing proteins merlin and expanded upstream of the Hippo Salvador pathway; positively regulating the Hippo complex (Hamaratoglu et al., 2006). A recent study identified a FERM domain binding consensus motif in Salvador, which likely mediates direct interaction with the FERM domain of merlin (Yu et al., 2010). Expanded has also been shown to co-immunoprecipitate with both Hippo and Salvador (Yu et al., 2010). Whether these interactions occur in a physiological setting remains unknown, but raises the possibility that merlin and expanded may activate the Hippo/Salvador complex via direct interaction. The C-terminal domain of expanded has also been identified to bind to Yorkie via WW domain-PY motif interactions (Badouel et al., 2009). In *Drosophila*, the C-terminal tail of expanded is also responsible for the activation and phosphorylation of the core Hippo pathway components (Boedigheimer et al., 1997).

Loss of merlin and/or expanded leads to the development of hyperplastic imaginal discs and overgrowth of adult wings (Boedigheimer and Laughon, 1993) (Figure 1.11), the same phenotypes that are observed in Hippo/Warts mutants. Additionally, over-expression of expanded induces apoptosis, reduces cell proliferation, decreases cell number in *Drosophila* wing, and severely disrupts eye development (Boedigheimer et al., 1997; Blaumueller and Mlodzik, 2000).

Merlin and expanded may have overlapping tumour suppressive functions in controlling cell growth, but inactivation of both proteins is required to result in a significant overgrowth phenotype (Boedigheimer and Laughon, 1993; McCartney et al., 2000; Hamaratoglu et al., 2006). Mutations of both merlin and expanded have a more pronounced effect on the adult antennae, thorax, wings and legs of *Drosophila* outgrowths, compared to mutants of either merlin or expanded alone (Hamaratoglu et al., 2006).

Expanded mutants in the *Drosophila* results in an over-proliferative phenotype in the eye wing and tarsal segments (Figure 1.12) although not as prominent as when both merlin and expanded genes are mutated (Figure 1.11). Loss of expanded resulted in an increase wing span and over-proliferative head capsule in addition to missing legs and swollen tarsal segments (Figure 1.12).

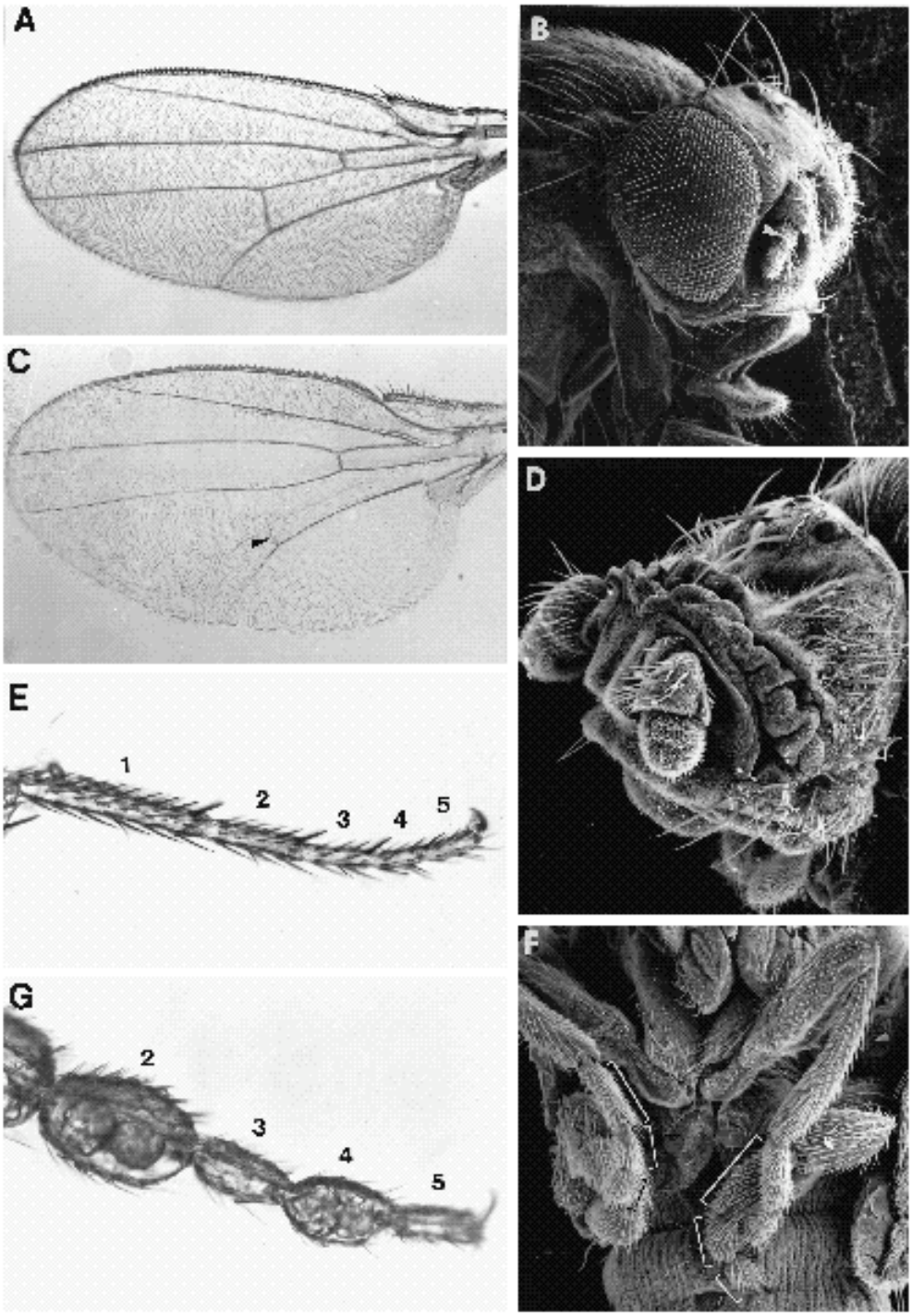

Figure 1.12: Expanded mutant *Drosophila* shows over-proliferation phenotypes in the eye, wing and tarsal segments. Wing **(A)** and head **(B)** from a wild-type *Drosophila*. *Drosophila* expanded mutants show over-proliferative defects in wing **(C)** head capsule **(D)**. **E)** Wild-type *Drosophila* with tarsal segments labelled. **F)** Expanded mutant show defects in the tarsal segments of the *Drosophila*, with 2 legs missing and 4 legs showing truncated tarsal segments. **G)** Expanded mutants also have characteristic swelling of the tarsal segments. Image taken from Boedigheimer and Laughon (1993).

Merlin and expanded co-localise in *Drosophila* (Boedigheimer and Laughon, 1993) and may heterodimerise with each other in order to function as an active tumour suppressor (McCartney et al., 2000). Loss of merlin results in an increase in expanded expression, either as a way of compensating for the loss of merlin or it may be possible that the expanded epitope is masked in the presence of merlin (McCartney et al., 2000). The latter supporting the formation of a merlin-expanded heterodimer, where expanded may function to stabilise the active tumour suppressor conformation by increasing the overall functional level of merlin. However, as more studies have shown that both merlin and expanded act as tumour suppressors, it is likely that expanded and merlin can act independently as monomers, able to compensate for the loss of the other.

Independent functions of merlin and expanded are further supported by recent experiments by Pellock et al. (2007), who have shown that merlin and expanded differentially regulate apoptosis and cell cycle exit in *Drosophila*. While expanded has a clear role in regulating cell cycle exit, merlin regulates apoptosis (Pellock et al., 2007). These observations increase the possibility that merlin and expanded may be regulated by different upstream receptors. Although the upstream events of expanded and merlin are unknown, there is evidence for an upstream protocadherin receptor, named Fat, to interact with expanded through an unknown mechanism (Bennett and Harvey, 2006; Silva et al., 2006; Tyler and Baker, 2007; Willecke et al., 2008). No upstream receptor for *Drosophila*'s merlin has yet been identified.

1.2.3 Other ERM proteins in *Drosophila*

Drosophila have only one ERM protein homologue, D-Moesin, which shares 58% sequence homology with human moesin, including 26% identity in the divergent C-terminal region (McCartney and Fehon, 1996). Loss of D-Moesin in *Drosophila* studies have shown that this protein is essential for cytoskeletal distribution, maintenance of apical-basal polarity and epithelial integrity (Miller, 2003). D-Moesin subcellular localisation is primarily in the apical membrane regions (McCartney and Fehon, 1996). Interestingly, the same subcellular apical membrane distribution is observed with Hippo pathway components, including merlin, FAT and expanded (Silva et al., 2006; Willecke et al., 2006; Bennett and Harvey, 2006; Cho et al., 2006; Maitra et al., 2006). Physio-

logically, loss of D-Moesin results in severe developmental problems, including missing posterior structures in the *Drosophila* fly in addition to defects in correct organisation and assembly in adherent junctions, photoreceptors, and imaginal discs (Polesello and Payre, 2004). Whether these developmental problems are due to moesin's role in the Hippo pathway remains, to date, unknown.

1.3 FERM proteins may modulate the Hippo pathway in mammals

1.3.1 The Hippo pathway is highly conserved between *Drosophila* and mammals

To date, most research identifying Hippo pathway components have been explored in *Drosophila*. Significant conservation of genes and pathway signalling of cellular processes between mammals and *Drosophila* have argued that studies of the Hippo pathway in flies can contribute directly to understanding the mammalian pathway (Potter et al., 2000). It is however important to note that unlike *Drosophila* studies, in which the Hippo pathway proteins are encoded by one single gene, most mammalian Hippo pathway proteins are composed of multiple isoforms (Sudol and Harvey, 2010). Therefore, the mammalian Hippo pathway cascade may be more complex, consisting of multiple isoforms, compared to the Hippo pathway in the *Drosophila* model. Figure 1.13 shows the corresponding orthologue components between the *Drosophila* and mammalian Hippo signalling proteins.

The relationship between the *Drosophila* Hippo, Salvador, Warts and Mats are conserved in mammals: MST/2 (Hippo homologue), SAV1 (Sav homologue), LATS1/2 (Wts homologue) and MOB (Mats homologue). Unknown upstream activators of the pathway activate the Hippo pathway by phosphorylating MST1/2, resulting in downstream activation and phosphorylation of the LATS1/2 kinase which binds in a complex with MOB1. LATS1/2 and MOB1 together phosphorylate and inhibit the downstream co-activator YAP. LATS1/2 phosphorylates YAP on five conserved HXRXXS motifs (Zhao et al., 2007). Phosphorylation of YAP on S127 site results in 14-3-3 binding, which further results in YAP-phosphorylation dependent cytoplasmic retention of

YAP (Zhao et al., 2007). YAP is also inhibited through phosphorylation at site S381, which primes CK1δ/ε phosphorylation of S384 and S387 on YAP, resulting in SCFβ-TRCP-mediated ubiquination and degradation (Zhao et al., 2010b). This mechanism of YAP degradation may provide a possible long-term YAP inhibition for cell contact inhibition.

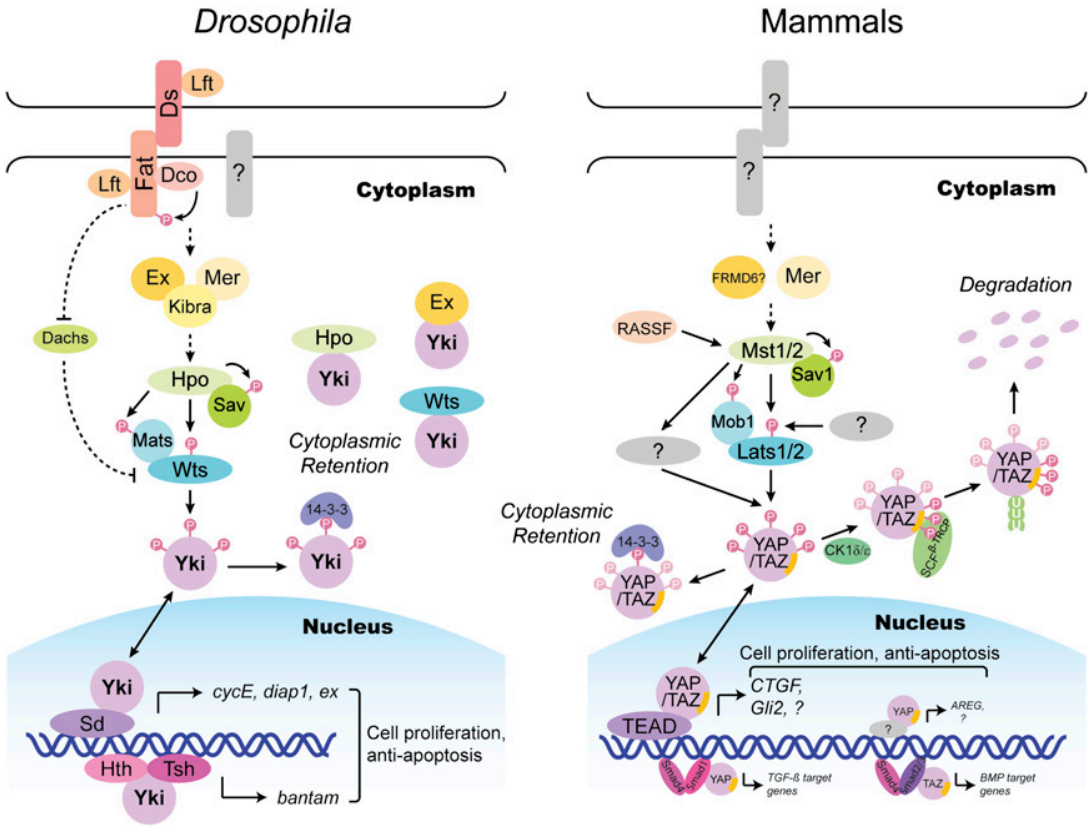

Figure 1.13: Schematic diagram of the Hippo pathway in *Drosophila* and mammals. Corresponding orthologue components of the *Drosophila* and mammals are shown in the same colour. Dashed arrows indicate unknown biochemical mechanisms. Image taken from Zhao et al. (2010a).

The downstream effects of YAP inhibition through cytoplasmic retention is the same as that observed with the *Drosophila* homologue, Yorkie, as YAP is inhibited through cytoplasmic retention by 14-3-3 protein binding (Zhao et al., 2007, 2008). YAP cytoplasmic retention prevents the co-transcriptional factor from binding to downstream transcriptional proteins in the nucleus, thereby preventing the transcription of cell survival proteins and promoting apoptosis. Sd homologue TEADs are the most studied YAP transcription factor targets. TEADs activation mediates expression of CTGF, Gli2 and

many other gene targets that results in cell proliferation and survival (Zhao et al., 2008). YAP also binds to Smad1 and Smad2/3 transcription factors to activate the expression of TGF-β and BMP target genes respectively, to maintain stem cell pluripotency (Varelas et al., 2008; Alarcon et al., 2009). Core Hippo pathway components have also been shown to affect the cell cycle. In human cells, LATS1/2 has been shown to affect cyclin E and cyclins A/B, inducing cell cycle arrest at G_1-S or G_2-M respectively (Xia et al., 2002; Li et al., 2003). Whether cyclin levels are affected by LATS converging onto YAP or whether this effect is observed through additional signalling cascades remains unknown.

1.3.2 Modulation and regulation of the mammalian Hippo pathway

The Hippo pathway, like many biological processes has to be tightly regulated and modulated. Many upstream proteins and negative feedback loops are therefore believed to exist, making the Hippo pathway signalling cascade more complex than that represented in Figure 1.13. Most research has focussed on downstream targets and physiological affects of the core Hippo pathway: MST1/2, LATS and YAP. Less is known about the upstream receptors, activators and modulators of the Hippo signalling cascade. The functional mechanistic actions of the mammalian homologues of merlin and expanded remain unclear and are further discussed in Section 1.3.2.1. The identity of other upstream members of the mammalian Hippo pathway has remained enigmatic. Recent studies have suggested that the proposed upstream Fat protocadherin receptor of the Hippo pathway in *Drosophila*, does not have the same control on organ size and activity of the Yorkie orthologues, YAP and TAZ, in mice (Saburi et al., 2008; Mao et al., 2011). Studying *Drosophila* models has clearly led to insight into some of the fundamental biological aspects of tumourigenesis within the mammalian system, but it should be noted that there will always be differences between the *Drosophila* and mammalian model.

1.3.2.1 FERM modulation on the Hippo pathway

As discussed in Section 1.2.2, the FERM domain containing proteins merlin and expanded activate the Hippo pathway in *Drosophila*. The mammalian genome contains potential homologous to the reported upstream

Hippo pathway regulators; including two possible expanded homologous (FRMD6=Expanded 1 and FRMD1=Expanded 2) and one merlin homologue (NF2/merlin).

Interestingly, the proposed homologue to the *Drosophila* expanded is willin (FRMD6). The expanded gene, 1427 amino acids in length, is significantly larger than the willin gene which is 614 amino acids in length, and may have split its functions during vertebrate evolution. The expanded and willin proteins are especially divergent in the carboxyl termini (Figure 1.14), which is the region proposed to activate and phosphorylate the *Drosophila* Hippo pathway (Boedigheimer et al., 1997) and bind to and inhibit Yorkie (Badouel et al., 2009). In *D. melanogaster*, Yorkie is believed to contact expanded via a WW domain-PY motif interaction (Badouel et al., 2009), but none of the three PY motifs in the expanded C-terminus are conserved in willin (Figure 1.14). A 55% protein similarity is, however, found in the FERM domain of expanded and willin (Figure 1.14).

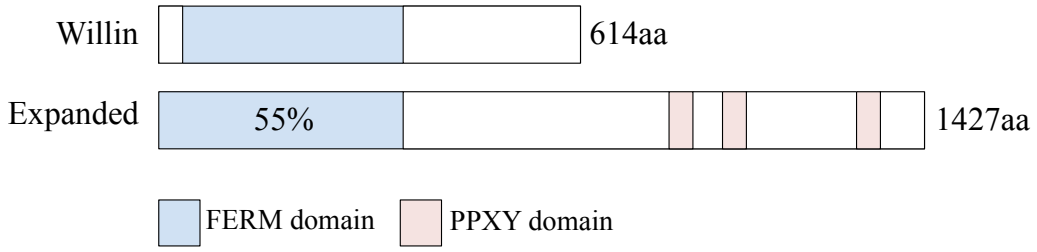

Figure 1.14: Schematic representation of protein domains in willin and expanded. Willin is composed of 614 amino acids (aa) and contains a FERM domain at the N-terminus. Expanded consists of 1427 amino acids and contains a FERM domain as well as three PPXY motifs. The FERM domain of willin and expanded share 55% similarity.

A study by Zhao et al. (2007) has shown that the expression of merlin and willin enhances the inhibition of YAP2, resulting in YAP nuclear to cytoplasmic translocation. Merlin and willin may therefore regulate cell proliferation through the Hippo pathway resulting in YAP translocation within the cell. Loss of merlin is associated with a clear increase in the protein levels of YAP, which has been shown to affect human meningioma cell growth by signalling through YAP (Striedinger et al., 2008). In addition to this increase, merlin loss was associated with nuclear localisation of YAP (Striedinger et al., 2008). Further evidence for the involvement of merlin in the Hippo pathway comes

from recent data which supports that merlin and the YAP oncoprotein function antagonistically to regulate liver development (Zhang et al., 2010). Strikingly, the merlin-deficient phenotypes in multiple tissues were largely suppressed by heterozygous deletion of YAP, suggesting that YAP is a major effector of merlin in growth regulation (Zhang et al., 2010).

Whether merlin and willin protein expression results in phosphorylation of the core Hippo signalling cassette (MST, LATS and YAP) remains unknown. In *Drosophila*, the FERM domain of expanded is not required for activation and phosphorylation of the core Hippo component (Boedigheimer et al., 1997) and the domains required for YAP cytoplasmic retention by merlin and willin remain unknown.

The involvement of other FERM domain containing proteins in the Hippo signalling pathway has not been studied and may suggest an essential role in signal modulation, as FERM proteins have been shown to modulate other FERM proteins. For example, ezrin, which is absent in *Drosophila*, may have an inhibitory role on the mammalian Hippo pathway as it can inhibit the functions of merlin (Section 1.1.4.2).

Evolutionary conservation between *Drosophila* and mammals is further supported by experiments showing that human LATS, MATS2 and YAP genes can all functionally rescue their respective *Drosophila* mutants *in-vivo* (Tao et al., 1999; Wu et al., 2003; Lai et al., 2005). However, the biological functions and consequences of these pathways might vary between different organisms. Willin displayed an overlapping localisation to expanded as it is predominantly localised at the apical junction of epithelial cells, possibly due to the conserved FERM domain. Despite this, willin did not display growth suppressive activity in *D. melanogaster* tissues (Figure 1.15). In addition, willin mis-expression did not limit the size of *D. melanogaster* wings and it failed to rescue the overgrowth defect and elevated Yorkie activity associated with *ex* deficiency (work done in collaboration with Dr Kieran Harvey, University of Melbourne, Australia; Figure 1.15). Divergence in the willin gene compared to that of expanded and the absence of the PPXY motifs in willin may explain why willin cannot compensate for the loss of expanded in *Drosophila*. Other mammalian proteins, such as angiomotin (Zhao et al., 2011) have also been proposed to inactivate YAP through PPXY motifs, a role fulfilled by the C-terminus of expanded in *D. melanogaster*.

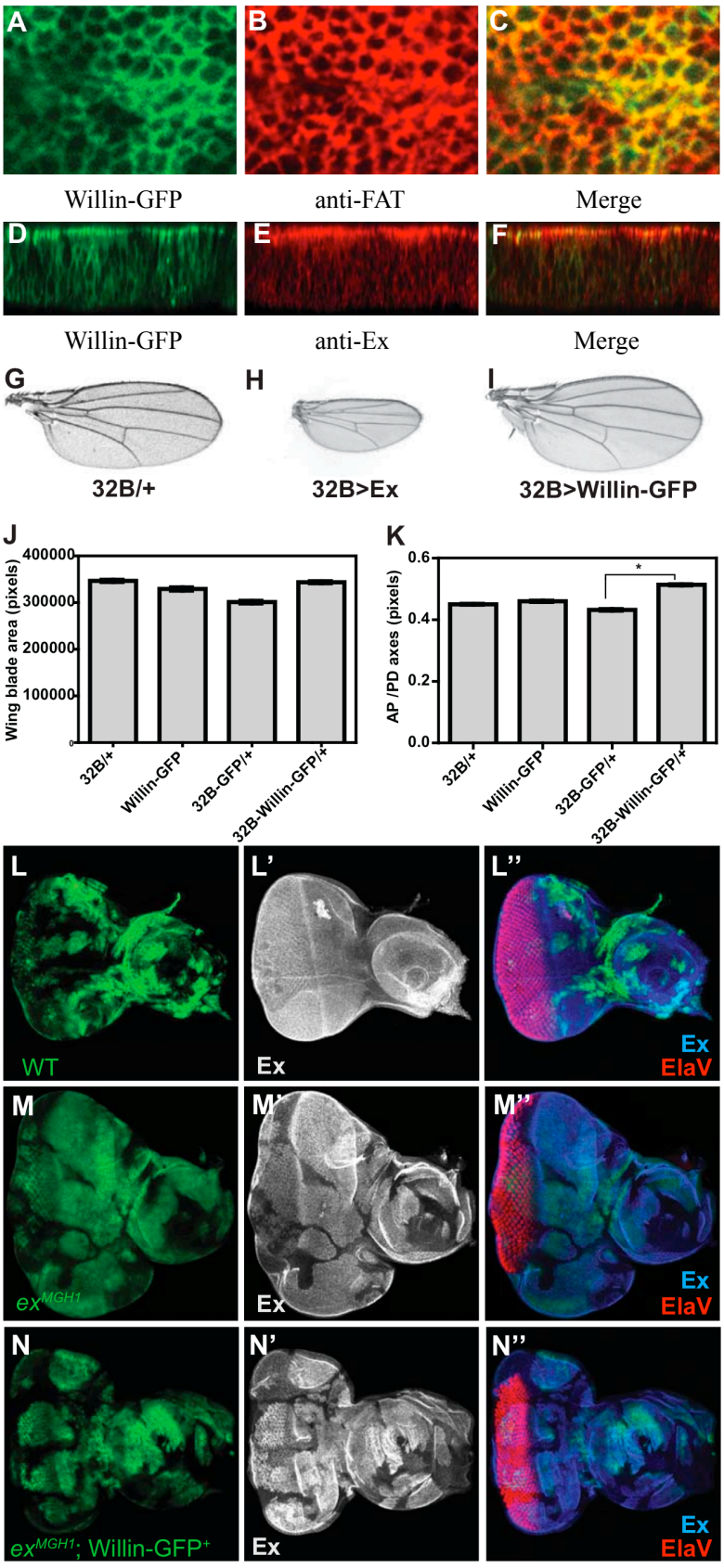

Figure 1.15: Willin displays similar subcellular localisation as expanded but cannot functionally replace it. Planar (A-C) and optical (D-F) cross sections of third instar larval wing imaginal discs expressing willin-GFP. Willin-GFP was detected at the apical plasma membrane, similar to Fat expression (red in B and C) and expanded (red in E and F). (G-I) Adult female D. melanogaster wings of the indicated genotypes. (J) Quantification of the area of adult wings of the indicated genotypes (n=32 for each genotype). (K) Quantification of the shape of adult wings of the indicated genotypes. (L-N) Third instar larval eye imaginal discs. Clones are positively marked with GFP (green) and are of the following genotypes: wild-type (L), exMGH1 (M), and exMGH1 also misexpressing willin-GFP (N). Image from a collaboration with Dr Kieran Harvey (University of Melbourne, Australia).

1.3.2.2 Cell density regulates Hippo signalling

Cell-to-cell contact, adhesion and polarity have all previously been described as important factors in activating the Hippo signalling cascade (Bennett and Harvey, 2006; Zhao et al., 2007; Graves et al., 2001; Lee et al., 2001; Chen et al., 2010). Extracellular signals from cell-to-cell contact provide neighbouring cells with vital information about the cell's external environment. The Hippo pathway has been proposed to play a role in regulating organ size by inhibiting cell growth at high cell density, where the pathway is believed to be suppressed at low cell density and activated at high cell density. This is supported by *in-vitro* work, where Zhao et al. (2007) have shown that YAP promotes cell proliferation as it is predominantly localised to the nucleus at low cell density, whereas at high cell density, YAP is localised to the cytoplasm. Several other components of the Hippo pathway have also been implicated in contact inhibition. Merlin becomes dephosphorylated and activated in confluent cells (Shaw et al., 1998; Morrison et al., 2001) which have been reported to be both necessary and sufficient to result in contact inhibition. LATS2 and WW45 are also involved in contact inhibition as their knock-out mouse embryonic fibroblast (MEF) cells show loss of contact inhibition (McPherson et al., 2004; Lee et al., 2008).

The Hippo signalling pathway may be regulated by the strength of cell-to-cell adhesion (Pan, 2007). Over-crowding of cells in an organ may result in quantitative or qualitative changes in the adherent junctions between neighbouring cells, which in turn might modulate the Hippo signalling activity. The mechanisms involved in cell density dependent regulation of the Hippo pathway remains unclear. One possible theory is that unknown upstream plasma membrane receptors of the Hippo pathway may be activated and up-regulated at high cell density upon interaction with other surface proteins upon cell-to-cell contact or through binding of an unknown extracellular ligand (Buttitta and Edgar, 2007). The activated receptor may then activate FERM domain containing proteins, which in turn stimulate the MST/LATS kinase cascade to inhibit oncogenic YAP, ultimately resulting in the inhibition of cell proliferation and apoptosis. FAT was identified as a potential transmembrane receptor for the Hippo pathway (Bennett and Harvey, 2006; Cho et al., 2006; Silva et al., 2006; Willecke et al., 2006). In this cell-density dependent proposed model, abundance of FAT, its ligand (possibly Dachsous), or the intensity of FAT can somehow respond to small differences in morphogen signalling levels

between two neighbouring cells (Harvey and Tapon, 2007).

1.3.2.3 Cell stress regulates Hippo signalling

As well as upstream proteins and plasma membrane receptors, extracellular cues are also vital in fully activating the Hippo pathway. Intracellular signals or mechanical tension on the cell membrane, might potentially regulate the Hippo signalling pathway. The mammalian homologue of Hippo, MST2, has been shown to be a pro-apoptotic responder to stress (O'Neill and Kolch, 2005). Recent studies have shown that for MST to result in an apoptotic downstream effect, MST has to be both phosphorylated and cleaved (Graves et al., 2001). The increased expression of MST merely sensitises the cells to cell death (Lee et al., 2001). Extracellular cell death signals are therefore believed to be required for full activation of the Hippo pathway to result in apoptosis.

1.3.3 Associated diseases with the mammalian Hippo pathway

1.3.3.1 Expression of Hippo pathway components

To date, it remains unclear in which mammalian tissues and cell types the Hippo pathway controls proliferation and apoptosis. In *Drosophila*, the Hippo pathway restricts growth of imaginal discs (Tapon et al., 2002; Harvey et al., 2003; Udan et al., 2003; Wu et al., 2003; Huang et al., 2005; Lai et al., 2005; Bennett and Harvey, 2006; Hamaratoglu et al., 2006; Silva et al., 2006), which are columnar epithelial cells, but does not limit tissue growth in other tissues such as salivary glands (Harvey and Tapon, 2007). This raises the possibility that the Hippo pathway regulates cell proliferation in a subset of human tissues and cell types that share similar growth, proliferative and apoptotic properties to *Drosophila* imaginal discs (Harvey and Tapon, 2007). Loss of Hippo pathway components and their associated contributions to tumour formation will give insight into the expression and importance of Hippo pathway components (Section 1.3.3.2).

1.3.3.2 Implications of Hippo components in disease

The physiological functions of the Hippo pathway components are harder to investigate in the mammalian system compared to the *Drosophila* model, as

most of the mammalian Hippo components knock-outs in mice are embryonically lethal (Table 1.2). However, consistent with the critical role of the Hippo pathway in mammalian physiology in regulating organ size control and cell proliferation, mutations in the Hippo pathway components have been implicated in human diseases, especially tumourigenesis. Table 1.2 summarises the importance of the Hippo components and their associations with cancer development.

The importance of merlin as a tumour suppressor has previously been discussed in Section 1.1.6.1. Genetic studies have demonstrated that MST1/2 are tumour suppressors. WW45 and MST1/2 mutant livers are significantly larger and histological analysis showed formation of a poorly differentiated hepatocellular carcinoma in WW45 mutants and cholangiocarcinoma was observed in MST1/2 mutants (Zhou et al., 2009; Song et al., 2010; Lu et al., 2010).

The loss of LATS proteins also promotes tumourigenesis. Mice deficient in LATS1 develop ovarian carcinomas and soft-tissue sarcomas (St John et al., 1999). Furthermore, methylation-dependent silencing of LATS1 and LATS2 correlates with an aggressive form of human breast cancer (Takahashi et al., 2005). LATS plays an important role in sister chromatid segregation (Bothos et al., 2005) and the loss of these proteins will greatly affect cell cycle progression and genomic instability that could ultimately result in cell defects. Converging mechanisms on the Hippo pathway components are also involved in the regulation of cell growth. For example, miRNA mediated silencing of LATS2 by miR372 and miR373 are also up-regulated in testicular germ cell tumours (Voorhoeve et al., 2007).

The oncogenic activity of YAP is supported by reports that showed that the YAP gene locus is amplified in a wide spectrum of human and murine tumours such as: oral squamous-cell carcinoma, and carcinomas of the lung, pancreas, oesophagus, liver and mammary gland (Imoto et al., 2005; Dai et al., 2003; Bashyam et al., 2005; Snijders et al., 2005; Overholtzer et al., 2006; Zender et al., 2006; Fernandez-L et al., 2009). Conversely, YAP has been reported to promote p73-dependent apoptosis in response to DNA damage, suggesting a potential pro-apoptotic and therefore tumour suppressive function under certain conditions (Strano et al., 2001; Basu et al., 2003; Matallanas et al., 2007; Oka et al., 2008; Yuan et al., 2008). Further studies are required to investigate the opposing functions of YAP as an oncogene, as the pro-apoptotic function of YAP was shown to be activated (Matallanas et al., 2007)

Protein	Phenotype of KO mice	Human disease	Reference
Merlin	Lethal before gestation	Neurofibromatosis, Schwannomas, Meningiomas	McClatchey et al. (1997) Hanemann (2008) Trofatter et al. (1993)
WW45	Perinatal lethality	Osteosarcoma, Hapatosarcoma	Lee et al. (2008)
MST1/2	Embryonic lethal	Hepatocellular carcinomas	Oh and Irvine (2009) Zhou et al. (2008)
LATS1	Partial lethality at P1 Survivors: mammary gland defects	Sacroma, Ovarian cancer, Breast cancer	St John et al. (1999) Takahashi et al. (2005) Hisaoka et al. (2002)
LATS2	Lethality at E10	Breast cancer	Takahashi et al. (2005) McPherson et al. (2004)
YAP	Lethality at E8	Cancer	Morin-Kensicki et al. (2006) Zender et al. (2006)
TAZ	Partial lethality at birth. Survivors: kidney and lung defects	Polycycsitc kidney disease cancer emphysema	Makita et al. (2008) Hossain et al. (2007)

Table 1.2: Mammalian Hippo signalling components and their contributions to tumourigenesis. KO= knock-out. Table adapted from Wang et al. (2009).

or inhibited (Oka et al., 2008) by LATS1 phosphorylation.

1.3.3.3 Hippo pathway components antagonise oncogenic properties *in-vitro*

YAP over-expression has been shown to enhance oncogenic activity in both immortalised mammary and pancreatic epithelial cells *in-vitro*. These oncogenic properties include the ability to support growth factor and anchorage independent growth, epithelial-to-mesenchymal transition and resistance to apoptosis (Overholtzer et al., 2006; Dong et al., 2007; Zhao et al., 2008; Chan et al., 2009; Zhang et al., 2009a). Over-expression of YAP *in-vitro* results in changes where a typical polarised uniform epithelial sheet of cells transforms into mesenchymal-like metastatic cells, exhibiting neither regimented structure nor tight intracellular adhesion. Interestingly, MST and LATS proteins can antagonise the oncogenic properties of YAP in these breast cancer cell lines (Overholtzer et al., 2006; Hao et al., 2008; Zhang et al., 2008a), further supporting the tumour suppressive functions of the Hippo pathway on YAP.

1.4 Key questions to be addressed in thesis

Studying *Drosophila* models has clearly led to insight into some fundamental biological aspects of tumourigenesis within the mammalian system and has opened up a new avenue for FERM domain containing proteins to modulate on the Hippo pathway in both *Drosophila* and mammals. To date, willin's involvement in growth signalling pathways in the mammalian system is unknown even though the *Drosophila* orthologue, expanded, has been shown to activate and modulate the Hippo pathway. It is predicted that willin plays a role in the Hippo pathway (Figure 1.16). The aim of this thesis is to investigate the role of willin in the mammalian Hippo pathway. Research will focus on the biological effect willin has on the mammalian Hippo pathway on cell proliferation and apoptosis *in-vitro* on both immortalised cell lines as well as primary cell cultures. The modulation of willin and other ERM proteins on the activation of the mammalian Hippo pathway will be investigated in order to directly contribute to the understanding of human cancers and potential therapeutics.

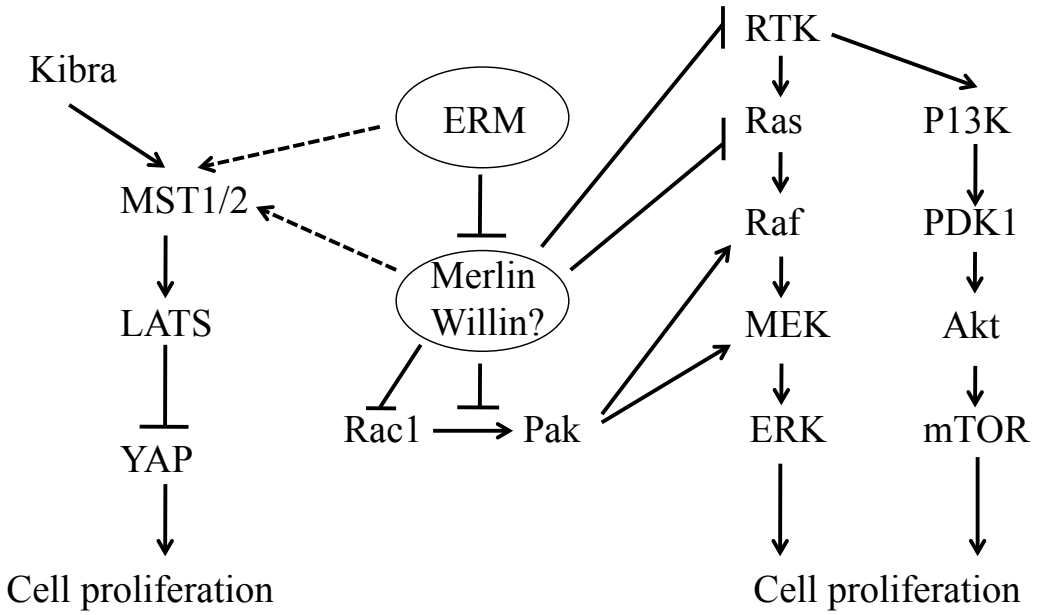

Figure 1.16: Schematic representation of the predicted interaction of willin on growth controlling signalling pathways. Merlin has been shown to inhibit cell proliferation by inhibiting MEK/ERK and Akt/mTOR signalling pathway as well as predicted interactions with the Hippo signalling pathway to inhibit cell growth. ERM proteins have growth promoting properties through inhibiting the actions of merlin. The effects of merlin, willin and ERM proteins on the Hippo pathway, to date, remain unknown (dashed line).

Chapter 2

Materials and Methods

2.1 Molecular cloning

2.1.1 Polymerase chain reaction (PCR)

PCR reactions for the amplification of full-length willin, the FERM domain and the C-terminal domain of willin contained: 0.5 units PfuTurbo DNA Polymerase (Roche), appropriate 10X buffer (Roche), 1% DMSO (Sigma), 0.5μM forward primer, 0.5μM reverse primer (Invitrogen; see Table 2.1 for list of PCR primers), 200μM dNTPs (Promega) and 100ng pWillin-GFP DNA template. The PCR reaction was conducted in a Biometra T-Gradient Thermal Cycler (Biometra, Germany) and the thermal PCR cycle was as described in Table 2.2. PCR reaction on cDNA contained Taq PCR master mix (Sigma), 0.5μM forward primer, 0.5μM reverse primer (Table 2.1) and 200ng cDNA. Biometra-T thermal cycler (Biometra, Germany) was set to the conditions described in Table 2.3.

NAME	NUCLEOTIDE SEQUENCE
BMP2-F	CGACCCTCGACCCCCGAGTC
BMP2-R	CACGCGGGGACACGTCCATT
Cterm-F	CGGGATCCACGATGAAGAAGCAGTACCGGGAATCTTAC
Cterm-R2	CGGAATTCCTAAGCGTAATCTGGGACGTCGTATGGGTA CACAACAAACTCTGGAACTTC
DR-500bp-F	GAGTGGAAGCAGGACTCTGG
DR-500bp-R	GTGAGTCCAAGCAATGCTGA
EF1a-F	ATGGCACGGTGACAACATGCT
EF1a-R	CCACATTACCACGACGGATG
FERM-F	CGGGATCCACGATGCGCAGTGTGTGCATTTTCCTT
FERM-R	CGGAATTCCTAAGCGTAATCTGGGACGTCGTATGG GTACTCTTCGTTTTCCTCCAGC
IGFBP2-F	CCAGCTCCAGGTGAGCCGC
IGFBP2-R	CCAGCAGAAGCCCCGCTTCC
m-actin-F	AGGCATTGTGATGGACTCCG
m-actin-R	AGTGATGACCTGGCCGTCAG
m-cyclo-F	AGGGTGGTGACTTTACACGC
m-cyclo-R	GGTTTGATGGGTAAAATGCC
mRT-PCR-F	AGCACAGATGGCCGTGTATT
mRT-PCR-R	TCAGTATCATCCCGACACGA
MST1/2-F	GAGAAGCTTGGAGAAGGGTC
MST1/2-R2	CCACAGTACTCCATAACAATCCA
PRL-F	ACCAGGAAAAGGGAAACGAATGCC
PRL-R	CGGCGCGGTCAAACAGGTCT
R-ezrin-F	CCCGGCCGATCCCAATTTGTGAA
R-ezrin-R	GGCGGAGACACGTCGGGAC
R-LATS1-F	TGCCGCAAAGGCCGAGCATA
R-LATS1-R	TGGCATTGATAGGTCTGGCAGCT
R-LATS2-F	TGAGCGCAGAGACGGTGGGT
R-LATS2-R	ACGTCCAATGTTTTGGCATAGCTGATT
R-merlin-F	TTTGCCATAGGCAGCCCGCC
R-merlin-R	GTTACACCCACCACTCCTCAAATACC
R-MST1-F	TGCTTACTTGGTAACCCAGCCTCAG
R-MST1-R	TGGGACTCGGTCCTCAGGGGA
R-MST2-F	AGCAGGACTTCAAGAACAAGAGTCATG
R-MST2-R	GGCGGCTTCAGTCGCAGGTT
r-willin-F	CAGCCCACAACACAATGAAC
r-willin-R	AGTGCAGCACCTGTTTCCTT
R-YAP-F	AGCCCAAGTCCCACTCGCGA
R-YAP-R	ACGAGGGTCAAGCCTTGGGTC
RASSF8-F	GGGGCTGGGCATAGAACTGTTGG
RASSF8-R	TTCCATGGTGCACCGGCCAGT
Willin2-F	GCTCAAGCTTCGAATTCGCCATGAAC
Willin2-R	ATAGCGGCCGCCACAACAAACTCTGGAACT

Table 2.1: Nucleotide primer sequences used for PCR, RT-PCR and qPCR.

Step	Temperature (^{o}C)	Time (sec)
1	94	300
2	94	30
3	50.2	60
4	72	120
5	72	600
6	4	pause

Table 2.2: Thermal PCR cycle for full-length willin PCR. Steps 2-4 were repeated a total of 40 times before steps 5 and 6 were performed.

Step	Temperature (^{o}C)	Time (sec)
1	94	300
2	94	30
3	52	40
4	72	60
5	72	600
6	4	pause

Table 2.3: Thermal PCR cycles for amplification of willin from cDNA. Steps 2-4 were repeated a total of 40 times before steps 5 and 6 were performed.

2.1.2 Agarose gel

1% (w/v) or 2% (w/v) agarose was melted in TBE buffer (0.45M Tris-borate, 10mM EDTA, pH 8.3; Sigma). Once cooled, a final concentration of 0.5μg/ml ethidium bromide (Sigma) was added. A 1% (w/v) agarose gel was used to separate DNA fragments larger than 1kb and 2% (w/v) for DNA fragments smaller than 1kb. The gel was left to set for 20 minutes at room temperature in a DNA gel rig. 6X agarose gel buffer (50% glycerol, 49.75% TBE, 0.25% bromophenol blue) was added to the samples before DNA was loaded into the wells. Hyperladder I (Bioline) was run simultaneously to analyse DNA band size. DNA gels were run at 60V for 1 hour and bands were visualised under UV light using GeneSnap software (Syngene).

2.1.3 Purification of DNA from agarose gel

DNA bands were visualised under low UV light (230-50Hz, Ultratec Ltd) and excised from the agarose gel using a sterile blade. The DNA band was purified using a Wizard SV gel and PCR Clean-up Kit (Promega) according the to manufacturer's protocol.

2.1.4 Restriction digest

5μg DNA was cut using 5 units restriction enzyme (Promega) and the appropriate 10X buffer (Promega) according to manufacturer's protocol. The restriction digest product was heat inactivated at 68^{o}C for 20 minutes. Double restriction digests were performed as follows: first restriction digest, heat inactivation, DNA clean up (Section 2.1.3), followed by a second restriction digest and heat inactivation. Restriction digest products were run on an agarose gel (Section 2.1.2) for analysis and extraction.

2.1.5 Ligation reaction

Restriction digested plasmid and the DNA insert were ligated using 5 units T4Turbo DNA ligase (Promega) and its appropriate 10X buffer (Promega) according to manufacturer's protocol; using a 1:5μl and 1:10μl vector:insert ratio. A control reaction was set up using 1μl vector in the absence of DNA insert. The ligation reaction was incubated at room temperature for a minimum of 4 hours.

2.1.6 Generating competent DH5α cells

A glycerol scrape of DH5α was added to 5ml Luria-Bertani (LB) medium (2% (w/v) tryptone, 0.5% bacto-yeast extract, 10mM NaCl, 2.5mM KCl, 10mM $MgCl_2$, 10mM $MgSO_4$, pH 7.5). DH5α bacterial cells were grown, shaking at 210rpm, in an orbital incubator at 37^{o}C for 15-18 hours. After incubation, 0.5ml of DH5α cell mixture was placed in fresh 50ml LB medium, shaking at 210rpm at 37^{o}C, until an absorbance reading between 0.3 and 0.4 was measured at 600nm (UV1601 Shimadzu Corporation). DH5α cells were harvested using a 4.2 Rotar Beckman J6-MC Centrifuge (Beckman) at 3,500g, at 4^{o}C, for 10 minutes. The DH5α cell pellet was resuspended in 20ml of 100mM $CaCl_2$ and incubated on ice for 30 minutes. DH5α competent cells were harvested at 400g

for 5 minutes at 4^{o}C. The cell pellet was resuspended in 1ml 100mM $CaCl_2$ and incubated on ice for 30 minutes before being used for transformations (Section 2.1.7). Competent DH5α cells were stored at -80^{o}C in 50% glycerol for future use.

2.1.7 Transformation

A 25μl ligation product (Section 2.1.5) was added to 200μl DH5α competent cells (Section 2.1.6) and left to incubate on ice for 30 minutes. The transformation mixture was heat shocked at 42^{o}C for 45 seconds and incubated on ice for an additional minute. 800μl SOC medium (2% (w/v) tryptone, 0.5% bacto-yeast extract, 10mM NaCl, 2.5mM KCl, 10mM $MgCl_2$, 10mM $MgSO_4$, 20mM glucose, pH 7.5) was added and incubated at 37^{o}C for 1 hour, shaking at 210rpm. 100μl of these cells were spread on agar plates that contained the appropriate antibiotic resistance (100μg/ml ampicillin or 50μg/ml kanamycin); dependent on the DNA plasmid's resistance. For DH5α transformations with pGEMT-easy plasmids, cells were spread onto X-gal plates (LB agar, 0.1mM IPTG and 2% X-gal and 100μg/ml ampicillin; protected from light).

2.1.8 Plasmid purification from transformed DH5α cells

A single colony from an agar plate (Section 2.1.7) or a glycerol stock scrape (Section 2.1.9) was added to 5ml LB medium, containing the appropriate antibiotic (100μg/ml ampicillin or 50μg/ml kanamycin). Transformed DH5α cells were grown at 210rpm, 37^{o}C, for 15-18 hours. DNA was purified using a Qiagen Spin Miniprep Kit (Qiagen), according to the manufacturer's manual. The DNA concentration of purified plasmid was measured at 260nm (UV1601 Shimadzu Corporation) and stored at -20^{o}C. DNA was sequenced at the DNA Sequencing Service (University of Dundee, UK).

2.1.9 Glycerol stocks

Glycerol stocks of transformed DH5α cells were made for long-term storage. 600μl LB overnight medium containing transformed DH5α cells and 400μl sterile 50% glycerol were mixed and stored at -80^{o}C.

2.2 Tissue culture

2.2.1 Cell culture

All cells were kept in an incubator at 37^{o}C with an atmospheric environment of 5% CO_2. Growth medium used for different cell lines are presented in Table 2.4.

CELL LINE	GROWTH MEDIUM COMPONENTS
HEK293	MEM, 10% FCS (Bethyl Laboratories), 2mM L-Glutamate, 100 units Penicillin, 0.1mg/ml Streptomycin, + 1% Non Essential Amino Acids
TRex	Same as HEK293 + 5 μg/ml Blasticidin (Invitrogen)
TRex-willinGFP	Same as TRex + 250μg/ml Zeocin (Invitrogen)
MCF10A	DMEM (Invitrogen), 5% Horse serum (Invitrogen), 20ng/ml EGF, 0.5μg/ml Hydrocortisone, 100ng/ml Cholera toxin, 10μg/ml Insulin, 100 units Penicillin + 0.1mg/ml Streptomycin
MCF10A-pBabe	Same as MCF10A + 2μg/ml Puromycin
MCF10A-YAP	Same as MCF10A + 300μg/ml Hygromycin
MCF10A-YAP + pBabe	Same as MCF10A-YAP + 2μg/ml Puromycin
Phoenix-A	DMEM, 10% FCS (Bethyl Laboratories), 2mM L-Glutamate, 100 units Penicillin + 0.1mg/ml Streptomycin
Schwann cells	DMEM, 10%FCS (Bethyl Laboratories), 2mM L-Glutamate, 100 units Penicillin, 0.1mg/ml Streptomycin, 10μM Forskolin + 20ng/ml Heregulin
Fibroblasts	DMEM, 10% FCS (Bethyl Laboratories), 2mM L-Glutamate, 100 units Penicillin and 0.1mg/ml Streptomycin

Table 2.4: Growth medium reagents for different tissue culture cell lines. All materials were from Sigma unless otherwise stated.

Cells were split, into T75 flasks, three times a week, in a class II sterile chamber. Growth medium was removed and the cells were rinsed with 1.5ml, pre-warmed to 37^{o}C, Trypsin-EDTA (Sigma). Cells were detached from the plastic surface by gently tapping the flask. Cells were harvested with 15ml fresh medium and the appropriate cell density was added back into the flask

containing 15ml fresh medium. Cells were passaged up to 40 times before being replaced with fresh cells that were stored in liquid nitrogen (Section 2.2.8). MCF10A cells were obtained from ATCC and were grown according to Debnath et al. (2003). HEK-293 cells were obtained from ATCC, TRex cells were are kind gift from Dr. Chris Tate (University of Cambridge, UK) and primary Schwann and fibroblast cells were a kind gift from Prof. Sue Barnett (University of Glasgow, UK).

2.2.2 DNA transfection

HEK-293 cells were transfected with DNA using GeneJammer transfection reagent (Stratagene) according to the manufacturer's manual (Table 2.5). HEK-293 cells were harvested and the appropriate cell density was added to dishes so that HEK-293 cells were 60-80% confluent on the day of transfection. Cells were placed in dishes with or without coverslips for use of immunofluorescence microscopy or western blotting respectively.

Size of dish (mm)	**GeneJammer (μl/dish)**	**DNA (μg/dish)**	**Optimem (μg/dish)**	**Medium (ml/dish)**
35	6	2	100	2
60	15	5	250	5
90	30	10	750	10
150	60	20	1000	15

Table 2.5: Volumes of reagents used in GeneJammer DNA transfection in different sized dishes.

2.2.3 siRNA transfection

HEK-293 cells were grown to 60-80% confluency in dishes with or without coverslips for use of immunofluorescence microscopy or western blotting respectively. Three duplex siRNA oligo-ribonucleotides specifically targeted against the willin gene were designed (Invitrogen): siRNA1 = GCCUCUAUAUGAAUCUGCAGCCUGUACAGGCUGCAGAUUCAUAUAGAGGC, siRNA2 = CACAGACUAUAUGUCGGAAACCAAAUUUGGUUUCCGACAUAUAGUCUGUG and siRNA3 = GACAGAGCAGCAAGAUACUAUUAUUAAU-

AAUAGUAUCUUGCUGCUCUGUC. siRNA was transfected into HEK-293 cells using GeneEraser (Stratagene) transfection reagent according to the manufacturer's protocol. The volume of siRNA was either split so that there was an equal volume of each siRNA duplex or made up of a single siRNA duplex.

2.2.4 Retroviral production and transfection

Retroviral infections were performed on MCF10A cell lines. Appropriate safety measures were taken when producing and transfecting a retrovirus. All viral work was done in a class II tissue culture hood designated for viral work only. All liquid waste was aspirated into a viral container containing Virkon (Antec International Ltd) and solid waste was placed in a double bag within the tissue culture hood after which it was placed within the viral waste. Both liquid and solid wastes were autoclaved before being disposed of.

Phoenix-A cells were harvested and $4x10^6$ cells were plated into 90mm dishes. After 24 hours, Phoenix-A cells were transfected with a pBabe vector containing the gene of interest and an empty vector was used as a control. For each 90mm transfection: 43μl Mirus LT1 (Mirus) was added to 1.5ml serum free Optimem (Invitrogen) and was left to incubate for 20 minutes at room temperature. 20μg of pBABE vector was added to Mirus LT1-Optimem solution and left to incubate for a further 30 minutes. The DNA-LT1-Optimem solution was then added drop by drop to the plate of Phoenix-A cells, which contained a total of 10ml of DMEM and 10% FCS. 24 hours post-transfection, the medium was removed and 4ml DMEM containing 10% FCS was added. Media was collected 48 hours post-transfection and 4ml DMEM containing 10% FCS was added back on the cells. 72 hours post-transfection, media containing the virus was collected. The media containing the virus from 48 hours and 72 hours post-transfection were pooled together and passed through a 0.45μm filter to remove cellular debris. The media containing the virus was used directly for retroviral transfection.

Cells to be transfected by retroviral transfection were harvested and $5x10^5$ cells were plated per 90mm dishes. 24 hours after seeding, culture media was aspirated from the 90mm dishes and 4ml of virus-media containing 8μg/ml polybrene (Sigma) was added to the cells and left to incubate for 8 hours in a 37^oC viral tissue culture incubator. Media was aspirated after the incubation and 10ml fresh culture media was added. Cells were selected with 2μg/ml

puromycin 48 hours post-infection. Four days after puromycin selection only puro-resistant cells remained.

2.2.5 Stable cell line production

Confluent T75 flasks were transfected with appropriate DNA plasmids using either the GeneJammer transfection (Section 2.2.2) or the retroviral transfection (Section 2.2.4) method. Cells were incubated in a sterile tissue culture incubator at 37^{o}C. 48 hours post-transfection, cells were selected for plasmid expression using appropriate antibiotics: 500μg/ml zeocin and 5μg/ml blasticidin were added to TRex-willin-GFP cell line; 2μg/ml puromycin was added to MCF10A-willin, MCF10A-FERM and MCF10A-Cterm cell lines; and 300μg/ml hygromycin was added to MCF10A-YAP cells. The cells were maintained in antibiotic containing medium thereafter.

2.2.6 Inducing TRex cell line

Willin-GFP expression was induced in the TRex-willin-GFP cells with growth medium containing 1μg/ml tetracycline. Fresh tetracycline was added every 48 hours for long inductions.

2.2.7 Storage of cell lines

Confluent T75 flask containing cells to be frozen down were trypsinised and resuspended in growth medium. Cells were harvested at 350g for 5 minutes at room temperature. The cell pellet was resuspended in freezing medium containing 40% FCS, 50% normal cell maintenance medium and 10% DMSO. 1.5ml aliquots were added to a cryotube and placed at -80^{o}C in a cryo-freezing container (Nalgene) for 24 hours. The cryotubes were placed in a liquid nitrogen store for long-term storage.

2.2.8 Rescue of frozen cell lines

Cells were quickly thawed at 37^{o}C and added to a sterile T75 flask containing 20ml growth cell medium. After 24 hours, the medium was aspirated and replaced with fresh medium.

2.3 Cell assays and treatments

2.3.1 Fixing and mounting cells for fluorescent microscopy

Cells were grown in dishes containing coverslips and treated as desired. When cell treatment was completed, the cells were washed three times with phosphate buffered saline (PBS; Sigma) and fixed with 1ml neutral buffered, filter sterilised, formalin (NBF; 10% (v/v) formalin, 0.4% (w/v) $NaH_2PO_4.H_2O$, 0.65% (w/v) Na_2HPO_4; Sigma) for 10 minutes at room temperature. Dishes were gently washed an additional three times with PBS and mounted with mowial (Sigma) and DAPI (4',6-diamidino-2-phenylindole; Sigma) on microscope slides. Images of the cells were taken using a DeltaVision deconvolution microscope (Applied Precision) or a multiphoton microscope (Leica). All images were taken from a Z-stack. Excitation wavelenght was 405nm for DAPI, 488nm for GFP and 633nm for mCherry. Slides were examined using either the X10 and X20 objectives under dry conditions or using the X40 and X63 objectives under oil immersion.

2.3.2 Propidium iodide staining for FACS analysis

Cells were washed three times in PBS and harvested in 10ml fresh growth medium at $350g$ for 5 minutes. The cell pellet was washed in ice-cold PBS and harvested at $350g$ for 5 minutes at 4^oC. For cell cycle analysis, $0.5x10^6$ cells were fixed in 80% ethanol and left overnight at -4^oC. Fixed cells were harvested at $350g$ for 5 minutes at 4^oC and the ethanol was aspirated. Fixed cells were resuspended in PBS containing $3\mu M$ propidium iodide (PI) and 500 units of RNaseA (Promega). Cells were incubated in PI solution for 30 minutes before being analysed on the FACS machine (FACscan Flow Cytometer, Becton Dickinson) at 615nm wavelength. For live/dead discrimination on cell populations, cells were harvested and resuspended in ice-cold PBS containing $3\mu M$ PI. Cells were incubated in PI solution for 5 minutes and analysed on the FACS flow cytometer (Becton Dickinson) at 615nm.

2.3.3 Nuclear versus cytoplasmic protein extraction

Cells were grown in two 90mm dishes and harvested at $300g$ for 5 minutes at 4^oC. The cell pellet was resuspended in 0.5ml ice-cold cytoplasmic extraction buffer (10mM HEPES pH7.9, 1.5mM $MgCl_2$, 10mM KCl, 0.5mM DTT) and incubated on ice for 5 minutes. Cells were lysed with 20 stokes using a Dounce homogeniser and the lysate was centrifuged at $228g$ for 5 minutes at 4^oC to pellet nuclei and other fragments. The supernatant, containing the cytoplasmic fraction, was stored at -20^oC. The nuclear pellet was resuspended in 0.5ml ice-cold nuclear extraction buffer (0.25mM sucrose, 10mM $MgCl_2$) and layered over a sucrose bed (0.88mM sucrose, 0.5mM $MgCl_2$). The nuclear fraction was pelleted by centrifugation at $2800g$ for 10 minutes at 4^oC. 5X protein sample buffer (250mM TrisHCl pH6.8, 10% SDS, 30% glycerol, 5% β-mercaptoethanol and 0.02% bromophenol blue) was added to both nuclear and cytoplasmic fractions and run on a protein SDS gel (Section 2.4.2.3). β-actin and coilin antibodies were used as a loading and a "carry-over contamination" control for cytoplasmic and nuclear extracts respectively.

2.3.4 Membrane and cytoplasmic sub-fractionation

Cells were grown in 90mm dishes, harvested at $300g$ for 5 minutes at 4^oC and washed twice in ice-cold PBS. The cell pellet was resuspended in 5ml hypotonic buffer (20mM Tris-HCl pH 7.4, 10mM KCl, 1mM EDTA, 1mM DTT, 1% aprotinin and 1mM PMSF) and incubated for 10 minutes on ice. Cells were lysed by 40 strokes using a Dounce homogeniser and equilibrated to 125mM NaCl. Cell lysates were spun at $1500g$ for 10 minutes at 4^oC. The pellet containing whole cells and nuclei was stored at -80^oC (P1 fraction). The supernatant was added to a Beckman ultraclear centrifuge tube and spun at $100{,}000g$ for 1 hour at 4^oC. The supernatant was incubated in 4 volumes of ice-cold acetone for 45 minutes and centrifuged at $3000g$ for 10 minutes at 4^oC. The acetone was aspirated and air-dried for an additional 40 minutes before the pellet was resuspended in 200μl 1% ice-cold Triton X-100 (S100). The pellet left in the Beckman centrifuge was resuspended in 200μl 1% ice-cold Triton X-100 and incubated on ice for 15 minutes. After incubation, the membrane fraction was centrifuged at $16{,}000g$ for 15 minutes at 4^oC. The Triton soluble supernatant (P100s) was removed and stored at -80^oC until needed. The Triton insoluble pellet (P100i) was resuspended in 200μl 1% ice-cold Triton

X-100 and stored at -80^{o}C until needed. 5XPSB (250mM TrisHCl pH6.8, 10% SDS, 30% glycerol, 5% β-mercaptoethanol and 0.02% bromophenol blue) was added to P1, P100s, P100i and S100 protein extracts and boiled for 10 minutes before being loaded on a SDS gel (Section 2.4.2.3).

2.3.5 Immunoprecipitation (IP)

2.3.5.1 Cross-linking antibody to Sepharose-G beads

10μl Sepharose-G beads (Sigma) were washed twice in PBS. Beads were resuspended in 100μl PBS containing 2μg of antibody and incubated with agitation for 1 hour at room temperature. Freshly prepared disuccinimidyl suberate (DSS, Pierce) was added to the antibody/Sepharose-G mixture to a final concentration of 650μg/ml and was incubated with agitation, for 1 hour at room temperature. After DSS cross-linking, Sepharose beads were washed four times with TBS. To release any unbound antibody, Sepharose beads were washed four times with 0.1M glycine (pH 2.8) followed by three washes with TBS. Before and after cross-linking samples were separated on a 10% Tris/glycine SDS gel (Section 2.4.2.3) to confirm that the heavy chain of the antibody was covalently linked to the beads.

2.3.5.2 Immunoprecipitation

Cells were grown in 90mm plates and transfected or induced for the desired protein expression. Cells were harvested at 420g for 5 minutes at 4^{o}C and resuspended in 300μl lysis buffer: 25mM Tris-HCl (pH 7.4), 150mM NaCl, 1mM $CaCl_2$, 1% TX-100 and 1% protease inhibitors (Roche). Cells were vortexed and incubated on ice for 15 minutes. Samples were sonicated twice for 10 seconds and centrifuged at 10,000g for 20 minutes at 4^{o}C to pellet insoluble material. To 20μl of protein-G Sepharose mixture conjugated to desired antibody (Section 2.3.5.1), cell lysate and wash buffer (25mM Tris-HCl pH 7.5, 150mM NaCl, 1% protease inhibitors) were added in a 1:1 ratio and incubated with agitation at 4^{o}C overnight. 15 hours after agitated incubation, protein-G Sepharose and the antibody solution were centrifuged for 1 minute and the supernatant was removed. The Sepharose complex was washed 3 times in wash buffer with a 30 second 500g spin. The pellet was resuspended in 50μl PSB (62.5mM Tris-HCl pH 6.8, 2% (w/v) SDS, 10% glycerol, 50mM DTT,

0.01% (w/v) bromophenol blue) and separated on a SDS gel (Section 2.4.2.3) to detect binding.

2.3.6 MTT assay

Cells were plated in 96 well plates in a total volume of 100μl medium. After cell treatment, MTT solution (3-(4,5-Dimethylthiazol-2-yl)-2,5-diphenyltetrazolium bromide; Sigma) was added to a final concentration of 1mg/ml. After a 3 hour incubation period in a sterile tissue culture incubator at 37^{o}C, all medium was aspirated and 100μl DMSO was added to each well. Plates were shaken for 5 minutes and the absorbance was measured at 590nm using MRX Microplate Reader (DYNEX Technologies).

2.3.7 TNFα treatment

Cells were treated, between 0-8 hours, with TNFα (Sigma) to a final concentration ranging from 0-200ng/ml.

2.3.8 Colorimetric caspase-3 assay

All materials for the caspase-3 assay were from the caspACE colorimetric assay kit (Promega).

2.3.8.1 Preparation of cell extract

Cells were grown in 35mm dishes and treated with either 50ng/ml TNFα, 50ng/ml TNFα and an apoptosis inhibitor Z-VAD-FMK (Promega) to a final concentration of 50μM, or left untreated. Cells were harvested at 450g for 10 minutes at 4^{o}C and washed in ice-cold PBS. The cell pellet was resuspended in lysis buffer provided in the caspase kit (Promega) at a concentration of 1x10^6 cells/ml. The cell extract was lysed by two freeze-thaw cycles and incubated on ice for 15 minutes. Cell lysates were centrifuged at 15,000g for 20 minutes at 4^{o}C and the supernatant was collected. The protein concentration of cell lysate was measured using a Bradford assay (Section 2.4.2.1).

2.3.8.2 Caspase assay

25μg of protein extract (Section 2.3.8.1) was used for the caspase-3 assay. Table 2.6 shows the components needed for a single reaction in a 96 well plate.

Plates were covered in parafilm and incubated for 4 hours at 37^{o}C and the absorbance was measured at 405nm using a MRX Microplate Reader (DYNEX Technologies). The difference between the amount of yellow produced in the absence and presence of Z-VAD-FMK inhibitor was a measure of the caspase-3 activity present in the sample. The specific activity (SA) of caspase-3 was calculated as described in CaspACE assay manual (Promega).

	Blank	**-ve control**	**induced apoptosis**	**inhibited apoptosis**
caspase buffer	32μl	32μl	32μl	32μl
DMSO	2μl	2μl	2μl	2μl
100mM DTT	10μl	10μl	10μl	10μl
untreated cell extract	-	Xμl	-	-
induced apoptosis extract	-	-	Xμl	-
inhibited apoptosis extract	-	-	-	Xμl
dH2O to total	98μl	98μl	98μl	98μl

Table 2.6: Volumes and reagents used in colorimetric caspase-3 assay (Promega).

2.3.9 Anchorage independence growth assay

Cells were harvested and seeded 2x10^4 cells per 35mm dish in a mixture of 0.35% agarose/DMEM:F12 complete media onto a lower layer of 0.5% agarose/DMEM:F12 complete media. Once the agarose was set, a layer of DMEM:F12 complete media was added above the agarose layers. Dishes were incubated at 37^{o}C in a humidified incubator for 3 weeks. Cell growth media was replaced twice a week and the number of colonies, defined as $\geq$5 cells, were counted after 14 and 21 days using a brightfield microscope.

2.3.10 Cell migration assay

Cells were harvested and 1x10^5-1x10^6 cells were placed in 0.5ml serum-free growth media. Media containing cells were added to the top chamber of 24 well 8.0μm pore Boyden chamber (Biocoat, Becton Dickinson). The lower chamber contained growth media with 20% serum. Cells were incubated at 37^{o}C in a humidified incubator for 24 hours. After 24 hours, media in the top Boyden chamber was removed and washed 3 times in sterile PBS and the top

membrane was scrubbed free of cells using a cotton swab. The bottom side of the porous membrane was stained with 0.1% crystal violet (Sigma) and a brightfield image of the cells was taken. Crystal violet dye was extracted with 500μl 0.1M sodium citrate in 50% ethanol and absorbance was measured at 570nm using a MRX Microplate Reader (DYNEX Technology).

2.3.11 Adhesion assay

A 96 well plate was coated with 10μg/ml laminin (Sigma) at 37^{o}C for 1 hour in a sterile chamber. Some wells were left uncoated for a negative control. Wells were washed twice with cell growth medium containing 0.1% BSA and blocked with cell medium containing 0.5% BSA for 1 hour at 37^{o}C. Wells were then washed with medium containing 0.1% BSA and plates were chilled on ice for 30 minutes. 2x10^4 cells were plated into each well and left to incubate at 37^{o}C for 30 minutes. After incubation, plates were shaken at 2000rpm for 10 seconds and wells were washed twice in PBS. Cells were fixed in 4% PFA for 10 minutes at room temperature and washed twice with PBS. Cells were stained with 5mg/ml crystal violet in 2% ethanol for 10 minutes and the total number of cells in the wells were counted using a brightfield microscope.

2.3.12 Scratch assay

The same number of cells were plated into 35mm dishes and left to grow until confluent. Once a monolayer of confluent cells was observed in the dishes, a scratch was made with the end of a yellow tip. Brightfield images were taken just after the scratch and at different time points depending on cell growth and migration. The percentage of scratch covered by cells was calculated using Image J software.

2.4 Protein and RNA detection

2.4.1 Reverse transcriptase PCR

2.4.1.1 RNA extraction

Lab surfaces and materials needed were cleaned with DEPC water (0.1% DEPC in sterilised water) and put under UV light for 10 minutes to create an RNase-free environment. RNA was extracted from cells using the RNeasy

Mini Kit (Qiagen), according to manufacturer's protocol. The extracted RNA concentration was measured at 260nm (UV1601 Shimadzu Corporation) and stored at -80^{o}C until needed.

2.4.1.2 DNase digestion of RNA samples

DNase digestion of 5μg RNA was achieved using 2 units RQ1 RNase Free DNase (Promega) and appropriate 10X buffer (Promega) according to the manufacturer's protocol. DNase digestion was incubated at 37^{o}C for 30 minutes. DNase treated RNA samples were stored at -80^{o}C until further required.

2.4.1.3 Reverse transcriptase PCR (RT-PCR)

2μg of DNase treated RNA was denatured at 65^{o}C for 10 minutes in 10μl RNase free water and 1μM random hexanucleotides (Roche). 20 units Protector RNase Inhibitor (Roche), 200μM dNTPs, 50 units AMV Reverse Transcriptase (Roche), and the appropriate 5X buffer were added and incubated at 25^{o}C for 10 minutes, 55^{o}C for 30 minutes and denatured at 95^{o}C for 2 minutes. Concentration of the cDNA product was measured at 260nm (UV1601 Shimadzu Corporation) and stored at -20^{o}C until further needed. The PCR was conducted on the cDNA as described in Section 2.1.1.

2.4.1.4 Quantitative PCR (qPCR)

Quantitative PCR (qPCR) was set up using Brilliant SYBR qPCR Master Mix (Stratagene) according to the manufacturers protocol. For each 20μl reaction: 10μl supermix, 0.5μM forward primer, 0.5μM reverse primer (for primer nucleotide sequences see Table 2.1) and 200ng DNase-treated cDNA were added to a PCR tube. A qPCR thermal cycle was set as described in Table 2.7. Fluorescence was read on a Mx3005P machine (Stratagene).

2.4.2 Western blotting

2.4.2.1 Bradford assay

A calibration curve was made by measuring the absorbance at 595nm for known amounts of BSA protein ranging from 0-8μg; 1μl protein, 500μl distilled water and 500μl Bradford reagent (Sigma). The protein concentration of the

Step	Temperature (^{o}C)	Time (sec)
1	95	300
2	94	30
3	56	60
4	72	60
5	72	600
6	4	pause

Table 2.7: qPCR thermal cycle profile. Steps 2-5 were repeated a total of 40 times before steps 5 and 6 were continued.

sample was determined by comparison with the standard curve when 1μl of the protein sample was mixed well with 500μl distilled water and 500μl Bradford reagent.

2.4.2.2 Whole cell protein extraction

To extract cells from transfection dishes, the cells were washed three times with PBS. Cells were scraped off and the same volume of protein sample buffer (2XPSB: 120mM Tris-HCl pH 6.8, 4% SDS, 20% glycerol, 10% 2-β-mercaptoethanol and 0.004% bromophenol blue) was added. Samples were sonicated on ice for three 5 seconds bursts and boiled for 15 minutes. Whole cell lysates were run on a SDS gel or stored at -20^{o}C. Lysates for phosphorylation studies were never stored and were always made and used fresh.

2.4.2.3 SDS PAGE gel

A separating gel was made using materials listed in Table 2.8. Upon the addition of APS and TEMED the gel was left to set for 30 minutes in a Mighty Small mini-Vertical Unit (Hoefer). Once set, a stacking gel was made (Table 2.9) and poured onto the separating gel. Combs were placed in the stacking gel and left to set for 30 minutes. Protein samples were run on polyacrylamide gels for 1 hour at 100 volts in Tris-glycine SDS running buffer (25mM Tris, 250mM glycine, 0.1% SDS, pH 8.3). A pre-stained protein standard ladder (Biolabs) was run simultaneously with the protein samples to analyse protein size.

Reagents	**Volume for 8% gel**	**Volume for 10% gel**	**Volume for 12% gel**	**Volume for 15% gel**
Distilled water	4.60ml	4.00ml	3.30ml	2.3ml
1.5M Tris-HCl, pH8.8	2.50ml	2.50ml	2.50ml	2.50ml
10% SDS	100μl	100μl	100μl	100μl
30% Acrylamide	2.70ml	3.30ml	4.00ml	5.00ml
10% APS	100μl	100μl	100μl	100μl
TEMED	10μl	10μl	10μl	10μl

Table 2.8: Composition of a 8%, 10%, 12% and 15% Tris/glycine SDS polyacrylamide gel electrophoresis gel. All reagents were from Sigma.

Reagents	**Volume**
Distilled water	2.68ml
0.5M Tris-HCl, pH6.8	1.25ml
10% SDS	50μl
30% Acrylamide	1.00ml
10% APS	15μl
TEMED	5μl

Table 2.9: Composition of the stacking gel for SDS gel. All reagents were from Sigma.

2.4.2.4 Transferring proteins to nitrocellulose membrane

Six blotting pads were fully soaked in Tris-glycine transfer buffer (25mM Tris, 190mM glycine, 0.1% SDS, 20% methanol, pH8.5). Four blotting papers and a nitrocellulose membrane (Protran, Scheicher) were soaked briefly in transfer buffer before a transfer stack was made. The transfer stack contained: 3 blotting pads, 2 blotting papers, SDS PAGE gel, nitrocellulose membrane, 2 blotting papers and 3 blotting pads (placed into electrophoresis chamber from the cathode to the anode end respectively). A blot module was filled with transfer buffer and the outer buffer chamber was filled with 650ml deionised water. Proteins were transferred from the SDS PAGE gel to the nitrocellulose membrane at 33V for 1 hour.

2.4.2.5 Western blotting

Nitrocellulose membrane was blocked overnight in 5% milk, 0.1% Tween (Sigma) in TBS (50mM Tris, 138mM NaCl, 2.7mM KCl, pH 8.0), with gentle agitation at 4^{o}C. Primary antibody was added in concentrations as described in Table 2.10 to 3% milk, 0.1% Tween and TBS, unless otherwise stated, for 1 hour at room temperature.

Antibody	Primary Antibody	Secondary Antibody
GFP	1:1,000 anti-GFP (Santa-Cruz)	1:10,000 anti-mouse HRP (Santa-Cruz)
FLAG	1:500 anti-FLAG M2 (Stratagene)	1:10,000 anti-mouse HRP (Santa-Cruz)
β-actin	1:10,000 anti-βactin (Sigma)	1:10,0000 anti-mouse HRP (Santa-Cruz)
MST1	1:1,000 anti-MST* (Cell Signalling)	1:10,000 anti-rabbit HRP (Santa-Cruz)
Phospho MST1/2 (thr183/180)	1:1,000 anti-pMST1/2* (Cell Signalling)	1:10,000 anti-rabbit HRP (Santa-Cruz)
Lats1	1:1,000 anti-Lats1* (Cell Signalling)	1:10,0000 anti-rabbit HRP (Santa-Cruz)
Phospho-Lats1 (ser909)	1:1,000 anti-pLats* (Cell Signalling)	1:10,000 anti-rabbit HRP (Santa-Cruz)
YAP	1:1,000 anti-YAP* (Cell Signalling)	1:10,000 anti-rabbit HRP (Santa-Cruz)
phospho-YAP (Ser127)	1:1,000 anti-pYAP* (Cell Signalling)	anti-rabbit HRP (Santa-Cruz)
caspase-3	1:1,000 anti-caspase 3 (Sigma)	1:10,000 anti-mouse HRP (Santa-Cruz)
coilin	1:1,000 anti-coilin (Sigma)	1:10,000 anti-rabbit HRP (Santa-Cruz)
HA	1:500 anti-HA (Sigma)	1:10,000 anti-mouse HRP (Santa-Cruz)

Table 2.10: Concentrations of primary and secondary antibody used in western blot protocol. All antibodies were diluted in TBS, 0.1% Tween, 5% milk with the exception of starred antibodies (*) that were incubated in 5% BSA, 0.1% Tween in TBS left gently shaking overnight at -4^{o}C.

Blots were washed three times, 5 minutes each, with 0.1% Tween in TBS. Secondary HRP antibody was added in concentrations as described in Table 2.10 to 3% (w/v) dried milk, 0.1% Tween in TBS for 1 hour at room temperature. The nitrocellulose blot was washed an additional 5 times, each lasting at least 6 minutes. The nitrocellulose membrane was incubated, for 5 minutes, with 4ml SuperSignal West Pico enhanced chemi-luminescence reagent (Pierce), before protein bands were visualised using a LAS-3000 Intelligent Dark Box (Fujifilm).

2.4.3 Wholemount in-situ hybridisation

2.4.3.1 Preparation of DNA template for RNA probe synthesis

The willin DNA sequence of interest was amplified using RT-PCR (Section 2.4.1) and cloned into the pGEMT easy vector (Promega) according to the manufacturer's protocol. Orientation of the insert was obtained through DNA sequencing (DNA Sequencing Service, University of Dundee, UK). 5μg of the DNA template was linearised using the *Sph*1 restriction enzyme (Section 2.1.4) to cut at the 5' or 3' end of the insert to make an anti-sense and sense probe respectively. The restriction digest was left overnight at 37^{o}C for complete linearisation. DNA was extracted by addition of 100μl phenol/chloroform (Sigma) to the restriction digest product, which was vortexed and centrifuged at 10,000g. The top layer was transferred to a nuclease-free 1.5ml microcentrifuge tube. The phenol/chloroform DNA extraction was repeated again. 10μl 3M sodium acetate (pH5.2) was added and the DNA was precipitated using ice-cold 70% ethanol (made with DEPC water). DNA was left to precipitate for 30 minutes at -80^{o}C, after which the DNA was pelleted at 10,000g for 15 minutes. The DNA pellet was air-dried for one hour and resuspended in 20μl DEPC treated water. The DNA concentration was measured on a spectrometer and 1μl of DNA template was run on an agarose gel (Section 2.1.2) to confirm linearisation.

2.4.3.2 RNA probe synthesis

Table 2.11 shows the materials and quantities needed for RNA probe synthesis. All reagents were added to a RNA-free PCR tube and both sense and anti-sense RNA probe were synthesised. The RNA probe reaction was incubated at 40^{o}C for 2 hours, after which 2μl of RNase free DNase (Roche) was added

to digest the DNA template at 37^{o}C for 15 minutes. 1μl 0.5M EDTA (pH 8.0) was added to stop the reaction. RNA was precipitated by the addition of 30μl of a lithium chloride precipitation solution (Ambion). RNA was precipitated for 4 hours at -20^{o}C and pelleted by centrifuged at 10,000g for 15 minutes. The pellet was washed with ice-cold 70% ethanol (made with DEPC treated water) and re-centrifuged at 10,000g for 15 minutes to maximise the removal of unincorporated nucleotides. Ethanol was carefully removed and the RNA was resuspended in 20μl DEPC water. 1μl of the RNA probe was run on an agarose gel to check whether RNA was present. 60μl of hybridisation mix (HM) (50% formamide (Sigma), 5X sodium chloride/sodium citrate buffer (Sigma), 1mg/ml tRNA (Roche), 100mg/ml heparin (Sigma), 0.1% Tween-20 (Sigma), made to pH4.5 with citric acid (Sigma)) was added to the RNA probe and stored at -20^{o}C.

Reagents	**Volume**
10X transcription buffer	2μl
10X DIG-NTP	2μl
linearilised DNA	1μg
SP6 RNA Polymerase	2μl
RNase inhibitor	1μl
DEPC treated water	to total of 20μl

Table 2.11: Volumes of reagents needed to make a RNA probe. All reagents were from Roche.

2.4.3.3 Zebrafish embryo collection

The night before eggs were collected, male and female zebrafish were placed in a breeding tank at 27^{o}C. The next morning, eggs were collected and unfertilised and abnormal eggs were removed. Fertilised embryos were placed in a Petri dish containing fish water at 27^{o}C until embryos developed to desired developmental stage (from 6-96 hours-post-fertilisation). Embryos were washed in fish water and dead and abnormal cells were removed from the Petri dish every 12 hours.

2.4.3.4 Zebrafish fixation, removal of chorion and pigmentation

Once the zebrafish embryos reached the desired developmental stage, the embryos were fixed for one hour at room temperature and then overnight at 4^{o}C with 4% paraformaldehyde in PBS. The chorions of the fixed embryos were manually removed using a needle and watchmakers forceps under a dissecting microscope. To remove zebrafish pigmentation, the fixed dechorionated embryos were incubated in PBS containing 3% H_2O_2 (Sigma) and 0.5% KOH (Sigma) at room temperature until pigmentation had completely disappeared. After the pigmentation was removed, the embryos were washed for 5 minutes in PBS.

2.4.3.5 Embryo dehydration and rehydration

Embryos were dehydrated in methanol for long-term storage at -20^{o}C. Embryos were washed for 5 minutes in 66% PBS/33% methanol, 5 minutes in 33% PBS/66% methanol and a final 10 minute wash with 100% methanol. Before the in-situ protocol was conducted, embryos needed to be rehydrated by a 5 minute wash in 66% methanol/33% PBS, 5 minutes in 33% methanol/66% PBS and four 5 minute washes in PBS with 0.2% Tween-20 (Sigma).

2.4.3.6 Permeabilisation and hybridisation of zebrafish embryos

Embryos were permeabilised by a 10μg/ml proteinase K (Roche) digestion at room temperature for the desired time as shown in Table 2.12. After proteinase K digestion, embryos were quickly washed in PBS containing 0.02% Tween and refixed in 4% paraformaldehyde in PBS for 20 minutes at room temperature. Embryos were then washed an additional 5 times for 5 minutes in PBS containing 0.02% Tween.

2.4.3.7 Wholemount hybridisation of zebrafish embryos

Embryos were pre-hybridised for 5 hours at 65^{o}C in 100μl hybridisation mix (HM). 100ng of the RNA probe was added to the HM containing embryos and left to incubate at 65^{o}C for 12 hours. After embryos were hybridised in the RNA probe, embryos were washed as described in Table 2.13.

Developmental stage	Duration of proteinase K digestion
1 cell-1 somite	30 sec
1-8 somite	1 min
9-18 somite	3 min
18 somite-24hpf	10 min
48hpf-4 days	30 min

Table 2.12: Duration of proteinase-K digestion at different zebrafish developmental stages in preparation for whole mount in-situ protocol.

Step	Temp (^{o}C)	Time (min)	Wash Components
1	65	1x10	75% HM/25% 2X SSC
2	65	1x10	50% HM/25% 2X SSC
3	65	1x10	25% HM/25% 2X SSC
4	65	1x10	2X SCC
5	65	1x20	0.2X SCC + 0.1% Tween
6	65	2x20	0.1X SSC + 0.1% Tween
7	20	1x5	66% 0.2X SCC/33% PBS-Tw
8	20	1x5	33% 0.2X SCC/66% PBS-Tw
9	20	2x5	PBS-Tw

Table 2.13: Washes conducted after RNA hybridisation of zebrafish embryos. PBS-Tw represents PBS containing 0.1% Tween-20.

2.4.3.8 NBT/BCIP staining

Hybridised embryos were pre-incubated in PBS containing 0.1% Tween, 5% foetal calf serum (Gibco) and 2mg/ml BSA (Sigma) for 2 hours at 4^{o}C. Embryos were incubated in anti-DIG (Roche) solution diluted 1:5,000 in PBS containing 0.1% Tween, 5% foetal calf serum (Gibco) and 2μg/ml BSA (Sigma) for 12 hours at 4^{o}C. Embryos were washed a total of seven times in PBS containing 0.1% Tween for 15 min each. Embryos were transferred to a 6 well dish and excess wash solution was removed. NBT/BCIP colouration buffer (100mM TrisHCl, pH9.5, 50mM $MgCl_2$, 100mM NaCl, 0.1% Tween, 0.4mg/ml NBT and 0.19mg/ml BCIP) was added to embryos and left for 10 minutes, protected from light exposure. Staining reaction was stopped by washing the

embryos in PBS containing 0.1% Tween. Embryos were stored at -20^{o}C in 50% glycerol.

2.4.3.9 Imaging and sectioning of embryos

Wholemount zebrafish embryos were studied in dark and brightfield mode using a dissecting Leica MZ7.5 binocular microscope (Leica Microsystems). Embryos were, additionally, flat-mounted in PBS by the addition of small jelly silicon drops underneath each corner of a glass coverslip. To prepare embryos for cryosectioning, embryos were placed in a cryomatrix in their desired orientation and snap frozen in isopentane (Fisher Scientific), which was cooled over liquid nitrogen to reach temperatures close to the isopentane freezing point (-159^{o}C). Wholemount embryos were cut at 10μm on a cryostat (Leica Microsystems, CM1850). All images were taken using a Leica DMRB microscope (Leica Microsystems) or Olympus CK40 microscope (Olympus) with a Nikon Coolpix 4500 digital camera (Nikon).

Chapter 3

Willin Expression Activates the Hippo Pathway

3.1 Introduction

Recent studies utilising *D. melanogaster* genetics have indicated that Merlin and a second FERM protein called Expanded, play a key role in controlling the Hippo signalling cascade; limiting organ size by inhibiting cell proliferation and promoting apoptosis (Edgar, 2006; Hamaratoglu et al., 2006; Harvey and Tapon, 2007). As the reported human orthologue sequence of Expanded (Ex1) is that of willin (Hamaratoglu et al., 2006), it was predicted that willin can act upstream of the mammalian Hippo pathway cassette, with the ability to activate and phosphorylate the highly conserved Hippo pathway components.

If willin is the true homologue of the *Drosophila* protein Expanded then willin will act upstream of the Hippo signalling pathway to phosphorylate and inhibit YAP, further resulting in downstream cell viability and cell cycle changes. Therefore, initial characterisation of willin, its ability to phosphorylate the core Hippo pathway components (MST1/2, LATS1 and YAP) and potential downstream apoptotic changes were investigated using the epithelial Human Embryonic Kidney (HEK-293) cell line as an *in-vitro* model system.

3.2 Results

3.2.1 Molecular cloning of TRex inducible plasmids

An inducible system was created as previous stable cell lines expressing willin have resulted in cell death (Herron, 2007). The TRex inducible system from Invitrogen was based on the tet-on system, where the gene of interest was expressed only upon the addition of tetracycline (Figure 3.1). Dr Chris Tate (University of Cambridge, UK) kindly provided HEK-293 cells stably expressing the tetracycline repressor plasmid (pcDNA6/TR). Consequently, only the inducible plasmid was cloned and transfected into the TRex-HEK-293 cells to create a stable willin-inducible cell line.

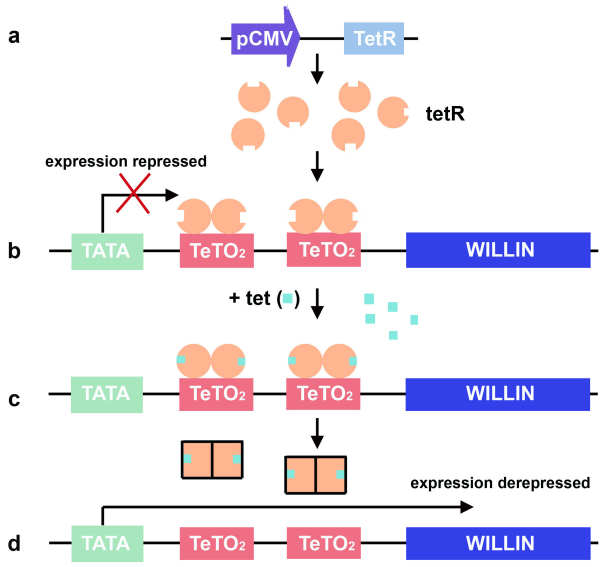

Figure 3.1: Schematic diagram demonstrating how willin expression was induced using the TRex system. Firstly the tetracycline repressor (tetR) protein was expressed from a pcDNA6/TR plasmid in HEK-293 cells **(a)**. The TetR formed homodimers and bound to Tet-operator-2 ($TetO_2$) sequences in the inducible expression vector, repressing the protein expression of willin **(b)**. Addition of tetracycline (tet) to the cell medium resulted in binding of the tetracycline to the TetR homodimers **(c)**, which resulted in a conformational change in tetR so that the TetR homodimers were released from the $TetO_2$ sequences and willin gene expression was induced **(d)**.

A TRex-willin-GFP plasmid was created to be used for the inducible cell line system. A willin-GFP fragment was cut out of the pWillin-GFP plasmid using *EcoR*1 and *Not*1 restriction enzymes. A DNA fragment encoding willin-GFP was then ligated into the pTRex plasmid (Figure 3.2). The correct full-length sequence of willin-GFP in the TRex plasmid was confirmed by the DNA Sequencing Service (University of Dundee, UK).

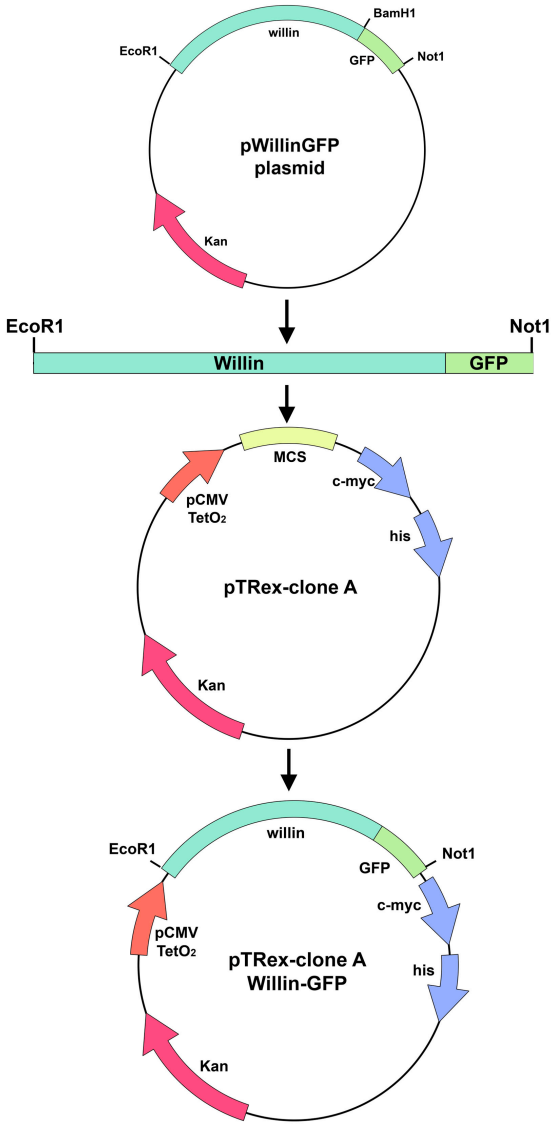

Figure 3.2: Cloning of the TRex-willin-GFP plasmid. pWillin-GFP plasmid was digested with *EcoR*1 and *Not*1 restriction enzymes to produce a willin-GFP fragment. This fragment was ligated into an empty pTRex plasmid clone A to produce the plasmid, TRex-willinGFP.

Full-length willin tagged to myc-his was also cloned into the TRex system. Full-length willin DNA was amplified by PCR using *willin2-F* and *willin2-R* primers (see Table 2.1 for primer sequence) as the forward and reverse primer respectively on the pwillin-GFP plasmid. The PCR fragment was then cut using *EcoR*1 and *Not*1 restriction enzymes and ligated into the pTRex-clone-C plasmid (Figure 3.3). The correct full-length willin-myc-his sequence was confirmed by the Sequencing Service (University of Dundee, UK).

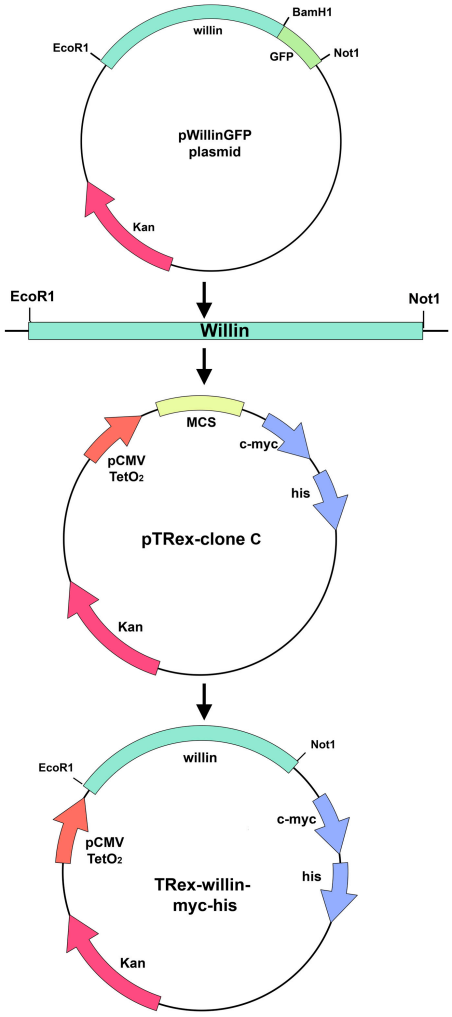

Figure 3.3: Schematic diagram of molecular cloning procedure used to construct the TRex-willin-myc-his plasmid. A PCR was conducted on the pWillin-GFP using *willin2F* and *willin2R* primers to produce a willin fragment with *EcoR*1 and *Not*1 restriction sites at the 5' and 3' end respectively. The willin PCR fragment was then ligated into the empty pTRex clone C plasmid, so that willin was in frame with the C-terminal myc and his tags, to create the TRex-willin-myc-his plasmid.

3.2.2 Tetracycline induces willin-GFP expression

The TRex-willin-GFP plasmid was transiently transfected into TRex HEK-293 cells (expressing the tetracycline repressor plasmid:pcDNA6/TR) and a stable cell line was created through antibiotic selection with 5μg/ml blasticidin and 500μg/ml zeocin. The TRex system worked as an on-off system and induced expression did not respond in a dose-response nature; increasing tetracycline concentrations did not increase willin-GFP expression levels. The recommended 1μg/ml of tetracycline was used to induce willin-GFP expression in all future experiments.

Willin-GFP fluorescence was observed when a final concentration of 1μg/ml tetracycline was added to the inducible cell line growth medium, and absent when no tetracycline was present (Figure 3.4). Western blot analysis confirmed that willin-GFP was only expressed in the presence of tetracycline (Figure 3.5). Upon addition of tetracycline, willin-GFP expression was induced within 2 hours (Figure 3.5). Figure 3.5 shows that the same amount of willin-GFP was expressed 6 to 24 hours post-induction. The TRex-willin-GFP cells no longer expressed willin-GFP 48 hours post-induction and fresh tetracycline had to be added to the cell culture medium for longer experiments as the half-life of tetracycline is about 6 hours and the protein turn-over of willin-GFP is approximately 2 days.

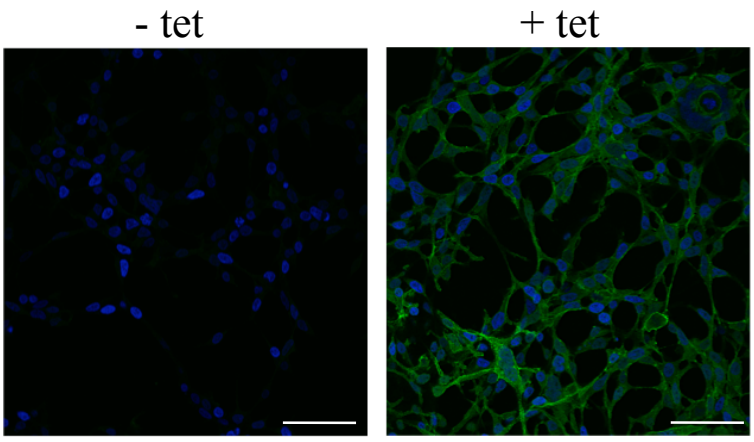

Figure 3.4: Fluorescence images of the TRex-willin-GFP inducible system. A stable HEK TRex-willin-GFP cell line was created so that only upon the addition of 1μg/ml tetracycline (tet) was willin-GFP expressed and absent when not induced. Cells were either incubated in 1μg/ml tetracycline (tet) for 48 hours or left untreated (-tet). After treatment, the cells were fixed and the nuclei were stained with DAPI. Images were taken on a Multiphoton microscope (Leica). *Bar*= 50μm.

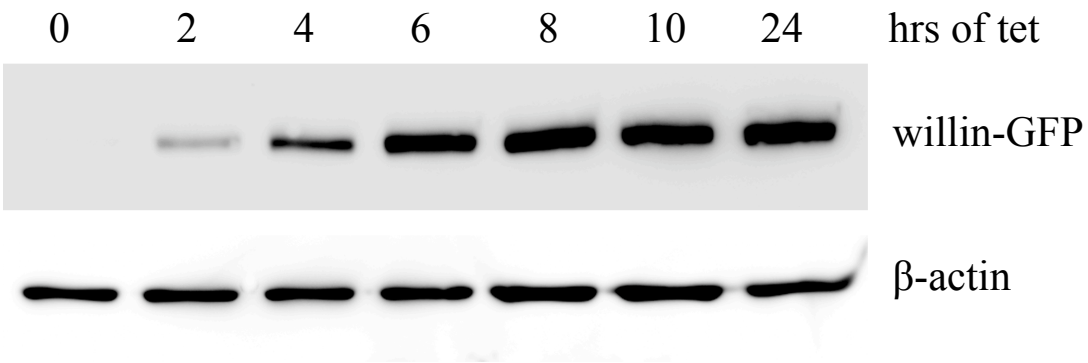

Figure 3.5: Western blot showing that willin-GFP was expressed in the TRex-willin-GFP inducible cell line upon the addition of tetracycline. Whole cell lysates were collected 0, 2, 4, 8, 10 or 12 hours after 1μg/ml tetracycline (tet) treatment and separated on a 10% SDS gel. The nitrocellulose membrane was probed with anti-GFP and β-actin antibodies.

3.2.3 siRNA willin knockdown using TRex system.

The TRex-willin-GFP inducible system was an ideal system to optimise siRNA knockdown experiments of willin. Cells were incubated in 5nM siRNA designed to specifically knockdown willin expression (see Section 2.2.3 for siRNA sequences). 24 hours prior to siRNA treatment completion, cells were incubated in 1μg/ml tetracycline to induce willin-GFP expression. Fluorescence microscopy images of siRNA treated cells (0-72 hours) showed that willin-GFP expression was decreased in the presence of siRNA (Figure 3.6). Willin-GFP fluorescence knockdown was observed 48-72 hours after siRNA treatment (Figure 3.6).

Western blot analysis confirmed willin-GFP knockdown using the custom designed siRNA duplexes (Figure 3.7). Cells were treated for 0, 24, 48, or 72 hours with siRNA against willin and incubated in 1μg/ml tetracycline 24 hours before siRNA treatment was completed. Whole cell lysates were separated on a SDS gel and knockdown of willin-GFP expression was observed 48-72 hours after siRNA treatment (Figure 3.6).

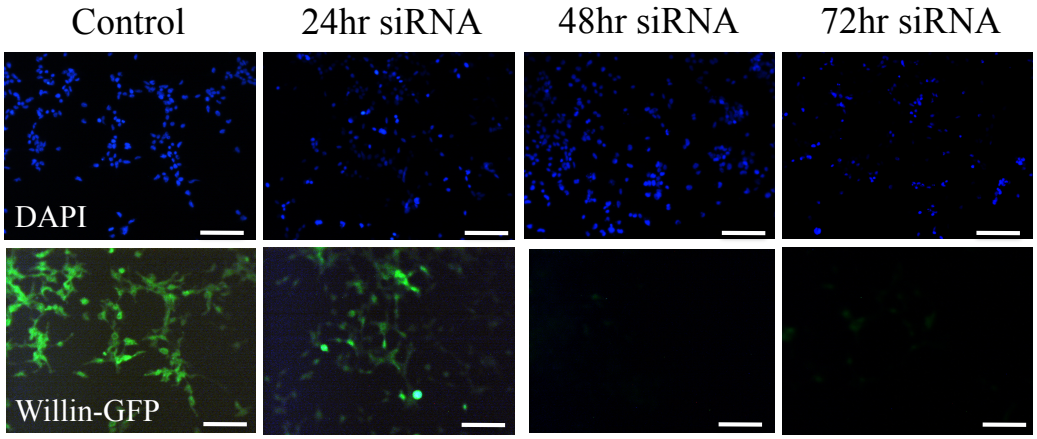

Figure 3.6: Fluorescence microscope images of siRNA willin knockdown using the TRex-willin-GFP inducible system. TRex-willin-GFP were incubated with siRNA against willin for either 0, 24, 48 and 72 hours. Cells were treated with 1μg/ml tetracycline 24 hours before siRNA treatment was completed. After treatment, the cells were fixed and the nuclei were stained with DAPI. Knockdown fluorescence of willin-GFP was observed 48-72 hours after siRNA treatment. *Bar*= 100μm.

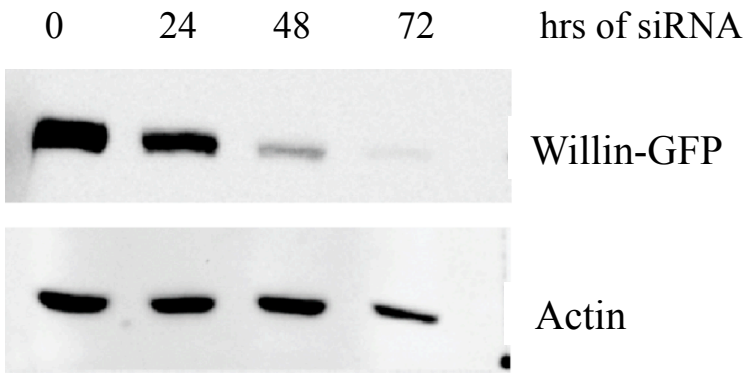

Figure 3.7: Western blot showing willin-GFP knockdown using siRNA designed specifically to knockdown willin expression. Cells were treated with either 0, 24, 48 and 72 hours of siRNA and treated with 1μg/ml tetracycline 24 hours before siRNA treatment was completed. Whole cell lysates were separated on a 10% SDS gel. Willin-GFP knockdown was observed 48-72 hours after siRNA treatment. The nitrocellulose membrane was probed with anti-GFP and β-actin antibodies.

An example of the success of developing siRNA specific to willin was shown by utilising a novel photoporation technique. In collaboration with the biophotonics group at the University of St Andrews, Maria Leilani Torres-Mapa was able to use the TRex-willin-GFP cell line to photoporate siRNA into a desired single cell and observe willin-GFP knockdown using a violet diode laser system (Torres-Mapa et al., 2010) (See Appendix E). For the photoporation studies, cells were incubated with 5nM siRNA duplexes and 10μg/ml Mito-DsRed encoding plasmid in the transfection media. Cells were targeted using a 3.4mW laser at the focus of a 1 second exposure time. Control dishes included (1) cells with Mito-DsRed plasmid and siRNA without laser treatment; (2) cells without Mito-DsRed plasmid but with siRNA without laser treatment, and (3) cells with neither Mito-DsRed plasmid and siRNA with laser treatment. Expression of willin-GFP was then induced with 1μg/ml tetracycline, and fluorescence was monitored over a 48 hour time period. For all control dishes, spontaneous DNA transfections or knockdown was not observed.

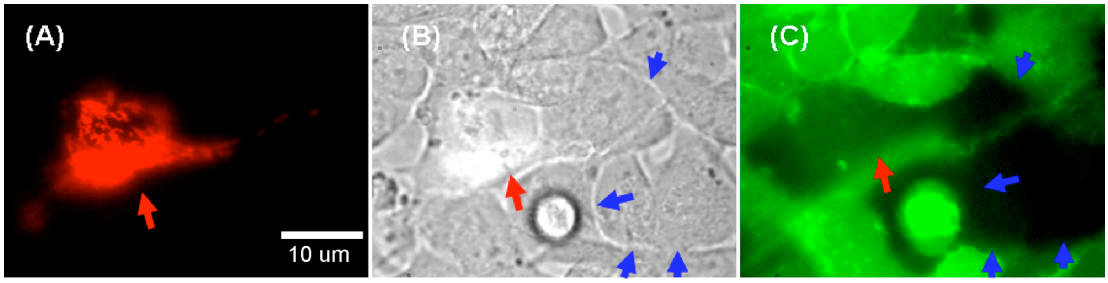

Figure 3.8: Gene knockdown using a violet diode system. **A)** A TRex-willin-GFP cell fluorescing red due to the expression of the Mito-DsRed and **B)** under brightfield imaging. **C)** Fluorescence image of the same field of view using a FITC HYQ, Nikon filter cube. Red arrow points to a cell which has been co-transfected with Mito-DsRed and willin specific siRNA. Blue arrows point to cells that have been transfected with siRNA only. Work done and published by Torres-Mapa et al. (2010).

Figure 3.8 shows immunofluorescent microscope images of TRex-willin-GFP cells which were photoporated in the presence of siRNA against willin and Mito-DsRed plasmid. Figure 3.8(a) shows a successfully transfected TRex-willin-GFP cells expressing Mito-DsRed protein. Clear knockdown of willin-GFP expression, as indicated by the absence of green fluorescence, was observed when TRex-willin-GFP cells were photoporated with willin siRNA (blue arrows in Figure 3.8). More cells were observed to have a lost willin-GFP

expression (blue arrows) than those that expressed the Mito-DsRed plasmid together with the loss of willin-GFP (red arrow; Figure 3.8). It can be concluded that the efficiency for gene knockdown will be higher compared to that of DNA transfection, as siRNA are much smaller in comparison to DNA plasmids (25bp versus ∼5000bp). No spontaneous Mito-DsRed plasmid and siRNA duplex transfections were observed in untreated dishes (Mito-DsRed plasmid and siRNA treatment but no laser treatment), indicating the specificity of action of the lasers.

3.2.4 Cellular distribution of willin, MST1 and LATS1 are cell density dependent.

Cell density and cell-to-cell contact play an important role in the activation of the Hippo pathway and the cellular distribution of many Hippo pathway components have been shown to be cell density specific (Zhao et al., 2007; Hao et al., 2008). ERM proteins, especially merlin, have also been shown to be cell density dependent (Muranen et al., 2005). The distribution of willin at different cell densities was therefore further investigated.

Figure 3.9 shows that willin's subcellular localisation is complex, since it can be localised within the cytoplasm, at the plasma membrane, but also within the nucleus of the cell. This mixed cellular distribution is common for ERM family proteins (Muranen et al., 2005) and has previously been published by Gunn-Moore et al. (2005). Fluorescence images showed that at low cell density, willin was predominately found within the cytoplasm of an isolated single cell. Punctate staining near the nucleus was sometimes observed in a single isolated cell (Figure 3.9.A). At higher cell density, willin was predominantly recruited to the plasma membrane; especially to cellular junctions between contacting neighbouring cells (Figure 3.9.B).

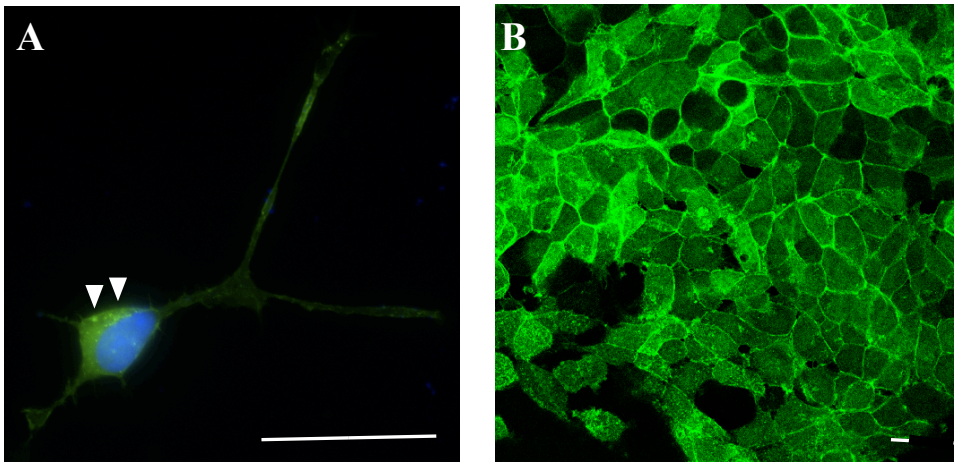

Figure 3.9: Fluorescence images of TRex-willin-GFP cells expressing willin-GFP. Cells were induced for willin-GFP expression with 1μg/ml tetracycline for 48 hours prior to being fixed. Willin-GFP localisation varied depending on cell density. **A)** Willin-GFP expression was predominately found within the cytoplasm of an isolated cell. Punctate staining was sometimes observed near the nucleus (shown by arrows). **B)** Upon contact with other neighbouring cells at higher density, willin-GFP expression was more predominately found at the plasma membrane. Willin-GFP expression was frequently observed to be recruited at cellular junctions between contacting cells. *Bar*= 100μm.

A biochemical membrane/cytoplasmic fractionation was conducted to further support the fluorescence observations that indicated that willin-GFP expression may be recruited to the plasma membrane upon cell-to-cell contact. 5x10^5 TRex-willin-GFP cells were plated onto either 35mm, 60 or 90mm dishes; to represent high, medium and low cell density respectively. The TRex-willin-GFP cells were induced for willin-GFP expression for 24 hours with 1μg/ml tetracycline and the membrane/cytoplasmic protein fractionations were extracted using the P100/S100 protocol (Section 2.3.4). Immunoblot analysis of the membrane and cytoplasmic fractions showed that as the cell density increased, willin-GFP expression was increased in the Triton X-100 soluble membrane fraction and decreased in the cytoplasmic fraction (Figure 3.10). Results from the membrane/cytoplasmic fractionation assay supported the previous fluorescence observations that willin was predominantly relocated to the plasma membrane at high cell density (Figure 3.9).

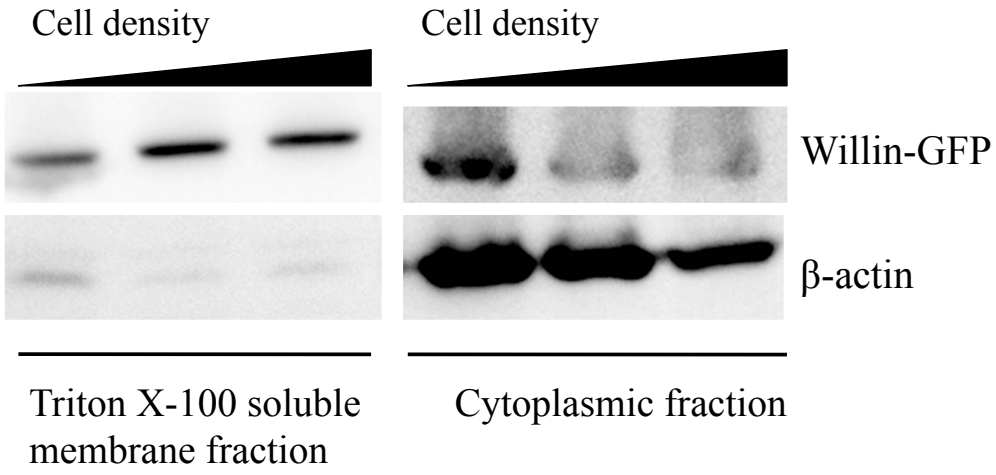

Figure 3.10: Willin-GFP expression translocated to the membrane fraction upon cell-to-cell contact. Increasing cell density resulted in an increased expression of willin-GFP within the Triton X-100 soluble membrane fraction and a decrease within the cytoplasmic fraction. TRex-willin-GFP cells were induced for willin-GFP expression for 24 hours with 1μg/ml tetracycline at low, medium and high density. Membrane and cytoplasmic protein extracts were obtained using the P100/S100 protocol and equal amounts of protein were separated on a 10% SDS gel. The nitrocellulose membrane was probed with anti-GFP and anti-β-actin antibodies.

As the Hippo pathway is activated at high cell density and willin is recruited to the plasma membrane at high cell densities, the expression of MST1 and LATS1 at different cell densities was further investigated in the Triton X-100 soluble membrane faction. The nitrocellulose membrane from Figure 3.10 was re-probed with MST1 and LATS1 antibodies. Interestingly, MST1 protein expression in the membrane soluble fraction decreased when cell density increased, inversely of that observed with willin (Figure 3.11). LATS1 expression however increased within the Triton X-100 soluble membrane fraction when cell density increased, which is the same correlation as that of willin expression (Figure 3.11).

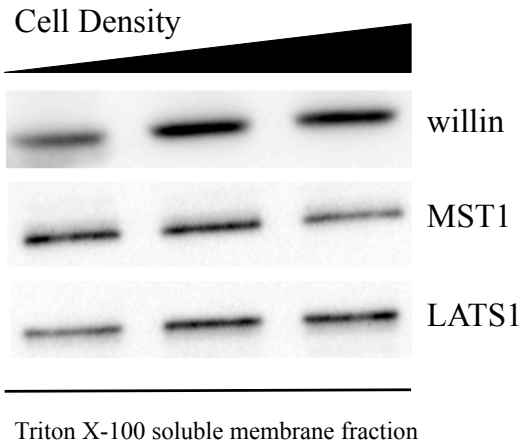

Figure 3.11: Cell density influenced willin, MST1 and LATS1 localisation to the membrane. The nitrocellulose membrane from Figure 3.10 was re-probed with MST1 and LATS1 primary antibodies followed by their respective anti-rabbit-HRP secondary antibody. Immunoblot analysis showed that willin and LATS1 expression increased within the Triton X-100 soluble membrane fraction when cell density increased, while MST1 expression decreased.

3.2.5 Expression of willin influences phosphorylation of MST1/2, LATS1 and YAP

Zhao et al. (2007) have recently demonstrated that the mammalian transcriptional co-activator YAP, the human orthologue of Yorkie, is inactivated by both willin and merlin by an unknown mechanism. Willin's ability to result in MST1/2, LATS1 and YAP phosphorylation, which thereby inactivates the ability of YAP to affect downstream targets, was further investigated. The stable inducible TRex-willin-GFP cell line was used to investigate the effect of willin expression upon the kinases upstream of YAP.

The TRex-willin-GFP cells were plated out into 60mm dishes and 1μg/ml tetracycline was added 0, 24, 48 or 72 hours after plating so that the cell density in all experimental dishes remained unchanged. Notably, YAP phosphorylation could only be studied over a two day induction period, since high cell density caused YAP phosphorylation in uninduced cells, as has been previously observed by Zhao et al. (2007). YAP phosphorylation experiments were therefore performed at an even lower cell density than MST1/2 and LATS1 phosphorylation studies. Image J analysis of the phosphorylation western blots (representative shown in Figure 3.12.A) showed that a significant increase in phosphorylation of MST1/2, LATS1 and YAP was observed when cells were

induced for willin-GFP expression (Figure 3.12.B, t-test: $p<0.01$, n=3).

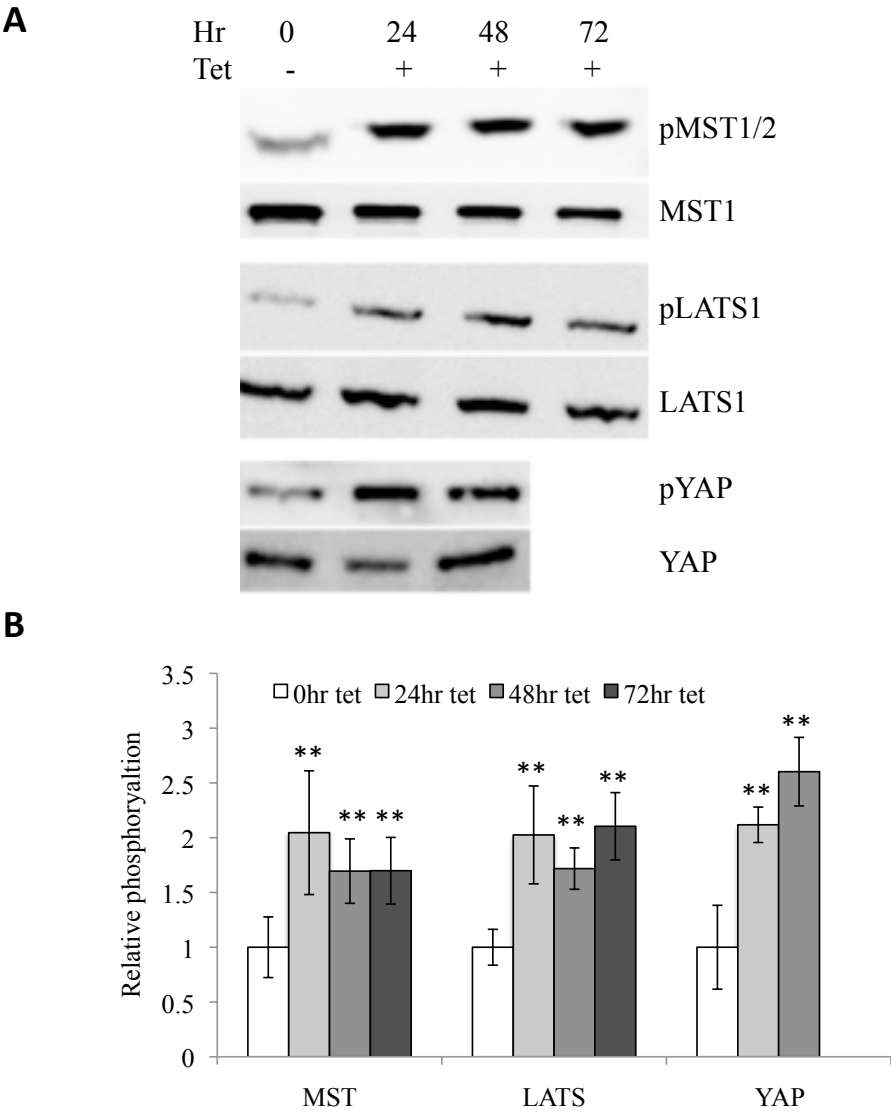

Figure 3.12: Willin expression induced significant phosphorylation of Hippo pathway components. TRex-willin-GFP cells were induced for willin-GFP expression with 1μg/ml tetracycline over a period of 0-4 days. Whole cell lysates were harvested and separated on a 10% SDS gel for immunoblot analysis with Hippo component antibodies; pMST1/2, MST1/2, LATS1, pLATS1, pYAP and YAP. **A**) Immunoblot showing that willin-GFP expression results in phosphorylation of Hippo pathway components MST1/2, LATS1 and YAP. **B**) Image J analysis, showed that induced willin expression resulted in significant phosphorylation of MST1/2, LATS1 and YAP compared to uninduced TRex-willinGFP cells (t-test: n=3, $p<0.01$**). Relative protein phosphorylation was calculated by measuring the integrated density (ID) of phosphorylated protein over the ID of whole protein present, relative to baseline phosphorylated protein when no tetracycline was added, which was set at 1 . Error bars represent ± standard deviation.

Experimental controls were performed to exclude the effects of tetracycline and the GFP-tag on phosphorylation of the Hippo pathway components: MST1/2, LATS1 and YAP. For the tetracycline control, the TRex cells were incubated in 1μg/ml tetracycline for 0, 24, 48 and 72 hours. Western blot analyses showed that no difference in MST1/2, LATS and YAP phosphorylation was observed when TRex cells were incubated in the presence or absence of tetracycline (Figure 3.12.A). For the latter GFP control, the TRex cells were transiently transfected with either an empty-GFP vector or treated with only GeneJammer transfection reagent. Western blot analysis showed that no changes in MST1/2, LATS1 and YAP phosphorylation was detected between the untransfected control and an empty-GFP expression plasmid (Figure 3.13.B).

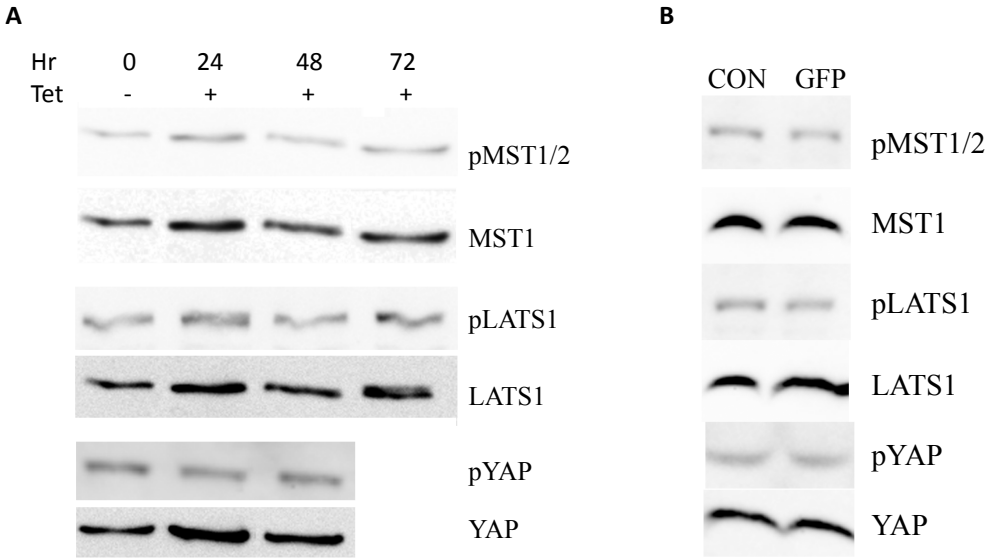

Figure 3.13: Addition of tetracycline and transient transfection of empty-GFP expression plasmid do not result in phosphorylation of Hippo pathway components. **A)** TRex cells were treated with 1μg/ml tetracycline and whole cell lysates were collected 0, 24, 48 and 72 hours after tetracycline treatment. The protein samples were separated on an 10% SDS gel and the nitrocellulose membrane was probed with antibodies against the core Hippo pathway components. **B)** TRex cells were either transfected with only GeneJammer transfection reagent (lane 1) or transfected with empty-GFP construct (lane 2). Whole cell lysates were collected 48 hours post-transfection and separated on a 10% SDS gel. The nitrocellulose membrane was probed with pMST1/2, MST1, pLATS1, LATS1, pYAP and YAP antibodies.

3.2.6 Willin expression results in YAP translocation to the cytoplasm

Activation of the Hippo pathway through phosphorylation of the core Hippo pathway cassette has been reported to translocate YAP from the nucleus to the cytoplasm through binding of the 14-3-3 protein to the YAP phosphorylation site Ser127 (Zhao et al., 2007; Hao et al., 2008).

The inducible TRex-willin-GFP cell line was used to investigate YAP translocation as phosphorylation of MST1/2, LATS1 and YAP was observed under induced willin-GFP conditions. The same induced conditions were therefore used, with the TRex-willin-GFP cells being induced for willin-GFP expression with 1μg/ml tetracycline. 50ng/ml TNFα was used as a positive control to promote YAP translocation into the cytoplasm, as cell death signals have been shown to promote full activation of the Hippo pathway (Lee et al., 2001; Graves et al., 2001).

Nuclear versus cytoplasmic fractionation on willin-GFP inducible cells showed that when willin-GFP expression was induced for two days with 1μg/ml tetracycline, YAP expression was highest in the cytoplasmic fraction and lower in the nuclear fraction (Figure 3.14). This pattern was unaltered by TNFα addition (Figure 3.14). YAP expression remained mostly within the nucleus when cells were not expressing willin-GFP (absence of tetracycline; Figure 3.14). Therefore, further supporting the observation that willin expression resulted in the activation and phosphorylation of the Hippo pathway.

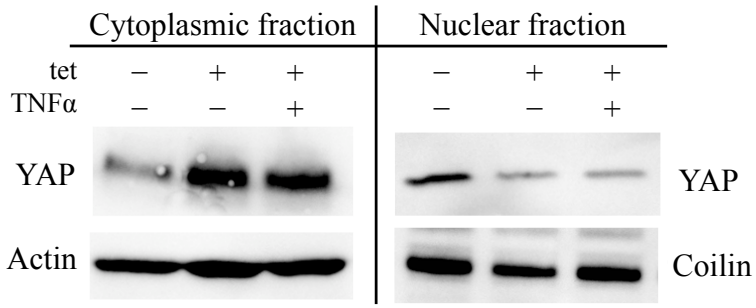

Figure 3.14: Willin-GFP expression resulted in YAP translocation from the nucleus to the cytoplasm. The TRex-willin-GFP cells were either uninduced, induced with 1μg/ml tetracycline for 48 hours, or induced and treated for 6 hours with 50ng/ml TNFα. The nuclear and cytoplasmic protein fractions were extracted and separated on a 10% SDS gel. The nitrocellulose membrane was probed with anti-YAP, β-actin and coilin antibodies.

3.2.7 Willin expression does not influence cell viability or the cell cycle

Studies examining the Hippo pathway in *D. melanogaster* have shown that Expanded and Merlin differentially regulate cell cycle exit and apoptosis (Pellock et al., 2007). Experiments using the controlled tetracycline inducible expression of willin-GFP in HEK-293 cells were therefore conducted to investigate potential changes in cell viability and cell cycle. A live/dead discrimination assay (Section 2.3.2) was performed using a propidium iodide (PI) stain, where cell viability was measured by FACS analysis. The PI entered the cell and bound to the DNA when the plasma membrane was leaky (necrosis and late apoptosis), whereas cells remained unstained when the plasma membrane remained intact (Figure 3.15).

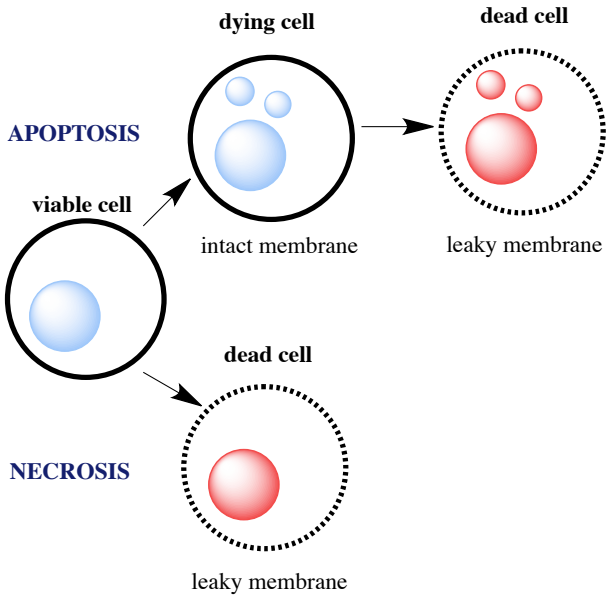

Figure 3.15: Schematic diagram showing how propidium iodide (PI) stain discriminated between viable and dying cells. Cells did not stain with PI (red) when the plasma membrane remained intact: in viable and early apoptotic cell. PI bound to the DNA when the plasma membrane was leaky in necrotic and late apoptotic cells.

TRex-willin-GFP and TRex control cells were treated with 1μg/ml tetracycline for a period of 0-97 hours. Willin-GFP expression was induced in the TRex-willin-GFP cells but not in the TRex cell line. Cells were harvested and analysed on a FACS machine (FACscan Flow Cytometer, Becton Dickinson) to detect cells positively stained with PI. A FACS compensation study was conducted to compensate for colour bleed-though of fluorescence emission, as the cells contained both green (GFP) and red fluorescence (PI) (Figure 3.16).

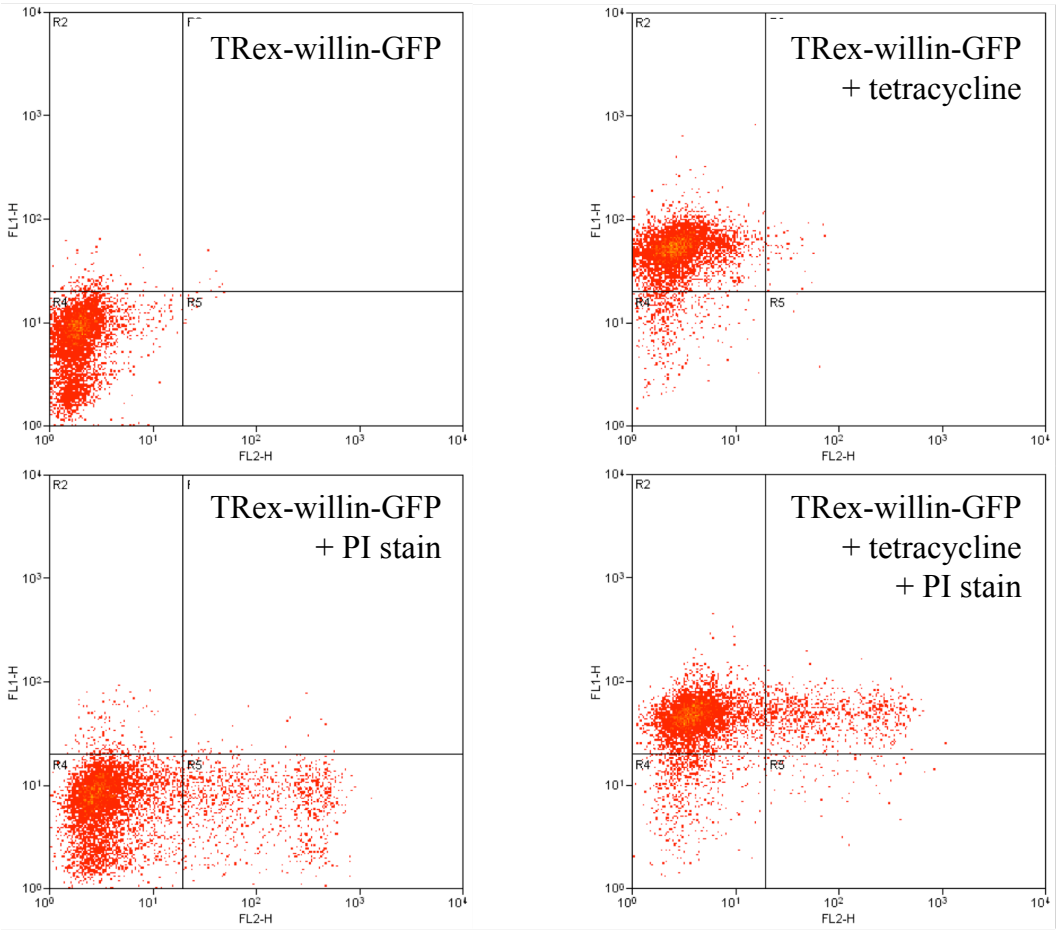

Figure 3.16: FACS analysis plots to compensate for colour bleed-through of fluorescence emission on a FACS machine. Every dot on the graph represents a cell and is plotted on a graph to measure green fluorescence (GFP) on the y-axis (FL1-H) and red fluorescence (PI stain) on the x-axis (FL2-H). TRex-willin-GFP cells were either untreated (not stained), induced with 1μg/ml tetracycline (green stain), stained with PI (red stain), or both induced with 1μg/ml tetracycline and stained with PI (red and green stain). 10,000 cells were counted in total.

Figure 3.17A shows the histogram outputs of a FACS live/dead discrimination experiment, where the first and second peaks represents live and dead cells respectively. Under the inducible conditions, willin-GFP expression in the TRex-willin-GFP cell line did not result in cell death. No significant cell viability changes were observed when both TRex and TRex-willin-GFP cells were treated with 1μg/ml tetracycline (24-96 hours) compared to untreated controls (0 hours tetracycline) (Figure 3.17b: t-test; $p>0.05$, n=3).

Even though no cell viability changes were observed, willin expression may result in cell cycle changes; such as a cell cycle arrest as seen with Expanded in the *D. melanogaster* model (Pellock et al., 2007). Cell cycle changes in the inducible TRex-willin-GFP cell line were therefore investigated. TRex and TRex-willin-GFP cells were treated with 1μg/ml tetracycline for 0-96 hours, fixed and stained with PI to detect the cell cycle stages in a 10,000 cell population. The first peak detected on the FACS cell cycle histogram represent cells in the G_1 phase of the cell cycle, the second peak represents cells in the G_2 phase of the cell cycle, and the plateau between the two peaks represent cells in the synthesis (S) phase.

Inducing cells for willin-GFP expression did not influence the cell cycle as the percentage of cells in the G_1, S and G_2 phases of the cell cycle remained unchanged when willin-GFP expression was induced (1-4 days with tetracycline) compared to uninduced (0 days of tetracycline) (Figure 3.18: t-test; $p>0.05$, n=3). Additionally no apoptotic bodies were observed in the FACS histograms (Figure 3.18A), supporting the observation that willin expression did not influence cell viability. Tetracycline itself did not result in any changes in the cell cycle as cells in the G_1, S and G_2 phases remained unchanged when TRex cells were incubated in the absence and presence of 1μg/ml tetracycline (Figure 3.18).

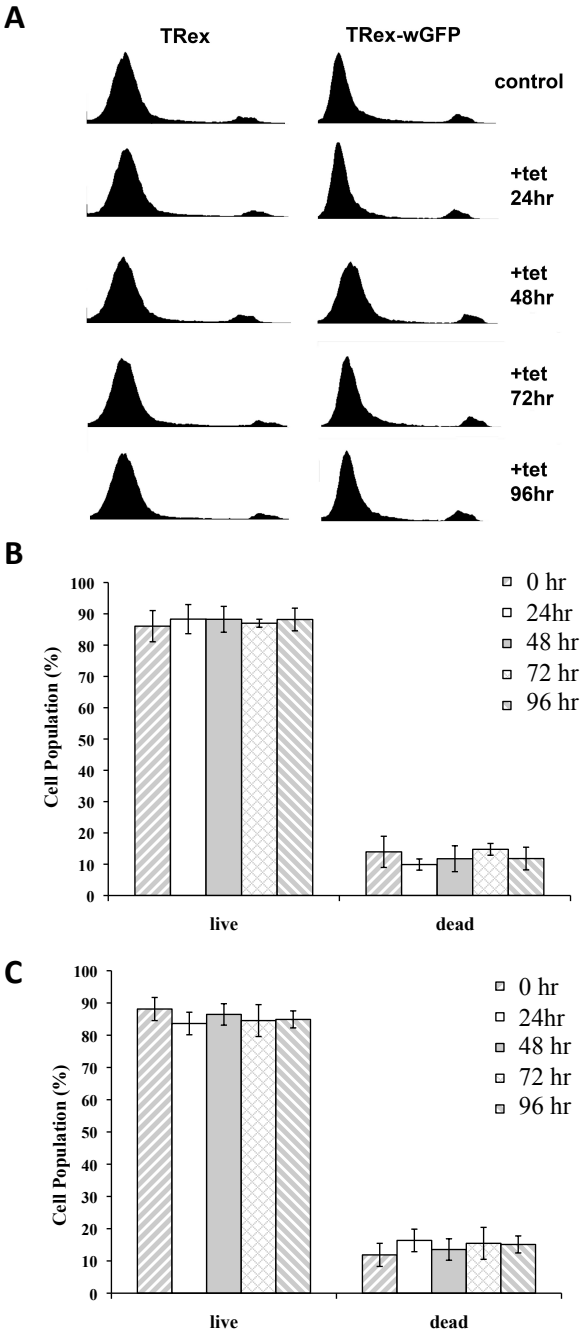

Figure 3.17: Controlled induced expression of willin-GFP did not result in changes in positively propidium iodide stained cells. TRex and TRex-willin-GFP cells were uninduced (0 hour tetracycline) or induced with 1μg/ml tetracycline for 24-96 hours. Cells were stained with PI and live/dead population peaks were observed on FACS histograms, showing cell counts on the y-axis and FL-2H fluorescence on the x-axis. In total 30,000 cells were counted (**A**). The percentage of TRex **(B)** and TRex-willin-GFP **(C)** cells in the live and dead peaks were analysed using Dako-cytometry software. No significant cell viability changes were observed when cells were uninduced or induced for willin-GFP expression (t-test; p >0.05, n=3). Error bars represent ± standard error.

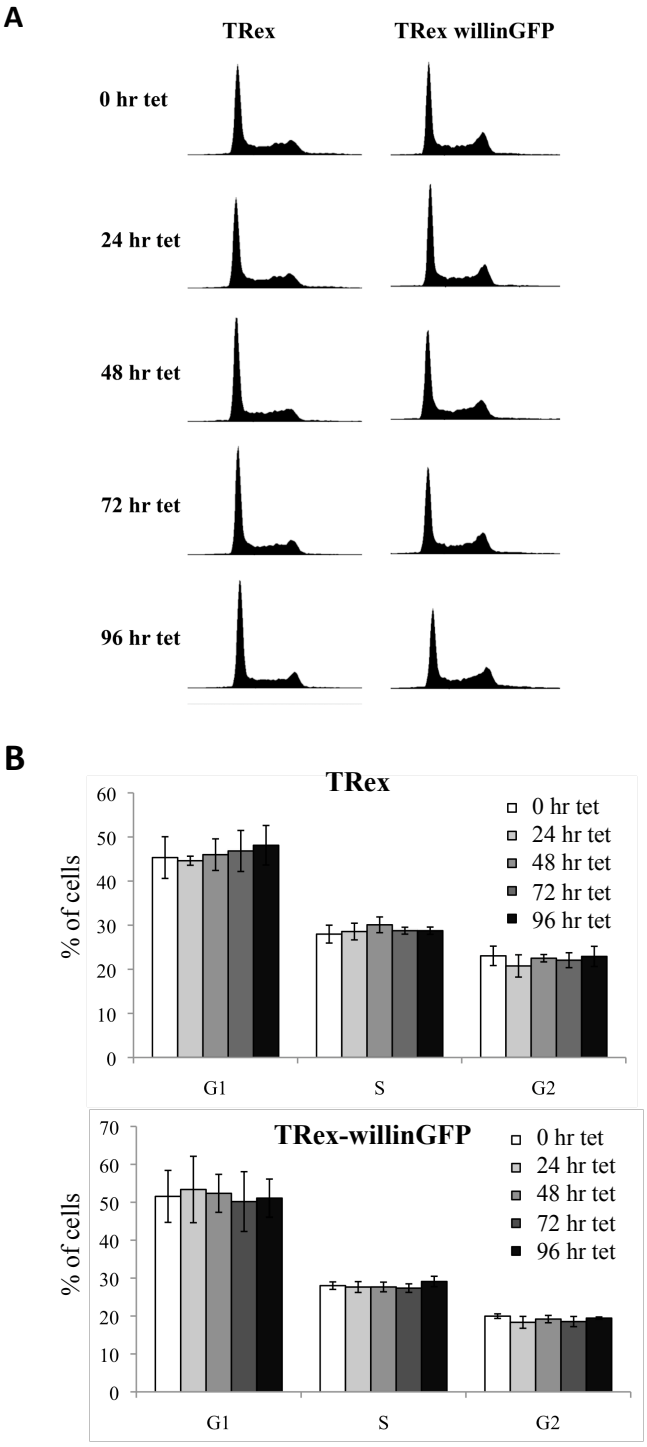

Figure 3.18: Willin expression did not influence the cell cycle. TRex and TRex-willin-GFP cells were incubated in 1μg/ml tetracycline for 0, 24, 48, 72, 96 hours. Cells were harvested, fixed and stained with PI. A total of 10,000 cells were analysed. **A**) FACS histogram output shows cell count on y-axis and intensity of PI fluorescence on the x-axis. **B**) Cell cycle analyses of three experiments were collated and the number of cells in the G1, S and G2 phases were calculated using Dako-cytometry software. No cell cycle changes were observed when the TRex and TRex-willin-GFP cells were induced with 1μg/ml tetracycline (t-test; $p>0.05$, n=3). Error bars represent $\pm$ standard error.

To investigate the downstream effect of YAP on the cell cycle in HEK-293 cells, HEK-293 cells were transiently transfected with a FLAG-YAP expression construct, a kind gift from Dr. D. Haber (Harvard University, USA), or left untreated. Cells were fixed and stained with PI to investigate cell cycle changes 48 hours post-transfection. No significant cell cycle changes were observed when HEK-293 cells were transfected with the FLAG-YAP expression plasmid compared to those left untreated (Figure 3.19; t-test; $p>0.05$, $n=3$).

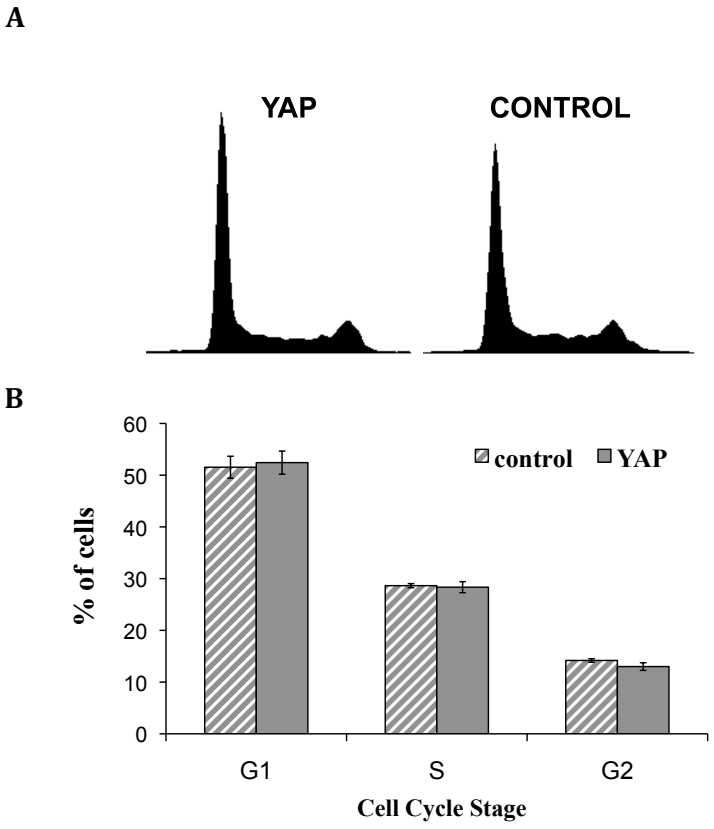

Figure 3.19: Transient transfection of a YAP-FLAG expression construct in HEK-293 cells did not result in cell cycle changes. HEK-293 cells were either transfected with YAP-FLAG or left untreated. Cells were harvested 48 hours post-transfection, fixed and stained with PI. A total of 10,000 cells were analysed in each individual experiment. **A**) FACS histogram output show the cell count on y-axis and the intensity of PI fluorescence on the x-axis. **B**) Cell cycle analyses of three experiments were collated and the number of cells in the G1, S and G2 phases of the cell cycle were calculated using Dako-cytometry software. The percentage of cells in each stage of the cell cycle remained unchanged when HEK-293 were untransfected (control) or transfected with a YAP-expression construct (t;test, $p>0.05$, $n=3$). Error bars represent $\pm$ standard error.

3.2.8 Ezrin and merlin modulate the ability of willin to phosphorylate MST1/2

As no cell cycle or cell viability changes were observed by induced willin-GFP expression alone, combinations of merlin and ezrin were transfected into the inducible system to see whether other upstream FERM domain containing proteins were needed to result in phosphorylation and complete downstream activation of the Hippo pathway.

To investigate the effect that ezrin and merlin expression has on willin's phosphorylation on MST1/2, combinations of transfections were used: merlin-GFP, GFP-ezrin, both merlin-FLAG and GFP-ezrin, and all the described combinations with willin-GFP expression induced by 1μg/ml tetracycline. Whole protein lysates were extracted 48 hours post-transfection.

A hierarchy in the ability to activate MST1/2 phosphorylation was observed, where the expression of either merlin or willin was sufficient to result in MST1/2 phosphorylation, whereas ezrin did not result in MST1/2 phosphorylation (Figure 3.20). A synergistic trend was observed on the phosphorylation of MST1/2 when cells were co-transfected with merlin and willin (Figure 3.20). However, this trend was not statistically significant (t-test; $p>0.05$, $n=3$). Ezrin had an inhibitory effect on both merlin's and willin's ability to induce phosphorylation of MST1 (Figure 3.20; t-test; $p<0.01$, $n=3$). Willin enhanced merlin's ability to induce the phosphorylation on MST (Figure 3.20), whereas merlin did not enhance or inhibit either willin's or ezrin's ability to phosphorylate MST (Figure 3.20).

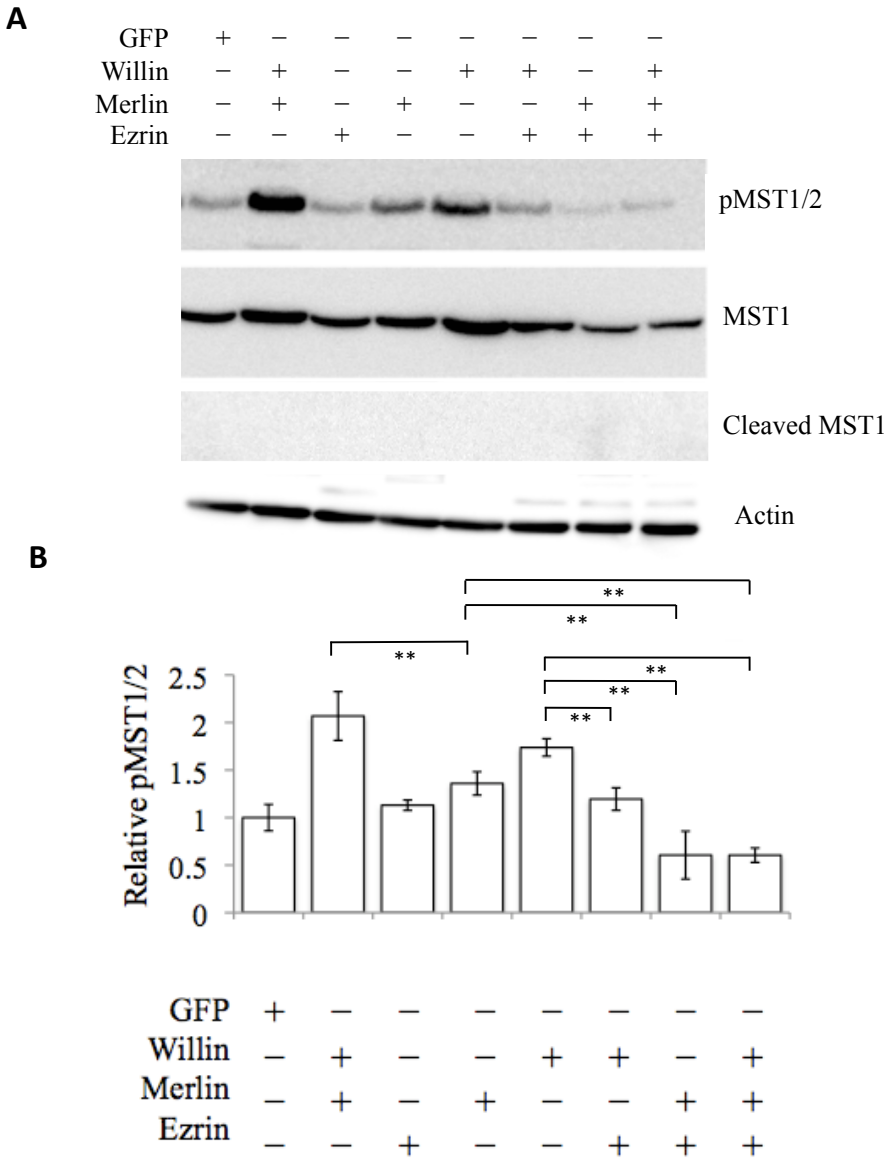

Figure 3.20: Ezrin and merlin expression modulated the ability of willin to induce phosphorylation of MST1/2. **A**) TRex-willin-GFP cells were transfected with 1μg of either GFP-ezrin and/or merlin-GFP and/or induced with 1μg/ml tetracycline. Whole cell lysates were separated on a 10% SDS gel and the nitrocellulose membrane was probed with pMST1/2, MST1 and actin antibodies. **B)** The relative protein phosphorylation was calculated by measuring the integrated density (ID) of phosphorylated protein over the ID of whole protein present, relative to the baseline phosphorylated protein of the empty-GFP transfection, which was set at 1. The presence of ezrin-GFP in cells expressing willin-GFP significantly decreased MST1/2 phosphorylation (t-test; $p<0.01$, $n=3^{**}$). Willin-GFP expression significantly enhanced MST1/2 phosphorylation when compared to only merlin transfected cells (t-test; $p<0.01$, $n=3^{**}$). No significant change in phosphorylation of MST1/2 was observed in merlin and willin expressing cells when compared to phosphorylation of MST1 by willin alone (t-test; $p>0.05$, $n=3$). Error bars represent $\pm$ standard error.

A MTT assay was performed to see whether willin could influence cell viability in cells transfected with ezrin or merlin. TRex-willin-GFP cells were transfected with merlin, ezrin or both merlin and ezrin, and willin-GFP expression was induced with 1μg/ml tetracycline. Willin expression did not affect MTT absorbance levels when cells were expressing merlin, ezrin or both merlin and ezrin (Figure 3.21; t-test; n=8, p>0.05).

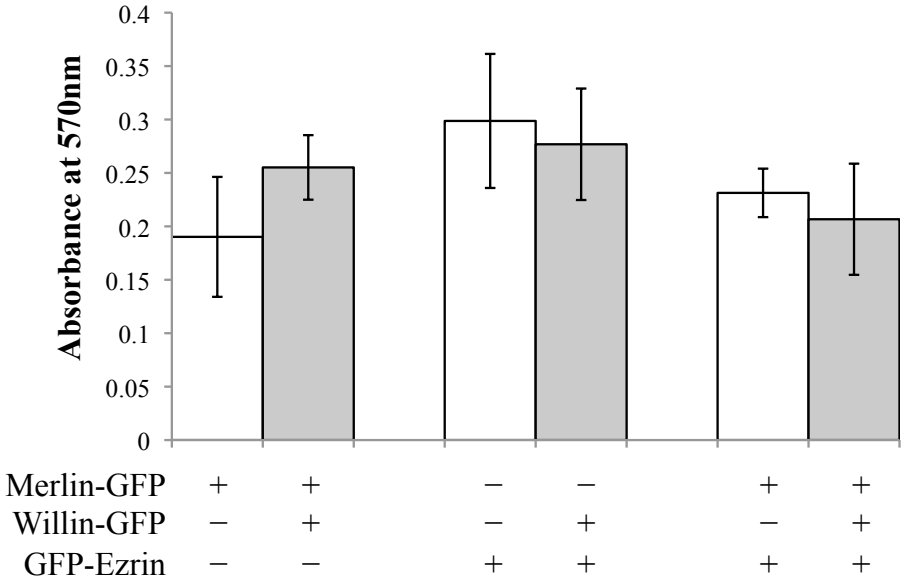

Figure 3.21: Induced willin-GFP expression did not affect MTT absorbance levels when cells were transiently transfected with merlin, ezrin or both merlin and ezrin. TRex-willin-GFP cells were transiently transfected with merlin-GFP, GFP-ezrin or both merlin-GFP and GFP-ezrin, and willin-GFP was induced with 1μg/ml tetracycline. MTT absorbance was read at a wavelength of 570nm, 48 hours post-transfection and induction. No significant change was observed in the presence or absence of willin-GFP expression (t-test; p>0.05, n=8). Error bars represent ± standard deviation.

Graves et al. (2001) have shown that for MST to result in a downstream apoptotic events, it needs to be both phosphorylated and cleaved. Over-expression of willin, merlin, ezrin or combinations of these in the TRex HEK-293 cell line did not result in MST1 cleavage (Figure 3.20), which further supported the observations that no downstream cell death occurred in the FERM containing protein combinations investigated.

3.2.9 Willin binds directly to ezrin and indirectly to merlin

Previous studies in *D. melanogaster* have indicated that Expanded and Merlin can bind to each other, co-localising in the plasma membrane, and that protein expression of one influences the cellular distribution of the other (McCartney et al., 2000). Merlin has previously been shown to co-precipitate with ezrin in mammalian cells (Meng et al., 2000), and therefore the same conditions were used to establish if willin would also co-precipitate with ezrin and merlin.

A previous Ph.D. student lab member, Dr Lissa Herron, has shown by immunoprecipitation experiments that willin can bind to merlin but not ezrin (Figure 3.22). In these experiments HEK-293 cells were transfected with plasmids expressing the following combinations of proteins and harvested 48 hours post-transfection: pCMVTag4a (empty FLAG) with willin-GFP or GFP-ezrin; willin-FLAG with GFP-ezrin; and merlin-FLAG with willin-GFP or GFP-ezrin. Immunoblot analyses of input and precipitate lanes (Figure 3.22) show that both merlin-FLAG and willin-FLAG are able to co-precipitate with GFP-ezrin under these conditions (lanes 8 & 10), but merlin-FLAG was not able to co-precipitate with willin-GFP (lane 4); the FLAG tag alone was not sufficient for precipitation of GFP-ezrin or willin-GFP (lanes 2 & 6). Neither empty FLAG, willin-FLAG nor merlin-FLAG co-precipitated untagged GFP (data not shown).

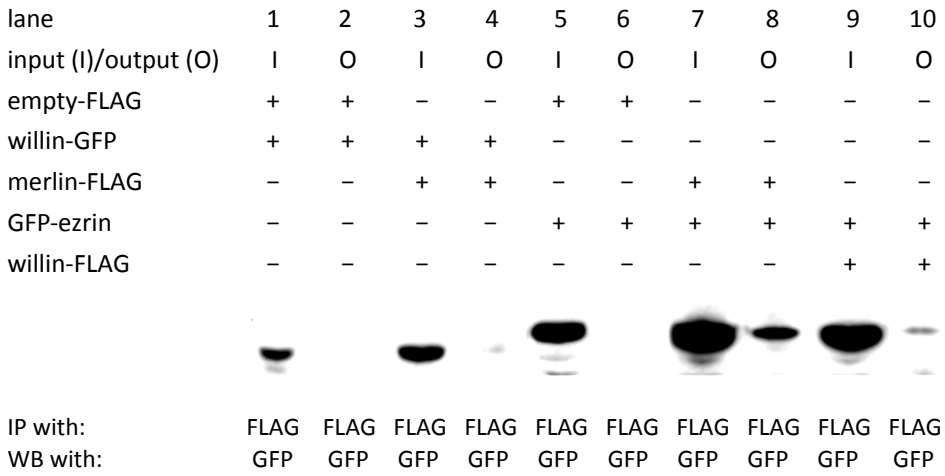

Figure 3.22: Willin can directly bind to merlin but not ezrin. HEK-293 cells were co-transfected with plasmids expressing either empty FLAG, Merlin-FLAG or Willin-FLAG and Willin-GFP or GFP-Ezrin. Input sample = whole cell extract. Output sample = final immunoprecipitated sample. *Lane 1.* empty FLAG/Willin-GFP input; *Lane 2.* empty FLAG/Willin-GFP IP; *Lane 3.* Merlin-FLAG/Willin-GFP input; *Lane 4.* Merlin-FLAG/Willin-GFP IP; *Lane 5.* empty FLAG/GFP-Ezrin input; *Lane 6.* empty FLAG/GFP-Ezrin IP; *Lane 7.* Merlin-FLAG/GFP-Ezrin input; *Lane 8.* Merlin-FLAG/GFP-Ezrin IP; *Lane 9.* Willin-FLAG/GFP-Ezrin input; *Lane 10.* IP= immunoprecipitation, WB= western blot. Work conducted by Dr. Lissa Herron.

A fluorescence co-localisation study was performed to further investigate the interactions between willin, merlin and ezrin using a deconvolution Deltavision microscope (Applied Precision). HEK-293 cells were transfected with plasmids expressing GFP-ezrin (kind gift from Dr R. Lamb, Institute of Cancer Research, London, UK) or merlin-GFP (kind gift from Dr W. Ip, University of Cincinnati, USA) and willin-mCherry (cloned by Andrew Robertson, University of St Andrews, UK). GFP-ezrin co-localised well with willin-mCherry within the plasma membrane (Figure 3.23 A-C). Conversely, the expression of merlin-GFP at the membrane appeared to exclude willin-mCherry expression at the membrane and no co-localisation was observed, supporting the biochemical data and suggesting that there is no direct interaction between merlin and willin (Figure 3.23 D-F).

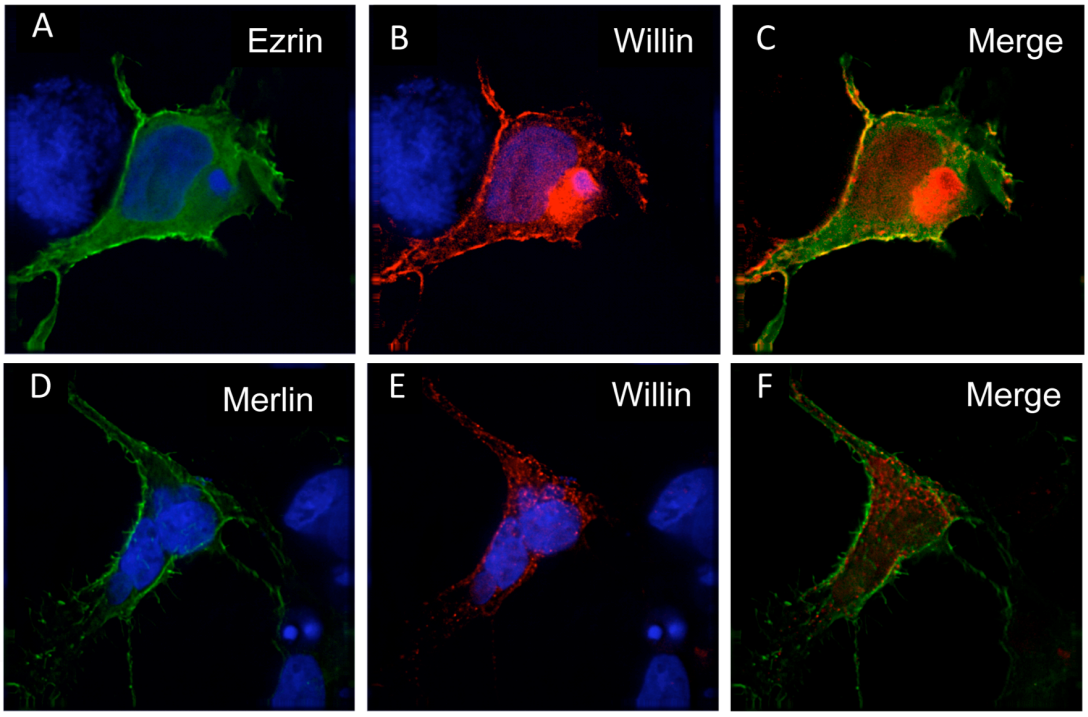

Figure 3.23: Willin co-localised with ezrin but not merlin in HEK-293 cells. HEK-293 cells were co-transfected with willin-cherry and either ezrin-GFP (**A-C**) or merlin-GFP (**D-F**) constructs. 48 hours post-transfection cells were fixed and fluorescence images were taken on a Deltavision microscope. Images displayed are representative and taken from a deconvoluted Z-stack. Co-localisation was seen at the plasma membrane when willin-cherry and ezrin-GFP constructs were co-transfected (**C**, yellow patches) but not when willin-cherry was co-transfected with merlin-GFP (**F**).

To investigate whether the FERM domain containing proteins could be found in a complex together, a triple transfection was performed with ezrin, merlin and willin expression plasmids. The same immunoprecipitation (IP) conditions (Section 2.3.5) were used as those used to obtain the IP data shown in Figure 3.22. HEK-293 cells were transfected with a combination of empty FLAG, GFP-ezrin, merlin-FLAG and willin-myc (cloned as described in Figure 3.3) expression plasmids. Cell lysates were collected 48 hours post-transfection and an immunoprecipitation was performed using FLAG and GFP antibodies conjugated to protein-G beads to pull out willin-myc, with either empty-FLAG, merlin-FLAG and ezrin-GFP proteins. Figure 3.24 shows that empty-FLAG did not pull out willin-myc (lane 1 & 2), ezrin-GFP pulled out willin-myc (lane 3 & 4) and merlin-FLAG pulled out willin-myc (lane 5 & 6). Merlin can therefore co-precipitate with willin, possibly through an indirect interaction via ezrin (Figure 3.24).

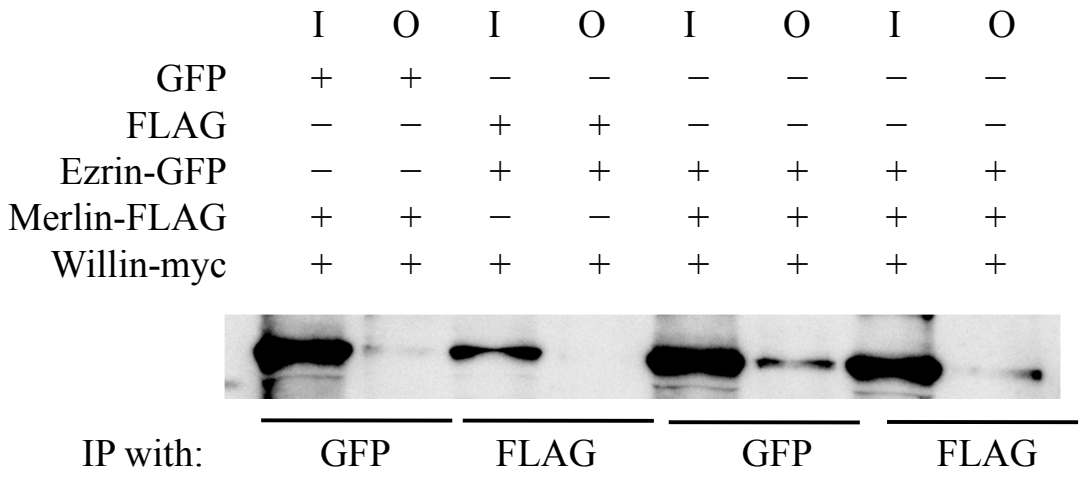

Figure 3.24: Willin binds indirectly to merlin via ezrin. HEK-293 cells were co-transfected with merlin-FLAG, GFP-ezrin and willin-myc constructs. 48 hours post-transfection cell lysates were collected and an immunoprecipitation assay was performed. Immunoprecipitation inputs (I) and outputs (O) were separated on a 10% SDS gel and the nitrocellulose membrane was probed with an anti-myc antibody to detect willin binding. Merlin-FLAG and GFP-ezrin were able to pull out willin-myc (lane 4 & 6). Empty-FLAG alone did not result in pull down of willin-myc protein (lane 2).

3.2.10 Willin expression sensitises cells to cellular death

Work by Lee et al. (2001) has shown that MST expression highly sensitises cells to cell death by the addition of TNFα and cycloheximide in Hela cells. Therefore, further investigations were conducted to see if willin expression sensitises cells to cell death, as only partial Hippo pathway signalling activation was observed thus far; where induction of willin expression resulted in no cell viability or cell cycle changes.

To test optimal conditions for TNFα-induced cell death, different TNFα concentrations (0-100ng/ml) were tested. Both TRex and TRex-willin-GFP cells were treated with 1μg/ml tetracycline, to induce willin-GFP expression in the latter only. The cells were incubated with 0, 25, 50 or 100ng/ml TNFα for 6 hours, 48 hours post-induction, before a MTT assay was performed as a measure of cell stress and viability. Figure 3.25 shows that increasing TNFα concentrations on TRex and TRex-willin-GFP cells decreased cell viability.

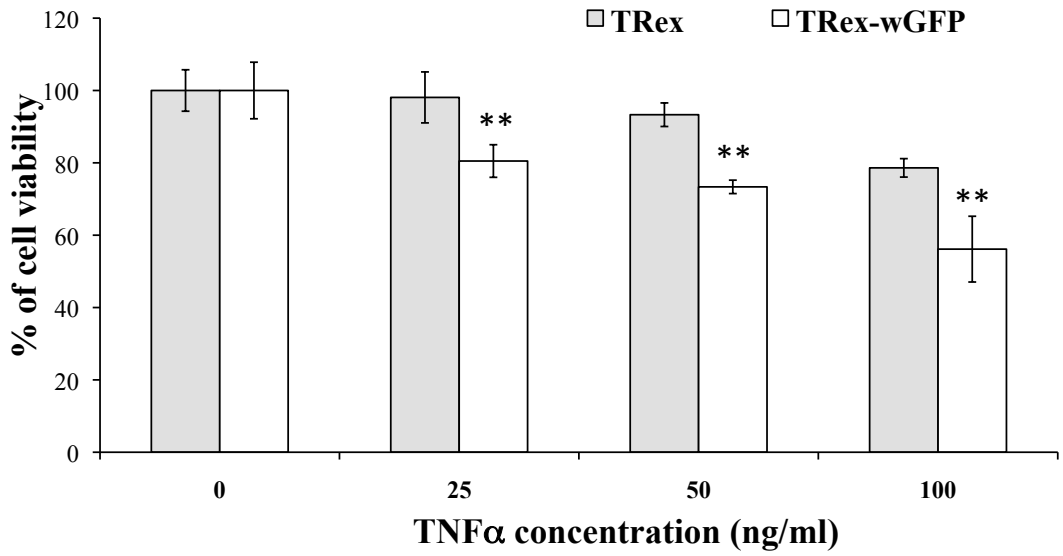

Figure 3.25: Increasing TNFα concentrations on TRex and TRex-willin-GFP cells decreased cell viability as measured by a MTT assay. Both TRex and TRex-willin-GFP cells were treated with 1μg/ml tetracycline 48 hours prior to a 6 hour TNFα treatment. The percentage of cell viability was measured as the absorbance level for treated/untreated cells, multiplied by 100. Significant cell viability differences between TRex and TRex-willin-GFP cells were observed when cells were treated with 25-100ng/ml TNFα compared to TRex-willin-GFP cells that were untreated (t-test; $p<0.01$, n=8**). Error bars represent $\pm$ standard deviation.

A MTT assay showed that when cells were incubated for 6 hours in 50ng/ml TNFα, cell viability significantly decreased to an average of 73% when willin-GFP was expressed, whereas the percentage of control cells not expressing willin-GFP was on average 93% (Figure 3.25). 50ng/ml TNFα was therefore the optimal concentration to test sensitisation to TNFα-induced cell death stimuli in further experiments.

Lee et al. (2001) have shown that MST over-expression resulted in sensitisation to cell death signals, resulting in caspase-3 activation. Caspase-3 activation was therefore further investigated when cells expressing willin were incubated in the presence or absence of TNFα. TRex and TRex-willin-GFP cells were both incubated with 1μg/ml tetracycline to control for the affect tetracycline has on caspase-3 activation, for a period of 0-4 days. Whole cell lysates were collected and immunoblot analysis showed that no caspase-3 cleavage was observed when TRex and TRex-willin-GFP cells were incubated with 1μg/ml tetracycline to induce willin-GFP expression in the latter only (Figure 3.26). This result supports the previous observation that willin-GFP induced expression did not result in cell death.

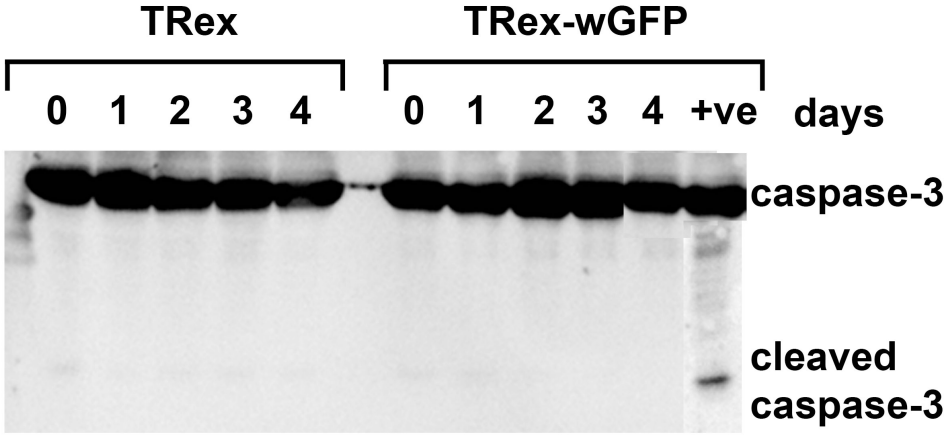

Figure 3.26: Induced willin-GFP expression with 1μg/ml tetracycline did not result in caspase-3 activation. TRex and TRex-willin-GFP cells were incubated in 1μg/ml tetracycline for 0-4 days. Whole-cell lysates were separated on a 20% SDS gel and the nitrocellulose membrane was probed with an anti-caspase-3 antibody. No active 17kDa caspase-3 was observed when both TRex and TRex-willin-GFP cells were induced with 1μg/ml tetracycline. As a positive control, TRex-willin-GFP cells were incubated in 50ng/ml TNFα for 4 hours.

To investigate whether willin expression resulted in cells being sensitised to TNFα-induced cell death, induced (1μg/ml tetracycline) TRex and TRex-willin-GFP cells were treated with 50ng/ml TNFα for a period of 0-4 hours. Whole cell lysates were collected and caspase-3 cleaved and un-cleaved protein levels were detected. Cleaved caspase-3 was observed within 1 hour of TNFα treatment and increased steadily over a period of 4 hours when willin-GFP expression was induced in TRex-willin-GFP cells (Figure 3.27.A). However, no caspase-3 cleavage changes were observed when TRex cells were treated with TNFα for 0-4 hours (Figure 3.27b; t-test; $p>0.05$, n=3). After 3 and 4 hours of 50ng/ml TNFα treatment, significantly more cleaved caspase-3 was observed when cells were over-expressing willin-GFP compared to control cells that did not express willin-GFP (Figure 3.27B; t-test: $p<0.01$, n=3).

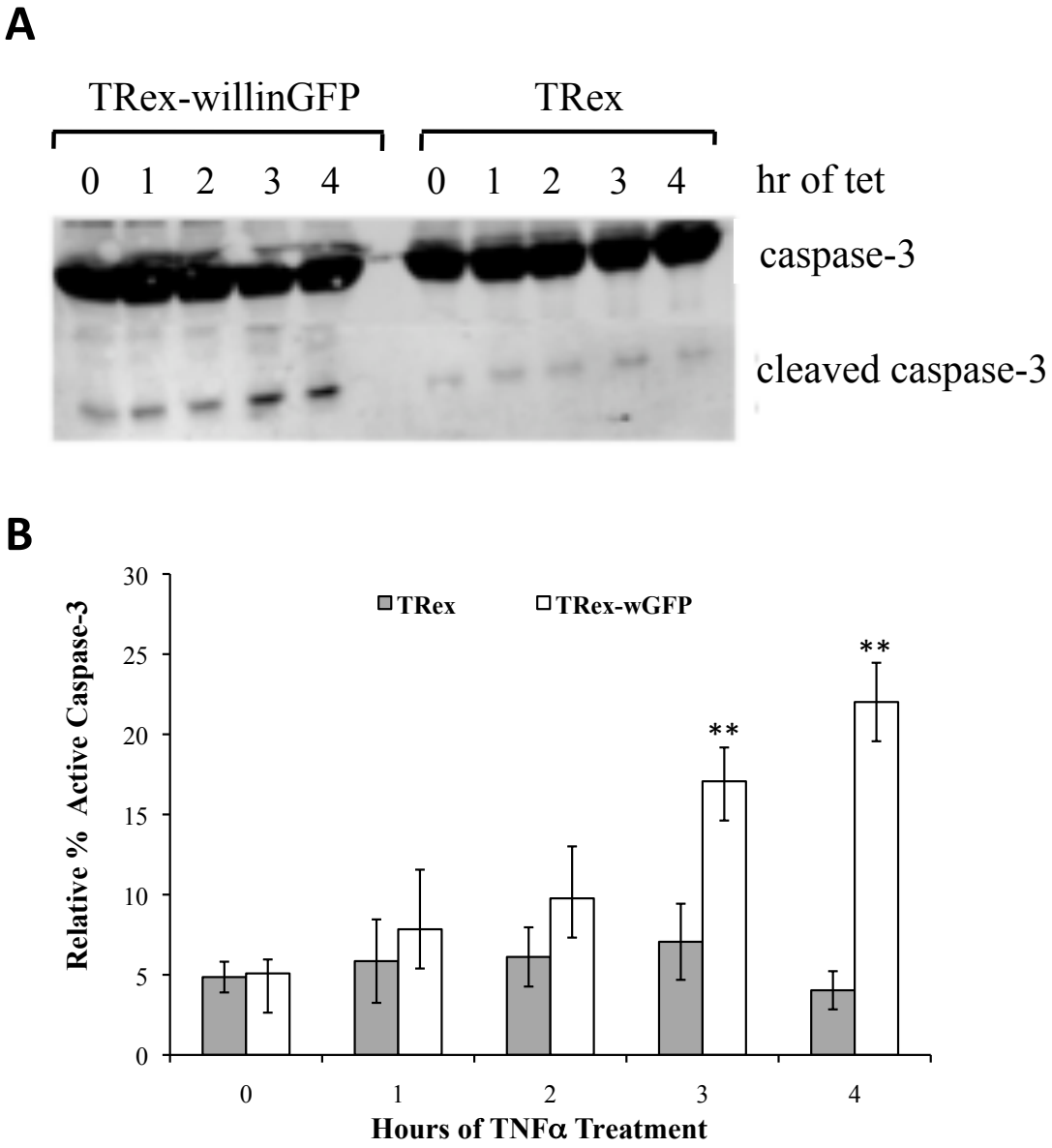

Figure 3.27: Controlled willin-GFP expression sensitised cells to apoptotic stress. TRex and TRex-willin-GFP cell lines were incubated in 1μg/ml tetracycline and treated with 50ng/ml TNFα for 0-4 hours. Whole-cell lysates were collected, separated on a 20% SDS gel and the nitrocellulose membrane was probed with an anti-caspase-3 antibody. **A)** Cleaved and active caspase-3 at the desired molecular weight of 17kDa was observed when willin-GFP was expressed within the TRex-willin-GFP cell line. **B)** Image J analysis was used to calculate % of active caspase present by dividing the integrated density (ID) of cleaved active caspase-3 over the ID of total caspase-3 present. TRex cells that expressed willin-GFP showed significant caspase-3 cleavage when under 3 and 4 hour TNFα stress compared to TRex cells not expressing willin-GFP (t-test; $p<0.01$, n=3**). Error bars represent $\pm$ standard deviation.

A colorimetric caspase-3 assay was conducted to measure the specific activity of active caspase-3 when the TRex cell lines were under TNFα-induced stress. The colorimetric substrate (AC-DEVD-pNA), labelled with a chromophore p-nitroaniline, was provided with the caspase-3 assay kit (Promega). Upon cleavage by caspase-3 (DEVDase), pNA was released from the substrate. Free pNA produced a yellow colour that was monitored by a spectrometer at a wavelength of 405nm (Figure 3.28). The amount of yellow produced was therefore proportional to the presence of active caspase-3. Z-VAD-FMK was provided within the kit to inhibit caspase-3 activity so that the difference between yellow produced in the absence and presence of the inhibitor was a direct measure of active caspase-3 present within the samples.

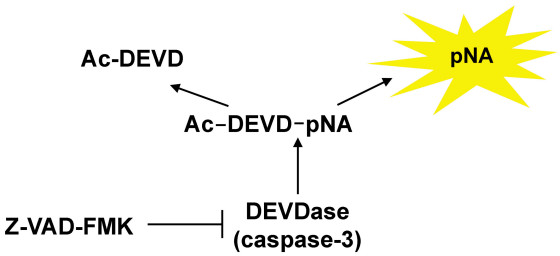

Figure 3.28: The colorimetric substrate (AC-DEVD-pNA) provided within the caspase-3 assay kit (Section 2.3.8: Promega) was labelled with a chromophore p-nitroaniline. Upon cleavage by caspase-3 (DEVDase), pNA was released from the substrate. Free pNA produced a yellow colour that was monitored by a spectrometer at a wavelength of 405nm. The amount of yellow produced was therefore proportional to the presence of active caspase-3. Z-VAD-FMK was provided within the kit to inhibit caspase-3 activity so that the difference between yellow produced in the absence and presence of the inhibitor was a direct measure of active caspase-3 present within the samples.

Both TRex and TRex-willin-GFP cells were induced with 1μg/ml tetracycline 2 days prior to a 6 hour treatment with either: 50ng/ml TNFα, with or without Z-VAD-FMK and untreated cells as a control. The difference between the accumulation of dye produced in the absence of inhibitor and in the presence of inhibitor was a measure of the caspase-3 activity present. Cell lysates were collected and a colorimetric assay was conducted to measure the specific activity (SA) of caspase-3. The results obtained confirmed active caspase-3 activity in TRex-willin-GFP cells expressing willin-GFP, whereas no caspase-3 activity was observed in the control TRex cells, when cells were put under 50ng/ml TNFα-induced apoptotic stress (Figure 3.29).

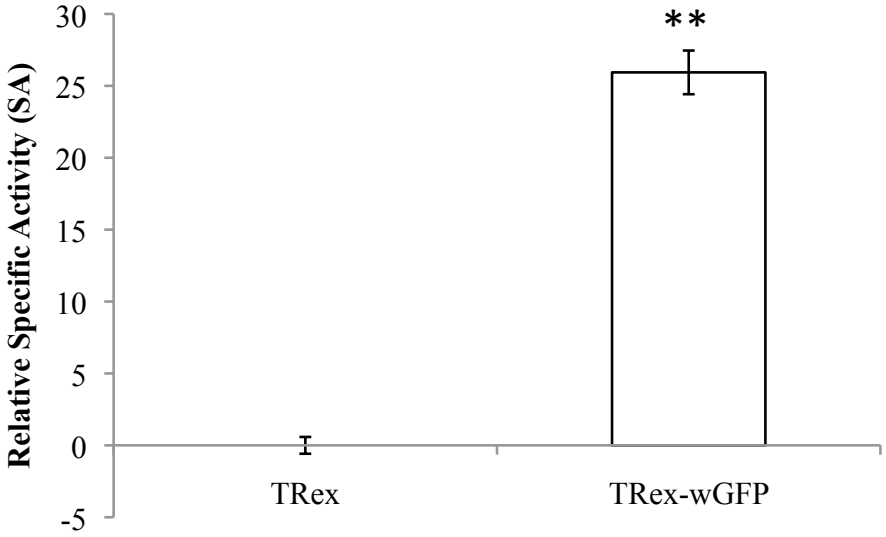

Figure 3.29: Under TNFα stress, willin expression resulted in caspase-3 activation (t-test; p<0.01, n=3**). TRex and TRex-willin-GFP cells were incubated in 1μg/ml tetracycline 2 days prior to 6 hour 50ng/TNFα treatment. Cell lysates were collected and a colorimetric assay was conducted to measure the specific activity (SA) of active caspase-3. Error bars represent ± standard error.

To further support that willin expression sensitises cells to TNFα-induced cell death, a live/dead PI FACS discrimination experiment (Section 2.3.2) was performed. Both TRex and TRex-willin-GFP cells were treated with 1μg/ml tetracycline for 48 hours and were either treated with or without 50ng/ml TNFα for 6 hours. Cells were harvested and 30,000 cells were analysed for cell viability. The percentage of live cells remained unchanged when TRex control cells, that did not express willin-GFP, were either treated with 50ng/ml TNFα or left untreated (Figure 3.30; t-test: p>0.05, n=3). However, a decrease from $\sim$ 80% to $\sim$ 60% was observed when cells were induced for willin-GFP expression in the presence of TNFα (Figure 3.30; t-test; p<0.01, n=3) further supporting previous experimental observations that the expression of willin resulted in cell sensitisation to cell death stimuli.

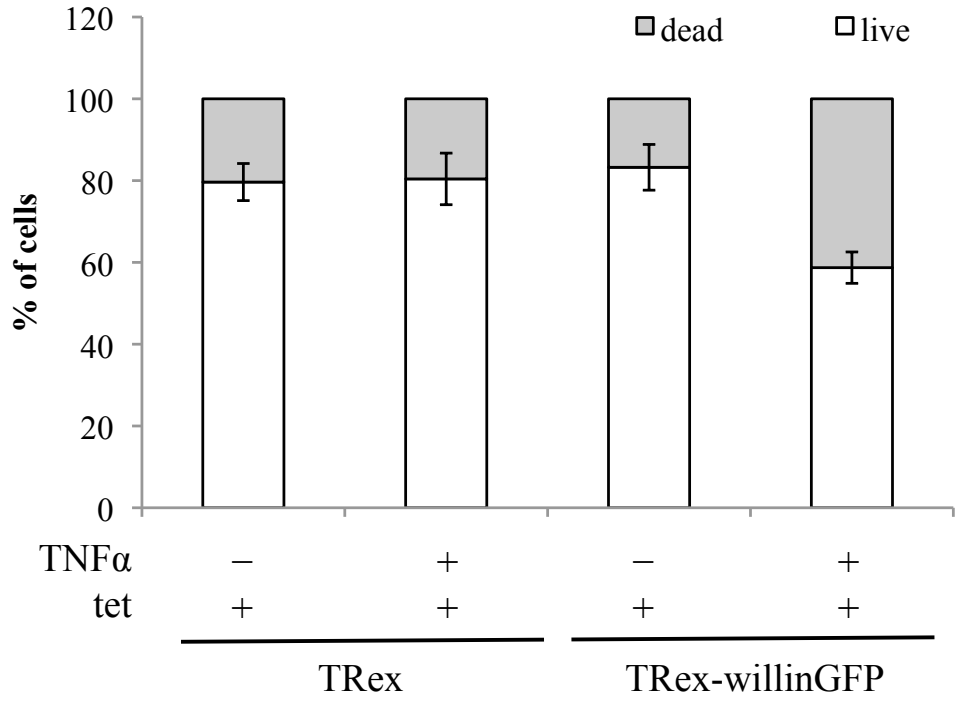

Figure 3.30: TNFα treatment on cells expressing willin-GFP resulted in cell death. TRex and TRex-willin-GFP cells were either treated with 1μg/ml tetracycline for 48 hours or both tetracycline (48 hours) and 50ng/ml TNFα (6 hours). The number of live and dead cells were measured, from a sample of 30,000 cells, using the PI staining detection protocol on a FACS machine and analysed using Dako-cytometry software. Cell viability decreased when cells were treated with TNFα and induced for willin-GFP expression compared to treated with TNFα alone (t-test; $p<0.01$, n=3). Error bars represent ± standard deviation.

3.2.11 Willin expression enhances MST1 cleavage under apoptotic stress

Graves et al. (2001) have shown that MST needs to be both phosphorylated and cleaved to result in an apoptotic downstream effect. Phosphorylation of MST1 occurred when willin expression was induced (as described in Section 3.2.5) and MST1 cleavage was therefore further investigated. As cell density is such an important factor for the activation of the Hippo pathway, cell density had to be tightly controlled in all experiments. To look at the effect of cell density on MST1 cleavage, TRex-willin-GFP cells were plated at either low, medium or high confluency levels and were left untreated, treated with 1μg/ml tetracycline for 48 hours, 50ng/ml TNFα for 6 hours or both. Whole

cell lysates were collected and MST1 protein expression was detected though immunoblot analysis. MST1 cleavage was not detected when cells were left untreated or induced for willin-GFP expression (Figure 3.31). However, MST1 cleavage was observed when 50ng/ml TNFα was added to the inducible cell line. Interestingly, this MST1 cleavage was enhanced when willin-GFP expression was induced by tetracycline at low cell density (Figure 3.31), further supporting that willin expression sensitised cells to cell death. However no such enhancement was seen when cells were plated out at medium to high confluency (Figure 3.31), suggesting that this observation was dependent on cell density.

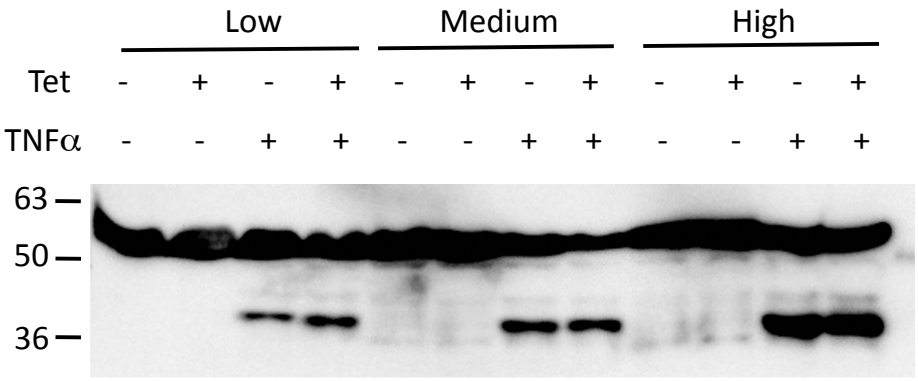

Figure 3.31: MST cleavage was observed under TNFα stress. TRex-willin-GFP cells were plated at different densities and either left untreated, treated with 1μg/ml tetracycline for 48 hours, 50ng/ml TNFα for 6 hours, or both. Whole cell lysates were separated on a 10% SDS gel and the nitrocellulose membrane was probed with an anti-MST antibody. MST cleavage was observed only when cells were treated with TNFα. At low cell density conditions, MST1 cleavage was increased when both TNFα treatment and willin-GFP expression were both present.

To further investigate that it was the expression of willin that resulted in enhanced MST1 cleavage when cells were under apoptotic stress at low cell density, an experiment was performed detecting MST1 cleavage when cells were either over-expressing willin or had reduced willin expression using siRNA in the absence and presence of TNFα. Immunoblot analysis showed that, at low cell density, willin expression resulted in an enhanced MST1 cleavage when cells where treated with TNFα compared to cells that were not expressing willin (t-test; $p<0.05$, $n=3$). However, no MST1 cleavage was observed when cells were not treated with TNFα (Figure 3.32), the same observation as that

observed in Figure 3.31. Knockdown of willin in the TRex-willin-GFP cells resulted in a further reduction of MST1 cleavage compared to cells that were endogenously expressing willin, however this reduction was not statistically significant (Figure 3.32; t-test: $p>0.05$, n=3).

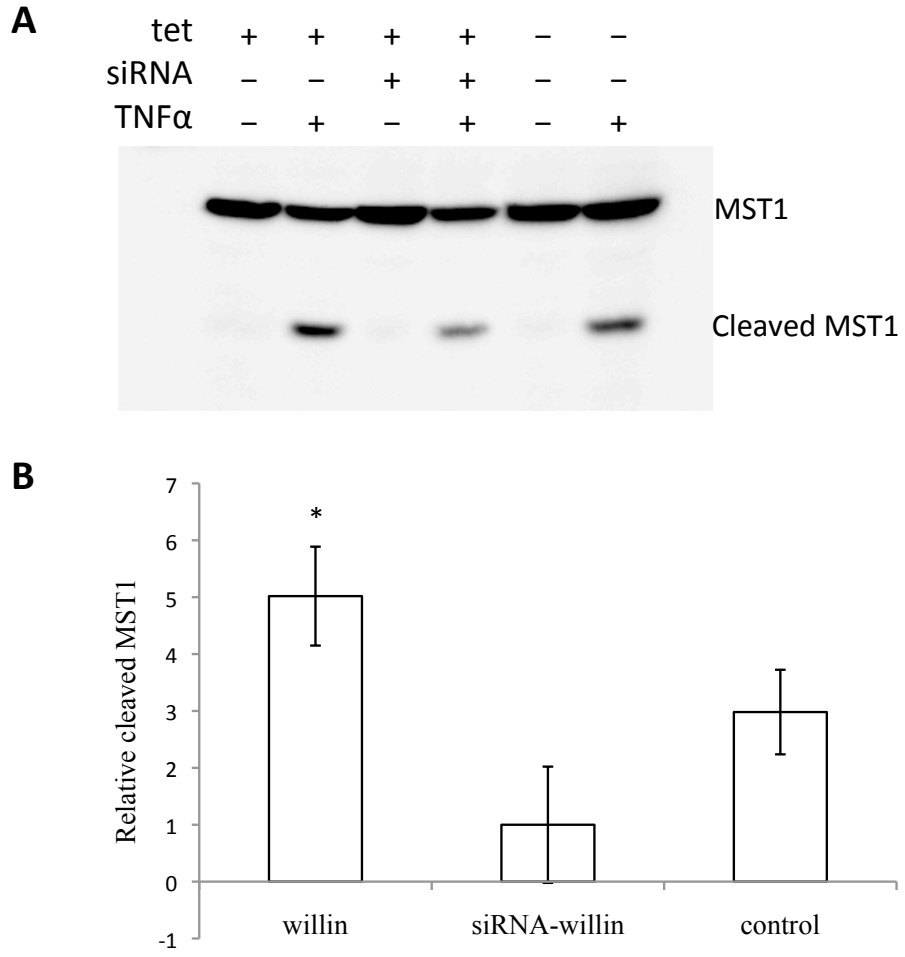

Figure 3.32: Willin expression enhanced MST1 cleavage under TNFα-induced stress. TRex-willin-GFP cells were either left untreated, treated with 1μg/ml tetracycline, 50ng/ml TNFα for 6 hours, both tetracycline (48 hours) and TNFα (6 hours), siRNA against willin (72 hours), and both siRNA (72 hours) and TNFα (6 hours) treatment. Whole cell lysates were separated on a 10% SDS gel and the nitrocellulose membrane was probed with an anti-MST antibody. **A**) Immublot showing that MST1 was cleaved only under TNFα stress. **B**) Image J analysis on immunoblots show that willin-GFP expression enhanced MST1 cleavage compared to TRex-willin-GFP cells that were not induced for willin-GFP expression (control) (t-test; $p<0.05$, n=3*). siRNA knockdown of willin reduced MST1 cleavage although not significantly (t-test; $p>0.05$, n=3) compared to untreated controls. Error bars represent ± standard deviation.

3.3 Discussion

3.3.1 Willin expression partially activates the Hippo pathway

The production of a tetracycline-inducible willin expression cell line (TRex-willin-GFP) proved to be a successful system to investigate Hippo signalling activation in HEK-293 cells. If willin is truly the human homologue of the *Drosophila* protein Expanded then willin will act upstream of the Hippo signalling pathway to activate and inhibit YAP, further resulting in downstream cell viability and cell cycle changes. As predicted, an increase in willin expression resulted in an increase in phosphorylation of the core Hippo pathway components: MST1/2, LATS1 and YAP (Section 3.2.5). Induced expression of willin resulted in an inhibition of YAP through YAP phosphorylation-induced cytoplasmic retention (Section 3.2.6); however this was not sufficient to result in further apoptotic downstream effects (Section 3.2.7). Willin over-expression resulted in partial activation of the Hippo pathway as no cell viability or cell cycle changes were observed when willin was expressed in HEK-293 cells.

The more upstream a protein is found within a signalling cascade, the less effect it can have on downstream targets. As willin is upstream of the core Hippo pathway cassette (MST, LATS and YAP) it is expected that full apoptotic downstream events are less likely to be observed. Other human signalling pathways, upstream proteins and negative feedback loops may all regulate and modulate the inhibition of YAP.

Another FERM domain containing protein called FRMD3 has previously been shown to have no impact on cell cycle progression or cell death in HEK-293 cells, even though it has been shown to be a novel putative tumour suppressor in non-small cell lung carcinoma (Haase et al., 2007). Partial activation of the Hippo pathway by willin expression therefore does not rule out willin's ability to be a tumour suppressor, as downstream cellular effects are very cell specific.

3.3.2 Willin expression results in sensitisation to TNFα-induced cell death

The partial activation of the Hippo pathway by willin expression may explain cell sensitisation to TNFα-induced cell death (Section 3.2.10). The reason for

this may be complex and MST may be a vital molecular switch for the Hippo pathway to lead to full downstream activation of the Hippo pathway; resulting in apoptosis and cell cycle changes. Lee et al. (2001) have previously reported that the MST kinase has to be both phosphorylated and cleaved to result in cellular death. Although phosphorylation of MST1/2 (and also LATS1 and YAP) occurred upon willin expression, cleaved MST1 was never observed in this scenario. Only upon TNFα stimulation was MST cleaved and an apoptotic downstream effect observed (Section 3.2.11). Interestingly, cells undergoing TNFα treatment and over-expressing willin had more cleaved MST1 compared to cells undergoing TNFα treatment alone. So the phosphorylation of MST caused by willin over-expression may have primed downstream apoptotic effect, however additional signals such as cell-to-cell contact or cell death signals are needed to promote the pre-apoptotic state of the cell into the full apoptotic downstream effects of the Hippo pathway (Figure 3.33).

The expression of willin enhances caspase-3 activation (Section 3.2.10) through an unknown mechanism. One possible theory is that willin expression may enhance caspase-3 mediated activation of MST1, which agrees with recent findings that suggest that TNFα-induced cell death in hepatocytes requires MST1/2 (Song et al., 2010). However, we cannot rule out the possibility that other factors are involved and that the effects of willin expression could be indirect.

3.3.3 Cell density is an important factor in the Hippo pathway

Cell density plays an important role in the activation of the Hippo pathway; with the pathway being activated at high cell densities and inhibited at lower cell densities. The mechanisms of Hippo pathway modulation remains, to this date, largely unknown. Cell-to-cell contact, adhesion and polarity have all previously been described as important factors in activating the Hippo signalling cascade (Graves et al., 2001; Lee et al., 2001; Bennett and Harvey, 2006; Zhao et al., 2007; Chen et al., 2010).

At high cell density, YAP phosphorylation was often observed in untreated control cells. These observations support those by Zhao et al. (2007) who have shown that, *in-vitro*, YAP becomes phosphorylated at high cell density. All experiments were therefore performed at very low density and phosphorylation

data for YAP when willin was induced could only be conducted over a 48 hour period, compared to 72 hours for MST1/2 and LATS1. MST1/2 and LATS1 may have been less prone to cell density variables as they are further upstream of other converging pathways onto YAP.

At low cell density, willin expression resulted in enhanced MST1 cleavage when cells were under TNFα stress. Whereas no increase in MST1 cleavage was observed, under TNFα-induced stress, when willin was expressed at medium and high cell density (Section 3.2.11). At medium and high cell densities, the Hippo pathway may have already been activated so that an increase in willin expression does not have an enhanced effect, as MST was already cleaved.

It is important to note that at high cell density *in-vitro*, the proportion of phosphorylated YAP protein increases, but this does not result in all cells dying, rather cells become contact inhibited and form a monolayer. In addition, YAP over-expression in HEK-293 cells did not result in changes in the cell cycle. Therefore in HEK-293 cells, it is likely that the mammalian Hippo pathway activation results in sensitisation to cell death, and additional signals such as cell contact and cell death signals are required to result in cell survival changes (Figure 3.33). This theory supports our data, as willin expression resulted in phosphorylation of MST1, LATS and YAP but had no impact on cell cycle progression or cell death.

3.3.4 Distribution of Hippo proteins is cell density dependent

The subcellular distribution of willin is varied as it can be localised at the plasma membrane, cytoplasm and nucleus (Section 3.2.4). This mixed cellular distribution is common within the ERM family of proteins (Gunn-Moore et al., 2005; Madan et al., 2006). The distribution of willin, like the distribution of other Hippo pathway proteins, changes depending on cell density. At low cell density, willin is predominately found in the cytoplasm, whereas at high cell density willin is re-distributed to the plasma membrane. As the Hippo pathway is activated though cellular contact, willin translocation to cellular junctions upon cellular contact with neighbouring cells may be vital in the downstream activation of the Hippo pathway. Future experiments should identify potential upstream receptors candidates such as FAT or CD44 (Chapter 6).

Complexes between the Hippo pathway components in the mammalian

system remains, to this date, largely unknown. Increasing cell density resulted in an increase of expression of willin and LATS1 in the Triton X-100 soluble membrane fraction. Whereas MST1 expression decreased in the Triton X-100 soluble fraction when cell density was increased. More research needs to be done to see whether willin and LATS can be found in a complex together. A complex between willin and LATS is plausible as localisation studies on LATS have shown similar distribution to that of willin. LATS has been shown to translocate to the plasma membrane upon cell-to-cell contact, with a high expression of these proteins found at cellular adherent junctions (Yang et al., 2004; Zhao et al., 2011).

3.3.5 Ezrin, merlin and willin can modulate activation of the Hippo pathway

A hierarchy in the ability to activate MST1/2 phosphorylation was observed, where the expression of either merlin or willin was sufficient to result in MST1/2 phosphorylation, whereas ezrin did not result in MST1/2 phosphorylation at the cell density tested (Section 3.2.8). A synergistic trend was observed on the phosphorylation of MST1/2 when cells were co-expressed with merlin and willin (Figure 3.20). Ezrin had an inhibitory modulation on both merlin's and willin's ability to phosphorylate MST1. Willin had an enhanced effect on merlin's ability to phosphorylate MST. Whereas merlin did not enhance or inhibit either willin's or ezrin's ability to induce the phosphorylation of MST.

Cell density is an important factor when studying the Hippo pathway and it is important to note that at different cell densities merlin and ezrin may have different modulation effects. The modulation on MST1 phosphorylation was chosen as it was the most upstream protein of the Hippo pathway complex, and future studies should also focus on the ability of ezrin and merlin to modulate the hippo pathway through phosphorylation of LATS1 and YAP.

The identification of possible binding factors is a key step in the characterisation of a novel protein. Willin can bind to ezrin, possibly via a head-to-tail conformation typically found between ERM protein binding. Previous results by Alfthan et al. (2004) have shown that ezrin binds with a strong affinity to merlin, resulting in the inhibition of merlin's downstream effects. The observed findings in this thesis support this theory as ezrin decreases phosphorylation

caused by increased expression of both merlin and willin. It is possible that the identified willin-ezrin interaction could be an important controlling mechanism for upstream activation of the Hippo pathway in mammals, and future studies will investigate this possibility.

Willin and merlin do not appear to co-localise or bind directly (Section 3.2.9). However when merlin, ezrin and willin are over-expressed within the cell, merlin can indirectly be associated with willin (Section 3.2.9). Whether this indirect binding occurs at a physiological level remains unknown. When merlin and willin are co-expressed in HEK-293 cells, the distribution of willin is altered as merlin appears to exclude willin expression at the membrane. This may be due to competition of upstream receptors. Willin's exclusion from the plasma membrane does, however, not affect willin's ability to phosphorylate the Hippo pathway, as the expression of willin in fact had an enhanced effect on merlin's ability to phosphorylate MST. ERM proteins distribution is of great importance in its ability to modulate the Hippo pathway and may explain why high cytoplasmic ezrin expression has prognostic significance for head and neck squamous cell carcinoma (Madan et al., 2006).

3.4 Conclusion

Figure 3.33 summarises the main findings of this chapter. Willin expression can induce the phosphorylation of the core Hippo pathway cassette (MST1/2, LATS1 and YAP) resulting in YAP inhibition through retention of YAP in the cytoplasm. Willin expression was not sufficient to result in cell viability or cell cycle changes in HEK-293 cells. However, willin expression did result in sensitisation to TNFα-induced cell death and enhanced MST1 cleavage in apoptotic stimuli conditions. Expression of merlin and ezrin can also modulate the Hippo pathway; where a synergistic trend was observed when both merlin and willin were expressed and where ezrin has an inhibitory role.

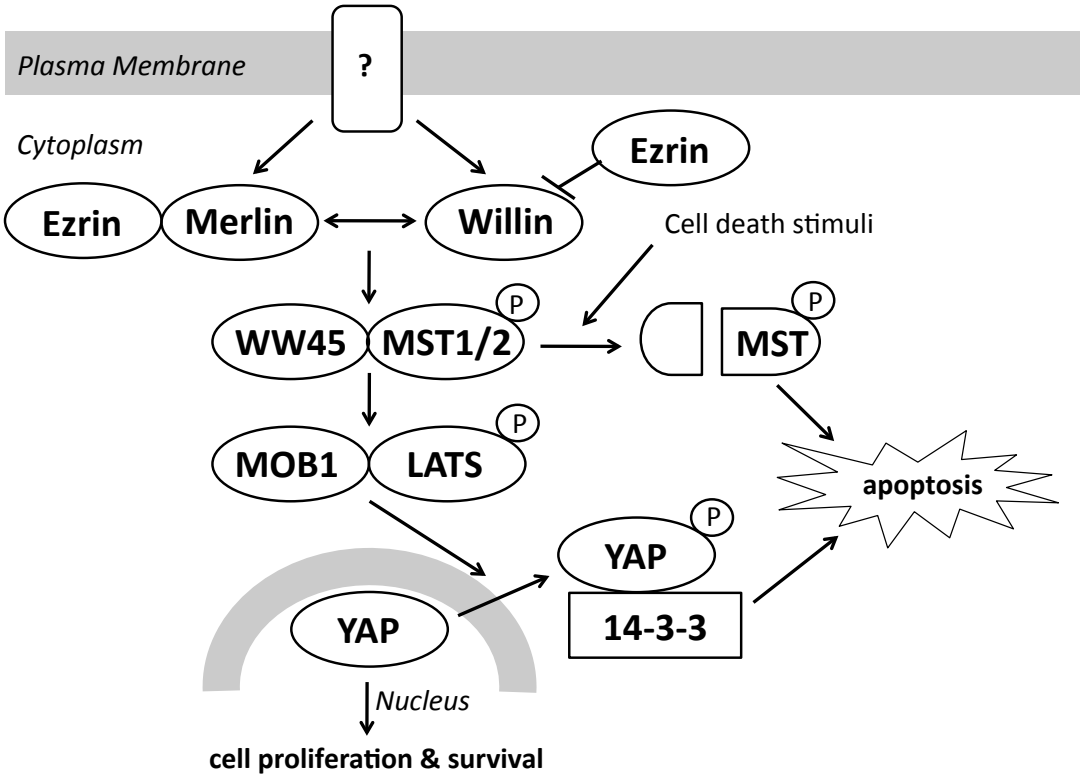

Figure 3.33: Updated Hippo pathway schematic to summarise results. Willin expression phosphorylates the core Hippo pathway cassette (MST1/2, LATS1 and YAP); resulting in YAP inhibition through retention of YAP in the cytoplasm, possibly through binding to 14-3-3 protein. Ezrin can bind directly to merlin and willin and has an inhibitory effect on the Hippo pathway. A synergistic effect was observed when both merlin and willin were expressed. For the Hippo pathway to result in apoptosis, the core proteins (MST, LATS and YAP) need to be phosphorylated and MST1 needs to be cleaved. MST1 cleavage can be induced with a cell death stimuli such as TNFα.

Chapter 4

Willin Expression Antagonises a YAP-induced EMT Phenotype

4.1 Introduction

In the previous chapter, willin expression in HEK-293 cells was shown to partially activate the Hippo pathway with no measurable physiological downstream outputs (Chapter 3). The function of willin in a non-tumourigenic, human mammary epithelial MCF10A cell line was further investigated as over-expression of YAP and deregulation of upstream Hippo components have previously been shown to induce a measurable epithelial-mesenchymal transition (EMT) in these cells (Overholtzer et al., 2006; Hao et al., 2008; Zhang et al., 2008a, 2009b).

Over-expression of YAP in MCF10A cells has been shown to induce an EMT response: where a typical polarised uniform epithelial sheet of cells transformed into mesenchymal-like cells, exhibiting neither regimented structure nor tight intracellular adhesion (Overholtzer et al., 2006; Zhao et al., 2007; Hao et al., 2008; Zhang et al., 2008a, 2009b). Hippo pathway components have been shown to antagonise a YAP-induced phenotype, resulting in functional downstream changes in anchorage-independent growth, cell migration, proliferation and adhesion (Overholtzer et al., 2006; Hao et al., 2008; Zhang et al., 2008a, 2009b). Willin's ability to antagonise a YAP-induced EMT phenotype in MCF10A cells was further investigated as willin has been placed upstream of the core Hippo pathway components (MST1/2, LATS1 and YAP; Chapter 3).

4.2 Results

4.2.1 Willin expression in MCF10A cells

4.2.1.1 Willin expression results in increased phosphorylation of MST1/2, LATS1 and YAP in MCF10A cells

To confirm that willin expression resulted in an increased phosphorylation of the core Hippo pathway components in MCF10A cells, and was not cell-specific to HEK-293 cells, MCF10A cells were retrovirally transfected with either pBabe-empty-vector or pBabe-willin-HA expression plasmids (kind gift from Dr. Paul Reynolds' lab, University of St Andrews, UK). 48 hours post retroviral transfection, whole cell lysates were collected and run on a 10% SDS gel. Immunoblot analysis confirmed that willin-HA was expressed in MCF10A cells retrovirally transfected with pBabe-willin-HA (Figure 4.1).

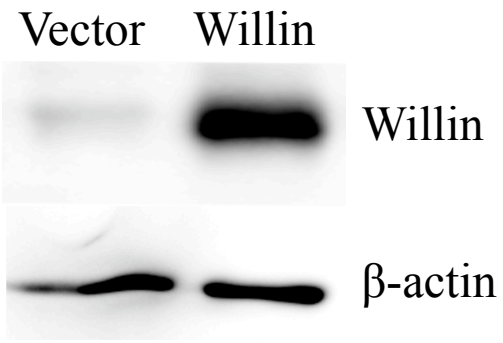

Figure 4.1: Immunoblot confirmed that willin-HA was expressed in MCF10A cells. MCF10A cells were retrovirally transfected with pBabe-willinHA or pBabe-vector plasmids. Whole cell lysates were collected and run on a 10% SDS gel. The nitrocellulose membrane was probed with an anti-HA antibody to detect willin-HA expression. β-actin detection was used as a loading control.

Expression of willin-HA in MCF10A cells resulted in an increase in phosphorylation of the core Hippo pathway cassette (Figure 4.2). Image J analysis of three phosphorylation western blots (representative shown in Figure 4.2.A) showed that a significant increase in phosphorylation of MST1/2, LATS1 and YAP was observed when MCF10A cells expressed willin-HA compared to an empty vector control (Figure 4.2.B, t-test: $p<0.01$, $n=3$).

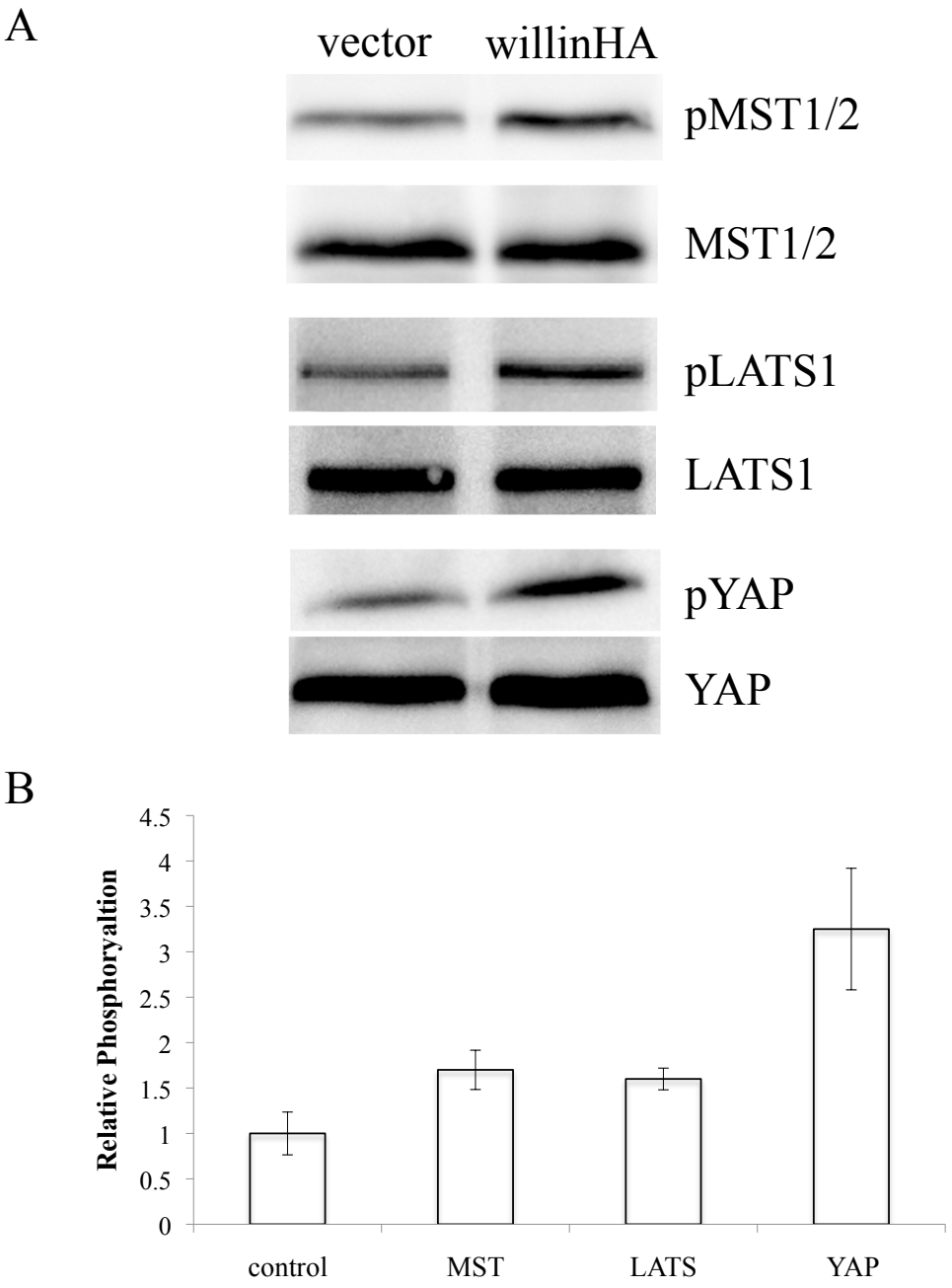

Figure 4.2: Expression of willin resulted in increased phosphorylation of MST1/2, LATS1 and YAP in MCF10A cells. pBabe-willin-HA and pBabe-vector were retrovirally transfected into MCF10A cells. 48 hours post-transfection, whole cell lysates were collected and run on a 10% SDS gel. **A)** The nitrocellulose membrane was probed with antibodies detecting both phosphorylated and total protein expression of MST1/2, LATS1 and YAP. **B)** Immunoblots were analysed using Image J software to calculate relative phosphorylation of MST1/2, LATS1 and YAP to empty vector controls that were standardised to 1. Relative phosphorylation was calculated by measuring the integrated density (ID) of phosphorylated protein/ID of total protein detected. Error bars represent ± standard error (n=3).

4.2.1.2 Willin expression results in YAP nuclear exit in MCF10A cells

Activation of the Hippo pathway through phosphorylation of the core Hippo pathway cassette has previously been reported to result in YAP translocation from the nucleus to the cytoplasm (Zhao et al., 2007; Hao et al., 2008). Nuclear to cytoplasmic translocation of YAP was observed when willin was over-expressed in HEK-293 cells (Section 3.2.6). To confirm that willin expression had the same effect on YAP translocation in MCF10A cells, nuclear fractionation experiments were conducted on stable MCF10A cells expressing empty vector and willin-HA.

MCF10A cells were retrovirally transfected with pBabe-willin-HA or pBabe-vector expression plasmids. Stable cell lines of each were created by antibiotic selection with 2μg/ml puromycin. Nuclear fractionation was performed on both cell lines and equal protein concentrations of nuclear cell lysates were run on a 10% SDS gel. Image J analysis of western blots (representative immunoblot shown in Figure 4.3.A) showed that nuclear YAP levels were significantly reduced, by $\sim$8 fold, in MCF10A cells that expressed willin-HA compared to MCF10A cells that expressed the empty vector (Figure 4.3.B; t-test: $p<0.01$, $n=3$).

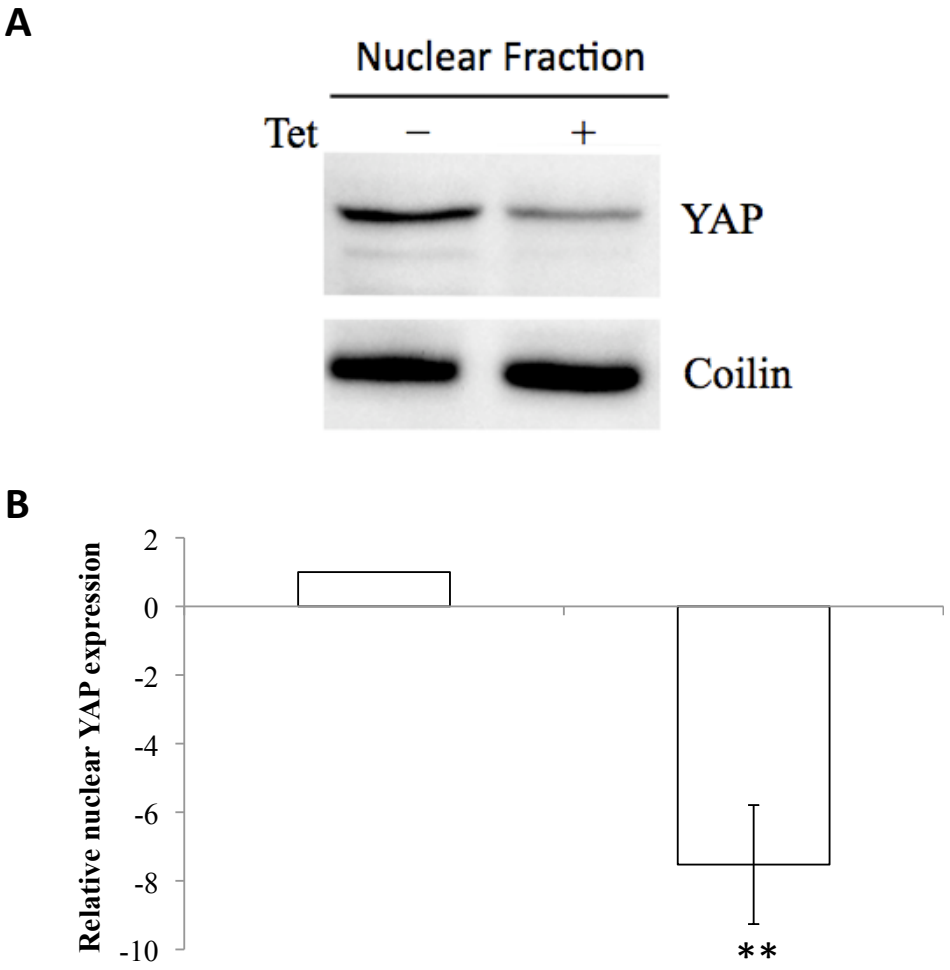

Figure 4.3: Expression of willin in MCF10A cells resulted in YAP nuclear exit. **A)** Nuclear fractions were collected from MCF10A cells over-expressing willin-HA and an empty vector, and run on a 10% SDS gel. The nitrocellulose membrane was probed with anti-YAP and coilin antibodies, where the latter was used as a nuclear fraction loading control. **B)** Image J analysis confirmed that a significant decrease in YAP nuclear expression was observed in MCF10A-willinHA compared to the MCF10A-vector cells (t-test; $p<0.01$, n=3**). YAP protein expression levels were relative to control MCF10A-vector cells which were set to 1. Error bars represent ± standard deviation.

4.2.1.3 Willin expression reduces cell proliferation at high cellular density

Previous studies have shown that the expression of the Hippo pathway kinases enhanced contact inhibition as proliferation rates were inhibited at high cell density but not at a low cell density (Camargo et al., 2007; Dong et al., 2007; Zhao et al., 2007). As willin expression was shown to activate the Hippo pathway (Section 4.2.1.1), its ability to influence cell proliferation was investigated.

MCF10A cells were retrovirally transfected with pBabe-vector or pBabe-willin-HA constructs. Stable cell lines were created and plated out into 96 well plates. A MTT assay was performed as a measure of cell proliferation every 24 hours for 7 days. Medium was replaced with fresh growth medium every 48 hours to prevent cells becoming nutrient deprived. Differences in proliferation curves were observed between MCF10A cells expressing an empty vector and MCF10A cells expressing willin-HA (Figure 4.4). At low cell density, the proliferation rate was the same in MCF10A cells over-expressing willin-HA or an empty vector (Figure 4.4). At high cell density (confluency was reached 3-4 days post plating), the rate of cell proliferation was reduced in MCF10A cells over-expressing willin-HA compared to that of MCF10A cells expressing an empty vector control (Figure 4.4).

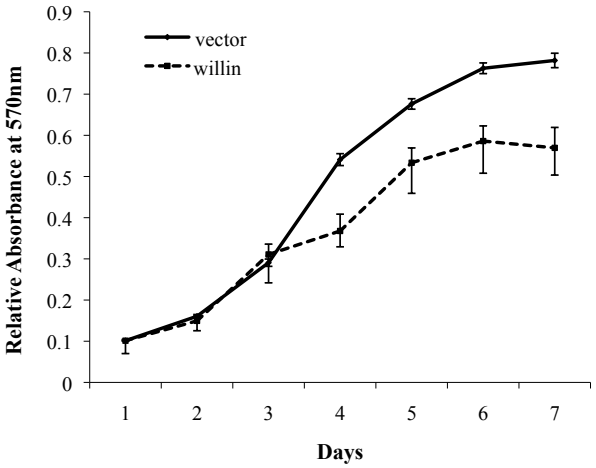

Figure 4.4: Willin expression in MCF10A cells (dashed line) reduced cell proliferation at high cell density. A MTT assay was performed on stable MCF10A-willinHA and MCF10A-vector cells as a measure of cell proliferation every 24 hours for 7 days. Error bars represent ± standard deviation.

To confirm that willin expression in MCF10A cells reduced proliferative growth at high cell density, the number of cells were counted using a haemocytometer. 2x10^6 MCF10A cells expressing willin-HA or an empty vector were plated out into 35mm dishes and the number of cells were counted every 24 hours for 5 days. Growth medium was replaced every 48 hours to prevent nutrient deprivation of the cells. A contact inhibition plateau in stable MCF10A cells expressing an empty vector was observed at ∼5x10^6 cells, whereas contact inhibition in MCF10A cells over-expressing willin-HA was observed at a lower cell number of ∼3x10^6 (Figure 4.5). This data supported previous observations from the MTT assay (Figure 4.4) that willin expression enhanced contact inhibition and reduced cell proliferation at high cell density.

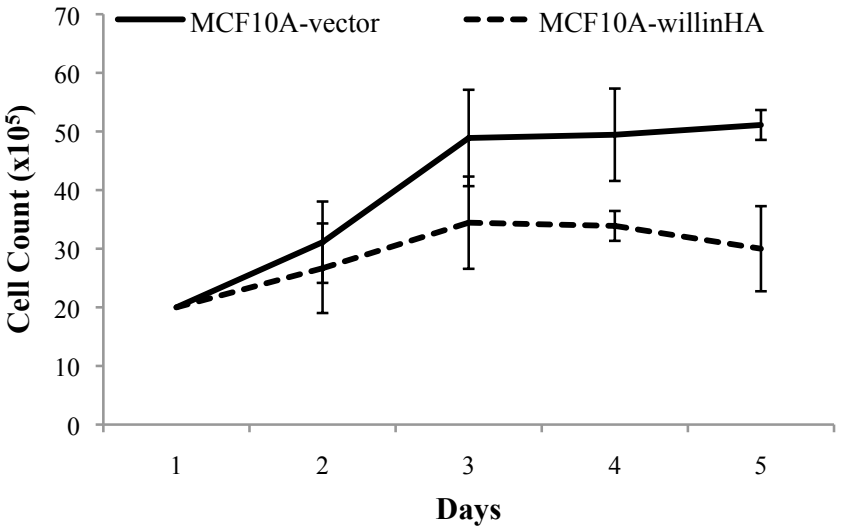

Figure 4.5: Willin expression slowed proliferation rate in MCF10A cells. 2x10^6 MCF10A cells over-expressing willin-HA or an empty vector were plated out into 35mm dishes and the number of cells were counted every 24 hours for 5 days. Less cells were counted in MCF10A cells expressing willin-HA (dashed line) when compared to MCF10A cells expressing an empty vector (solid line). Error bars represent ± standard deviation (n=6).

In human cells, LATS1/2 have been shown to affect cyclin E and cyclins A/B, inducing cell cycle arrest at G_1-S or G_2-M respectively (Xia et al., 2002; Li et al., 2003). The effect of willin on the cell cycle at high cell density was further investigated as willin expression reduced cell proliferation at high cell density. MCF10A cells were retrovirally transfected with pBabe-vector or pBabe-willin-HA vectors and plated into 35mm dishes. Cells were harvested at a high confluency, fixed with ethanol and stained with propidium

iodide for cell cycle analysis (Section 2.3.2). Willin expression in MCF10A cells resulted in a small G_1 arrest (Figure 4.6: t-test; $p<0.05$, $n=6$). Willin expression in MCF10A cells did not affect cell viability as stable MCF10A cells over-expressing willin-HA were successfully passaged and willin expression in MCF10A cells did not result in an increase of cells in the sub-G_1 phase of the cell cycle (Figure 4.6.A).

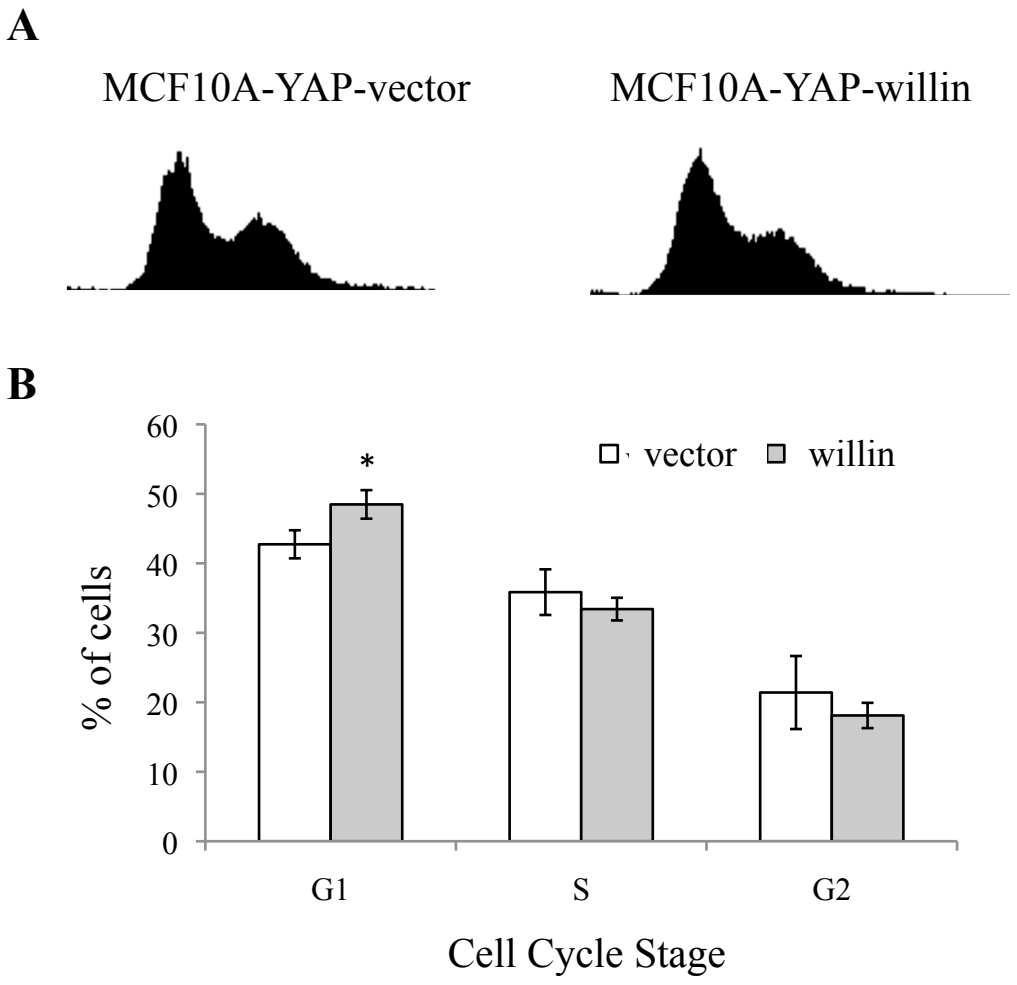

Figure 4.6: Willin expression in MCF10A cells resulted in a small G_1 arrest at high cell density. 10,000 MCF10A cells expressing either willin-HA or an empty vector were harvested at high cell density, fixed with ethanol, and stained with PI. **A)** The FACS histogram outputs show cell count on the y-axis and PI fluorescence intensity on the x-axis. **B)** Cell cycle histograms were analysed using Dako-cytometry software and the percentage of cells in G_1, S and G_2 phases of the cell cycle were calculated. Willin expression in MCF10A cells resulted in a small G_1 arrest (t-test; $p<0.05$, $n=6$*). Error bars represent ± standard deviation.

4.2.1.4 Willin expression modulates cellular migration

Hippo pathway components have been shown to inhibit cell migration at high cell densities (Zhao et al., 2007; Hao et al., 2008; Zhang et al., 2008a). Willin's ability to inhibit cell migration was therefore further investigated. MCF10A cells were retrovirally transfected with pBabe-willin-HA or pBabe-vector expression plasmids and migration through a Boyden chamber was measured. MCF10A cells were plated at either low ($5x10^5$) or high ($1x10^6$) cell density within the Boyden chamber and cell migration through the 8.0μm pores was measured 24 hours after plating. Figure 4.7 shows that the expression of willin-HA in MCF10A cells reduced cellular migration through a Boyden chamber by $\sim$ 25% at high cell density (t-test; $p<0.05$, n=3), whereas the reduction in cell migration upon expression of willin in MCF10A cells was not statistically significant at low cell density (t-test; $p>0.05$, n=3).

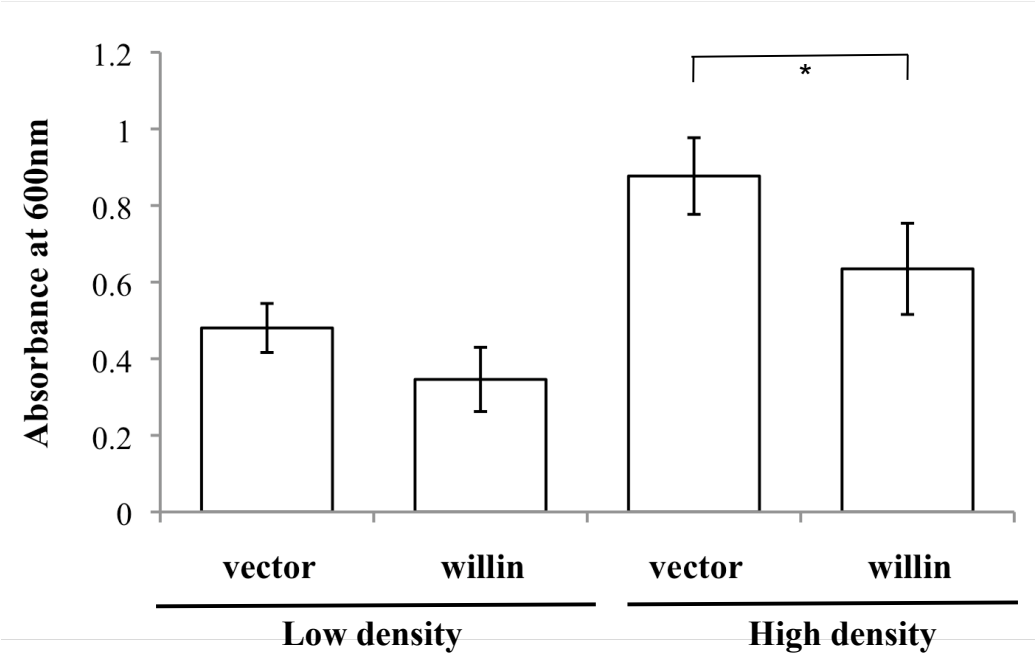

Figure 4.7: Willin expression in MCF10A cells reduced cell migration. MCF10A cells over-expressing willin-HA or an empty vector were seeded into a Boyden chamber at low ($5x10^5$) and high ($1x10^6$) cell density. Cell migration though a Boyden chamber was measured 24 hour after plating. No significant reduction in migration was observed at low cell density (t-test; $p>0.05$, n=3). However, willin expression in MCF10A reduced cell migration significantly at high cell density (t-test; $p<0.05$, n=3*). Error bars represent ± standard deviation.

4.2.2 Expression of willin and its FERM domain can antagonises a YAP-induced EMT phenotype in MCF10A cells

Hippo pathway components have been shown to antagonise a YAP-induced EMT phenotype, resulting in functional downstream changes in anchorage-independent growth, cell migration, adhesion as well as changes in epithelial and mesenchymal markers (Overholtzer et al., 2006; Zhao et al., 2007; Hao et al., 2008; Zhang et al., 2008a, 2009b). Further studies were performed to investigate whether full-length willin and its conserved FERM domain were sufficient to negatively regulate an oncogenic YAP-induced EMT phenotype in MCF10A cells: reducing cell migration and anchorage independent growth, and enhancing cell adhesion.

4.2.2.1 Cloning and expression of the FERM and C-terminal domain of willin

To investigate whether the conserved FERM domain of willin was sufficient to antagonise a YAP-induced EMT phenotype, both the FERM and the C-terminal domain of willin were cloned into a pBabe(puro) expression vector and expressed in MCF10A cells over-expressing YAP. The amino acid and DNA nucleotide sequences of the defined FERM and C-terminal domains of willin are shown in Figure 4.8.

Using PCR, the FERM and C-terminal domains of willin were amplified from a willin-GFP plasmid using primers (FERM domain: *FERM-F & FERM-R*; C-terminal domain: *Cterm-F & Cterm-R2*. See Table 2.1 for primer sequence) that contained a *BamH*1 and *EcoR*1 restriction site at the 5' and 3' end respectively. A hemagglutinin tag (HA: YPYDVPDYA) was incorporated into the reverse primer so that cloned FERM and C-terminal plasmids were C-terminally tagged with HA. A restriction digest using *BamH*1 and *EcoR*1 enzymes was performed on the PCR inserts and the pBabe-puro vector. The FERM and C-terminal domain PCR products were ligated into a pBabe vector and constructs were named pBabe-FERM and pBabe-Cterm respectively (Figure 4.9). The DNA Sequencing Service (University of Dundee, UK) confirmed that unmutated FERM and C-terminal domains of willin, C-terminally tagged with HA, were cloned into a pBabe(puro) expression vector.

Amino acid sequence:

MNKLNFHNNRVMQDR**RSVCIFLPNDESLNIIINVKILCHQLLVQVCDLLRLKDCHLFGLSVI**
QNNEHVYMELSQKLYKYCPKEWKKEASKGIDQFGPPMIIHFRVQYYVENGRLISDRAARYYY
YWHLRKQVLHSQCVLREEAYFLLAAFALQADLGNFKRNKHYGKYFEPEAYFPSWVVSKRGKD
YILKHIPNMHKDQFALTASEAHLKYIKEAVRLDDVAVHYYRLYKDKREIEASLTLGLTMRGI
QIFQNLDEEKQLLYDFPWTNVGKLVFVGKKFEILPDGLPSARKLIYYTGCPMRSRHLLQLLS
NSHRLYMNLQPVLRHIRKLEENEEKKQYRESYISDNLDLDMDQLEKRSRASGSSAGSMKHKR
LSRHSTASHSSSHTSGIEADTKPRDTGPEDSYSSSAIHRKLKTCSSMTSHGSSHTSGVESGG
KDRLEEDLQDDEIEMLVDDPRDLEQMNEESLEVSPDMCIYITEDMLMSRKLNGHSGLIVKEI
GSSTSSSSETVVKLRGQSTDSLPQTICRKPKTSTDRHSLSLDDIRLYQKDFLRIAGLCQDTA
QSYTFGCGHELDEEGLYCNSCLAQQCINIQDAFPVKRTSKYFSLDLTHDEVPEFVVstop

Nucleotide sequence:

atgaacaaattgaattttcataacaacagagtcatgcaagaccgc***cgcagtgtgtgcatttt***
ccttcccaacgatgaatctctgaacatcatcataaatgttaagattctgtgtcaccagttgc
tggtccaggtttgtgacctgctcaggctaaaggactgccacctctttggactcagtgttata
caaaataatgaacatgtgtatatggagttgtcacaaaagctttacaaatattgtccaaaaga
atggaagaaagaggccagcaagggtatcgaccaatttgggcctcctatgatcatccacttcc
gtgtgcagtactatgtggaaaatggcagattgatcagtgacagagcagcaagatactattat
tactggcacctgagaaaacaagttcttcattctcagtgtgtgctccgagaggaggcctactt
cctgctggcagcctttgccctgcaggctgatcttgggaacttcaaaaggaataagcactatg
gaaaatacttcgagccagaggcttacttcccatcttgggttgtttccaagaggggaaggac
tacatcctgaagcacattccaaacatgcacaaagatcagtttgcactaacagcttccgaagc
tcatcttaaatatatcaaagaggctgtccgactggatgacgtcgctgttcattactacagat
tgtataaggataaaagggaaattgaagcatcgctgactcttggattgaccatgaggggaata
cagattttcagaatttagatgaagagaaacaattactttatgatttcccctggacaaatgt
tggaaaattggtgtttgtgggtaagaaatttgagattttgccagatggcttgccttctgccc
ggaagctcatatactacacggggtgccccatgcgctccagacacctcctgcaacttctgagc
aacagccaccgcctctatatgaatctgcagcctgtcctgcgccatatccggaagctggagga
aaacgaagagaagaagcagtaccgggaatcttacatcagtgacaacctggacctcgacatgg
accagctggaaaaacggtcgcgggccagcgggagcagtgcgggcagcatgaaacacaagcgc
ctgtcccgtcattccaccgccagccacagcagttcccacacctcgggcattgaggcagacac
caagccccgggacacggggccagaagacagctactccagcagtgccatccaccgcaagctga
aaacctgcagctcaatgaccagtcatggcagctcccacacctcaggggtggagagtggcggc
aaagaccggctggaagaggacttacaggacgatgaaatagagatgttggttgatgacccccg
ggatctggagcagatgaatgaagagtctctggaagtcagcccagacatgtgcatctacatca
cagaggacatgctcatgtcgcggaagctgaatggacactctgggttgattgtgaaagaaatt
gggtcttccacctcgagctcttcagaaacagttgttaagcttcgtggccagagtactgattc
tcttccacagactatatgtcggaaaccaaagacctccactgatcgacacagcttgagcctcg
atgacatcagactttaccagaaagacttcctgcgcattgcaggtctgtgtcaggacactgct
cagagttacacctttggatgtggccatgaactggatgaggaaggcctctattgcaacagttg
cttggcccagcagtgcatcaacatccaagatgcttttccagtcaaaagaaccagcaaatact
tttctctggatctcactcatgatgaagttccagagtttgttgtgtaa

Figure 4.8: Amino acid and DNA nucleotide sequence of full-length willin. The N-terminal FERM domain sequence of willin is underlined and in bold. The underlined FERM domain was cloned into pBABE vector. The sequence located at the 3' end of the FERM domain to the stop codon was also cloned into the pBabe-puro vector and was termed the C-terminal domain of willin.

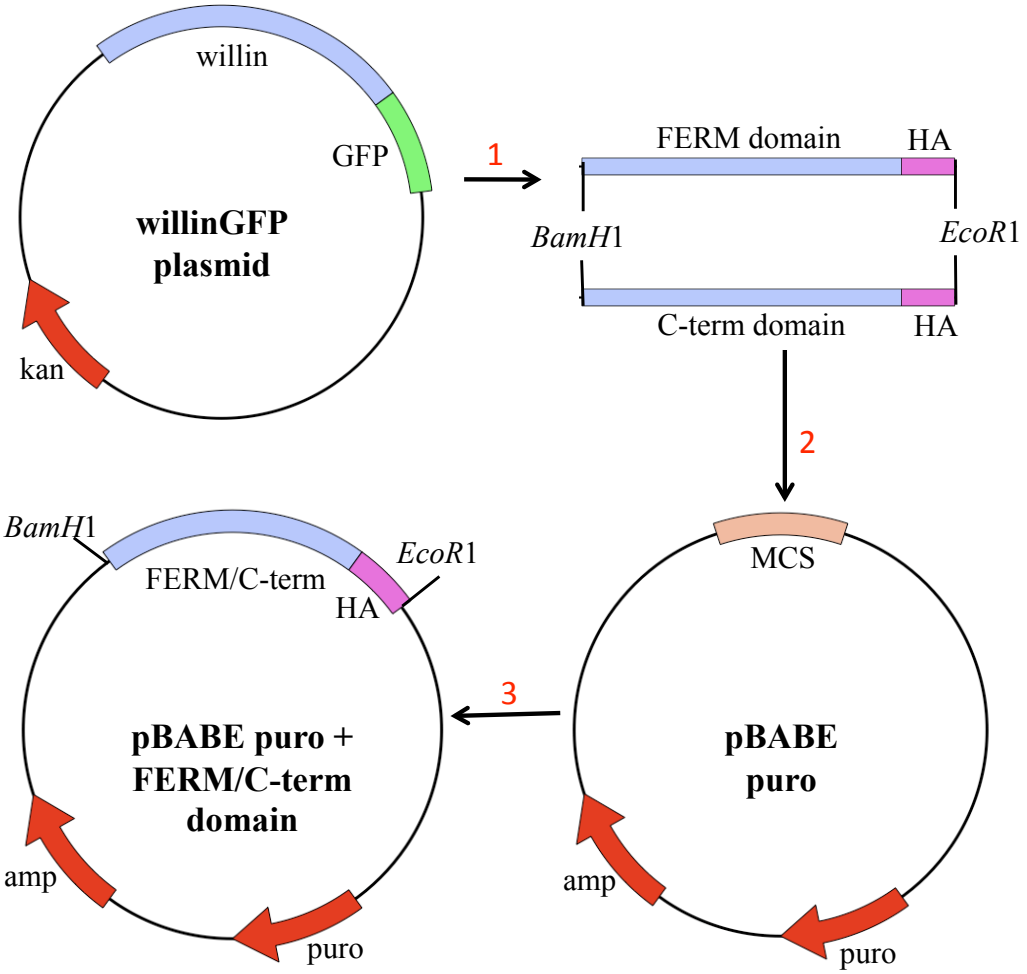

Figure 4.9: Schematic diagram of molecular cloning techniques performed to construct pBabe-FERM and pBabe-Cterm expression plasmids. PCR was conducted on the willin-GFP plasmid using *FERM-F & FERM-R* or *Cterm-F & Cterm-R2* primers to produce a FERM and C-terminal fragment with *BamH1* and *EcoR1* restriction sites at the 5' and 3' end respectively (1). A restriction digest was performed using *BamH*1 and *EcoR*1 enzymes on both the PCR inserts and pBabe-puro so that the PCR fragments could be cloned into the multiple cloning site (MCS) of the pBabe vector (2). The PCR fragments were ligated into the pBabe vector and constructs were named pBabe-FERM and pBabe-Cterm (3).

pBabe-willin-HA, pBabe-FERM, pBabe-Cterm and pBabe-vector were retrovirally transfected into MCF10A cells over-expressing YAP-FLAG (kind gift from Dr. D. Haber, Harvard University, USA). Stable cell lines were created by 2μg/ml puromycin selection. Immunoblot analysis confirmed that full-length willin, the FERM and the C-terminal domain of willin were expressed in the MCF10A-YAP cell lines created (Figure 4.10).

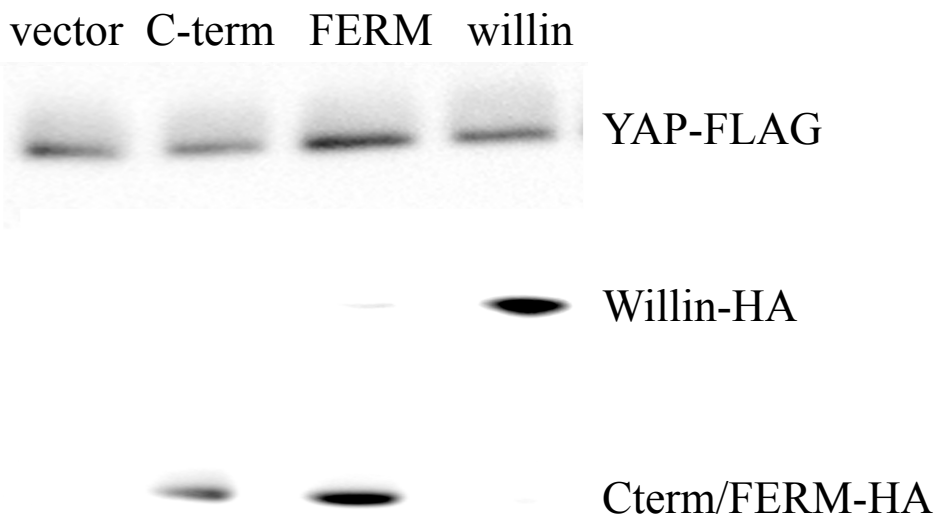

Figure 4.10: MCF10A-YAP stable cell lines were created over-expressing an empty vector, full-length willin, the FERM domain or the C-terminal domain of willin. Whole cell lysates were collected from MCF10A-YAP (YAP-FLAG) stable cell lines created to express either willin-HA, FERM-HA or the C-terminal-HA domain of willin. Lysates were run on a 10% SDS gel and the nitrocellulose membrane was probed with anti-FLAG and high affinity anti-HA antibody, to detect YAP and willin expression respectively.

4.2.2.2 Willin expression results in a morphological change in MCF10A-YAP cells

A mesenchymal-like phenotype of MCF10A-YAP cells was reverted back to a more epithelial-like phenotype when full-length willin and the FERM domain of willin were expressed in MCF10A-YAP cells (Figure 4.11). The mesenchymal-like phenotype of MCF10A cells remained unchanged when an empty vector or the C-terminal domain of willin were retrovirally transfected

into MCF10A-YAP cells (Figure 4.11). Expression of full-length willin and its FERM domain resulted in cellular morphological alternations, where the morphology of a cell changed from a spindle-shaped mesenchymal appearance with increased scattering to more uniform and polarised epithelial appearance (Figure 4.11).

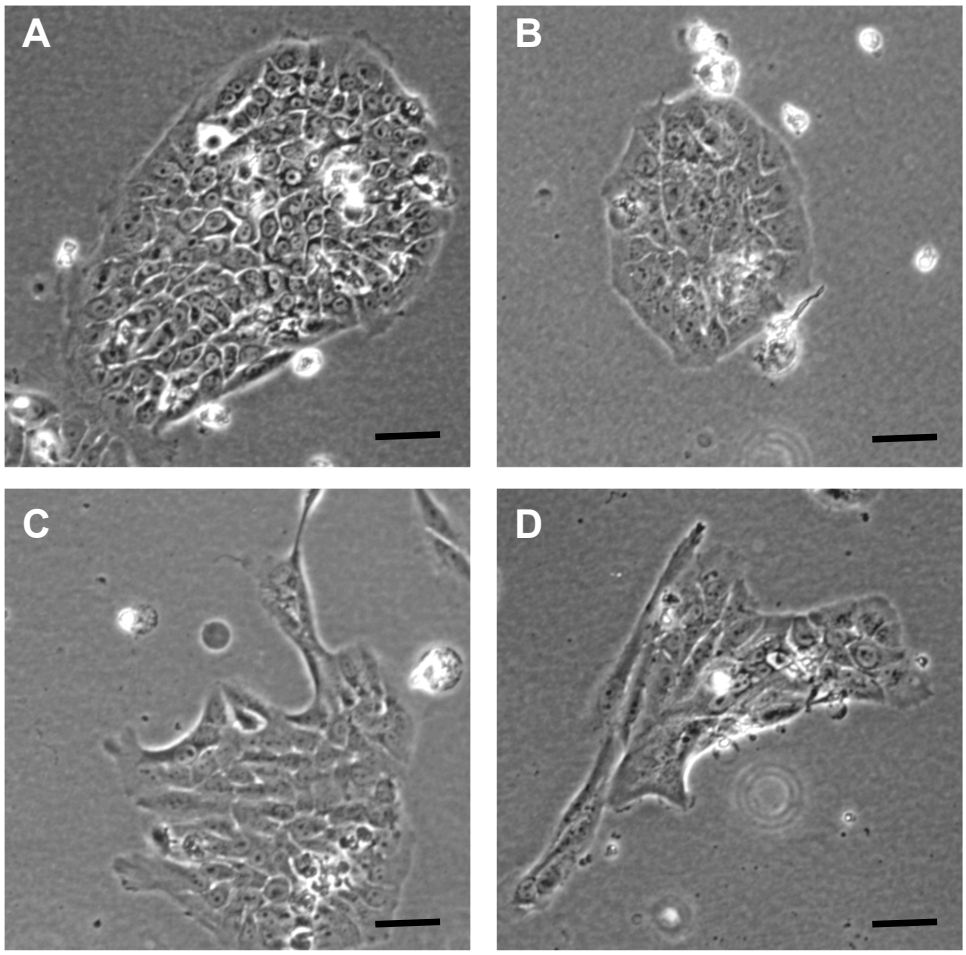

Figure 4.11: Willin and FERM expression antagonised a YAP-induced EMT morphological phenotype. Brightfield images were taken of MCF10A-YAP cells expressing either full-length willin (**A**), the FERM domain of willin (**B**), the C-terminal domain of willin (**C**) or an empty vector (**D**). A more epithelial-like phenotype was observed when MCF10A-YAP cells expressed full-length willin or the FERM domain of willin, while a more mesenchymal-like morphology was observed when cells expressed the C-terminal domain of willin or an empty vector. $Bar = 50\mu$m.

Susana Moleirinho, a Ph.D. student in our lab, showed that the levels of mesenchymal and epithelial markers varied between MCF10A-YAP cells expressing an empty vector or full-length willin, confirming the morphological EMT phenotype observations shown in Figure 4.11. Expression of willin-HA in MCF10A cells resulted in a decrease of the mesenchymal marker vimentin and N-cadherin and an increase in the epithelial marker occludin and E-cadherin (Figure 4.12).

To further investigate that the EMT changes observed were due to activation of the Hippo pathway converging through phosphorylation of the Ser127 YAP site, a mutant MCF10A-YAP(S127A) cell line was created. Susana Moleirinho retrovirally transfected MCF10A-YAP(S127A) cells with a pBabe-vector or pBabe-willin-HA expression plasmids. Immunoblot analysis showed that no changes in either epithelial (E-cadherin and occludin) or mesenchymal (vimentin and N-cadherin) markers were observed when willin-HA or an empty vector were expressed in MCF10A-YAP(S127A) cells (Figure 4.12).

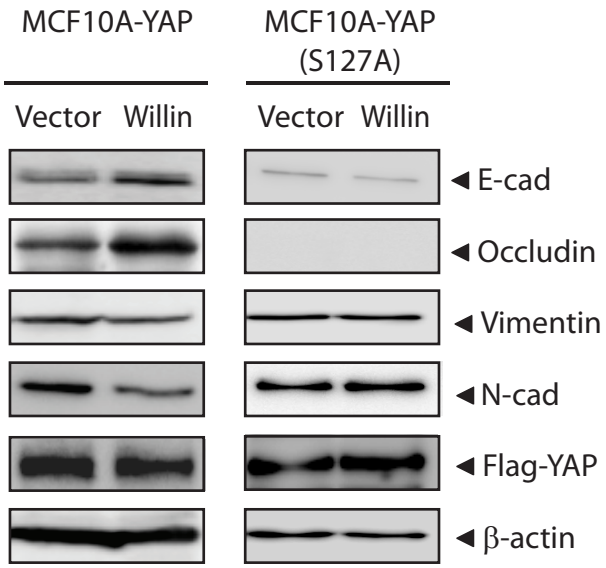

Figure 4.12: Willin expression antagonised a YAP-induced EMT phenotype in MCF10A cells. Whole cell lysates were collected of MCF10A-YAP or MCF10A-YAP(S127A) cells over-expressing vector or willin-HA and run on a 10% SDS gel. The nitrocellulose membrane was probed with epithelial (E-cad and occludin) and mesenchymal antibodies (vimentin and N-cad). Immunoblots show increased E-cadherin, occludin and decreased vimentin, N-cadherin in MCF10A-YAP cells expressing willin, but no changes were observed between MCF10A-YAP(S127A) cells expressing willin and an empty vector control. Work done by Susana Moleirinho.

4.2.2.3 Expression of willin and its FERM domain reduces anchorage-independent growth

Stable MCF10A-YAP cells over-expressing either an empty vector, full-length willin, FERM or the C-terminal domain of willin were seeded and grown in soft-agar to measure anchorage-independent growth. The number of colonies, defined as 5 or more cells, were counted 2 and 3 weeks after plating. The experiment was conducted as a double-blind study to reduce counting bias. Brightfield images in Figure 4.13.A show that the colony sizes observed in MCF10A-YAP cells over-expressing the FERM domain of willin and full-length willin was different to the colony sizes observed in MCF10A-YAP cells over-expressing an empty vector or the C-terminal domain of willin. Colony sizes were larger in MCF10A-YAP cells expressing an empty vector and the C-terminal domain of willin compared to MCF10A-YAP cells that were expressing willin and the FERM domain of willin (Figure 4.13.A).

In addition to cell colony size differences, variations in the total number of colonies formed in MCF10A-YAP cells over-expressing full-length willin and the FERM domain of willin were observed when compared to MCF10A-YAP cells over-expressing the C-terminal domain of willin or an empty vector (Figure 4.13.B). A $\sim$50% reduction in colony formation was observed, both 2 and 3 weeks after plating, when either full-length willin or the FERM domain of willin was over-expressed in MCF10A-YAP cells, compared to MCF10A-YAP cells that expressed an empty vector (Figure 4.13.B; t-test, $p<0.01$, $n=6$). Expression of the C-terminal domain of willin in MCF10A-YAP cells did not alter the cells ability to grow in soft agar when compared to MCF10A control cells expressing an empty vector (Figure 4.13B; t-test; $p>0.05$, $n=6$). Two weeks post-seeding, a slight trend was observed where the FERM domain of willin seemed to have a stronger effect on the ability to inhibit anchorage-independent growth than full-length willin; however this effect was not statistically significant (Figure 4.13B; t-test, $p>0.05$, $n=6$).

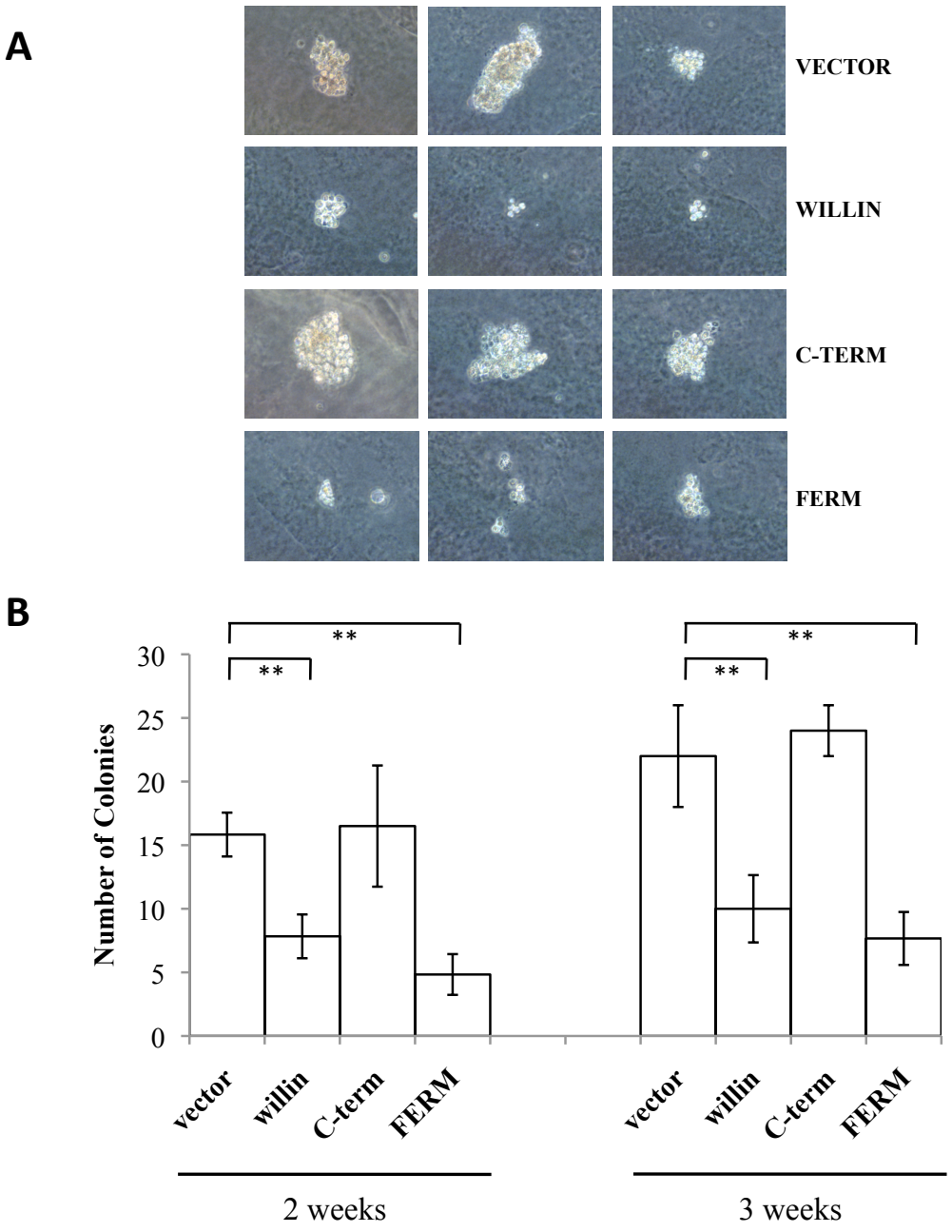

Figure 4.13: Expression of willin and its FERM domain reduced anchorage-independent growth. Stable MCF10A-YAP cells over-expressing either an empty vector, full-length willin, the FERM or the C-terminal domain of willin were grown in soft-agar. **A**) Brightfield images taken of formed colonies. Colony sizes were larger in MCF10A-YAP cells expressing an empty vector and the C-terminal domain of willin compared to MCF10A-YAP cells that expressed full-length willin and its FERM domain. **B**) Number of colonies (>5 cells) were counted 2 and 3 weeks after plating. Expression of willin and its FERM domain significantly reduced anchorage-independent growth in MCF10A-YAP cells compared to MCF10A-YAP cells that expressed an empty vector or the C-terminal domain of willin (t-test; $p<0.01$, n=6**). Error bars represent ± standard deviation.

4.2.2.4 Expression of willin and its FERM domain reduces cell migration

Previous studies have shown that YAP over-expression in MCF10A cells results in an increase in cell migration (Overholtzer et al., 2006; Zhao et al., 2007). To investigate the negative regulation on YAP by willin, cell migration was measured using both a wound healing scratch assay and a Boyden chamber assay.

Stable MCF10A-YAP cells over-expressing an empty vector, full-length willin, the FERM domain and the C-terminal domain of willin were plated out onto 35mm dishes. Once the dishes were confluent, a scratch was made using the end of a yellow tip and brightfield images were taken after the scratch was made 24 hours post wound formation. Representative brightfield images of the wound healing assay for MCF10A-YAP cells over-expressing an empty vector, full-length willin, the FERM and the C-terminal domain of willin are shown in Figure 4.14.A. The percentage of scratch covered with cells was measured using image J, 24 hours post wound formation. Cell migration was reduced by ∼50% when MCF10A-YAP cells over-expressed full-length willin and its truncated FERM domain compared to MCF10A-YAP that expressed an empty vector (Figure 4.14.B; t-test: $p<0.01$, n=9). Expression of the C-terminal domain of willin in MCF10A-YAP cells did not affect cell migration when compared to the empty vector control (Figure 4.14.B; t-test: $p>0.05$, n=9).

A second migration assay was conducted to confirm that the expression of willin and its FERM domain reduced cell migration. MCF10A-YAP cells expressing an empty vector, full-length willin, FERM or the C-terminal domain of willin were plated into Boyden chambers. 24 hours after incubation, the number of cells migrated through the 8.0μm pores in the chamber were measured. Consistent with data obtained for the scratch assay, cell migration through a Boyden chamber was reduced by ∼50% when MCF10A-YAP cells over-expressed full-length willin and its truncated FERM domain compared to MCF10A-YAP cells that expressed an empty vector (Figure 4.15; t-test: $p<0.01$, n=3). Furthermore, expression of the C-terminal domain of willin in MCF10A-YAP cells did not affect cell migration when compared to the empty vector control (Figure 4.15; t-test: $p>0.05$, n=3).

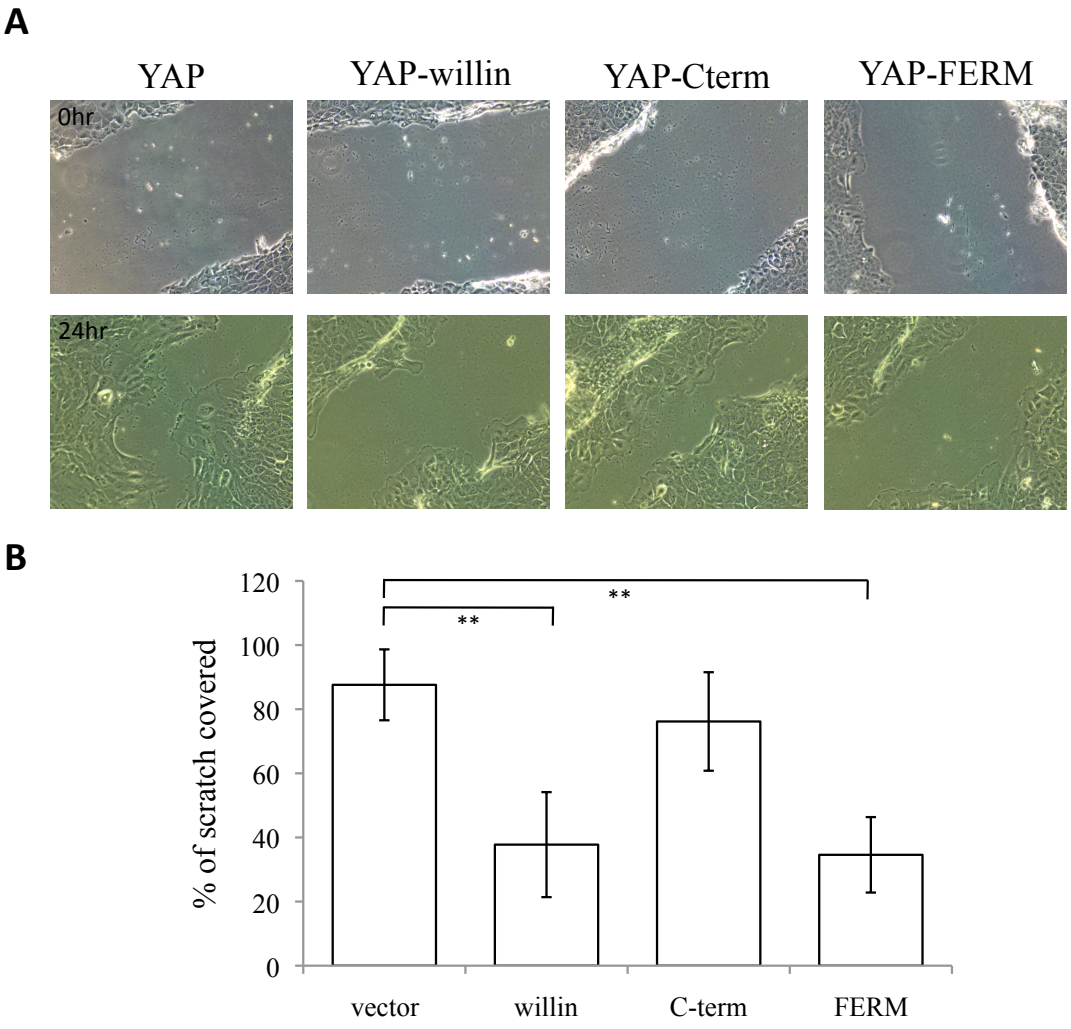

Figure 4.14: Expression of willin and its FERM domain in MCF10A-YAP cells reduced cell migration. A scratch was made with a yellow pipette tip in confluent MCF10A-YAP cells expressing an empty vector, full-length willin, the FERM or the C-terminal domain of willin. **A**) Brightfield images were taken before and 24 hours after the scratch was made. **B**) The percentage of the scratch covered after 24 hours was measured using Image J software. Expression of willin and its FERM domain in MCF10A-YAP cells significantly reduced cell migration when compared to MCF10A cells that expressed an empty vector or the C-terminal domain (t-test; $p<0.01$, $n=9^{**}$). Error bars represent ± standard deviation.

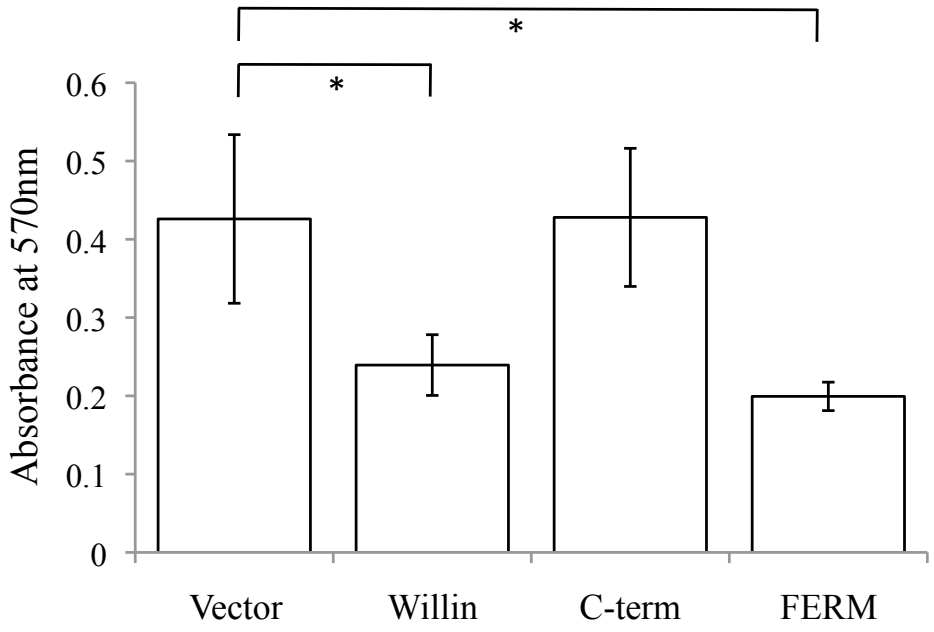

Figure 4.15: Expression of willin and its FERM domain reduced cell migration through a Boyden chamber. MCF10A-YAP cells expressing an empty vector, full-length willin, the FERM or the C-terminal domain of willin were plated into Boyden chambers. 24 hours after incubation, the number of cells migrated through the chamber were fixed and stained with crystal violet (CV). The CV dye was extracted and measured at a wavelength of 570nm. Expression of willin and the FERM domain of willin significantly reduced cell migration through a Boyden chamber (t-test; $p<0.05$, n=3*). Error bars represent ± standard deviation.

4.2.2.5 Expression of willin and its FERM domain enhances cell adhesion

During cell culture maintenance, it was noted that MCF10A-YAP cells over-expressing full-length willin and the FERM domain of willin took twice as long to trypsinise compared to MCF10A-YAP cells over-expressing an empty vector or the C-terminal domain of willin. Taking together this observation and the fact that changes in cell adhesion is a hallmark of EMT, the ability of willin to affect cell adhesion was further investigated.

Stable MCF10A-YAP cells expressing an empty vector, full-length willin, the FERM or the C-terminal domain of willin were seeded onto a laminin coated 96 well plate. After a 30 minute incubation, an adhesion assay was performed and the number of cells adherent to the laminin plate were fixed and counted (Section 2.3.11). Expression of full-length willin and its truncated

FERM domain enhanced cell adhesion to a laminin-coated dish, by a 1.6-1.8 fold respectively, compared to MCF10A-YAP cells that expressed an empty vector (Figure 4.16: t-test; $p<0.05$ n=4). The truncated C-terminal domain of willin had no effect on cell adhesion when compared to MCF10A-YAP cells that expressed an empty vector (Figure 4.16: t-test; $p>0.05$, n=4).

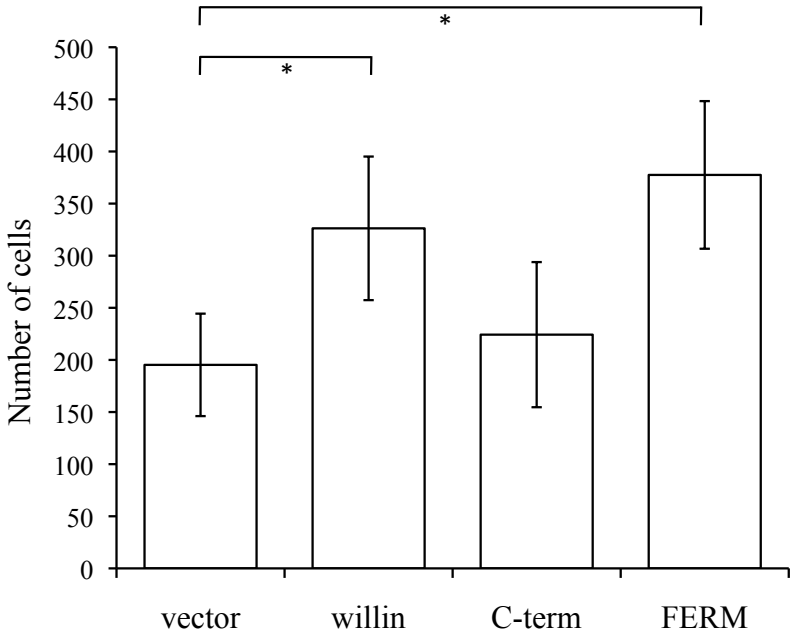

Figure 4.16: Expression of willin and its FERM domain enhanced cell adhesion. An adhesions assay was performed on stable MCF10A-YAP cells expressing either an empty vector, full-length willin, the FERM or the C-terminal domain of willin. Number of cells adherent to laminin-coated dishes, after adhesion assay was performed, was increased in MCF10A-YAP cells expressing both full-length willin and the FERM domain of willin when compared to MCF10A cells over-expressing an empty vector (t-test; $p<0.05$, n=4*). Error bars represent ± standard deviation.

4.2.3 The FERM domain of willin increases phosphorylation of MST1/2, LATS1 and YAP

As the FERM domain of willin can antagonise a YAP-induced phenotype, with observed changes in cell migration, adhesion and anchorage-independent growth, experiments were conducted to investigate whether the FERM domain of willin could activate the core Hippo pathway components. As investigations into phosphorylation of the core Hippo pathway components had to be performed at low cell density, transfection into HEK-293 cells were preferred over

the longer retroviral transfection method required for MCF10A cells.

HEK-293 cells were plated at low cell density and were transiently transfected with pBabe-willin-HA, pBabe-FERM, pBabe-Cterm or pBabe-vector. Whole cell lysates were collected 48 hours post-transfection and run on a 10% SDS gel. The nitrocellulose membrane was probed with antibodies detecting both total and phosphorylated core Hippo pathway components: MST1/2, LATS1 and YAP. Immunoblot analysis showed that an increased phosphorylation of MST1/2, LATS1 and YAP was observed when HEK-293 cells expressed full-length willin or its truncated FERM domain (Figure 4.17). Expression of the C-terminal domain of willin in HEK-293 cells did not result in phosphorylation changes of MST1/2, LATS1 and YAP when compared to an empty vector control (Figure 4.17).

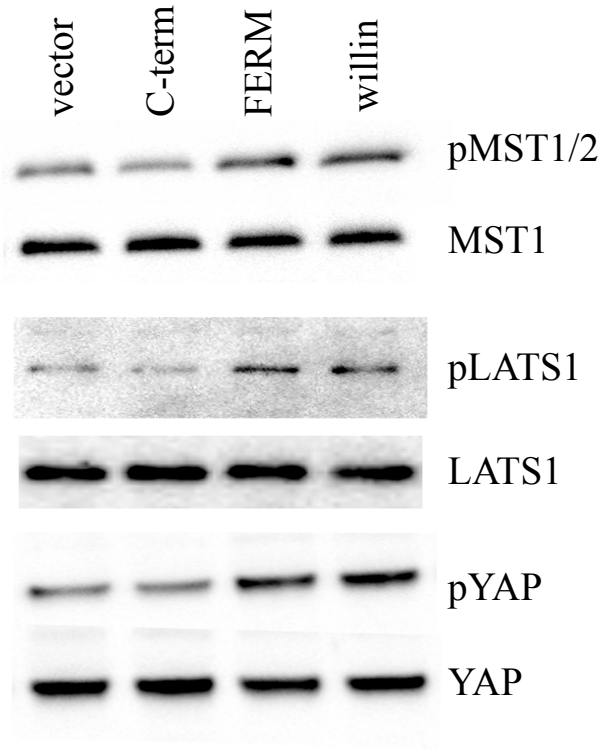

Figure 4.17: Expression of full-length willin and its FERM domain resulted in an increased phosphorylation of core Hippo components: MST1/2, LATS1 and YAP. HEK-293 cells were transfected with either an empty vector, willin-HA, FERM-HA or Cterm-HA expression plasmids. Whole cell lysates were collected 48 hours post-transfection and run on a 10% SDS gel. The nitrocellulose membrane was probed with core Hippo pathway antibodies; pMST1/2, MST1, pLATS1, LATS1, pYAP and YAP.

4.2.4 Expression of willin and its FERM domain negatively regulate YAP target gene expression

Hao et al. (2008) have recently reported genes, involved in cell proliferation, migration and adhesion, that are either up- or down-regulated by YAP and are negatively regulated by LATS1. qPCR analysis was conducted to see if willin could be a negative regulator of YAP by affecting the regulation of some of the genes listed to be affected by YAP: PRL, IGFB3, BMP2 (Hao et al., 2008) and RASSF8. The RASSF8 gene was chosen as a prospective regulator of willin as it has previously been shown to be a potential binding partner of willin (Rual et al., 2005). qPCR analysis was performed on stable MCF10A-YAP cells over-expressing an empty vector, full-length willin, the FERM or the C-terminal domain of willin. Expression of full-length willin and its conserved FERM domain altered the expression of YAP gene targets: increasing BMP2 and RASSF8; and decreasing PRL and IGFBP3 RNA levels (Table 4.1, Figure 4.18; t-test; $p<0.01$, $n=5$). Expression of the C-terminal domain of willin did not result in changes in total RNA levels of YAP downstream targets when compared to MCF10A-YAP cells expressing an empty vector (Figure 4.18; t-test; $p>0.05$).

Gene name	Accession #	Description
Down-regulated		
PRL	NM000948	Prolactin
IGFBP3	NM001013398	Insulin growth factor-binding protein 3
Up-regulated		
BMP2	NM001200	Bone morphogenetic protein 2
RASSF8	NM001164746	Ras association domain family 8

Table 4.1: List of genes up-regulated and down-regulated by the expression of willin and the FERM domain of willin in MCF10A-YAP cells.

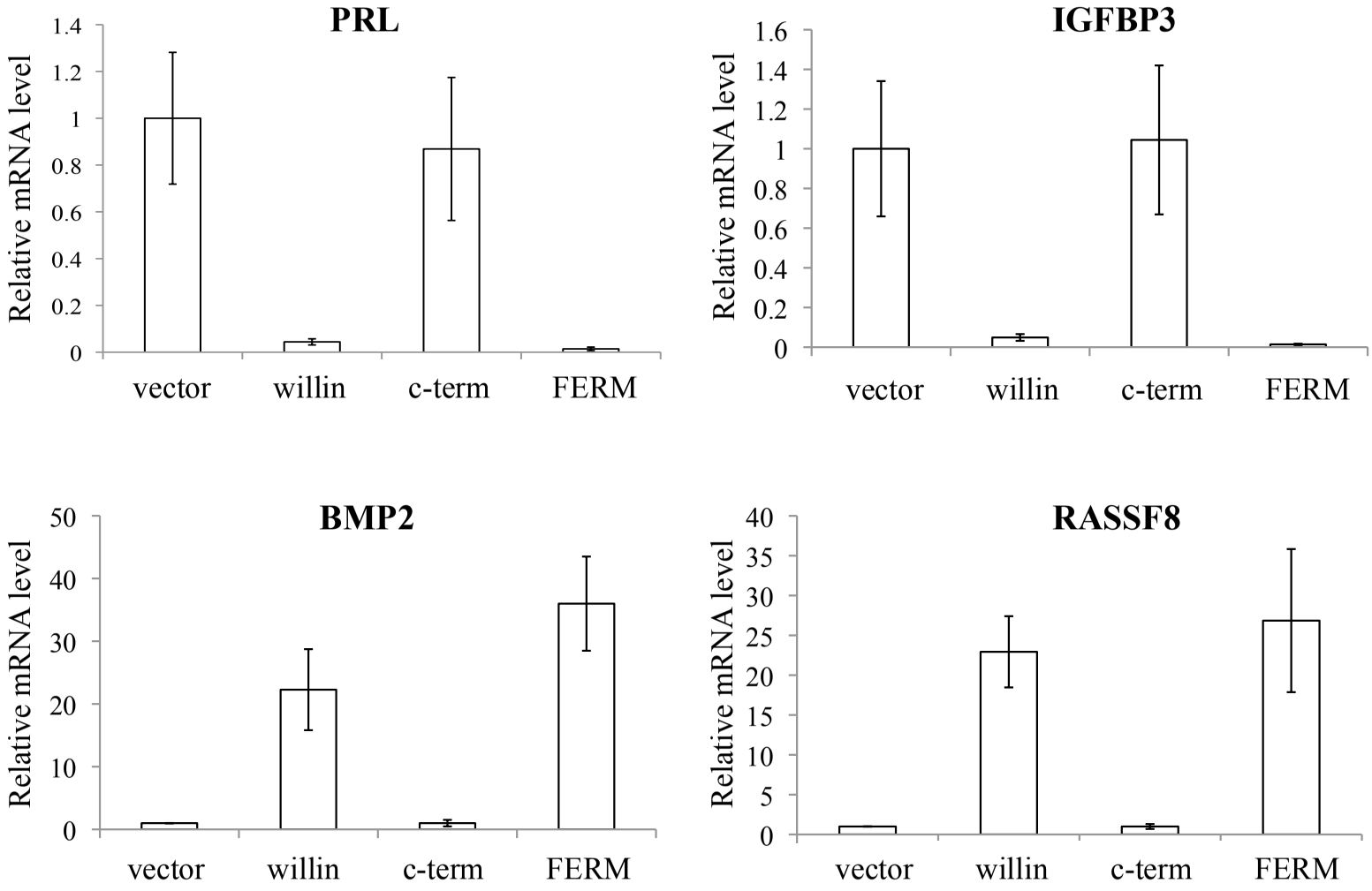

Figure 4.18: Expression of willin and its FERM domain antagonised YAP target proteins. qPCR analysis was performed on known YAP downstream targets: PRL, IGFBP3, BMP2 and RASSF8. Expression of willin and its FERM domain in MCF10A-YAP cells significantly decreased RNA levels of PRL and IGFBP3, and increased RNA levels of BMP2 and RASSF8 (t-test; $p<0.01$, $n=5$). Error bars $\pm$ represent standard deviation.

4.3 Discussion

4.3.1 Willin expression activates the Hippo pathway cassette in MCF10A cells

Willin's ability to activate the Hippo pathway is not exclusive to HEK-293 cells, as willin expression in MCF10A cells leads to an increase in phosphorylation of MST1/2, LATS1 and YAP, which further resulted in downstream YAP nuclear exit. Future studies should focus on willin's ability to antagonise YAP in different cell types, as YAP has also been reported to function as a tumour suppressor, rather than a oncogene, in MDA-231 breast cell line (Yuan et al., 2008). The function of willin may therefore be cell-specific.

4.3.2 Willin expression enhances contact inhibition

The Hippo tumour suppressor pathway regulates organ size and tumourigenesis through activation of the cascade at high cell densities to inhibit cell proliferation. Consistent with data that showed that Hippo pathway components reduce cell proliferation (Camargo et al., 2007; Dong et al., 2007; Zhao et al., 2007), willin expression in MCF10A cells enhanced contact inhibition; reducing cell proliferative rate and migratory capacity at high cell density, whereas the cell proliferation rate and migration at low cell density remained unchanged to wild-type MCF10A cells (Section 4.2.1). Whether the change in proliferation rate is due to activation of the Hippo pathway or alternative signalling cascades remains unclear and requires further investigation.

Core Hippo pathway components have been found to affect the cell cycle. In human cells, LATS1/2 have been shown to affect cyclin E and cyclins A/B, inducing cell cycle arrest at G_1-S or G_2-M respectively (Xia et al., 2002; Li et al., 2003). At high cell density, willin expression in MCF10A cells resulted in a slight but significant cell cycle arrest at G_1 (Section 4.2.1.3). This G_1 cell cycle arrest may have been enhanced if cells were synchronised before cell cycle analysis was performed. Congruous with willin expression in HEK-293 cells, willin expression in MCF10A cells did not result in cell death as stable cell lines were successfully passaged and no increase in cells in sub-G_1 phase of the cell cycle was observed.

4.3.3 Willin expression antagonises a YAP induced EMT phenotype

The induction of EMT by YAP over-expression is consistent with an emerging concept of EMT inducers as oncogenes. The loss of contact inhibition by cells over-expressing YAP and the gain of anchorage-independent growth in soft agar are hallmarks of cancer cells *in-vitro* (Hanahan and Weinberg, 2000). A protein that antagonises the YAP-induced phenotype may therefore have tumour suppressive properties. Upstream Hippo components have previously been confirmed to negatively regulate YAP in human cell lines (Overholtzer et al., 2006; Zhao et al., 2007; Hao et al., 2008; Zhang et al., 2008a, 2009b). In addition, ectopic willin expression antagonised a YAP-induced EMT phenotype in MCF10A cells, in terms of changes in functional outputs of anchorage-independent growth, adhesion and migration, but also in EMT marker expression changes.

Willin expression in MCF10A-YAP cells resulted in morphological cell alteration from a spindle-shaped mesenchymal-like appearance with increased scattering to more uniform and polarised epithelial-like phenotype (Section 4.2.2). EMT markers confirmed a mesenchymal-epithelial transition when willin was expressed in MCF10A-YAP cells, with a decrease in N-cadherin levels and a production of E-cadherin. The presence of E-cadherin in epithelial cells allows for greater cell-cell adhesive strength compared with that of a N-cadherin expressing mesenchyme (Chu et al., 2004, 2005). Regular shaped cell-cell junctions and adhesion between neighbouring epithelial cells holds them tightly together and inhibits the movement of individual cells away from the epithelial monolayer. The EMT reversion in MCF10A-YAP cells by willin expression therefore resulted in an increased cell adhesion and decreased cell migratory capacity and anchorage-independent growth.

Furthermore, willin expression did not result in changes to EMT marker expression in cells expressing a constitutively active YAP mutant (MCF10A-YAP-S127A), demonstrating that the downstream antagonistic EMT effects of willin on YAP were via YAP's Ser127 phosphorylation site. Other studies, conducted by Susana Moleirinho, confirmed that the inhibition of anchorage-independent growth and cell migration by over-expression of willin in MCF10A-YAP cells was due to willin's downstream effects converging onto the YAP Ser127 phosphorylation site.

4.3.4 FERM domain of willin activates the Hippo pathway

The conserved FERM domain of willin was sufficient, and as efficient as full-length willin, to antagonise a YAP-induced EMT phenotype in MCF10A cells whereas the C-terminal domain of willin could not (Section 4.2.3). In addition to antagonising a YAP-induced EMT phenotype in MCF10A cells (changing cell migration, adhesion and anchorage-independent growth), the expression of the FERM domain of willin resulted in an increase in phosphorylation of MST1/2, LATS1 and YAP in HEK-293 cells. The FERM domain contains a motif that is able to activate the Hippo kinase complex, whether the FERM domain activates and/or regulates upstream Hippo pathway receptors, that contain a FERM-binding motif, or activates downstream Hippo pathway kinases directly, remains unknown and requires further studies.

The FERM domain of willin is a scaffolding domain which can bind to different proteins that contain a FERM binding motif. For example, the CD44 plasma membrane receptor contains a FERM-binding peptide motif composed of KKKLVIN (Mori et al., 2008) and may explain why the FERM domain of willin is efficient, and as effective as full-length willin, to activate the Hippo pathway. The binding of the FERM domain of willin to potential upstream receptors may also inhibit other proteins from binding (Figure 4.19). For example, the FERM domain of willin may bind to the CD44 receptors and inhibit ezrin or merlin's ability to bind to CD44; thereby having a modulatory role on the Hippo pathway, rather than having a direct effect on the Hippo pathway itself (Figure 4.19). A second explanation on how the FERM domain of willin is able to phosphorylate the Hippo pathway is that the FERM domain of willin may bind to other ERM proteins, resulting in the masking of potential binding motifs or phosphorylation sites to promote a closed and inactive ERM protein conformation. The inhibition of ERM proteins that may result in the suppression of the Hippo pathway will be released to further result in the activation of the Hippo pathway (Figure 4.19). Finally, the FERM domain of willin may also regulate the distribution, aggregation and availability of upstream Hippo pathway receptors. The FERM domain of willin may potentially regulate the number of Hippo pathway receptors. The more upstream Hippo pathway receptors there are, which may include CD44 or FAT, the more cells will become sensitised to extracellular stimuli that activate the Hippo cascade. Merlin has

been shown to affect the up-regulation of various upstream plasma membrane receptors to enhance the growth inhibitory effects of merlin (McClatchey and Giovannini, 2005; Curto and McClatchey, 2008).

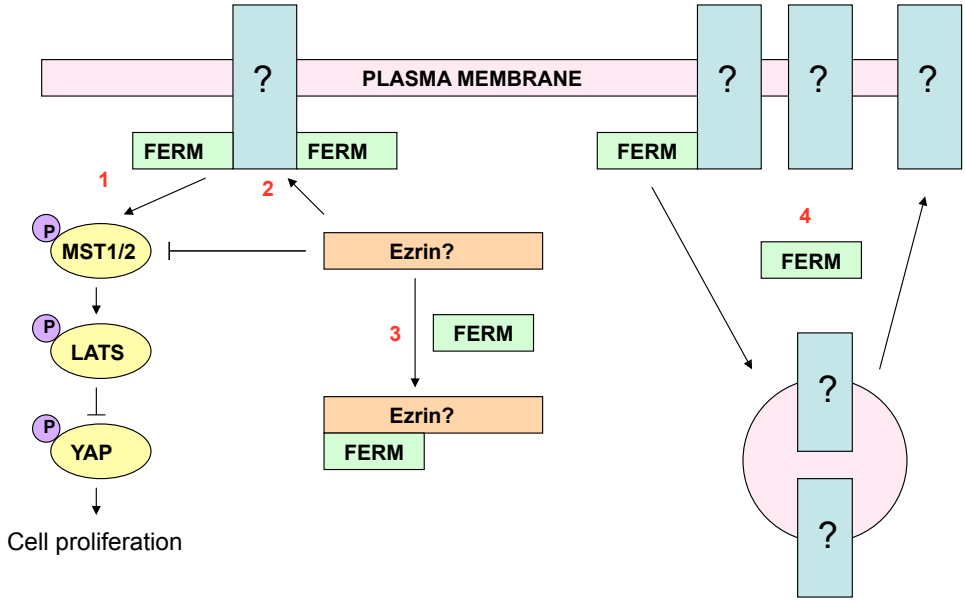

Figure 4.19: Schematic diagram illustrating the possible theories on how the FERM domain of willin may modulate the Hippo pathway. **1**) The FERM domain of willin may bind to upstream plasma membrane receptors that contain a FERM binding motif. Binding to the plasma membrane localises the FERM domain of willin to the correct cellular location to activate the core Hippo pathways. **2**) Binding of the FERM domain to unknown upstream receptors may saturate the receptors and prevent other proteins from binding. Proteins that may inhibit the Hippo pathway are therefore prevented from binding to upstream Hippo pathway activators, resulting in the suppression of the Hippo pathway to activate the Hippo pathway. **3**) The FERM domain may also bind to the C-terminal end of other ERM proteins. The binding of the FERM domain of willin to other proteins may result in the masking of potential binding motifs or phosphorylation sites to promote a closed and inactive protein conformation. Inhibition of ERM proteins that may result in suppression of the Hippo pathway will be released to result in the activation of the Hippo pathway. **4**) The binding of the FERM domain may also result in the up-regulation of upstream Hippo pathway receptors.

Willin shares sequence homology with the *D.melanogaster* protein Expanded only within its conserved FERM domain (Gunn-Moore et al., 2005; Hamaratoglu et al., 2006). The Expanded and willin proteins are especially divergent in the carboxyl termini, which is the region of Expanded that is proposed to phosphorylate the Hippo pathway in *D.melanogaster* (Boedigheimer

et al., 1997). Differences between the *D. melanogaster* and mammalian Hippo pathway would explain why willin cannot rescue the function of its orthologue in *D. melanogaster* tissues (Dr Kieran Harvey, unpublished work: Section 1.3.2.1), since the C-terminal domain of Expanded resulted in activation of the Hippo pathway in *D. melanogaster* (Boedigheimer et al., 1997), while the FERM domain activates the Hippo pathway in mammals. Importantly, not all FERM domain containing proteins can activate the Hippo pathway, since ezrin has been shown to have an inhibitory effect (Chapter 3).

4.3.5 Willin and its FERM domain negatively regulate YAP targets

Hao et al. (2008) have recently reported genes that are either up- or down-regulated by YAP. Expression of willin and its truncated FERM domain can negatively regulate previously reported YAP downstream targets (Hao et al., 2008): decreasing PRL & IGFBP3 and increasing BMP2 & RASSF8 (Section 4.2.4). PRL, IGFBP3, BMP2 and RASSF8 genes are all involved in cell proliferation, migration and adhesion. PRL enhances cell proliferation and migration in MCF7 cells (Doll et al., 2007) and IGFBP3 has been shown to have a protective role against the carcinogenic effects of growth hormone (Grimberg, 2000). BMP2 belongs to TGFβ family of proteins which acts as an anti-proliferative factor in epithelial cells (Massagu et al., 1994) whereas RASSF8 acts as tumour suppressor (Falvella et al., 2006; Lock et al., 2010). Down-regulation of PRL and IGGBP3 and up-regulation of BMP2 and RASSF8 may explain the negative effects on cell proliferation, migration and tumourigenic cell characteristics when willin and the FERM domain of willin are expressed. It remains unclear whether willin regulates these genes by converging on YAP through the Hippo pathway or if the regulation of these genes is YAP-independent through other signalling cascades.

4.4 Conclusion

The Hippo pathway is an important signalling cascade controlling EMT and cellular proliferation. Figure 4.20 summarises the main findings of this chapter. Expression of willin and its FERM domain can antagonise a YAP-induced EMT phenotype in MCF10A cells. EMT is a reversible process, where over-

expression of YAP results in a morphological change towards a mesenchymal-like phenotype in MCF10A cells and willin expression can revert this phenotype back into a more epithelial-like phenotype. This changes cell migration, proliferation, anchorage-independent growth and cell adhesion ability of MCF10A-YAP cells. Expression of willin and its active FERM domain in MCF10A-YAP cells can also antagonise known YAP targets: decreasing PRL and IGFBP3 and increasing BMP2 and RASSF8 RNA expression.

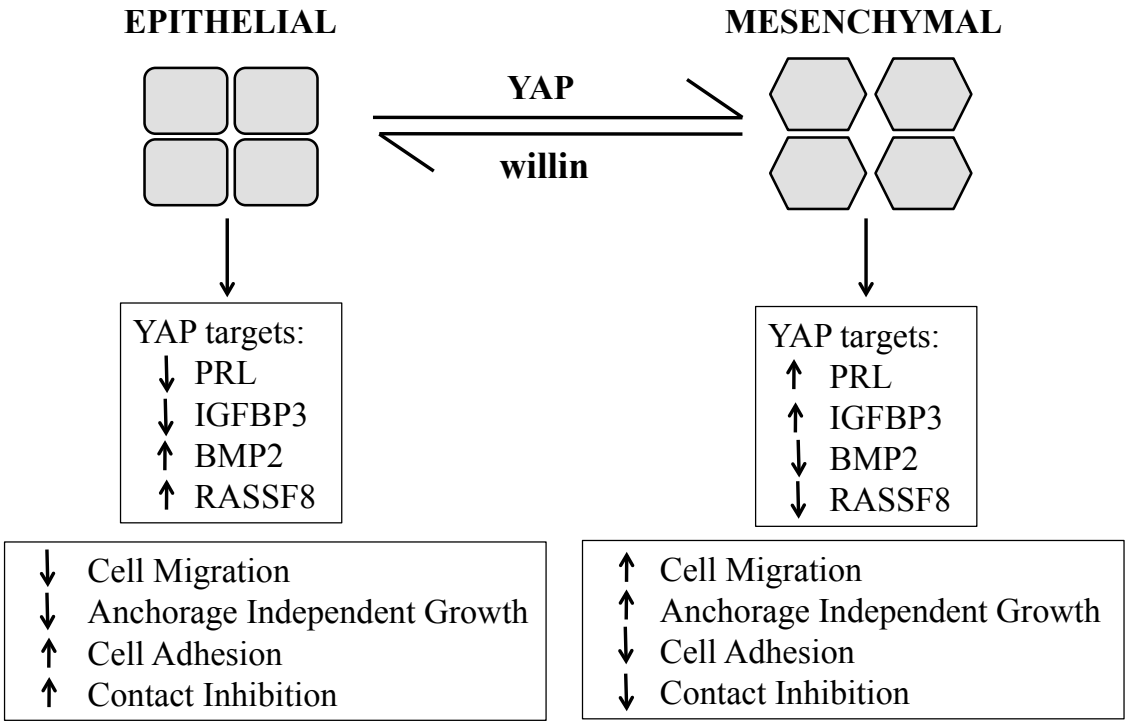

Figure 4.20: Summary of chapter's findings showing that expression of willin can antagonise a YAP-induced EMT phenotype. EMT is a reversible process: where over-expression of YAP results in a morphological change towards a mesenchymal-like phenotype in MCF10A cells, and willin expression can revert this phenotype back into a more epithelial-like phenotype. This changes cell migration, proliferation, anchorage independent growth and cell adhesion ability of MCF10A-YAP cells. Expression of willin and its active FERM domain in MCF10A-YAP cells can also antagonise known YAP targets: decreasing PRL and IGFBP3 and increasing BMP2 and RASSF8 RNA expression.

Chapter 5

Willin Expression Within The Peripheral Nervous System

5.1 Introduction

5.1.1 Willin expression in the mammalian PNS

Willin was initially isolated as a potential binding partner to neurofascin through a yeast two-hybrid screen of a rat sciatic nerve library (Gunn-Moore et al., 2005; Herron et al., 2007). However, expression of willin in the sciatic nerve during different developmental stages remains unknown and was therefore investigated. The sciatic nerve is composed of different cell types, of which neurons, fibroblast and Schwann cells are the major components. Further studies were conducted to define where willin was expressed within the sciatic nerve. The level of Hippo pathway components, as well as ERM proteins, were also investigated in these cells to examine whether the Hippo pathway proteins were present within both the fibroblast and Schwann cells.

The Hippo pathway has been extensively studied in the fibroblast cell line, NIH-3T3, and the core Hippo pathway components have previously been identified in primary mouse embryonic fibroblast (Guo et al., 2007; Zhang et al., 2008a). To date, the expression of the Hippo pathway components in Schwann cells is unknown. ERM proteins have been identified in Schwann cells and it is well documented that the gene responsible for schwannomas formation is NF2, a gene encoding the merlin protein (Rouleau et al., 1993; Trofatter et al., 1993). Willin expression in Schwann cells may therefore have a protective role in schwannoma formation by compensating for merlin's loss, as both merlin

and willin have been proposed to have similar cell proliferative functions and have been shown to activate the Hippo pathway (Chapter 3). Additionally, ERM proteins have been shown to compensate for each other's loss (Fehon et al., 2010).

5.1.2 Willin expression in the zebrafish PNS

There is a greater emphasis and need for physiological genomics (Cowley, 1999) in research today and the zebrafish (*Danio rerio*) is a powerful model organism for the study of vertebrate biology (Amatruda et al., 2002), being well suited to both developmental and genetic analysis. A comparison between the human genome and the nearly completed zebrafish genome demonstrates conservation of cell-cycle regulating genes, tumour suppressors and oncogenes (Dooley and Zon, 2000; Amatruda et al., 2002). In additional to conservation of genes between humans and zebrafish, its external development, transparency of embryos, small size, ease and cost of maintenance are all factors that contribute to the zebrafish organism being a good model system for cancer cell biology.

Recently, work has been conducted to investigate the role of the Hippo tumour suppressor kinase in zebrafish. YAP has been shown to be required for the development of brain, eyes, and neural crest during embryogenenis in zebrafish (Jiang et al., 2009). The Hippo pathway has also been proposed to be essential for normal pronephros development in the zebrafish (Skouloudaki et al., 2009). Wholemount in-situ hybridisations were therefore performed as a quick and efficient method to establish spatial and temporal gene expression of willin in embryos and early stage zebrafish larvae. As willin is expressed in the peripheral nervous system (sciatic nerve) in the mammalian system, emphasis was placed on identifying willin expression in the PNS of the zebrafish model.

5.2 Results

5.2.1 Willin Expression in the Sciatic Nerve

5.2.1.1 Willin is expressed in mouse sciatic nerve from developmental stages E18.5 to adult

Willin was initially isolated as a potential binding partner to neurofascin through a yeast two-hybrid screen of a rat sciatic nerve library (Gunn-Moore et al., 2005; Herron et al., 2007). However, the expression of willin in the sciatic nerve during different developmental stages remained unknown and was therefore investigated. Stuart Gillespie (University of Edinburgh, UK) kindly provided sciatic nerve RNA samples from E18.5, P4, P8, P15, P21 and 6 month-old mice. RT-PCR reactions using *mRT-PCR-F* and *mRT-PCR-R* primers (see Table 2.1 for primer sequence) were performed to detect willin expression at different developmental stages of the mouse sciatic nerve. Figure 5.1 shows that willin expression is detected in the sciatic nerve of E18.5, P4, P8, P15, P21 and 6 month-old mice.

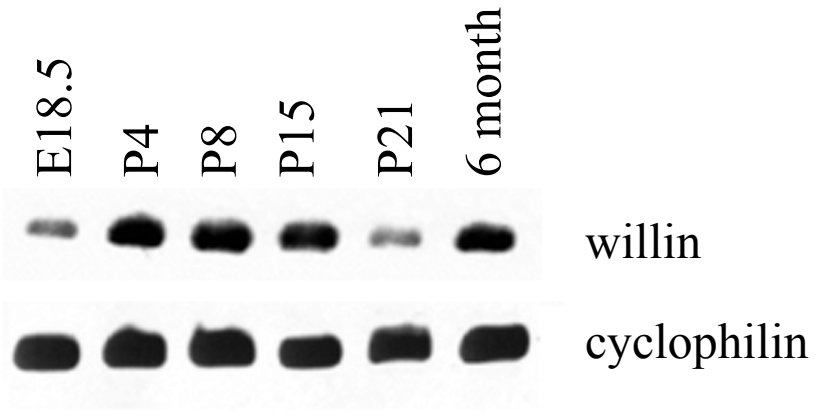

Figure 5.1: Willin expression at different developmental stages (E18.5 to 6 month) of the mouse sciatic nerve. *mRT-PCR-F* & *mRT-PCR-R* primers were used for the amplification of willin and *m-cyclo-F* & *m-cyclo-R* primers for cyclophilin (loading control) from mouse sciatic nerve cDNA. PCR products were run on a 2% agarose gel and DNA bands were detected under UV light.

The PCR product was cloned into a pGEMT easy vector (Promega; Figure 5.2) and the plasmid, containing the PCR insert, was sent to the Sequencing Service (University of Dundee, UK). The Sequencing Service confirmed that

the PCR products using *mRT-PCR-F* and *mRT-PCR-R* primers (see Table 2.1 for primer sequence) on mouse cDNA specifically amplified the correct mouse willin gene of interest (NM-028127; see Appendix B for sequence).

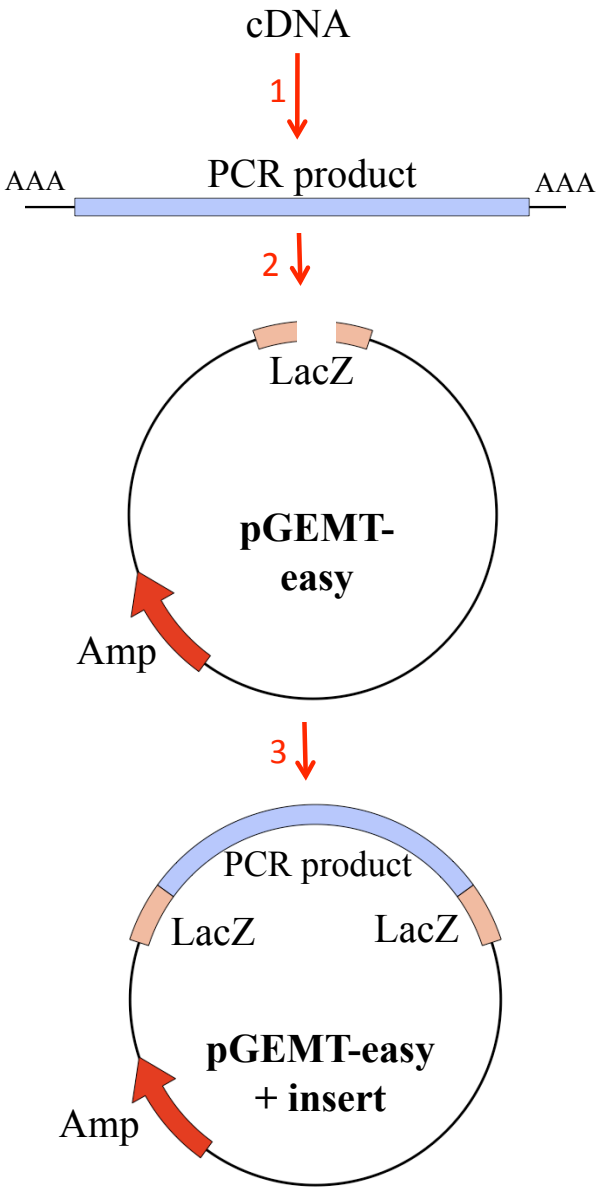

Figure 5.2: Schematic diagram of molecular cloning of PCR products into the pGEMT-easy vector system in preparation for DNA sequencing. PCR was performed on cDNA **(1)**. The PCR product contained an A-tail due to Taq PCR enzyme used in the PCR reaction. The PCR product could therefore be ligated into the pre-cut pGEMT-easy vector (Promega) containing T-tails at each cut end **(2)**. When PCR product was inserted into the pGEMT easy vector, the LacZ operon was affected **(3)**, resulting in white colony formation on ampicillin agar plates.

RT-PCR analysis data of willin expression at the different developmental stages of the sciatic nerve (Figure 5.1) suggested that RNA expression levels may vary during development. Quantitative PCR was therefore conducted on sciatic nerve RNA of E.18.5, P4, P8, P15, P21 and 6 month-old mice. In addition to detecting willin levels, qPCR analysis also detected mouse MST1/2 levels to investigate a potential correlation between the expression levels of willin and downstream Hippo kinases at the different developmental stages.

MST1/2 RT-PCR product was amplified from a sciatic nerve RNA of a 6 month-old adult mice using *MST1/2-F* and *MST1/2-R* primers (see Table 2.1 for primer sequence; Figure 5.3). The PCR product was cloned into a pGEMT easy vector (Figure 5.2) and the DNA Sequencing Service (University of Dundee, UK) confirmed that the PCR using *MST1/2-F* and *MST1/2-R* primers on mouse cDNA was able to amplify both the MST1 (NM021420.3) and MST2 (NM019635.2) gene.

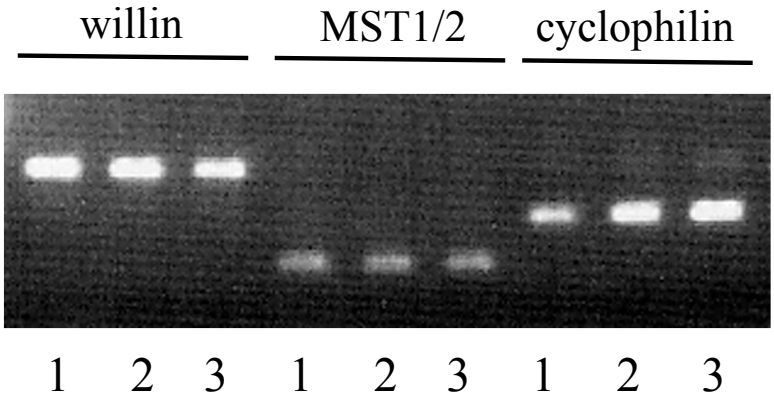

Figure 5.3: RT-PCR products of willin, MST1/2 and cyclophilin from sciatic nerve tissue of a 6 month-old mouse. RT-PCR reaction was done in triplicate using the following primers: willin, *mRT-PCR-F* & *mRT-PCR-R*; MST1/2, *MST1/2-F* & *MST1/2-R2*; cyclophilin, *m-cyclo-F* & *m-cyclo-R*. RT-PCR products were run on a 2% agarose gel and detected at their correct corresponding sizes: willin, 511bp; MST1/2, 218bp; cyclophilin, 344bp.

qPCR analysis showed that the RNA levels of both willin and MST1/2 in the mouse sciatic nerve varied throughout the developmental stages (Figure 5.4). However, no correlation was detected between willin and MST1/2 mRNA expression in the sciatic nerve from E18.5 to 6 month-old adult mice (Figure 5.3). The level of RNA expression of MST1/2 in the mouse sciatic nerve remained unchanged during development with the exception of a ∼2.5 fold

increased peak at P21 (Figure 5.4). In contrast, willin RNA levels in the mouse sciatic nerve increased ∼4 fold from E18.5 to P8, with a slight drop in expression at P15 and again an increased peak at stage P21 (Figure 5.3). Both willin and MST1/2 expression in the mouse sciatic nerve were highest at P21 and lowest in a 6 month-old adult mice (Figure 5.3).

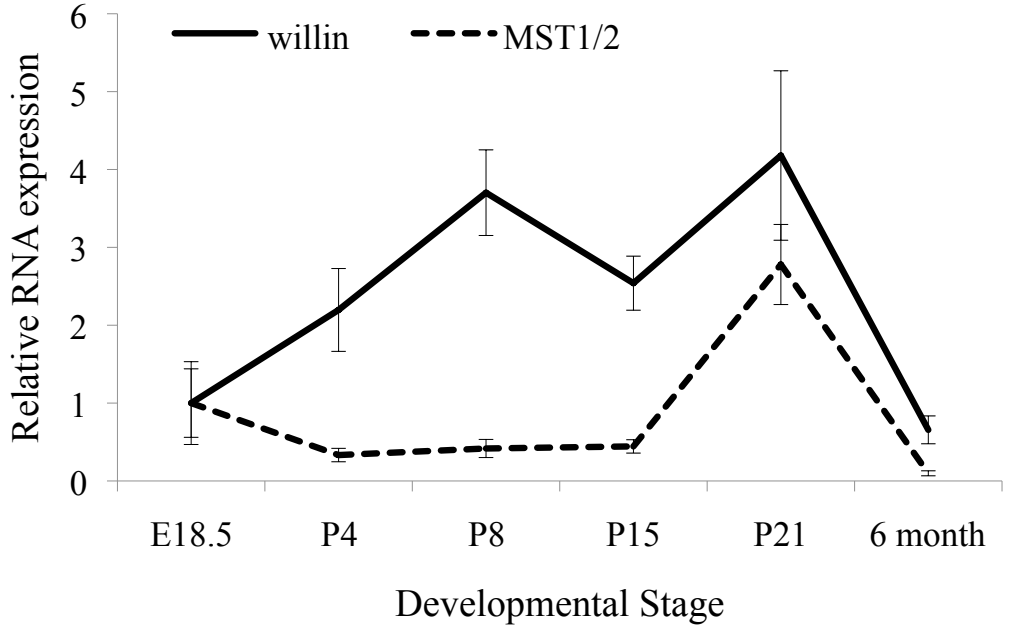

Figure 5.4: Relative quantification of willin and MST1/2 levels in the mouse sciatic nerve at different developmental stages (E18.5 to 6 months old). qPCR was conducted on cDNA samples and gene expression was standardised to cyclophilin levels; relative to expression at E18.5 which was set to 1. Error bars represent ± standard deviation.

5.2.1.2 ERM and Hippo pathway components are differently expressed in primary Schwann and fibroblast cells

The major components of a sciatic nerve are neurons, Schwann cells and fibroblast cells. qPCR analysis was performed to investigate the level of expression of willin, and core Hippo pathway components, in primary Schwann and fibroblast cultures. Dr Jennifer R. Higginson (University of Glasgow, UK), kindly provided primary Schwann and fibroblast cell cultures isolated from a rat sciatic nerve. RNA was isolated from both the primary fibroblast and Schwann cells and RT-PCR products of willin (*r-willin-F* & *r-willin-R* primers), merlin

(*R-merlin-F* & *R-merlin-R* primers), ezrin (*R-ezrin-F* & *R-ezrin-R* primers), MST1 (*R-MST1-F* & *R-MST1-R* primers), MST2 (*R-MST2-F* & *R-MST2-R* primers), LATS1 (*R-LATS1-F* & *R-LATS1-R* primers), LATS2 (*R-LATS2-F* & *R-LATS2-R* primers) and YAP (*R-YAP-F* & *R-YAP-R* primers) all separated at their correct corresponding sizes on a 2% agarose gel (Figure 5.5; see Table 2.1 for primer sequence). PCR products were cloned into a pGEMT easy vector and the DNA Sequencing Service (University of Dundee, UK) confirmed that the PCR products amplified were that of willin (XM-001064688.2; see Appendix C for sequence), merlin (NM-013193.1), ezrin (NM-019357), MST1 (NM-001107800.1), MST2 ((NM-031735.1), LATS1 (NM-001134543.1), LATS2 (NM-001107267.1) and YAP (NM-001034002).

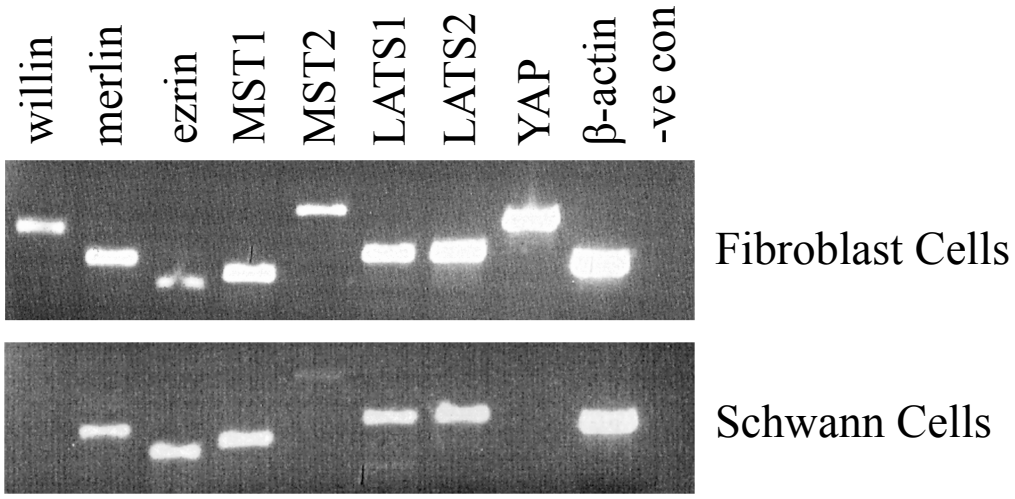

Figure 5.5: RT-PCR products of ERM proteins (merlin, ezrin and willin) and Hippo pathway proteins (MST1/2, LATS1/2, YAP) on rat primary fibroblast and Schwann cells. RT-PCR products were run on an agarose gel and PCR products were detected at their correct corresponding sizes: willin (417bp), merlin (324bp), ezrin (245bp), MST1 (276bp), MST2 (549bp), LATS1 (347bp), LATS2 (346bp), YAP (419bp).

qPCR analysis showed that ERM and the core Hippo pathway proteins are differently expressed in primary rat Schwann and fibroblast cells (Figure 5.6). Both ERM (willin, merlin & ezrin) and Hippo components proteins (MST1, MST2, LATS1, LATS2 & YAP) were more abundant in primary fibroblast cells than Schwann cells, with the exception of ezrin which was equally expressed in both fibroblast and Schwann cells (Figure 5.6). The levels of willin, MST2 and YAP1 are very low, and possibly absent, in Schwann cells (Figure 5.6).

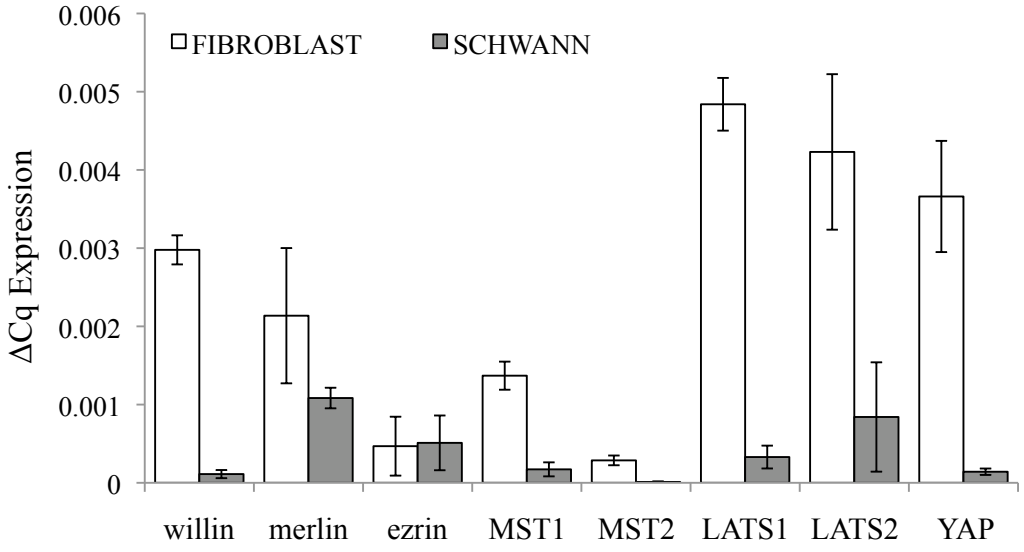

Figure 5.6: qPCR analysis of ERM and Hippo pathway proteins in primary rat fibroblast and Schwann cells. ΔCq gene expression was calculated and standardised to β-actin expression levels. Error bars represent ± standard deviation.

Immunohistochemical staining of willin in a human nerve bundle confirmed that willin was absent in Schwann cells (Figure 5.7). Dr Michael Prystowsky (Albert Einstein College of Medicine, USA) showed that willin expression within the human nerve bundle is sparse, with higher expression levels of willin observed in the surrounding tissues that may possibly be fibroblast cells (Figure 5.7).

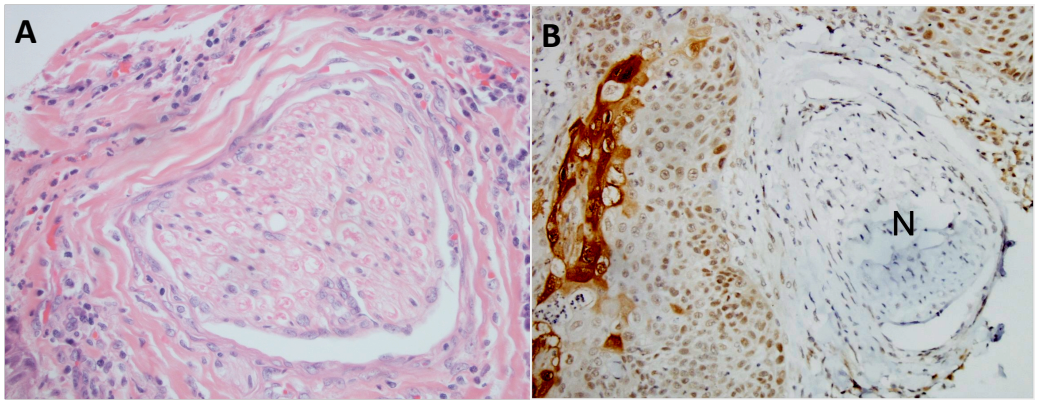

Figure 5.7: Immunohistochemistry staining of willin in the PNS. **A)** Haematoxylin and eosin staining of a nerve bundle in the PNS. **B)** Immunohistochemistry staining of willin on a PNS nerve bundle (N). Willin staining (brown) is low in the nerve bundle and more willin staining is observed within its surrounding tissue. Immunohistochemistry was done by Dr Michael Prystowsky (Albert Einstein College of Medicine, USA).

5.2.2 Wholemount Zebrafish In-Situ Hybridisation

5.2.2.1 Willin is endogenously expressed in Zebrafish embryos

Before a wholemount *Danio rerio* (zebrafish) in-situ hybridisation was performed, RT-PCR was conducted to confirm that willin was expressed in the zebrafish embryos. Total RNA from whole zebrafish was extracted 24, 48 and 96 hours post-fertilisation (hpf). cDNA was synthesised from the RNA and a PCR reaction was used to amplify willin and a positive EF1α control; using *DR-500bp-F* & *DR-500bp-R* and *EF1a-F* & *EF1a-R* primers (see Table 2.1 for primer sequences) respectively. Figure 5.8 shows that willin was expressed in zebrafish embryos 24, 48 and 72 hpf. The willin RT-PCR product was cloned into a pGEM-T easy vector (Promega; Figure 5.2) and the DNA Sequencing Service (University of Dundee, UK) confirmed that the zebrafish willin gene of interest (NM001111187; see Appendix D for sequence) was amplified.

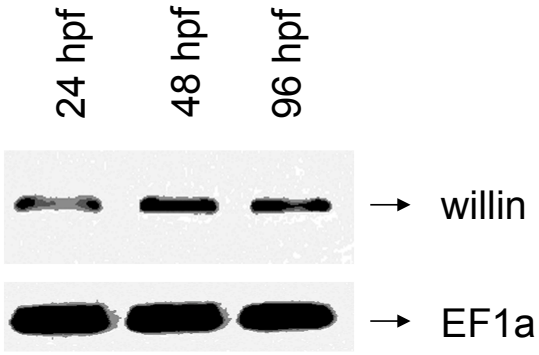

Figure 5.8: Willin expression in zebrafish 24, 48 and 96 hours post-fertilisation (hpf). RNA from whole zebrafish was extracted and RT-PCR was performed using *DR-500bp-F* and *DR-500bp-R* primers to amplify willin expression. RT-PCR of EF1α, using *EF1a-F* and *EF1a-R* primers, was conducted as a positive control. RT-PCR products were run on a 2% SDS gel and detected under UV light.

5.2.2.2 RNA probe synthesis

As willin was found to be expressed in the zebrafish embryos (24-96 hpf), a wholemount in-situ hybridisation was performed to establish spatial and temporal gene expression of willin in a zebrafish embryo. Firstly, a RNA probe to detect specifically willin RNA was synthesised. RNA was isolated from a 48 hpf zebrafish embryo and RT-PCR was performed to amplify a $\sim$500bp product of the zebrafish willin gene using *DR-500bp-F* and *DR-500bp-R* primers (see Table 2.1 for primer sequence). The PCR product was cloned into a pGEMT easy vector system and orientation of the PCR insert was confirmed by the DNA Sequencing Service (University of Dundee, UK). Both willin orientations (5'-3' and 3'-5) within the pGEMT easy vector were used to make RNA probes (Figure 5.9).

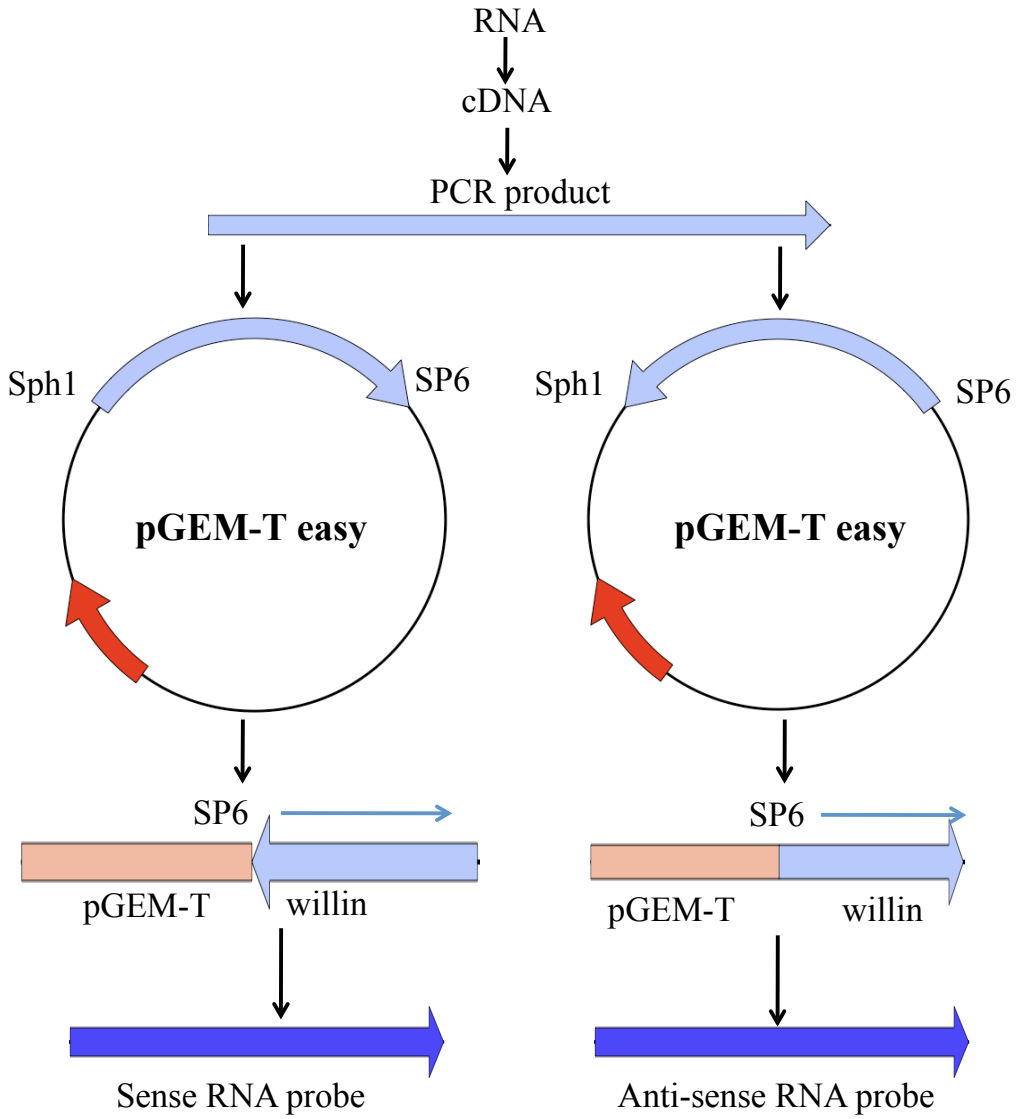

Figure 5.9: Schematic diagram showing techniques used for RNA probe synthesis. Zebrafish RNA was isolated and cDNA was made through a reverse transcription reaction. PCR was conducted using primers specific to willin (*DR-500bp-F* + *DR-500bp-R*). PCR product was ligated into the pGEMT easy vector system and orientation of the PCR insert was confirmed by DNA sequencing. Plasmid was linearised using *Sph*1 and SP6 RNA polymerase was used to create both sense and anti-sense RNA probes, depending on original orientation of willin in the pGEMT easy vector.

To check the integrity and quality of the newly synthesised RNA probe, the RNA probe was run at high voltage (180 volts) on an agarose gel for 5 minutes. Figure 5.10 shows that both sense and anti-sense RNA probes were of good quality as one clear single RNA band was observed and the RNA was not degraded.

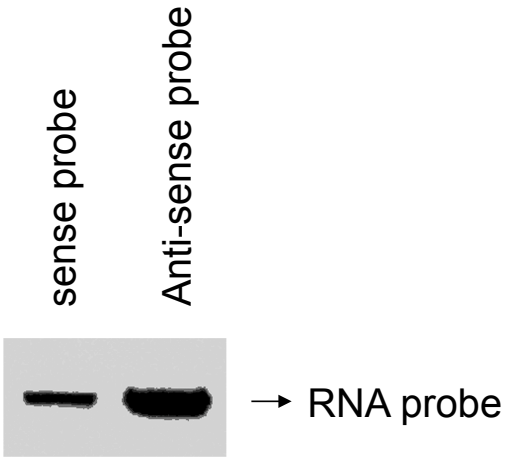

Figure 5.10: Sense and anti-sense RNA probes were of good quality. RNA probes were synthesised and run at high voltage (180 volts) on a 1% agarose gel for 5 minutes. RNA probes were visualised under UV light.

5.2.2.3 Willin is expressed in lateral line neuromast cells

Wholemount in-situ hybridisations were performed using both sense and anti-sense RNA probes in zebrafish embryos 24-96 hpf. The anti-sense RNA probe should specifically detect endogenous willin RNA expression, whereas the sense RNA probe was used as a negative control to detect non-specific binding. Figure 5.11 illustrates the in-situ protocol used for wholemount zebrafish embryos.

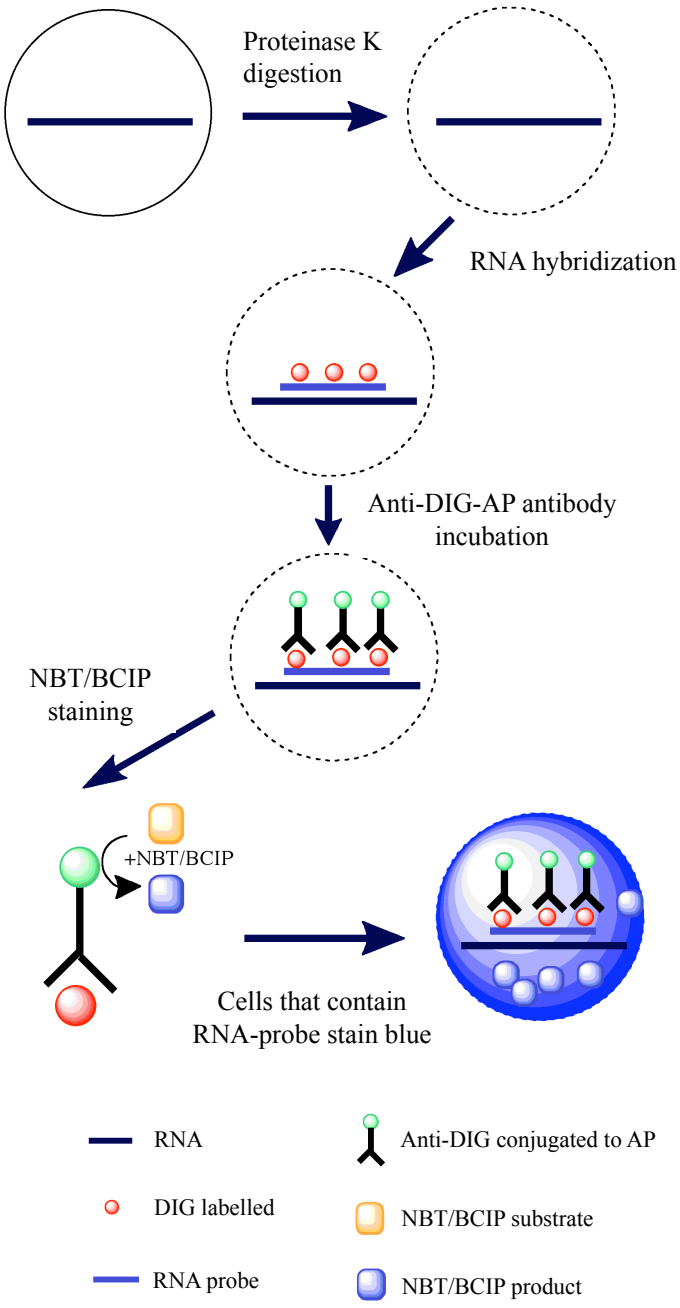

Figure 5.11: Schematic diagram of zebrafish in-situ hybridisation protocol using RNA probes. Zebrafish embryos were fixed and membrane was permeabilised with by a proteinase-K digestion. DIG labelled sense and anti-sense RNA probes were incubated overnight to bind to specific mRNA sequence of interest. After washes, zebrafish embryos were incubated in anti-DIG antibody that were conjugated to alkaline phosphatase. The presence of bound antibody to RNA probe was detected using NBT/BCIP staining. NBT and BCIP together yield an insoluble blue/purple precipitate when reacted with alkaline phosphatase. Cells that contained the RNA probe therefore stain blue whereas in the absence of a bound RNA probe the cell remained unchanged.

In-situ hybridisation of wholemount zebrafish using the sense willin RNA probe resulted in a small amount of non-specific binding to the phospholipid-rich yolk sac. No non-specific binding was observed using willin sense RNA probe in zebrafish embryo's anterior trunk, posterior trunk, and tail at 24, 48, 72 and 96 hpf (Figure 5.12).

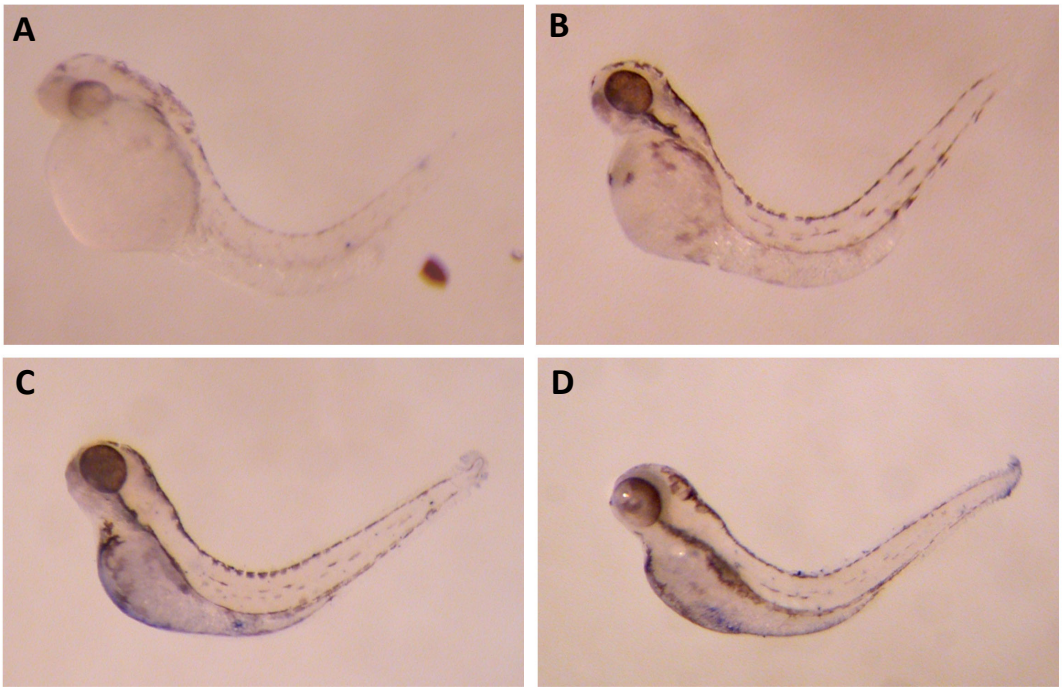

Figure 5.12: Wholemount zebrafish in-situ control with sense-RNA probe. Wholemount in-situ hybridisations were performed on **A)** 24, **B)** 48, **C)** 72 and **D)** 96 hpf zebrafish embryos with sense-RNA probe.

Specific willin expression was detected by in-situ hybridisation using willin anti-sense RNA probe in zebrafish embryos aged 24-97 hpf. The expression pattern of willin observed represented that of both anterior and posterior lateral line neuromast cells (Figure 5.13 & 5.14). Neuromast cells are part of the PNS in zebrafish and are deposited along the trunk and head to respond to water movements and pressures (Dijkgraaf, 1963; Ma and Raible, 2009; Montgomery et al., 2000).

Figure 5.13 shows whole zebrafish embryos 24, 48, 69 and 72 hpf, hybridised with the willin anti-sense RNA probe. Microscopic images of the embryos confirmed that willin was expressed in typical neuromast cells in both the posterior and anterior lateral line of the zebrafish embryo (Figure 5.14).

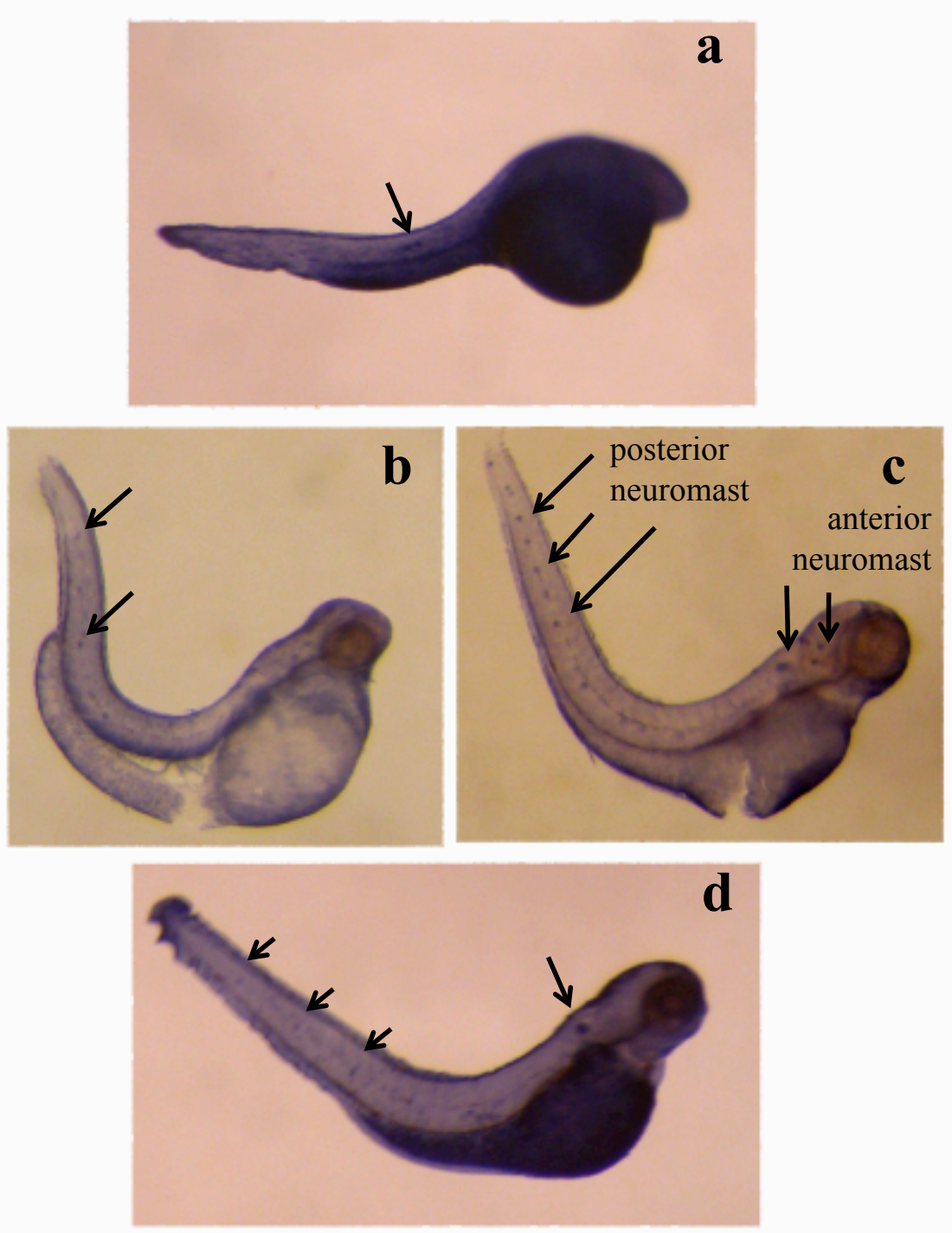

Figure 5.13: Wholemount zebrafish in-situ staining of willin 24-96 hpf. Wholemount in-situ experiments were conducted **a)** 24, **b)** 48, **c)** 72 and **d)** 96 hours post-fertilisation using a 500bp anti-sense RNA probe specifically designed to detect willin expression. **a**) at 24 hpf the whole embryo epithelium was stained with 2-3 neuromast detected in the posterior lateral line (arrow). **b-d**) at 48-96 hpf these neuromast become more apparent and were observed every 5-10 somites in the posterior lateral line and neuromast rosettes were also stained in the anterior lateral line in the head (arrows).

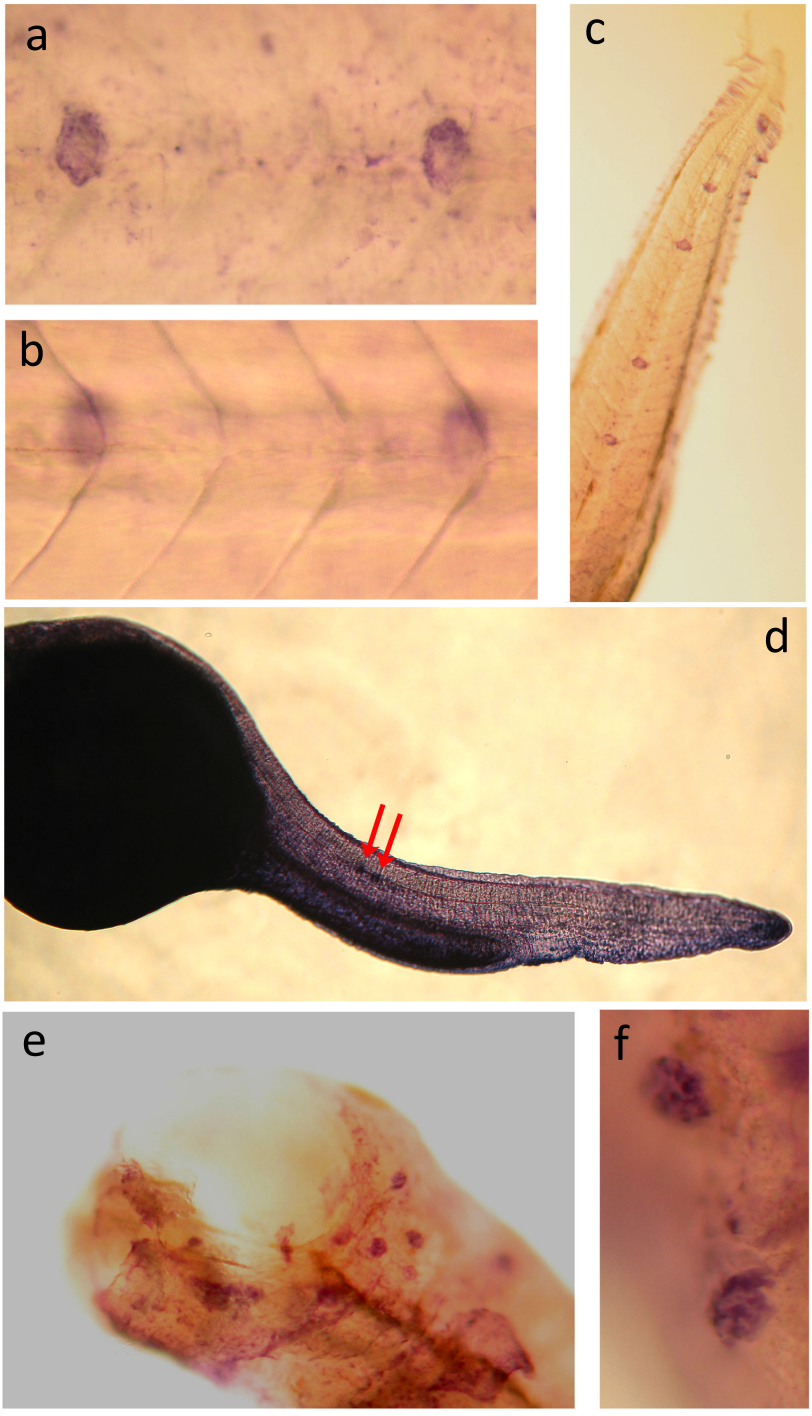

Figure 5.14: Zebrafish willin expression in neuromast cells. In-situ hybridisation was performed with anti-sense probes on 24-96 hpf zebrafish embryos, and willin expression were observed in neuromast cells. **a**, **b** and **c** show that the distinctive neuromasts were stained and observed every 3-6 somites along the posterior lateral line in a 72 hpf zebrafish. **d)** Two neuromasts were stained in the anterior end of the 24 hpf embryo's tail. No additional neuromasts were observed in the 24 hpf embryo. **e)** Neuromast cells in the form of distinctive rosettes were observed in anterior lateral line just posterior to the developing ear in a 72 hpf embryo. **f)** A close-up of willin stained anterior lateral line neuromast in a 72 hpf zebrafish embryo.

Two willin stained neuromasts were deposited within the posterior lateral line in 24 hpf embryos (Figure 5.14.D). No additional stained neuromasts were observed in 24 hpf zebrafish embryos. As the zebrafish embryo developed (48-97 hpf) more willin stained neuromasts were detected every 5-10 somites along the posterior lateral line (Figure 5.14.A-B). At 72 hpf, willin stained neuromast cells in the form of distinctive rosettes were observed in the anterior lateral line just posterior to the developing ear (Figure 5.14.E-F). The number of positively stained neuromasts in both the anterior and posterior lateral line of the zebrafish declined in more developed (96 hpf) embryos (Figure 5.13). However, some willin staining, distinctive of neuromasts, was still observed in the posterior and anterior lateral line in 96 hpf zebrafish embryos (Figure 5.13).

Cryo-cross-sections were performed on the zebrafish in-situ hybridisations to investigate the spatial and temporal gene expression of willin in more detail. In addition to willin being expressed in the distinct neuromast cells, willin was also expressed in the epithelial layer of the zebrafish embryos (Figure 5.13, 5.15). Figure 5.15.A shows a cross-section through a 48 hpf zebrafish head, were willin expression was found to be within the epithelial layer. In addition, a cross section through the tail of a 48 hpf zebrafish fish also showed willin expression in the epithelial layer (Figure 5.15B-C). The cryosection of the tail was sliced through a superficial neuromast cells which was observed in the epidermis, above the basement membrane (shown by an arrow in Figure 5.15C).

Epithelial expression of willin in the head and tail of the 48 hpf zebrafish embryo was polarised to one side of the epithelium. Predominantly more willin was expressed in the epithelial layer dorsal of the zebrafish head compared to the ventral side (Figure 5.15.A). Additionally, more willin was expressed on one side of the 48 hpf embryo tail compared to the other. Notably, the lateral epithelial side that contained the superficial neuromast was predominantly stained with willin compared to the opposite lateral side in the tail of the zebrafish (Figure 5.15.B-C).

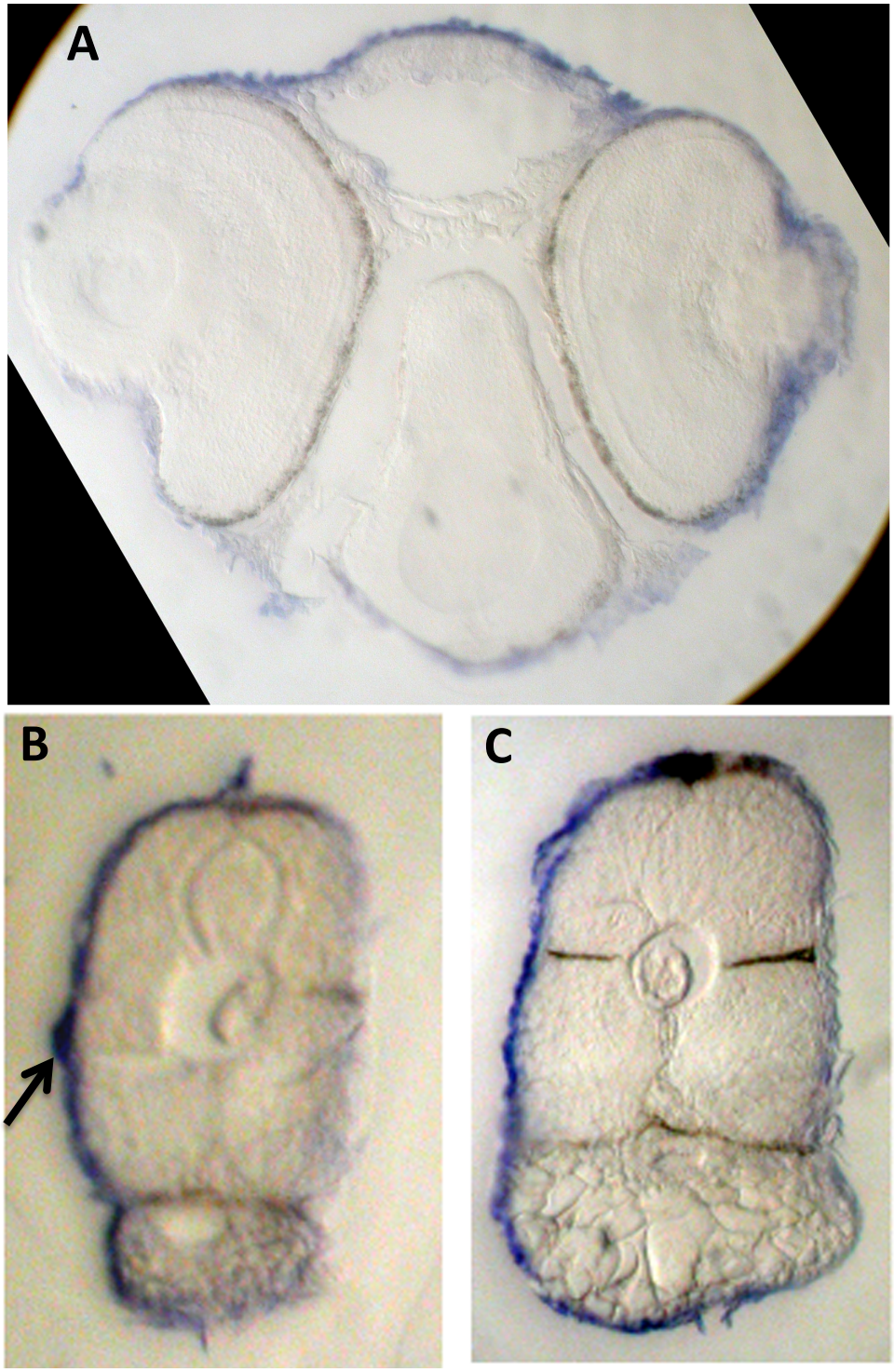

Figure 5.15: Cross section of wholemount zebrafish in-situ hybridisation using a 500bp anti-sense RNA probe to detect willin RNA. **A)** Cross section of 48 hpf zebrafish embryo's head, where willin staining was observed at the epithelial layer. **B)** Cross section of 48 hpf zebrafish embryo's tail. Cryosection was sliced through a superficial neuromast (arrow) which was observed in the epidermis that sits above the basement membrane. **C)** Cross section of a 48 hpf zebrafish embryo's tail more anterior to cross section in B.

5.3 Discussion

5.3.1 Willin expression in the mammalian PNS

5.3.1.1 Willin is expressed in the mouse sciatic nerve

Previous work showed that willin was expressed in the sciatic nerve, where willin was initially isolated as a potential binding partner to neurofascin through a yeast two-hybrid screen of a rat sciatic nerve library (Gunn-Moore et al., 2005; Herron et al., 2007). However, willin expression during the developmental stages of the mouse remained unknown.

RT-PCR analysis confirmed that willin was expressed in the mouse sciatic nerve from the developmental stages of E18.5 to 6 month-old adult. Quantitative PCR showed that the RNA levels of both willin and MST1/2 in the mouse sciatic nerve varied at different developmental stages. However no correlation was observed between the expression of willin and MST1/2. The lack of correlation between willin and MST1/2 expression may be due to willin acting on other proteins and pathways during development. It is also important to note that it is not the total level of MST1/2 expressed that is critical, but whether it is in an active (phosphorylated) or inactive (unphosphorylated) state.

Even though no correlation between willin and MST1/2 RNA levels in the sciatic nerve were observed during development, both willin and MST1/2 levels peaked at P21 and were lowest in the 6 month-old adult mice. At P21, myelination is in the late and final stages (Fern et al., 1998); where Schwann cells have insulated the axon and sheath formation is inhibited. Transforming growth factor (TGF)-βs plays a role in inhibiting myelination and are believed to up-regulate cell adhesions molecules such as neural cell adhesion molecule (NCAM) and L1 (Mirsky and Jessen, 1996). Willin and MST1/2 may be up-regulated during late myelination in response to extracellular matrix signals such as TGF-β to reduce cell proliferation. Expression of both willin and MST1/2 in the sciatic nerve was lowest in adult mice, supporting the concept that the Hippo pathway is critical during early stages of development, thereby regulating organ size and proliferation.

5.3.1.2 Willin, ERM proteins and the Hippo components are differently expressed in primary Schwann and fibroblast cells

Primary fibroblast and Schwann cells were isolated to define and characterise which cell type in the sciatic nerve endogenously expressed willin. qPCR analysis showed that willin, ERM and Hippo pathway components were all expressed in the primary rat fibroblast cells. This is consistent with data by Zhang et al. (2008a) and Guo et al. (2007) who identified the core Hippo pathway components in primary mouse embryonic fibroblast (MES) and in a fibroblast cell line, NIH-3T3. Intriguingly, 40% of fibroblast cells arise through epithelial to mesenchymal transition (Iwano et al., 2002) and willin and the Hippo pathway have been shown to control EMT (Chapter 4). Fibroblasts have a prominent role in the progression, growth and spread of cancer, by producing growth factor, chemokines and extracellular matrix facilitating angiogenic recruitment of endothelial cells and pericytes (Kalluri and Zeisberg, 2006). Willin and the Hippo pathway components may have a tumour suppressive function in the fibroblast cells though inhibition of the cancer enhancing properties of these cells and this requires further investigations.

Significantly lower willin, ERM proteins and Hippo pathway components were expressed in primary Schwann cells compared to fibroblast cells; with the exception of ezrin, which was equally expressed in both. Willin, MST2 and YAP1 appear to be absent in the primary Schwann cells. However, it is important to note three major factors. Firstly, the expression of different isoforms of willin, ERM proteins and Hippo pathway components may be cell specific. Secondly, isolated primary cell culture do not represent cells in their physiological environment and may have resulted in different protein levels being expressed, as neighbouring cells *in-vivo* may affect proteins expression within the Schwann cells. Finally, cell density is an important factor in the activation of the Hippo pathway and the fact that the primary Schwann cells did not proliferate as fast as the fibroblast cells, and were therefore harvested at a lower cell density, may explain why the levels of Hippo pathway proteins were lower in Schwann cells.

5.3.2 Willin expression in the zebrafish PNS

5.3.2.1 Willin is expressed in neuromast cells

In-situ hybridisation showed that willin was expressed in distinctive neuromast cells found within the anterior and posterior lateral line of the zebrafish (*Danio rerio*). Neuromast cells are part of the peripheral nervous system of the fish and form the sensory lateral line organ. Neuromast cells consists of a core mechanosensory hair cells surrounded by support cells; which are innervated by sensory neurons that are localised in a cranial ganglion (Ghysen and Dambly-Chaudiere, 2004). Neuromast cells are deposited along the trunk and head of the zebrafish to respond to changes in water movements and pressure relative to the zebrafish's body (Dijkgraaf, 1963; Montgomery et al., 2000) (Figure 5.16). Neuromast mechanosensory hair cells are therefore of importance in a wide variety of zebrafish behaviour such as prey detection, predator avoidance, school swimming and sexual courtship (Coombs and Meunz, 1989). The lateral line hair cells share structural, functional and molecular similarities with the hair cells in the vertebrate inner ear (Ma and Raible, 2009).

Willin expression in the neuromast cells at different developmental stages (24-96 hpf) of the zebrafish embryo coincide with previous data which showed that neuromast cells are deposited along the posterior lateral line 24 hpf and that all neuromasts are deposited 72 hpf (Ma and Raible, 2009). Neuromast deposition resulted in 5-6 neuromast being positioned every 5-10 somites along the trunk and tail as well as 2-3 terminal neuromasts formed at the top of the tail (Gompel et al., 2001).

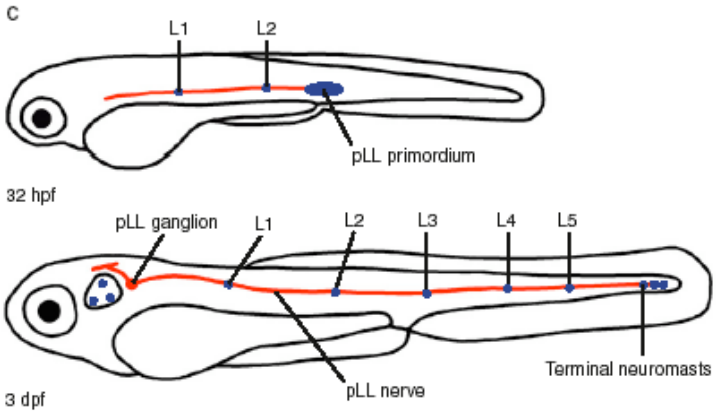

Figure 5.16: Schematic representation of neuromast migration in zebrafish development. At 32 hours post-fertilisation, the posterior lateral line primordium has migrated halfway down the length of the trunk with two neuromast being deposited, L1 and L2. At 3 days after fertilisation, the posterior lateral line consists of five neuromast (L1-L5) with 2-3 terminal neuromasts. The posterior lateral line ganglion is located caudal to the developing ear and neuromasts are innervated by the posterior lateral line. Diagram obtained from Ma and Raible (2009).

The rosette appearance of the willin stained neuromast cells (Figure 5.14) suggests that the surrounding supportive neuromast cells express willin. Many proteins involved in cell adhesion are present within the neuromast cells as neuromast cells undergo apicobasal polarisation before actin-rich membranes become enriched in the focal points to form the classical rosette like appearance of the neuromast cells (Lecaudey et al., 2008; Hava et al., 2009; Ma and Raible, 2009). Willin, like other FERM domain containing proteins, is involved in cell adhesion and translocates to cellular junctions upon cell-to-cell contact (Chapter 3) and to focal adhesion sites during cytokinesis (Yang et al., 2004). Willin's role as a scaffolding protein to maintain cellular structure may explain why willin is expressed within these actin-enriched focal point neuromast cells.

Willin may be involved in the development of neuromast cells as positively stained neuromasts appeared to decline in embryos at 96 hpf. In zebrafish, all neuromasts are deposited and matured 3 days after fertilisation (Ghysen and Dambly-Chaudiere, 2007). Proteins involved in the deposition and development of neuromast cells can therefore be transiently expressed in neuromast until they are matured. As willin expression appeared to decline in neuromast cells it may be that willin is involved in the developmental stages in neuromast development and redundant once the neuromast mature. However, it is

important to note that other factors could also explain this scenario. Willin expression at 96 hpf seems to be expressed widely within the epithelial layer of the zebrafish so that the neuromast, which are deeper in the dermal layer cannot be observed as clearly. Cryosectioning and co-staining with a neuromast marker should clarify whether willin staining declines in mature neuromasts. One such neuromast marker is Sox2 (Hernandez et al., 2007). Willin expression within the neuromast of a 96 hpf zebrafish embryo might be lower, and a longer incubation with the NBT/BCIP substrate may be required to visualise the expression.

5.3.2.2 Willin expression in the zebrafish epithelial layer

Willin is not only expressed in the neuromast cells but seems to be widely expressed in the epithelial layer of the zebrafish. It is important to note that willin expression in more tissues may have been observed if the NBT/BCIP in-situ substrate reaction was left longer to incubate. We can therefore not rule out that willin may be expressed at lower levels in other zebrafish tissues. As YAP has previously been shown to be required for the development of the brain, eyes, and neural crest during embryogenenis in zebrafish (Jiang et al., 2009), willin may also have a role in the development of these organs, possibly through the Hippo pathway.

At hatching, neuromasts are present in the epithelium on both the head and trunk (Tarby and Webb, 2003). Cryosection through the tail showed that the neuromast at 48 hpf was present within the epithelium. Previous data support this observation and the migration of the neuromast from the epithelial layer into the dermis to form the lateral line is illustrated in Figure 5.17. The neuromasts develop from the lateral side of the epithelium (Tarby and Webb, 2003). The polarised expression of willin observed in Figure 5.15 is possibly an in-situ hybridisation artifact as the lateral line is formed on both sides of the zebrafish.

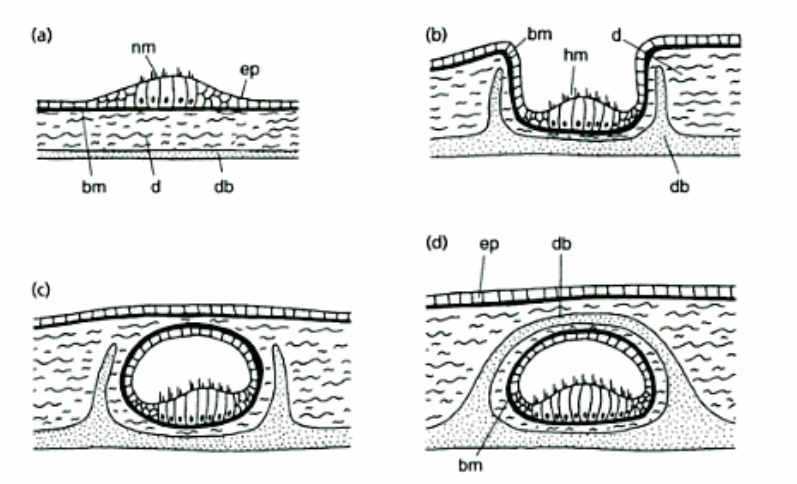

Figure 5.17: Schematic representation of the morphogenesis of the lateral line canal. **A**) A superficial neuromast (nm) is located in the epidermis (ep) that sits above the basement membrane (bm). **B**) Bony canal walls ossify intramembraneously and expand upwards from the underlying dermal bone (db) on either side of the neuromast, which appears to sink into an epithelial groove. **C**) The epithelium fuses over the neuromast forming an epithelial canal. **D**) The dermal canal bone continues to ossify and the canal walls fuse to form the canal roof. nm= neuromast, bm= basement membrane, d= dermis, dm= dermal bone, ep = epithelium. Image obtained from Tarby and Webb (2003).

5.4 Conclusion

To conclude, willin is expressed in both the mammalian and zebrafish peripheral nervous system. qPCR analysis has shown that willin is endogenously expressed in the sciatic nerve, where a high abundance level of expression is observed in primary isolated fibroblast cells. ERM (merlin, ezrin & willin) and Hippo signalling proteins were identified in fibroblast cells. A lower level of expression was observed in primary Schwann cells and willin, MST2 and YAP1 appear to be absent. Willin is also expressed in the zebrafish PNS. In-situ hybridisation of wholemount zebrafish embryos identified willin expression in the distinctive neuromast cells of both the anterior and posterior lateral line. This data suggests that willin and the Hippo pathway may play an essential role in the developmental regulation within the peripheral nervous system.

Chapter 6

Future Experiments

Willin, like other ERM proteins, is placed at a crucial juncture for the integration of the extracellular environment and intracellular signalling pathways. FERM domain containing proteins (Expanded and merlin) have been shown to activate a novel Hippo signalling cascade that regulates cell contact inhibition, organ size control, cell growth, proliferation, apoptosis and cancer development in *Drosophila*. Work described in this thesis has shown that willin, the predicted human homologue of Expanded, is a novel FERM containing protein candidate that can partially activate the tumour suppressor Hippo signalling pathway cassette in the mammalian system.

Induced willin expression resulted in an increased phosphorylation of the Hippo pathway components MST1/2, LATS1 and YAP (Chapter 3). Willin expression in HEK-293 cells resulted in a partial activation of the Hippo pathway as no cell cycle or cell viability changes were observed, even though YAP translocated from the nucleus to the cytoplasm (Chapter 3). Willin expression in HEK-293 cells did however sensitise cells to TNFα-induced cell death, possibly because the core Hippo components MST1/2, LATS1 and YAP were phosphorylated and YAP translocated from the nucleus to cytoplasm when willin expression was induced (Chapter 3). However, it can not be ruled out that willin expression sensitised cells to cell death stimuli, independent of the Hippo pathway, through activation of other signalling pathways.

Quantifiable changes were, however, observed when willin was overexpressed in MCF10A cells as willin expression was able to antagonise a YAP-induced EMT phenotype: increasing cell adhesion and contact inhibition and decreasing cell migration and anchorage independent growth (Chapter 4). EMT changes are hallmarks of the development and progression of

cancers. The control of EMT by the Hippo pathway is, therefore, vital during development. Interestingly, the FERM domain of willin alone was able to antagonise a YAP-induced EMT phenotype and phosphorylate the core Hippo pathway cassette, suggesting that the scaffolding function of the FERM domain may be the key to the activation and modulation of the Hippo pathway (Chapter 4). The FERM domain contains a motif that is able to activate the Hippo kinase complex, whether the FERM domain activates and/or regulates upstream Hippo pathway receptors that contain a FERM binding motif or activates downstream Hippo pathway kinases directly remains unknown and requires further studies (see Figure 4.19 for possible theories on how the FERM domain may activate the Hippo pathway).

Preliminary studies have shown that willin is expressed during early stages of development in the mouse sciatic nerve (Chapter 5). Isolation and qPCR analysis on primary rat Schwann and fibroblast cells have identified that willin and the Hippo pathway components are expressed predominantly within the fibroblast cells (Chapter 5). As fibroblast cells have a prominent role in the progression, growth and spread of cancers, willin and the Hippo pathway components may play an important role in tumour suppression through inhibition of cancer enhancing properties of the fibroblast cells. Intriguingly, 40% of the fibroblast cells arise from epithelial to mesenchymal transition (Iwano et al., 2002). The expression of willin and the Hippo pathway components in the fibroblast cells may therefore be related to the cell's origin as willin and the Hippo pathway components have been shown to modulate EMT in MCF10A cells (Chapter 4).

This work has demonstrated that willin is a novel protein involved in the activation of the Hippo pathway and may therefore act as a tumour suppressor. The initial characterisation work on the novel willin protein has placed willin upstream of the mammalian Hippo pathway, like its *Drosophila* homologue Expanded. Although both willin and Expanded can activate the Hippo pathway, similarities and differences are observed between the two proteins. In the mammalian system, willin activates the Hippo pathway through the FERM domain (Chapter 4), whereas Expanded activates the Hippo pathway through the C-terminal end (Boedigheimer et al., 1997).

Despite amassing a wealth of knowledge about the novel willin protein and its involvement in the Hippo pathway, the modulatory mechanisms of willin on the newly expanding mammalian Hippo pathway still remains unknown. Fur-

ther progress into the novel mammalian Hippo pathway is likely to continue as the signalling cascade is crucial for organ size control and differentiation during normal development, and misregulation of this pathway results in cancer development. Further studies should focus on identifying Hippo binding proteins and complexes, determining the modulation of the Hippo pathway and investigating the Hippo signalling cascade in a physiological *in-vivo* system.

6.1 Binding proteins and complexes

The Hippo pathway in the *D. melanogaster* model has been extensively studied. Less is known about the tumour suppressor signalling cascade in the mammalian system. The aim of this project was to investigate the role of willin in the Hippo pathway. Willin was shown to activate the Hippo pathway, however the molecular details of how willin expression resulted in the phosphorylation of the Hippo pathway or the Hippo protein complexes formed remains unknown.

Biomolecular studies in HEK-293 cells have proposed that willin can bind directly to ezrin and indirectly to merlin (Chapter 3). Future studies should focus on identifying further upstream and downstream binding partners of willin. Emphasis on upstream willin receptors is important to understand how the Hippo pathway is initially activated and modulated. Potential candidate upstream receptors include Fat and CD44, which have previously been shown to activate the Hippo pathway (Reddy and Irvine, 2008; Xu et al., 2010). The CD44 plasma membrane receptor contains a FERM binding peptide motif composed of KKKLVIN (Mori et al., 2008) and may explain why the FERM domain of willin is efficient, and as effective as full-length willin, to activate the Hippo pathway (Chapter 4). Further truncation of the FERM domain of willin should identify the peptide motif necessary for the phosphorylation and activation of the core Hippo pathway.

In *Drosophila*, Expanded's C-terminal domain is essential for the phosphorylation and activation of the Hippo pathway, whereas the FERM domain of Expanded localises the protein to the apical membrane in order to bind to upstream plasma membrane receptors (Boedigheimer et al., 1997). In the mammalian system, the FERM domain of willin has been shown to activate the Hippo pathway (Chapter 4). It is hypothesised that the FERM domain of willin also localises the protein to upstream plasma membranes receptors that

contain a FERM binding motif. The function of the C-terminal domain of willin remains to this date unknown but may have an inhibitory effect on its FERM domain through head-to-tail binding, or may be required for cellular protein localisation. Further localisation studies using both the FERM and C-terminal domains of willin are required to support this hypothesis.

Even though a high protein sequence conservation is observed between the *Drosophila* and mammalian system, experiments in this thesis have shown that differences between the two systems are also observed; as the FERM domain of willin can activate the Hippo pathway in the mammalian system (Chapter 4), whereas the C-terminal domain of Expanded results in activation of the *Drosophila* Hippo pathway (Boedigheimer et al., 1997). Differences and similarities between the *Drosophila* and mammalian Hippo signalling cascade requires further investigation as the function of the Hippo kinase complexes may have split during vertebrate evolution to result in differences in the Hippo pathway complexes formed between *Drosophila* and mammals. For example, the C-terminal domain of Expanded has been identified to bind to Yorkie and Yorkie is believed to contact Expanded via WW domain-PY motif interactions (Badouel et al., 2009). However, none of these three PY motifs in Expanded are conserved between willin and YAP in mammals (Figure 1.14). The Hippo complexes formed in the *Drosophila* and mammalian model may therefore be very different. Further investigations are therefore required to identify Hippo kinase complexes in the mammalian system and to investigate whether the core Hippo components form a complex with willin and translocate as one unit or whether activations are transient and proteins act independently. Live imaging and immunoprecipitation studies will provide this information. The production of a willin antibody to detect endogenous willin expression is however essential.

Preliminary results suggest that willin and LATS may co-localise as both willin and LATS translocate to the membrane fraction at high cell density in HEK-293 cells, whereas MST1 protein levels decreased in the membrane fraction at increasing cell density (Chapter 3). A complex between willin and LATS is plausible as localisation studies on LATS have shown similar distribution to that of willin. LATS has been shown to translocate to the plasma membrane upon cell-to-cell contact, with a high expression of these proteins found at cellular adherent junctions (Yang et al., 2004; Zhao et al., 2011). More research into the molecular binding complexes formed in the Hippo pathway

will result in a greater understanding on how the Hippo pathway is activated and modulated.

6.2 Modulation of the Hippo pathway

As with all biological processes and pathways, modulation and negative feedback loops are essential. The same is true for the modulation of the Hippo pathway which has to be tightly regulated to balance cell death and proliferation. Therefore, upstream activation and inhibition of the Hippo pathway needs to be strictly controlled. To date, little is known about upstream factors that activate the Hippo pathway cascade. High cell density and extracellular cell death signals have thus far been proposed. It can therefore not be ruled out that willin may have both growth inhibitory and growth proliferative functions at different cell densities.

The expression of willin can enhance merlin's ability to phosphorylate MST1/2, whereas ezrin has an inhibitory effect on MST1/2 phosphorylation by willin, merlin and both willin and merlin (Chapter 3). How merlin, ezrin and willin modulate the Hippo pathway cascade is not known. Whether ezrin, merlin and willin modulate the Hippo pathway by competing for the same upstream receptor, or whether the classical head-to-tail binding of ERM proteins results in conformational changes, which in turn blocks upstream or downstream protein binding motifs, is unknown and requires further investigation.

Future work should also focus on identifying the protein structure of willin. The protein conformation of willin may change from an open (active) to a closed (inactive) state, as has been proposed for the activation and inhibition of Expanded by merlin (McCartney et al., 2000). The open conformation may expose the FERM domain or potential phosphorylation sites that are necessary for the activation of the Hippo pathway. Binding of ezrin to willin may result in a conformational change in willin from an open and active state that is growth inhibitory to a closed and inactive state that is growth promoting.

The Hippo pathway, like many signalling cascades, is composed of a complex network of proteins. An increasing number of novel mammalian proteins, such as Kibra (Genevet et al., 2010; Yu et al., 2010), have been shown to activate the Hippo pathway. To date, nothing is known about how the expression of these proteins results in an increased phosphorylation of MST1/2, LATS1 and YAP. Future identification of the kinases involved in activation of MST1/2

will provide vital information on the activation of the Hippo pathway and how the signalling cascade may be regulated.

Modulation of the Hippo pathway can be further analysed using the MCF10A cell line. The reversion of an EMT phenotype in MCF10A-YAP cells is quantifiable using different combinations of ERM proteins, as well as other novel upstream proteins of the Hippo pathways such as Kibra. Combinations of shRNA knock-outs of ERM proteins and double knock-outs with YAP, will provide vital information on the modulation and hierarchy of activation of the Hippo pathway. As ERM proteins can compensate for each other's loss (Fehon et al., 2010) it would also be interesting to investigate whether the loss of willin results in an increase in other upstream Hippo components such as merlin or Kibra.

6.3 Role of willin in a physiological system

Extensive information about proteins can be obtained through cell culture analysis. However, the role of proteins may be very cell specific. For example, YAP has been shown to have tumour suppressive functions as well as being oncogenic (Yuan et al., 2008). In addition, different isoforms of the mammalian Hippo pathway proteins are expected to be present in different cell types. The physiological downstream effect of the Hippo pathway, as well as the different isoforms expressed in an array of cell tissues and cell lines, requires further investigation. Unlike in *Drosophila*, in which the Hippo pathway proteins are encoded by one single gene, most mammalian Hippo pathway proteins are composed of multiple isoforms (Sudol and Harvey, 2010). To date, a total of three isoforms of willin have been proposed. For this reason the mammalian Hippo pathway cascade may be more complex, consisting of multiple isoforms, when compared to the Hippo pathway in the *Drosophila* model. Furthermore, co-culture of primary cells such as fibroblast and Schwann cells will represent a more physiological setting.

The ultimate aim of this project is to shift to a physiological *in-vivo* system. One such system is the zebrafish (*Danio rerio*) model. Preliminary data has shown that willin is expressed in the epithelial layer and distinct lateral line neuromast cells of the zebrafish (Chapter 5). Willin expression, localisation, embryonic micro-injection and morpholino knock-out (Eisen and Smith, 2008) experiments will provide more detailed information of the role of willin and

its regulation of cellular growth. The core Hippo pathway components have recently been studied in the zebrafish model (Jiang et al., 2009; Skouloudaki et al., 2009) and further studies are anticipated to see whether willin has a similar distribution and function in the zebrafish. Future studies will also focus on creating a transgenic knock-out mouse. As willin knock-out mice may be embryonic lethal, as seen with merlin (McClatchey et al., 1997), an inducible Cre-lox recombination system (Brocard et al., 1997) may be preferable.

6.4 The bigger picture

In-vivo experiments in this thesis have shown that willin can, as predicted from the *Drosophila* homologue Expanded, activate and phosphorylate the core Hippo signalling cascade. It is however very plausible that willin may be involved in a number of other pathways to regulate cell growth; such as the inhibition of the MEK/ERK and AKT/mTOR signalling pathways (Figure 6.1). Willin's involvement in regulating and modulating cellular growth may therefore be more complex, with multiple downstream cell proliferative signalling pathways involved (Figure 6.1). Future work should therefore investigate other potential signalling avenues of willin on cell proliferation, especially as its closely related family member, merlin, has been shown to be involved in a complex network of signalling pathways (Section 1.1.4.2; Figure 6.1).

While this project showed that willin expression activates the novel Hippo pathway tumour suppressor signalling cassette *in-vitro*, the question of whether willin is a tumour suppressor gene in human cancer awaits further analysis, since no studies have addressed if this gene is mutated or silenced in cancer. Advances in upstream Hippo pathway components such as willin may not only solve the puzzle of size control and cell proliferation, but will also provides new targets for treatment of human diseases such as atrophy and cancers, as well as utilising tissue engineering and regenerative medicine.

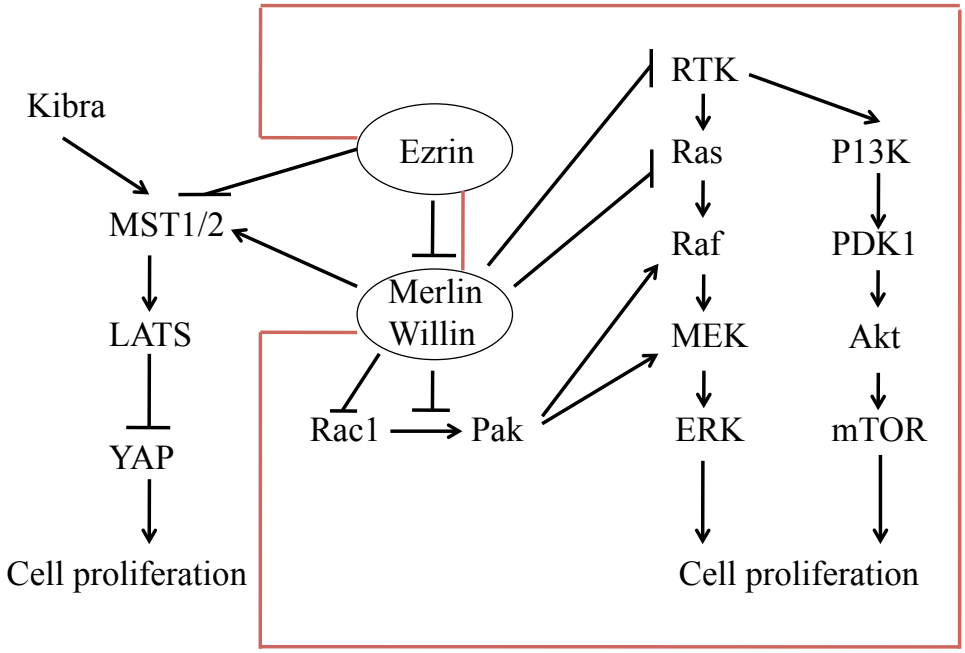

Figure 6.1: Potential growth signalling pathways modulated by willin. Only one of the signalling pathways predicted to be activated by willin was investigated within this thesis. Work in this thesis focused on the novel Hippo tumour suppressor pathway. Other potential signalling pathways that may be modulated by willin include the MEK/ERK and AKT/mTOR signalling pathways. Unknown potential pathways modulated by willin are boxed in red.

Bibliography

C Alarcon, A Zaromytidou, Q Xi, S Gao, J Yu, S Fujisawa, A Barlas, AN Miller, K Katia Manova-Todorova, MJ Macias, G Sapkota, D Pan, and J Massague. Nuclear CDKs drive smad transcriptional activation and turnover in BMP and TGF-beta pathways. *Cell*, 139:757–769, 2009.

K Alfthan, L Heiska, M Gronholm, GH Renkema, and Carpen O. Cyclic AMP-dependent protein kinase phosphorylates Merlin at serine 518 independently of p21-activated kinase and promotes Merlin-Ezrin heterodimerization. *J Biol Chem*, 279:18559–18566, 2004.

JF Amatruda, JL Shepard, HM Stern, and LI Zon. Zebrafish as a cancer model system. *Cancer Cell*, 1:229–231, 2002.

MR Amieva and H Furthmayr. Subcellular localization of moesin in dynamic filopodia, retraction fibers, and other structures involved in substrate exploration, attachment, and cell-cell contacts. *Experimental Cell Research*, 219: 180–196, 1995.

C Badouel, L Gardano, N Amin, A Garg, R Rosenfeld, TL Bihan, and H McNeill. The FERM domain protein Expanded regulates Hippo pathway activity via direct interactions with the transcriptional activator Yorkie. *Dev Cell*, 16:411–420, 2009.

Y Bai, YJ Liu, H Wang, Y Xu, I Stamenkovic, and Q Yu. Inhibition of the hyaluronan-CD44 interaction by merlin contributes to the tumor-suppressor activity of merlin. *Oncogene*, 2007.

MD Bashyam, RB Young, H Kim, P Wang, T Hernandez-Boussard, CA Karikari, R Tibshirani, A Maitra, and JR Pollack. Assay-based comparative genomic hybridization identifies localized DNA amplifications and homozygous deletions in pancreatic cancer. *Neoplasia*, 7:556–562, 2005.

S Basu, NF Totty, MS Irwin, M Sudol, and J Downward. Akt phosphorylates the yes-associated protein, yap, to induce interaction with 14-3-3 and attenuation of p73-mediated apoptosis. *Mol Cell*, 11:11–23, 2003.

FC Bennett and KF Harvey. Fat cadherin modulates organ size in drosophila via the salvador/warts/ hippo signaling pathway. *Curr. Biol.*, 16:2101–2110, 2006.

CM Blaumueller and M Mlodzik. The Drosophila tumor suppressor expanded regulates growth, apoptosis, and patterning during development. *Mechanisms of Development*, 92:251–262, 2000.

M Boedigheimer and A Laughon. Expanded: a gene involved in the control of cell proliferation in imaginal discs. *Development*, 118:1291–1301, 1993.

MJ Boedigheimer, KP Nguyen, and Bryant PJ. Expanded functions in the apical cell domain to regulate the growth rate of imaginal discs. *Dev Genet*, 20:103–110, 1997.

J Bothos, RL Tuttle, M Ottey, FC Luca, and TD Halazonetis. Human LATS1 is a mitotic exit network kinase. *Cancer Research*, 65:6568–6575, 2005.

A Bretscher, D Chambers, R Nguyen, and D Reczek. ERM-Merlin and EBP50 protein families in plasma membrane organization and function. *Annual Review of Cell and Developmental Biology*, 16:113–143, 2000.

A Bretscher, K Edwards, and RG Fehon. ERM proteins and merlin: integrators at the cell cortex. *Nat Rev Mol Cell Biol*, 3:586–599, 2002.

J Brocard, X Warot, O Wendling, N Messaddeq, JL Vonesch, P Chambon, and D Metzger. Spatio-temporally controlled site-specific somatic mutagenesis in the mouse. *Proceedings of the National Academy of Sciences of the United States of America*, 94:14559–14563, 1997.

LA Buttitta and BA Edgar. How size is controlled: from Hippos to Yorkies. *Nat Cell Biol*, 9:1225–1227, 2007.

FD Camargo, S Gokhale, JB Johnnidis, D Fu, GW Bell, R Jaenisch, and TR Brummelkamp. YAP1 increases organ size and expands undifferentiated progenitor cells. *Current Biology*, 17:2054–2060, 2007.

SW Chan, CJ Lim, LS Loo, YF Chong, C Huang, and W Hong. TEADs mediate nuclear retention of TAZ to promote oncogenic transformation. *J Biol Chem*, 284:1434714358, 2009.

P Charles, S Tait, C Faivre-Sarrailh, G Barbin, F Gunn-Moore, N Denisenko-Nehrbass, A Guennoc, J Girault, PJ Brophy, and C Lubetzki. Neurofascin is a glial receptor for the paranodin/caspr-contactin axonal complex at the axoglial junction. *Current Biology*, 12:217–220, 2002.

CL Chen, KM. Gajewski, F Hamaratoglu, W Bossuyt, L Sansores-Garcia, C Tao, and G Halder. The apical-basal cell polarity determinant Crumbs regulates Hippo signaling in Drosophila. 107:15810–15815, 2010.

AH Chishti, AC Kim, SM Marfatia, M Lutchman, M Hanspal, H Jindal, SC Liu, PS Low, GA Rouleau, N Mohandas, JA Chasis, JG Conboy, P Gascard, Y Takakuwa, SC Huang, EJ Benz Jr, A Bretscher, RG Fehon, JF Gusella, V Ramesh, F Solomon, VT Marchesi, S Tsukita, S Tsukita, M Arpin, D Louvard, NK Tonks, JM Anderson, AS Fanning, PJ Bryant, DF Woods, and KB Hoover. The FERM domain: a unique module involved in the linkage of cytoplasmic proteins to the membrane. *Trends in Biochemical Sciences*, 23:281–282, 1998.

E Cho, Y Feng, C Rauskolb, S Maitra, R Fehon, and KD Irvine. Delineation of a Fat tumor suppressor pathway. *Nat Genet*, 38:1142–1150, 2006.

YS Chu, WA Thomas, O Eder, F Pincet, E Perez, Thiery JP, and S Dufour. Force measurements in E-cadherin-mediated cell doublets reveal rapid adhesion strengthened by actin cytoskeleton remodeling through Rac and Cdc42. *J. Cell. Biol*, 2004.

YS Chu, O Eder, WA Thomas, I Simcha, F Pincet, A Ben-Zeev, E Perez, Thiery JP, and S Dufour. Prototypical type-I E-cadherin and type-II cadherin-7 mediate very distinct adhesiveness through their extracellular domain. *J. Biol. Chem*, 281:365–373, 2005.

JG Conboy. Molecular-Cloning and Characterization of the Gene Coding for Red-Cell Membrane Skeletal Protein-4.1. *Biorheology*, 23:218–128, 1986.

JG Conboy. Structure, function, and molecular genetics of erythroid membrane

skeletal protein 4.1 in normal and abnormal red blood cells. *Semin Hematol*, 30:58–73, 1993.

SGP Coombs and H Meunz. *The mechanosensory lateral line: neurobiology and evolution*, volume 17. New York: Springer-Verlag, 1989.

SW Coons. Pathology of schwannomas of the eighth cranial nerve. *Operative Techniques in Neurosurgery*, 4:53–57, 2001.

AW Cowley. The emergence of physiological genomics. *Journal of Vascular Research*, 36:83–90, 1999.

M Curto and AI McClatchey. Nf2/merlin: a coordinator of receptor signalling and intercellular contact. *British Journal of Cancer*, 98:256–262, 2008.

Z Dai, WG Zhu, CD Morrison, RM Brena, DJ Smiraglia, A Raval, YZ Wu, LJ Rush, P Ross, JR Molina, GA Otterson, and C Plass. A comprehensive search for DNA amplification in lung cancer identifies inhibitors of apoptosis cIAP1 and cIAP2 as candidate oncogenes. *Human Molecular Genetics*, 12: 791–801, 2003.

J Debnath, SK Muthuswamy, and JS Brugge. Morphogenesis and oncogenesis of MCF-10A mammary epithelial acini grown in three-dimensional basement membrane cultures. *Methods*, 30:256–268, 2003.

C Dichamp, S Taillibert, L Aguirre-Cruz, J Lejeune, Y Marie, ME Kujas, JY Delattre, K Hoang-Xuan, and M Sanson. Loss of 14q chromosome in oligodendroglial and astrocytic tumors. *Journal of Neuro-Oncology*, 67:281–285, 2004.

S Dijkgraaf. The functioning and significance of the lateral line organs. *Biological Reviews*, 38:51–105, 1963.

F Doll, J Pfeilschifter, and A Huwiler. Prolactin upregulates sphingosine kinase-1 expression and activity in the human breast cancer cell line MCF7 and triggers enhanced proliferation and migration. *Endocrine-Related Cancer*, 14:325–335, 2007.

J Dong, G Feldmann, J Huang, S Wu, N Zhang, SA Comerford, MF Gayyed, RA Anders, A Maitra, and D Pan. Elucidation of a universal size-control mechanism in drosophila and mammals. *Cell*, 130:1120–1133, 2007.

K Dooley and LI Zon. Zebrafish: a model system for the study of human disease. *Current Opinion in Genetics and Development*, 10:252–256, 2000.

BA Edgar. From cell structure to transcription: Hippo forges a new path. *Cell*, 124:267–273, 2006.

SD Edwards and NH Keep. A crystal structure of the activated FERM domain of moesin: an analysis of structural changes on activation. *Biochemistry*, 40:7061–7068, 2001.

JS Eisen and JC Smith. Controlling morpholino experiments: don't stop making antisense. *Development*, 135:1735–1743, 2008.

B Elliott, J Meens, S SenGupta, D Louvard, and M Arpin. The membrane cytoskeletal crosslinker ezrin is required for metastasis of breast carcinoma cells. *Breast Cancer Research*, 7:365–373, 2005.

DGR Evans, M Sainio, and ME Baser. Neurofibromatosis type 2. *J Med Genet*, 37:897–904, 2000.

FS Falvella, G Manenti, M Spinola, C Pignatiello, B Conti, U Pastorino, and TA. Dragani. Identification of RASSF8 as a candidate lung tumor suppressor gene. *Oncogene*, 28:3934–3938, 2006.

RG Fehon, AI McClatchey, and A Bretscher. Organizing the cell cortex: the role of ERM proteins. *Nat Rev Mol Cell Biol*, 11:276–287, 2010.

R Fern, P Davis, SG Waxman, and BR Ransom. Axon conduction and survival in CNS white matter during energy deprivation: A developmental study. *Journal of Neurophysiology*, 79:95–105, 1998.

A Fernandez-L, PA Northcott, J Dalton, C Fraga, D Ellison, S Angers, MD Taylor, and AM Kenney. YAP1 is amplified and up-regulated in hedgehog-associated medulloblastomas and mediates sonic hedgehog-driven neural precursor proliferation. *Genes and Development*, 23:2729–2741, 2009.

Z Franck, R Gary, and A Bretscher. A. moesin, like ezrin, colocalizes with actin in the cortical cytoskeleton in cultured cells, but its expression is more variable. *J Cell Sci*, 105:219–231, 1993.

T Fukasawa, JM Chono, S Sakurai, N Koshiishi, R Ikeno, A Tanaka, Y Matsumoto, Y Hayashi, M Koike, and M Fukayama. Allelic loss of 14q and 22q, NF2 mutation, and genetic instability occur independently of c-kit mutation in gastrointestinal stromal tumor. *Japanese Journal of Cancer Research*, 91: 1241–1249, 2000.

R Gary and A. Bretscher. Ezrin self-association involves binding of an N-terminal domain to a normally masked C-terminal domain that includes the F-actin binding site. *Mol. Biol. Cell*, 6:1061–1075, 1995.

A Gautreau, D Louvard, and M Arpin. ERM proteins and NF2 tumor suppressor: the Yin and Yang of cortical actin organization and cell growth signaling. *Current Opinion in Cell Biology*, 14:104–109, 2002.

A Genevet, MC Wehr, R Brain, BJ Thompson, and N Tapon. Kibra is a regulator of the Salvador/Warts/Hippo signaling network. *Developmental Cell*, 18:300–308, 2010.

A Ghysen and C Dambly-Chaudiere. Development of the zebrafish lateral line. *Current Opinion in Neurobiology*, 14:67–73, 2004.

A. Ghysen and C. Dambly-Chaudiere. The lateral line microcosmos. *Genes Dev*, 21:2118–2130, 2007.

M Giovannini, E Robanus-Maandag, M Valk, M Niwa-Kawakita, V Abramowski, L Goutebroze, JM Woodruff, A Berns, and G Thomas. Conditional biallelic NF2 mutation in the mouse promotes manifestations of human neurofibromatosis type 2. *Genes and Development*, 14:1617–1630, 2000.

N Gompel, N Cubedo, C Thisse, B Thisse, C Dambly-Chaudire, and A Ghysen. Pattern formation in the lateral line of zebrafish. *Mechanisms of Development*, 105:69–77, 2001.

Y Goulev, JD Fauny, B Gonzalez-Marti, D Flagiello, J Silber, and A Zider. Scalloped interacts with yorkie, the nuclear effector of the hippo tumor-suppressor pathway in Drosophila. *Current Biology*, 18:435–441, 2008.

JD Graves, KE Draves, Y Gotoh, EG Krebs, and EA Clark. Both phosphorylation and caspase-mediated cleavage contribute to regulation of the

ste20-like protein kinase Mst1 during CD95/Fas-induced Apoptosis. *J Biol Chem*, 276:14909– 14915, 2001.

A Grimberg. p53 and IGFBP-3: Apoptosis and Cancer Protection. *Molecular Genetics and Metabolism*, 70:85–98, 2000.

FJ Gunn-Moore, GI Welsh, LR Herron, F Brannigan, K Venkateswarlu, S Gillespie, M Brandwein-Gensler, R Madan, JM Tavar, PJ Brophy, MB Prystowsky, and Guild S. A novel 4.1 ezrin radixin moesin (FERM)-containing protein. *FEBS letters*, 579:5089–5094, 2005.

FJ Gunn-Moore, M Hill, F Davey, LR Herron, S Tait, D Sherman, and Brophy PJ. A functional FERM domain binding motif in neurofascin. *Mol Cell Neurosci*, 33:441–446, 2006.

C Guo, S Tommasi, L Liu, JK Yee, R Dammann, and GP Pfeifer. RASSF1A is part of a complex similar to the Drosophila Hippo/Salvador/Lats tumor-suppressor network. *Current Biology*, 17:700–705, 2007.

DH Gutmann, CA Haipek, and K Hoang Lu. Neurofibromatosis 2 tumor suppressor protein, merlin, forms two functionally important intramolecular associations. *J Neurosci Res*, 58:706–16, 1999.

DH. Gutmann, J Donahoe, A Perry, N Lemke, K Gorse, K Kittiniyom, SA Rempel, JA Gutierrez, and IF Newsham. Loss of DAL-1, a protein 4.1-related tumor suppressor, is an important early event in the pathogenesis of meningiomas. *Human Molecular Genetics*, 9(10):1495–1500, 2000.

D Haase, M Meister, T Muley, J Hess, S Teurich, P Schnabel, B Hartensteinand, and P Angel. FRMD3, a novel putative tumour suppressor in NSCLC. *Oncogene*, 26:4464–4468, 2007.

K Hamada, T Shimizu, T Matsui, S Tsukita, and T Hakoshima. Structural basis of the membrane-targeting and unmasking mechanisms of the radixin FERM domain. *Embo J*, 19:4449–4462, 2000.

F Hamaratoglu, M Willecke, M Kango-Singh, R Nolo, E Hyun, C Tao, H Jafar-Nejad, and G Halder. The tumour-suppressor genes NF2/Merlin and Expanded act through hippo signalling to regulate cell proliferation and apoptosis. *Nat Cell Biol*, 8:27–36, 2006.

D Hanahan and RA Weinberg. The hallmarks of cancer. *Cell*, 100:57–70, 2000.

CO Hanemann. Magic but treatable? Tumours due to loss of Merlin. *Brain*, 131:606–615, 2008.

Y Hao, A Chun, K Cheung, B Rashidi, and X Yang. Tumor suppressor LATS1 is a negative regulator of oncogene YAP. *J Biol Chem*, 283:5496–5509, 2008.

GM Harrison, G Davies, TA Martin, WG Jiang, and MD Mason. Distribution and expression of CD44 isoforms and Ezrin during prostate cancer-endothelium interaction. *International Journal of Oncology*, 21:935–940, 2002.

K Harvey and N Tapon. The Salvador-Warts-Hippo pathway: an emerging tumour-suppressor network. *Nat Rev Cancer*, 7:182–191, 2007.

KF Harvey, CM Pfleger, and IK Hariharan. The Drosophila Mst ortholog, hippo, restricts growth and cell proliferation and promotes apoptosis. *Cell*, 114:457–467, 2003.

D Hava, U Forster, M Matsuda, S Cui, BA Link, J Eichhorst, B Wiesner, A Chitnis, and S Abdelilah-Seyfried. Apical membrane maturation and cellular rosette formation during morphogenesis of the zebrafish lateral line. *J Cell Sci*, 122:687–695, 2009.

PP Hernandez, FA Olivari, AF Sarrazin, PC Sandoval, and M Allende. Regeneration in zebrafish lateral line neuromasts: expression of the neural progenitor cell marker sox2 and proliferation-dependent and-independent mechanisms of hair cell renewal. *Developmental Neurobiology*, 67:637654, 2007.

LR Herron. *A study of the behaviour and interactions of the novel FERM protein Willin*. PhD thesis, University of St Andrews, 2007.

LR Herron, F Davey, M Hill, D Sherman, P Brophy, and F Gunn-Moore. The L1 cell adhesion family and their interaction with the 4.1 superfamily. *Neuron Glia Biology*, 2007.

DA Hilton, N Ristic, and CO Hanemann. Activation of ERK, AKT and JNK signalling pathways in human schwannomas in situ. *Histopathology*, 55: 1365–2559, 2009.

M Hisaoka, A Tanaka, and H Hashimoto. Molecular alterations of h-warts/LATS1 tumor suppressor in human soft tissue sarcoma. *Lab Invest*, 82:1427–1435, 2002.

Z Hossain, SM Ali, HL Ko, J Xu, CP Ng, K Guo, Z Qi, S Ponniah, W Hong, and W Hunziker. Glomerulocystic kidney disease in mice with a targeted inactivation of WWTR1. *National Academy of Sciences*, 104:1631–1636, 2007.

J Huang, S Wu, J Barrera, K Matthews, and D Pan. The hippo signaling pathway coordinately regulates cell proliferation and apoptosis by inactivating Yorkie, the Drosophila homolog of YAP. *Cell*, 122:412–434, 2005.

KW Hunter. Ezrin, a key component in tumor metastasis. *Trends in Molecular Medicine*, 2004.

I Imoto, H Tsuda, A Hirasawa, M Miura, M Sakamoto, S Hirohashi, and Inazawa J. Expression of cIAP1, a target for 11q22 amplification, correlates with resistance of cervical cancers to radiotherapy. *Cancer Res.*, 7:556–562, 2005.

M Iwano, D Plieth, TM Danoff, C Xue, H Okada, and EG Neilson. Evidence that fibroblasts derive from epithelium during tissue fibrosis. *J. Clin. Investig*, 110:341–350, 2002.

Q Jiang, D Liu, Y Gong, Y Wang, S Sun, Y Gui, and H Song. YAP is required for the development of brain, eyes, and neural crest in zebrafish. *Biochemical and Biophysical Research Communications*, 2009.

R Kalluri and M Zeisberg. Fibroblasts in cancer. *Nat Rev Cancer*, 6:392–401, 2006.

S Kitajiri, K Fukumoto, M Hata, H Sasaki, T Katsuno, T Nakagawa, J Ito, S Tsukita, and S Tsukita. Radixin deficiency causes deafness associated with progressive degeneration of cochlear stereocilia. *J Cell Biol*, 166:559–570, 2004.

AG Knudson. Antioncogenes and human cancer. *Proc Natl Acad Sci USA*, 90: 10914–10921, 1993.

T Kondo, K Takeuchi, Y Doi, S Yonemura, S Nagata, and S Tsukita. ERM (Ezrin/Radixin/Moesin)-based molecular mechanism of microvillar breakdown at an early stage of apoptosis. *J. Cell Biol*, 139:749–758, 1997.

H Kusunoki and T Kohno. Solution structure and glycophorin C binding studies of the protein 4.1R FERM alpha-lobe domain. *Proteins*, 76:255–260, 2009.

ZC Lai, X Wei, T Shimizu, E Ramos, M Rohrbaugh, N Nikolaidis, LL Ho, and Y Li. Control of cell proliferation and apoptosis by MOB as tumor suppressor, Mats. *Cell*, 120:675–685, 2005.

V Lecaudey, G Cakan-Akdogan, WHJ Norton, and D Gilmour. Dynamic FGF signaling couples morphogenesis and migration in the zebrafish lateral line primordium. *Development*, 135:2695–2705, 2008.

HS Lee, RM Bellin, DL Walker, B Patel, P Powers, H Liu, B Garcia-Alvarez, JM de Pereda, RC Liddington, N Volkmann, D Hanein, DR Critchley, and RM Robson. Characterization of an actin-binding site within the talin FERM domain. *Journal of Molecular Biology*, 2004.

JH Lee, TS Kim, TH Yang, BK Koo, SP Oh, K Lee, HJ Oh, SH Lee, YY Kong, JM Kim, and DS Lim. A crucial role of WW45 in developing epithelial tissues in the mouse. *EMBO*, 27:1231–1242, 2008.

KK Lee, T Ohyama, N Yajima, S Tsubuki, and S Yonehara. MST, a physiological caspase substrate, highly sensitizes apoptosis both upstream and downstream of caspase activation. *J. Biol. Chem.*, 276:19276–19285, 2001.

PE Leone, MJ Bello, JM de Campos, J Vaquero, JL Sarasa, A Pestana, and JA Rey. NF2 gene mutations and allelic status of 1p, 14q and 22q in sporadic meningiomas. *Oncogene*, 18:2231–2239, 1999.

B Levy, T Mukherjee, and K. Hirschhorn. Molecular cytogenetic analysis of uterine leiomyoma and leiomyosarcoma by comparative genomic hybridization. *Cancer Genetics and Cytogenetics*, 121:1–8, 2000.

Y Li, J Pe, H Xia, H Wang, and W Tao. Lats2, a putative tumor suppressor, inhibts G1/S transition. *Oncogene*, 22:4398–405, 2003.

FE Lock, N Underhill-Day, T Dunwell, D Matallanas, W Cooper, L Hesson, A Recino, A Ward, T Pavlova, E Zabarovsky, MM Grant, ER Maher, AD Chalmers, W Kolch, and F Latif. The RASSF8 candidate tumor suppressor inhibits cell growth and regulates the Wnt and NF-KB signaling pathways. *Oncogene*, 29:4307–4316, 2010.

L Lu, Y Li, SM Kim, W Bossuyt, P Liu, Q Qiu, Y Wang, G Halder, MJ Finegold, JS Lee, and RL Johnson. Hippo signaling is a potent in vivo growth and tumor suppressor pathway in the mammalian liver. *Proceedings of the National Academy of Sciences*, 107:14371442, 2010.

M Lutchman and GA Rouleau. The neurofibromatosis type 2 gene product, schwannomin, suppresses growth of NIH3T3 cells. *Cancer Res.*, 55:2270–2274, 1995.

EY Ma and DW Raible. Signaling pathways regulating zebrafish lateral line development. *Current Biology*, 2009.

R Madan, M Brandwein-Gensler, NF Schlecht, K Elias, E Gorbovitsky, TJ Belbin, R Mahmood, D Breining, H Qian, G Childs, J Locker, R Smith, M Jr Haigentz, F Gunn-Moore, , and MB Prystowsky. Differential tissue and subcellular expressionof erm proteins in normal and malignant tissues: cytoplasmic ezrin expression has prognostic signficance for head and neck squamous cell carcinoma. *Head and Neck*, 28:1018–1027, 2006.

R Maddala, VN Reddy, DL Epstein, and V Rao. Growth factor induced activation of Rho and Rac GTPases and actin cytoskeletal reorganization in human lens epithelial cells. *Molecular Vision*, 9:329–336, 2003.

S Maitra, RM Kulikauskas, H Gavilan, and RG Fehon. The tumor suppressors merlin and expanded function cooperatively to modulate receptor endocytosis and signaling. *Current Biology*, 16:702–709, 2006.

R Makita, Y Uchijima, K Nishiyama, T Amano, Q Chen, T Takeuchi, A Mitani, T Nagase, Y Yatomi, H Aburatani, O Nakagawa, EV Small, P Cobo-Stark, P Igarashi, M Murakami, J Tominaga, T Sato, T Asano, Y Kurihara, and H Kurihara. Multiple renal cysts, urinary concentration defects, and pulmonary emphysematous changes in mice lacking taz. *American Journal of Physiology - Renal Physiology*, 294:542–553, 2008.

P Mangeat, C Roy, and M Martin. ERM proteins in cell adhesion and membrane dynamics. *Trends in Cell Biology*, 9:187–192, 1999.

Y Mao, J Mulvaney, S Zakaria, T Yu, KM Morgan, S Allen, MA Basson, P Francis-West, and KD Irvine. Characterization of a Dchs1 mutant mouse reveals requirements for Dchs1-Fat4 signaling during mammalian development. *Development*, 138:947–957, 2011.

CJ Marshall. Specificity of receptor tyrosine kinase signaling - transient versus sustained extracellular signal-regulated kinase activation. *Cell*, 80:179–185, 1995.

V Martel, C Racaud-Sultan, S Dupe, C Marie, F Paulhe, A Galmiche, MR Block, and C Albiges-Rizo. Conformation, localization, and integrin binding of talin depend on its interaction with phosphoinositides. *Journal of Biological Chemistry*, 276:21217–21227, 2001.

J Massagu, L Attisano, and JL Wrana. The tgf-β family and its composite receptors. *Trends in Cell Biology*, 4:172–178, 1994.

D Matallanas, D Romano, K Yee, K Meissl, L Kucerova, D Piazzolla, M Baccarini, JK Vass, W Kolch, and E O'neill. RASSF1A elicits apoptosis through an MST2 pathway directing proapoptotic transcription by the p73 tumor suppressor protein. *Mol Cell*, 21:962–975, 2007.

T Matsui, M Maeda, Y Doi, S Yonemura, M Amano, K Kaibuchi, S Tsukita, and S Tsukita. Rho-kinase phosphorylates COOH-terminal threonines of Ezrin/Radixin/Moesin (ERM) proteins and regulates their head-to-tail association. *J. Cell Biol*, 140:647–657, 1998.

B McCartney, RM Kulikauskas, DR LaJeunesse, and RG Fehon. The neurofibromatosis-2 homologue, merlin, and the tumor suppressor expanded function together in drosophila to regulate cell proliferation and differentiation. *Dev*, 127:1315–1324, 2000.

BM McCartney and RG Fehon. Distinct cellular and subcellular patterns of expression imply distinct functions for the Drosophila homologues of moesin and the neurofibromatosis 2 tumor suppressor, merlin. *J Cell Biol*, 133:843–852, 1996.

AI McClatchey and M Giovannini. Membrane organization and tumorigenesis-the nf2 tumor suppressor, merlin. *Genes and Development*, 19:2265–2277, 2005.

AI McClatchey, I Saotome, V Ramesh, JF Gusella, and T Jacks. The NF2 tumor suppressor gene product is essential for extraembryonic development immediately prior to gastrulation. *Genes and Development*, 11:1253–1265, 1997.

JP McPherson, L Tamblyn, A Elia, E Migon, A Shehabeldin, E Matysiak-Zablocki, B Lemmers, L Salmena, A Hakem, J Fish, F Kassam, J Squire, BG Bruneau, MP Hande, and R Hakem. Lats2/Kpm is required for embryonic development, proliferation control and genomic integrity. *EMBO J*, 23: 3677–3688, 2004.

C Meignin, I Alvarez-Garcia, I Davis, and IM Palacios. The Salvador-Warts-Hippo pathway is required for epithelial proliferation and axis specification in Drosophila. *Current Biology*, 17:1871–1878, 2007.

JJ Meng, DJ Lowrie, H Sun, E Dorsey, PD Pelton, AM Bashour, J Groden, N Ratner, and W Ip. Interaction between two isoforms of the NF2 tumor suppressor protein, merlin, and between merlin and ezrin, suggests modulation of ERM proteins by merlin. *Journal of neuroscience research*, 62: 491–502, 2000.

KG Miller. A role for moesin in polarity. *Trends in Cell Biology*, 13:165–168, 2003.

R Mirsky and KR Jessen. Schwann cell development, differentiation and myelination. *Current Opinion in Neurobiology*, 6:89–96, 1996.

J Montgomery, G Carton, R Voigt, C Baker, and C Diebel. Sensory processing of water currents by fishes. *Philosophical Transactions of the Royal Society of London. Series B: Biological Sciences*, 355:1325–1327, 2000.

T Mori, K Kitano, S Terawaki, R Maesaki, Y Fukami, and T Hakoshima. Structural basis for CD44 recognition by ERM proteins. *J. Biol. Chem*, 283:29602–29612, 2008.

E M. Morin-Kensicki, BN Boone, M Howell, JR Stonebraker, J Teed, JG Alb, TR Magnuson, W O'Neal, and SL Milgram. Defects in yolk sac vasculogenesis, chorioallantoic fusion, and embryonic axis elongation in mice with targeted disruption of yap65. *Mol. Cell. Biol.*, 26:77–87, 2006.

H Morrison, LS Sherman, J Legg, F Banine, C Isacke, CA Haipek, DH Gutmann, H Ponta, and P Herrlich. The NF2 tumor suppressor gene product, merlin, mediates contact inhibition of growth through interactions with CD44. *Genes and Development*, 15:968–980, 2001.

H Morrison, T Sperka, J Manent, M Giovannini, H Ponta, and P Herrlich. Merlin/neurofibromatosis type 2 suppresses growth by inhibiting the activation of ras and rac. *Cancer Research*, 67:520–527, 2007.

T Muranen, M Gronholm, GH Renkema, and O Carpen. Cell cycle-dependent nucleocytoplasmic shuttling of the neurofibromatosis 2 tumour suppressor merlin. *Oncogene*, 24:1150–1158, 2005.

H Oh and KD Irvine. In vivo analysis of yorkie phosphorylation sites. *Oncogene*, 28:19161927, 2009.

T Oka, V Mazack, and M Sudol. Mst2 and Lats kinases regulate apoptotic function of Yes Kinase-associated Protein (YAP). *Journal of Biological Chemistry*, 283:27534–27546, 2008.

E O'Neill and W Kolch. Taming the Hippo: Raf-1 controls apoptosis by suppressing MST2/Hippo. *Cell Cycle*, 4:365–367, 2005.

M Overholtzer, J Zhang, GA Smolen, B Muir, and W et al. Li. Transforming properties of YAP, a candidate oncogene on the chromosome 11q22 amplicon. *Proceedings of the National Academy of Sciences*, 103:12405–12410, 2006.

D Pan. Hippo signaling in organ size control. *Genes Dev*, 21:886–897, 2007.

ST Pang, X Fang, A Valdman, G Norstedt, A Pousette, L Egevad, and P Ekman. Expression of ezrin in prostatic intraepithelial neoplasia. *Urology*, 63: 609–612, 2004.

S Pantalacci, N Tapon, and P Leopold. The Salvador partner Hippo promotes apoptosis and cell-cycle exit in Drosophila. *Nat Cell Biol*, 5:921–927, 2003.

MA Pearson, D Reczek, A Bretscher, and PA Karplus. Structure of the ERM protein moesin reveals the FERM domain fold masked by an extended actin binding tail domain. *Cell*, 101:259–270, 2000.

BJ Pellock, E Buff, K White, and IK Hariharan. The drosophila tumor suppressors expanded and merlin differentially regulate cell cycle exit, apoptosis, and wingless signaling. *Developmental Biology*, 304:102, 2007.

C Polesello and F Payre. Small is beautiful: what flies tell us about ERM protein function in development. *Trends Cell Biol*, 14:294–302, 2004.

CJ Potter, GS Turenchalk, and T Xu. Drosophila in cancer research: an expanding role. *Trends in Genetics*, 16:33–39, 2000.

V Ramesh. Merlin and the ERM proteins in Schwann cells, neurons and growth cones. *Nat Rev Neurosci*, 5:462–470, 2004.

BV Reddy and KD Irvine. The FAT and Warts signaling pathways: new insights into their regulation, mechanism and conservation. *Development*, 135:2827–2838, 2008.

GA Rouleau, P Merel, M Lutchman, M Sanson, J Zucman, C Marineau, K Hoang-Xuan, S Demczuk, C Desmaze, B Plougastel, SM Pulst, G Lenoir, E Bijlsmaparallel, R Fashold, J Dumanski, P Jong, D Parry, R Eldrige, A Aurias, O Delattre, and G Thomas. Alteration in a new gene encoding a putative membrane-organizing protein causes neuro-fibromatosis type 2. *Nature*, 363:515–521, 1993.

JF Rual, K Venkatesan, T Hao, T Hirozane-Kishikawa, A Dricot, N Li, FG Berriz, FD Gibbons, M Dreze, N Ayivi-Guedehoussou, N Klitgord, C Simon, M Boxem, S Milstein, J Rosenberg, DS Goldberg, LV Zhang, SL Wong, G Franklin, S Li, JS Albala, J Lim, C Fraughton, E Llamosas, S Cevik, C Bex, P Lamesch, RS Sikorski, J Vandenhaute, HY Zoghbi, A Smolyar, S Bosak, R Sequerra, L Doucette-Stamm, ME Cusick, DE Hill, FP Roth, and M Vidal. Towards a proteome-scale map of the human protein-protein interaction network. *Nature*, 437:1173–1178, 2005.

S Saburi, I Hester, E Fischer, M Pontoglio, V Eremina, M Gessler, SE Quaggin, R Harrison, R Mount, and H McNeill. Loss of Fat4 disrupts PCP signaling

and oriented cell division and leads to cystic kidney disease. *Nat Genet*, 40: 1010–1015, 2008.

I Saotome, M Curto, and AI McClatchey. Ezrin is essential for epithelial organization and villus morphogenesis in the developing intestine. *Dev. Cell*, 6:855–864, 2004.

RJ Shaw, AI McClatchey, and T Jacks. Regulation of the neurofibromatosis type 2 tumor suppressor protein, merlin, by adhesion and growth arrest stimuli. *J Biol Chem*, 273:7757–7764, 1998.

L Sherman, HM Xu, RT Geist, S Saporito-Irwin, N Howells, H Ponta, P Herrlich, and DH Gutmann. Interdomain binding mediates tumor growth suppression by the NF2 gene product. *Oncogene*, 15:2505–2509, 1997.

E Silva, Y Tsatskis, L Gardano, N Tapon, and H McNeill. The tumor suppressor gene fat controls tissue growth upstream of expanded in the hippo signaling pathway. *Curr Biol*, 16:2081–2089, 2006.

K Skouloudaki, M Puetz, M Simons, J Courbard, C Boehlke, B Hartleben, C Engel, MJ Moeller, C Englert, F Bollig, T Schafer, H Ramachandran, M Mlodzik, TB Huber, EW Kuehn, E Kim, A Kramer-Zucker, and G Walz. Scribble participates in Hippo signaling and is required for normal zebrafish pronephros development. *Proceedings of the National Academy of Sciences*, 106:8579–8584, 2009.

AM Snijders, BL Schmidt, J Fridlyand, N Dekker, D Pinkel, RCK Jordan, and DG Albertson. Rare amplicons implicate frequent deregulation of cell fate specification pathways in oral squamous cell carcinoma. *Oncogene*, 24: 42324242, 2005.

H Song, KK Mak, L Topol, K Yun, J Hu, L Garrett, Y Chen, O Park, J Chang, RM Simpson, CY Wang, B Gao, J Jiang, and Yang Y. Mammalian Mst1 and Mst2 kinases play essential roles in organ size control and tumor suppression. *Proc Natl Acad Sci USA*, 2010.

MAR St John, W Tao, X Fei, R Fukumoto, ML Carcangiu, DG Brownstein, AF Parlow, SJ McGrath, and T Xu. Mice deficient of Lats1 develop soft-tissue sarcomas, ovarian tumours and pituitary dysfunction. *Nature Genetics*, 21:182–186, 1999.

AO Stemmer-Rachamimov, L Xu, C Gonzalez-Agosti, JA Burwick, D Pinney, R Beauchamp, LB Jacoby, JF Gusella, V Ramesh, and DN Louis. Universal absence of merlin, but not other erm family members, in schwannomas. *Am J Pathol*, 151:1649–1654, 1997.

JT Stickney, WC Bacon, M Rojas, N Ratner, and W Ip. Activation of the tumor suppressor Merlin modulates its interaction with lipid rafts. *Cancer Res*, 64:2717–2724, 2004.

S Strano, E Munarriz, M Rossi, L Castagnoli, Y Shaul, A Sacchi, M Oren, M Sudol, G Cesareni, and G Blandino. Physical interaction with yes-associated protein enhances p73 transcriptional activity. *Journal of Biological Chemistry*, 18:15164–15173, 2001.

K Striedinger, SR VandenBerg, GS Baia, MW McDermott, DH Gutmann, and A Lal. The neurofibromatosis 2 tumor suppressor gene product, merlin, regulates human meningioma cell growth by signaling through YAP. *Neoplasia*, 10:1204–12, 2008.

M Sudol and KF Harvey. Modularity in the hippo signaling pathway. *Trends in Biochemical Sciences*, 35:627–633, 2010.

CX Sun, VA Robb, and DH Gutmann. Protein 4.1 tumor suppressors: getting a FERM grip on growth regulation. *J Cell Sci*, 115:3991–4000, 2002.

Y Takahashi, Y Miyoshi, C Takahata, N Irahara, T Taguchi, Y Tamaki, and S Noguchi. Down-Regulation of LATS1 and LATS2 mRNA Expression by Promoter Hypermethylation and Its Association with Biologically Aggressive Phenotype in Human Breast Cancers. *Clinical Cancer Research*, 11: 1380–1385, 2005.

K Takeuchi, N Sato, H Kasahara, N Funayama, A Nagafuchi, S Yonemura, S Tsukita, and S Tsukita. Perturbation of cell adhesion and microvilli formation by antisense oligonucleotides to ERM family members. *The Journal of Cell Biology*, 125:1371–1384, 1994.

W Tao, S Zhang, GS Turenchalk, RA Stewart, MAR St John, W Chen, and T Xu. Human homologue of the Drosophila melanogaster lats tumour suppressor modulates CDC2 activity. *Nat Genet*, 21:177–181, 1999.

N Tapon, KF Harvey, DW Bell, DCR Wahrer, TA Schiripo, DA Haber, and IK Hariharan. Salvador promotes both cell cycle exit and apoptosis in Drosophila and is mutated in human cancer cell lines. *Cell*, 2002.

ML Tarby and JF Webb. Development of the supraorbital and mandibular lateral line canals in the cichlid, archocentrus nigrofasciatus. *Journal of Morphology*, 255:44–57, 2003.

M Theobald, H Christiansen, A Schmidt, B Melekian, N Wolkewitz, NM Christiansen, C Brinkschmidt, F Berthold, and F Lampert. Sublocalization of putative tumor suppressor gene loci on chromosome arm 14q in neuroblastoma. *Genes Chromosomes and Cancer*, 26:40–46, 1999.

M Tokunou, T Niki, Y Saitoh, H Imamura, M Sakamoto, and S Hirohashi. Altered expression of the ERM proteins in lung adenocarcinoma. *Lab Invest*, 80:1643–1650, 2000.

ML Torres-Mapa, L Angus, M Ploschner, K Dholakia, and FJ. Gunn-Moore. Transient transfection of mammalian cells using a violet diode laser. *J Biomed Opt*, 15, 2010.

JA Trofatter, MM MacCollin, JL Rutter, JR Murrell, MP Duyao, DM Parry, R Eldridge, N Kley, AG Menon, K Pulaski, VH Haase, CM Ambrose, D Munroe, C Bove, JL Haines, RL Martuza, ME MacDonald, BR. Seizinger, M Short, AJ Buckler, and JF Gusella. A novel moesin-, ezrin-, radixin-like gene is a candidate for the neurofibromatosis 2 tumor suppressor. *Cell*, 72: 791–800, 1993.

JYM Tse, HK Ng, KM Lau, KW Lo, WS Poon, and DP Huang. Loss of heterozygosity of chromosome 14q in low- and high-grade meningiomas. *Human Pathology*, 28:779–785, 1997.

S Tsukita, K Oishi, N Sato, J Sagara, A Kawai, and S Tsukita. ERM family members as molecular linkers between the cell surface glycoprotein CD44 and actin-based cytoskeletons. *J. Cell Biol.*, 126:391–401, 1994.

O Turunen, T Wahlstrom, and A. Vaheri. Ezrin has a COOH-terminal actin-binding site that is conserved in the ezrin protein family. *J. Cell Biol.*, 126: 1445–1453, 1994.

DM Tyler and NE Baker. Expanded and fat regulate growth and differentiation in the Drosophila eye through multiple signaling pathways. *Dev Biol*, 305: 187–201, 2007.

RS Udan, M Kango-Singh, R Nolo, C Tao, and G Halder. Hippo promotes proliferation arrest and apoptosis in the Salvador/Warts pathway. *Nat Cell Biol*, 5:914–920, 2003.

X Varelas, R Sakuma, P Samavarchi-Tehrani, R Peerani, BM Rao, J Dembowy, Yaffe MB, PW Zandstra, and JL Wrana. TAZ controls Smad nucleocytoplasmic shuttling and regulates human embryonic stem-cell self-renewal. *Nature Cell Biology*, 10:837–848, 2008.

K Venkateswarlu, F Gunn-Moore, JM Tavare, and PJ Cullen. EGF- and NGF-stimulated translocation of cytohesin-1 to the plasma membrane of PC12 cells requires PI 3-kinase activation and a functional cytohesin-1 PH domain. *Journal of Cell Science*, 112:1957–1965, 1999.

PM Voorhoeve, C le Sage, M Schrier, AJ Gillis, H Stoop, R Nagel, YP Liu, J van Duijse, J Drost, A Griekspoor, E Zlotorynski, N Yabuta, G De Vita, H Nojima, LH Looijenga, and R Agami. A genetic screen implicates mirna-372 and mirna-373 as oncogenes in testicular germ cell tumors. *Adv Exp Med Biol*, 604:17–46, 2007.

K Wang, C Degerny, M Xu, and XJ Yang. YAP, TAZ, and Yorkie: a conserved family of signal-responsive transcriptional coregulators in animal development and human disease. *Biochemistry and Cell Biology*, 87:77–91, 2009.

YF Wang, JN Shen, XB Xie, J Wang, and Huang G. Expression change of ezrin as a prognostic factor in primary osteosarcoma. *Med Oncol*, pages 685–697, 2010.

W Wick, C Grimmel, C Wild-Bode, M Platten, M Arpin, and M Weller. Ezrin-dependent promotion of glioma cell clonogenicity, motility, and invasion mediated by BCL-2 and transforming growth factor-beta 2. *Journal of Neuroscience*, 21:3360–3368, 2001.

M Willecke, F Hamaratoglu, M Kango-Singh, R Udan, CL Chen, C Tao, X Zhang, and G Halder. The fat cadherin acts through the hippo tumor-suppressor pathway to regulate tissue size. *Curr Biol*, 16:2090–2100, 2006.

M Willecke, F Hamaratoglu, L Sansores-Garcia, C Tao, and G Halder. Boundaries of dachsous cadherin activity modulate the hippo signaling pathway to induce cell proliferation. *Proc Natl Acad Sci USA*, 30:14897–14902, 2008.

KL Wu, S Khan, S Lakhe-Reddy, G Jarad, A Mukherjee, CA Obejero-Paz, M Konieczkowski, JR Sedor, and JR Schelling. The NHE1 Na+/H+ exchanger recruits ezrin/radixin/moesin proteins to regulate Akt-dependent cell survival. *Journal of Biological Chemistry*, 279:26280–26286, 2004.

S Wu, J Huang, J Dong, and D Pan. Hippo encodes a ste-20 family protein kinase that restricts cell proliferation and promotes apoptosis in conjunction with salvador and warts. *Cell*, 114:445–456, 2003.

S Wu, Y Liu, Y Zheng, J Dong, and D. Pan. The TEAD/TEF family protein Scalloped mediates transcriptional output of the Hippo growth-regulatory pathway. *Dev. Cell*, 14:388–398, 2009.

H Xia, H Qi, J Pei, J Barton, M Blackstad, T Xu, and W Tao. LATS1 tumor suppressor regulates G2/M transition and apoptosis. *Oncogene*, 21: 1233–1241, 2002.

HM Xu and DH Gutmann. Merlin differentially associates with the microtubule and actin cytoskeleton. *J Neurosci Res*, 51:403–415, 1998.

Y Xu, I Stamenkovic, and Q Yu. CD44 Attenuates Activation of the Hippo Signaling Pathway and Is a Prime Therapeutic Target for Glioblastoma. *Cancer Research*, 70:2455–2464, 2010.

X Yang, K Yu, Y Hao, D Li, R Stewart, KL Insogna, and T Xu. LATS1 tumour suppressor affects cytokinesis by inhibiting LIMK1. *Nat Cell Biol*, 6:609–617, 2004.

J Yu, Y Zheng, J Dong, S Klusza, W Deng, and D Pan. Kibra functions as a tumor suppressor protein that regulates hippo signaling in conjunction with Merlin and Expanded. *Dev Cell*, 18:288–299, 2010.

M Yuan, V Tomlinson, D Holliday, C Chelala, T Harada, R Gangeswaran, C Manson-Bishop, P Smith, SA Danovi, O Pardo, T Crook, CA Mein, LZ Jones, and S Basu. Yes-associated protein (YAP) functions as a tumor suppressor in breast. *Cell Death and Differentiation*, 15:1752–1759, 2008.

L Zender, MS Spector, W Xue, P Flemming, C Cordon-Cardo, J Silke, ST Fan, JM Luk, M Wigler, GJ Hannon, D Mu, R Lucito, S Powers, and SW Lowe. Identification and validation of oncogenes in liver cancer using an integrative oncogenomic approach. *Cell*, 125:1253–1267, 2006.

H Zhang, CY Liu, ZY Zha, B Zhao, J Yao, S Zhao, Y Xiong, QY Lei, and KL Guan. TEAD transcription factors mediate the function of TAZ in cell growth and epithelial-mesenchymal transition. *J Biol Chem*, 15:13355–13362, 2009a.

J Zhang, GA Smolen, and DA Haber. Negative regulation of YAP by LATS1 underscores evolutionary conservation of the Drosophila Hippo pathway. *Cancer Res*, 68:2789–2794, 2008a.

L Zhang, F Ren, Q Zhang, Y Chen, B Wang, and J Jiang. The TEAD/TEF family of transcription factor Scalloped mediates Hippo signaling in organ size control. *Dev. Cell*, 14:377–387, 2008b.

N Zhang, H Bai, KK David, J Dong, Y Zheng, J Cai, M Giovannini, P Liu, RA Anders, and D Pan. The Merlin/NF2 Tumor Suppressor Functions through the YAP Oncoprotein to Regulate Tissue Homeostasis in Mammals. *Developmental Cell*, 19:27–38, 2010.

X Zhang, CC Milton, PO Humbert, and Harvey KF. Transcriptional output of the Salvador/Warts/Hippo pathway is controlled in distinct fashions in Drosophila melanogaster, and mammalian cell lines. *Cancer Res.*, 69:6033–6041, 2009b.

B Zhao, X Wei, W Li, RS Udan, Q Yang, J Kim, J Xie, T Ikenoue, J Yu, L Li, P Zheng, K Ye, A Chinnaiyan, G Halder, Z Lai, and KL Guan. Inactivation of yap oncoprotein by the hippo pathway is involved in cell contact inhibition and tissue growth control. 21(21):2747–2761, 2007.

B Zhao, X Ye, J Yu, L Li, W Li, S Li, J Yu, JD Lin, CY Wang, AM Chinnaiyan, ZC Lai, and KL Guan. TEAD mediates YAP-dependent gene induction and growth control. *Genes Dev*, 22:1962–1971, 2008.

B Zhao, L Li, Q Lei, and KL Guan. The Hippo-YAP pathway in organ size control and tumorigenesis: an updated version. *Genes and Development*, 24:862–874, 2010a.

B Zhao, L Li, K Tumaneng, CY Wang, and Guan KL. A coordinated phosphorylation by lats and ck1 regulates yap stability through scf(beta-trcp). *Genes Dev*, 24:72–85, 2010b.

B Zhao, L Li, Q Lu, LH Wang, CY Liu, Q Lei, and Guan KL. Angiomotin is a novel Hippo pathway component that inhibits YAP oncoprotein. *Genes Dev*, 25:51–63, 2011.

D Zhou, BD Medoff, L Chen, L Li, X Zhang, M Praskova, M Liu, A Landry, RS Blumberg, VA Boussiotis, R Xavier, and J Avruch. The Nore1B/Mst1 complex restrains antigen receptor-induced proliferation of native T cells. *Proceedings of the National Academy of Sciences*, 105:20321–20326, 2008.

D Zhou, C Conrad, F Xia, JS Park, B Payer, Y Yin, GY Lauwers, W Thasler, JT Lee, J Avruch, and N Bardeesy. Mst1 and Mst2 maintain hepatocyte quiescence and suppress hepatocellular carcinoma development through inactivation of the Yap1 oncogene. *Cancer Cell*, 6:425–438, 2009.

Appendix A

Human willin sequence (BC020521)

Amino acid sequence:

MNKLNFHNNRVMQDRRSVCIFLPNDESLNIIINVKILCHQLLVQVCDLLRLKDCHLFGL
SVIQNNEHVYMELSQKLYKYCPKEWKKEASKGIDQFGPPMIIHFRQYYVENGRLISDRA
ARYYYYWHLRKQVLHSQCVLREEAYFLLAAFALQADLGNFKRNKHYGKYFEPEAYFPSW
VVSKRGKDYILKHIPNMHKDQFALTASEAHLKYIKEAVRLDDVAVHYYRLYKDKREIEA
SLTLGLTMRGIQIFQNLDEEKQLLYDFPWTNVGKLVFVGKKFEILPDGLPSARKLIYYT
GCPMRSRHLLQLLSNSHRLYMNLQPVLRHIRKLEENEEKKQYRESYISDNLDLDMDQLE
KRSRASGSSAGSMKHKRLSRHSTASHSSSHTSGIEADTKPRDTGPEDSYSSSAIHRKLK
TCSSMTSHGSSHTSGVESGGKDRLEEDLQDDEIEMLVDDPRDLEQMNEESLEVSPDMCI
YITEDMLMSRKLNGHSGLIVKEIGSSTSSSSETVVKLRGQSTDSLPQTICRKPKTSTDR
HSLSLDDIRLYQKDFLRIAGLCQDTAQSYTFGCGHELDEEGLYCNSCLAQQCINIQDAF
PVKRTSKYFSLDLTHDEVPEFVVstop

Nucleotide sequence:

atgaacaaattgaattttcataacaacagagtcatgcaagaccgccgcagtgtgtgc
attttccttcccaacgatgaatctctgaacatcatcataaatgttaagattctgtgt
caccagttgctggtccaggtttgtgacctgctcaggctaaaggactgccacctcttt
ggactcagtgttatacaaaataatgaacatgtgtatatggagttgtcacaaaagctt
tacaaatattgtccaaaagaatggaagaaagaggccagcaagggtatcgaccaattt
gggcctcctatgatcatccacttccgtgtgcagtactatgtggaaaatggcagattg
atcagtgacagagcagcaagatactattattactggcacctgagaaaacaagttctt
cattctcagtgtgtgctccgagaggaggcctacttcctgctggcagcctttgccctg
caggctgatcttgggaacttcaaaaggaataagcactatggaaaatacttcgagcca
gaggcttacttcccatcttgggttgtttccaagaggggaaggactacatcctgaag
cacattccaaacatgcacaaagatcagtttgcactaacagcttccgaagctcatctt
aaatatatcaaagaggctgtccgactggatgacgtcgctgttcattactacagattg
tataaggataaaagggaaattgaagcatcgctgactcttggattgaccatgagggga
atacagattttcagaatttagatgaagagaaacaattactttatgatttcccctgg
acaaatgttggaaaattggtgtttgtgggtaagaaatttgagattttgccagatggc
ttgccttctgcccggaagctcatatactacacggggtgccccatgcgctccagacac
ctcctgcaacttctgagcaacagccaccgcctctatatgaatctgcagcctgtcctg
cgccatatccggaagctggaggaaaacgaagagaagaagcagtaccgggaatcttac
atcagtgacaacctggacctcgacatggaccagctggaaaaacggtcgcgggccagc
gggagcagtgcgggcagcatgaaacacaagcgcctgtcccgtcattccaccgccagc
cacagcagttcccacacctcgggcattgaggcagacaccaagccccgggacacgggg
ccagaagacagctactccagcagtgccatccaccgcaagctgaaaacctgcagctca
atgaccagtcatggcagctcccacacctcaggggtggagagtggcggcaaagaccgg
ctggaagaggacttacaggacgatgaaatagagatgttggttgatgacccccgggat
ctggagcagatgaatgaagagtctctggaagtcagcccagacatgtgcatctacatc
acagaggacatgctcatgtcgcggaagctgaatggacactctgggttgattgtgaaa
gaaattgggtcttccacctcgagctcttcagaaacagttgttaagcttcgtggccag
agtactgattctcttccacagactatatgtcggaaaccaaagacctccactgatcga
cacagcttgagcctcgatgacatcagactttaccagaaagacttcctgcgcattgca
ggtctgtgtcaggacactgctcagagttacacctttggatgtggccatgaactggat
gaggaaggcctctattgcaacagttgcttggcccagcagtgcatcaacatccaagat
gcttttccagtcaaaagaaccagcaaatacttttctctggatctcactcatgatgaa
gttccagagtttgttgtgtaa

Appendix B

Mouse willin sequence (NM028127)

Amino acid sequence:

MNKLTFHNNKAMQDRRRVCIFLPNDKSVSIIINVKILCHQLLVQVCDLLRLKDSHLF
GLSVIQNNEHVYMELSQKLYKYCPKEWKKEASKVRQYEVTWGIDQFGPPMIIHFRVQ
YYVENGKLISDRIARYYYYWHLRKQVLHSQCVLREEAYFLLAAFALQADLGNFKRKL
HHGDYFEPEAYFPAWVVSKRGKDYILKHIPNMHKDQFALTASEAYYIKEAVRLDDVA
IHYYRLYKDKREAEGSLTLGLTMRGIQIFQNLEEEKQLLYDFPWTNVGKLVFVGKKF
EILPDGLPSARKLVYYTGCPTRSRHLLQLLSNSHRLYMNLQPVLRHLRKQEENEEKK
QYRESYISDNLDLDMDPLEKRSRASGSSAGSVKHKRLSRHSTASHSSSHTSGIEADT
KPRDPGPEDSCSGSAMHRKLKTCSSMTSHGSSHTSGVESGGKDRLEEDSQDEEIEML
VDDPRDLEPMPEESLEVSPEMCIYITEDMLLSRKLNGHSGLIVKEIGSSTSSSSETV
VRLRGQSTDSLPQTICRKPKTSTDRHSLSLDDIRLYQKDFLRIAGLCQDTAQSYTFG
CGHELDESGLYCNSCLAQQCVNIQDAFPVKRASKYFSLDLTHDEVPEFVV

Nucleotide sequence:

cggcgccgctggagcagacgccggttgtgagtcggaagcctggcgctgtcgactttggaggtctcccag
tggactttctacagctatgaaacctacactgtggggcaccacgatgcttccgttggccgtatgatgagg
aggagaagttggctttggagtgctgggagcctgagaagttgctgagcacccagcgcccccagcccgccc
actggcccgcccataacacaatgaacaaactgaccttccataacaacaaagccatgcaggaccgtcgca
gagtgtgtattttcctccccaatgacaagtccgtgagcatcatcataaatgttaaaattctgtgtcacc
agttgctggtccaggtgtgtgacctgctcaggttaaaggacagtcacctctttggtctcagtgttatac
aaaataatgaacatgtatatatggaattgtcacaaaagctttataagtattgtccaaaagaatggaaaa
aggaggccagcaaggtacggcaatacgaagtcacttggggcatcgaccagtttgggccccccatgatca
tccacttccgggtgcagtactacgtggagaatgggaagctgatcagtgaccgaattgcaagatactatt
attactggcacctacggaaacaggtgctgcactcccagtgtgtgctcagagaggaggcctacttcctgc
tggcagcctttgcactgcaagctgacctcggcaacttcaaaaggaaactgcaccacggagactactttg
agccagaggcttacttcccggcatgggttgtttccaagcgggggaaggactacatcctgaaacacatcc
caaacatgcacaaggaccagtttgccctgacggcctccgaggcctacctaaagtacatcaaagaagccg
tccgactggacgacgtcgccatccattactacagactgtacaaggataaaagggaggctgaaggctcac
tgaccctaggactgaccatgcgaggaatacagattttcagaatctagaagaagagaaacaattgctct
atgatttcccctggacaaatgttgggaagttggtgtttgtgggcaagaagtttgagattttgccagatg
gccttccctccgccaggaagctggtctactacacagggtgtcccacgcgctcccggcatctcctgcagc
tcctgagcaacagccaccgcctctacatgaacctgcagcccgtcctgcgccacctccgcaagcaggagg
agaatgaagagaaaaagcagtaccgggaatcctacatcagcgacaacctggaccttgacatggacccgc
tggaaaagcggtcccgagccagtgggagcagcgctggcagcgtgaagcataagcgcctgtcccgccact
ccacggccagccacagcagctcccacacctccggcatcgaggcagacaccaagccccgggacccagggc
cggaagacagctgttcaggcagcgccatgcaccggaagctgaagacctgcagctccatgaccagccacg
gcagctcccacacctctggggttgagagtggaggcaaagaccgcctggaagaggactcgcaagatgagg
aaatcgagatgctggtggatgaccccagggacctggagccgatgcctgaagagtcgctggaagtcagcc
cagagatgtgtatctacatcacggaagatatgctcctgtcgaggaagctgaacggacactcagggttaa
ttgtgaaagaaatcggctcctccacctccagctcttcggaaacggttgtcaggctgcgtggacagagca
ccgactcccttccacagacgatatgtcgaaaaccaaagacttccaccgatcgccatagcctgagccttg
acgacatcagactgtaccagaaagacttcctgcgcatcgcgggcctgtgtcaggacactgctcagagct
acacgtttgggtgtggccatgaactggatgagagcggtctctactgcaacagctgcctggctcagcagt
gtgtcaacatacaggacgcattcccagtgaaaagagccagcaagtacttttctctggaccttactcacg
acgaagtcccagagttcgtcgtctgagtcgcccctgcgggcagccctgcgggcagccgctgtctgctgg
aggctgtggagtctgagggtctttacacattatttgtgccataacttttcaccccaaacttagctttt
tctttatagtattcgagatggaaacaaaagccttgggacagttgcactttaagtattatgcagaggtaa
aagaaacagagaatgtaagaggaagacaagtgcccagattgtctattgccccttggaaggaagtgtgc
tttccagctttacccagatttcagactgtcagactgcagtgtgtttgttcatctcttgtgttccggttc
aaatttatgtttatcacgtgaaagatgttataggcttatctgtttgcttatgggtttttcagccacttc
ctcatgaggcacggtttgaggggggaggacaaaaggggagttctctcttctttttctggagagccattcta
gtacatagccattgttgcctcacagaggttggtccgaaatgaacactgaagttggtgggagtcttatgt
tctagccaaagatgtgtatgtgatggaagatggaagccccactcagagtccagaaggcgtgtgccggga
cactgggctccttcacaaatggacagtgctctgtccgctgttttgttcttccatgaccttcccaggaag
ctctgggattggcctgtgcttgtgacatggtacattttgcagtttacaaagctggtgtatgttaacaac
cattgggaatgtctcagaagacatttgtttggttgtatttcctttgttggtttttaatggtggccaaca
gatggtgatgctagtttctgctttaacaagatacccttactgtatgtatatgttatacgtatctagata
cgtgggactctgtgtgtttatgtgtttgaagcttagtgactcttcatttggacttcagtatatgtcttg
cacacatagaatttcttgtttaatgtcaaggatgcttagacacagacaatcagttgataaatgtagagt
taagagtgacttttccatgtgtgcctttggccaagattctcaaccctgattgcataatagacttgtcca
gagagcttttaaaacatgcccgggtcccaccaggccagtttaaaccagtctcctgtggctgggagattg
atttaaagtgtaccaggttgagacagtaatgcacagtaggattggagatccaagagtgtctttctattc
attttgaagtaaaagtatacagaaaatattagtgatagagaatgggccacttttaagacagggcctgct
actgttacagtgtataatgaagccaggagaatgagtttggtcaacttgatatccattgaagacgttgct
cgcccttcaggagagaacttcatagcacaatgtctttctaggagatgtttttaatgatttagtatttta
caacatttgtttaccatattttgatactccatttttgctatctgccaggttttattaaaaagaagacta
tgtattattttctaaagaaactcatatttttgtacaaacttatgtttccaagtaaggaagaaatagatg
tagggtcaggcagaacatagcagtgtttccccctggctaggtcagtgtcccagagcccgtggtggccac
agacatgcccggtcaccatgctgccctcctgtgctggcacggcctcagcagggtcacatccagtaactc
tcacctgacactaaagaaggaaaaagaagttctgtgctcatgacttttattttgcttttgttgaatgctt
ttagaagaaccaaagtttcagatgccagaatgtataagtgtctcagtgtccacagataggcaaagggca
aaggggtccgtcacctgatggcttcttttgcttccgagtcattgcatagtctcatcattgctcacagat
gcttaggggccacaccctggtgaagtacgcgatctccagagcacagatggccgtgtattcccacagccc
tcggcatctcttgcagatgcagagatggaaaggttgcttgcttggctgtgtgctttataccttttttct
ctctgctccagaatccagtcttcagggttctgcccaggctgtcgatcgccatttgccctcttccaggca
gacttggaaatagtcttaaagggttttcaaagacaagatcagccaggaaacagtttctcatttctgacc
cacgggagaatcatagacatatatgtatgtggagctccactttgaagaattgacattcttgtattgggc

Appendix C

Rat willin sequence (163scII)

Amino acid sequence:

QRTLPDHWPAHNTMNKLTFHNNKVMQDRRRVCIFLPNDKSVSIIINVKILCHQLLVQVC
DLLRLKDSHLFGLSVIQNNEHVYMELSQKLYKYCPKEWKKEASKGIDQFGPPMIIHFRV
QYYVENGKLISDRIARYYYYWHLRKQVLHSQCVLREEAYFLLAAFALQADLGNFKRKVH
HGDYFEPEAYFPAWVVSKRGKDYILKHIPNMHRDQFALTASEAYLKYIKEAVRLDDVAI
HYYRLYKDKREVEGSLTLGLTMRGIQIFQNLEEEKQLLYDFPWTNVGKLVFVGKKFEIL
PDGLPSARKLVYYTGCPTRSRHLLQLLSNSHRLYMNLQPVLRHLR

Nucleotide sequence:

cagcgcaccctgcctgaccactggccagcccacaacacaatgaacaaactgaccttccataa
caacaaagtcatgcaggaccgccgcagagtgtgtatttcctccccaatgacaagtctgtga
gcatcatcataaatgttaaaattctgtgtcaccagttgctggtccaggtgtgtgacctgctc
aggttgaaggatagtcacctctttggtctcagtgttatacaaaataatgaacacgtatatat
ggaattgtcacaaaagctctataagtattgtccaaaagaatggaaaaaggaggccagcaagg
gcatcgaccagtttgggcctcccatgatcatccatttccgggtgcagtactatgtggagaac
gggaagctgatcagtgaccggattgcgagatactattattactggcacctaaggaaacaggt
gctgcactctcagtgtgtgctcagagaggaggcctacttcctgctggcagcctttgcactgc
aggctgacctcgggaacttcaaaaggaaagtgcaccatggagactactttgagccagaggct
tacttcccagcatgggtggtttccaagcgggggaaggactacatcctgaaacacattccaaa
catgcacagagaccagtttgcactgacagcctccgaggcatatctaaagtacatcaaagagg
ccgtccgactggatgacgtcgccatccattactacagactgtacaaggataaaagagaggtt
gaaggttcactgaccctgggactgaccatgcgagggatacagatctttcagaatctagaaga
agagaaacagttgctgtatgatttcccctggacaaatgttgggaagttggtgtttgtgggca
agaagtttgagattttgcccgatggcctcccctccgccaggaagctggtctactacaccggg
tgccccacacgctcccggcatctcctgcagctgctgagcaacagccaccggctctacatgaa
cctgcagcccgtcctgcgccacctccgc

Appendix D

Zebrafish willin sequence (NM001111187)

Amino acid sequence:

MSVPTKQERTVCVLLPNKETLDITVGVKATGQDVFHRVCELLGVRELHYFGLTLVKNNE
HIFLDLEEKLAKYFPKEWKQDSGKGSHRRSIPPLLCLKVQYYVENGRLICERKARKLYY
YDLRERVLRSECRQQEEVYFQLAGFALQADHSDHSSEGQSHGHAMYFQPKEYFPPWIIA
KRGIDYLLCHGPKVHKELWGMSCRDAVLLFIRESCRLEDVPVTFYRLQKDKKEEKGSAL
LGLTLRGMQVFQEVNNVRDLLYDFPWFHVGRLTFLGKKFEIQPDGLPSARKLVYYTGSA
FRSRHLLLHLSSCHRLYLSLQPALKHLRQLEETEEKKRYRESYISDELDLDQPCSEGSP
RLSRHSTSSSGIEADTRQNSVSVEMVSVEEKEKSSINTSSTAQSHEEHWQETDSQEPGE
VSVDDPVDLLRLAELLEGVSVDCPTIQSVKDSKDQHMSSVTGKDQTDLSDPDGLKQVLN
QKLSNPSDCYNLSLEDVRQLSPLLPLGTPTAPNASIGYTFALPHSPTNPCPDDTSLCVQ
RPTNCLSLARLDDNQPLELVL

Nucleotide sequence:

ctcaaaacaaacacacacggactttaatacgcgatattcacaatgaaggaaccaatacct
gtgagcaaagcactttgaagaaaaagattcaagtcgtagtgtgtgattgtgtgtgtgtgtgt
gtgtgtgtgtgtgtgtgtcagtgtttttgtttctgtgtgtgtgtgtgtgtgtatatgt
gtgagtggatgagctcttatagaccatgtctgtccccaccaaacaagagaggaccgtatgtg
tcctccttcccaacaaggagacactggacatcacagtgggggtgaaagcaactggtcaagat
gtgtttcaccgtgtctgcgagcttctcggtgtcagagagctgcactactttggattaacttt
agtcaaaaacaatgagcacatctttctggacttggaagagaaacttgccaagtatttcccca
aggagtggaagcaggactctgggaaggggtcacacaggaggtccatccctcccctgctctgt
ctgaaggtccagtattatgtggagaacggcagactcatctgtgagcgtaaagcgagaaagct
gtactactatgaccttcgtgagcgagtcctgcgctctgaatgccgacagcaggaggaagtgt
atttccagctggcaggattcgctctacaggccgatcactctgaccactcatcagaaggacag
agtcacggacatgccatgtatttccaacccaaagaatattttcctccatggataatagcaaa
gcgtggcatcgactacctgctgtgtcacgggcccaaggtccataaggagctgtggggaatgt
cctgtcgagacgctgtcctgctgttcatcagagagtcctgccgtctggaggacgtcccagtc
accttctatcgtctgcagaaggacaagaaagaagagaagggttcagcattgcttggactcac
tctcagaggaatgcaagtgtttcaggaggtgaacaacgtgcgtgatctgctctatgatttcc
cctggtttcatgtgggacgactcactttcttgggaaaaaagtttgagatccagccggacggt
ttgccctcagcgaggaagctggtttactatacgggttcggcatttcgctctcgtcatctgct
tctgcatctgagctcatgtcatcgcttatatctgagtttacagcctgccctcaaacacctgc
ggcagctggaagagactgaggagaagaagcggtatcgtgaatcttacatcagtgatgagctg
gacctggaccagccatgcagtgaaggcagtcctcgtctgtccagacactccaccagcagctc
cggcatcgaggcggacaccagacagaacagcgtctcggtagagatggtctcagtggaggaga
aagagaaatccagcatcaacaccagcagcacagctcagagccatgaagagcactggcaggag
acagattcgcaggagccgggagaggtttctgtggacgatcctgtggatctcttgcgattggc
tgagctactggagggagtgtccgtcgactgtcccaccatccaatcagtcaaggactctaaag
atcagcatatgagctcagtcacaggtaaagaccaaacagacctaagtgatccagacggcctg
aaacaggttttgaatcagaagctttctaacccatccgactgctataatctaagcctggagga
cgtgcgacagttatctcctcttcttccgctgggaacgccgacagctccaaacgcctccatcg
gctacacatttgcgctcccacattccccaaccaacccatgtccagatgacacttcactctgt
gtccagagacccacgaactgcctttctctggcccgcctggatgataaccagccgctggagct
tgtgctataaaatctggacttgtgatagtattttgttccttattttgacatattttcatctg
aacaagaaagaagaccatgatttggtccatatggagttgatcgggttgttggatcattgcta
tcggtcgatctcatgtgagcgacaggttgatcccgccccttgtgccagtaatcatcatcat
catcatcatcatcattatcatcatcatcagaaaagagaatagatgactctgacatacactat
ttgtaataaataatgcaataattcatccgattgactgcttaaagactttaaagtccatgtga
accggacgatgctgagacgtttatttcaggatgttgatgtgcttccaactgaaacagaatat
tgagaaggggcggggctttcctgtgcacattattacgtaaagcgtaacctaactgcaagag
atggtattaatatgcagttgctatggaaaccctcaagctgacatcaagggaaggaccgccac
tctaaacacggaagcaaatggtcatactttgattgaagattaccaaaacaaatacatttttc
agtggattaacttgcatgtattaattattcaccttaagaatggcaatgtgagctagcaaatt
tgattttaagcggactttaaagcccaaagttcacttgaagtttccaattattgtatagtcca
acataaagtgtcaatttttttgtgattgcatgtatagtacaagtacagtttatctggtact
ttgtccacaaggtgtcaacactcagattagatgctcttttaagtccaaaataaattgagat
ggaaaaaaagcaacaacaaactactgaagacagcaaaaaaaaaaaaaaaaaaaaaaaaaa
aa

Appendix E

Published papers

Journal of Biomedical Optics 15(4), 041506 (July/August 2010)

Transient transfection of mammalian cells using a violet diode laser

Maria Leilani Torres-Mapa
University of St. Andrews
Scottish University Physics Alliance (SUPA)
School of Physics and Astronomy
North Haugh
St. Andrews KY16 9SS, Scotland
United Kingdom

Liselotte Angus
University of St. Andrews
School of Biology
Fife, St. Andrews
KY16 9TS, Scotland
United Kingdom

Martin Ploschner
Kishan Dholakia*
University of St. Andrews
Scottish University Physics Alliance (SUPA)
School of Physics and Astronomy
North Haugh
St. Andrews KY16 9SS, Scotland
United Kingdom

Frank J. Gunn-Moore*
University of St. Andrews
School of Biology
Fife, St. Andrews
KY16 9TS, Scotland
United Kingdom

Abstract. We demonstrate the first use of the violet diode laser for transient mammalian cell transfection. In contrast to previous studies, which showed the generation of stable cell lines over a few weeks, we develop a methodology to transiently transfect cells with an efficiency of up to ~40%. Chinese hamster ovary (CHO-K1) and human embryonic kidney (HEK293) cells are exposed to a tightly focused 405-nm laser in the presence of plasmid DNA encoding for a mitochondrial targeted red fluorescent protein. We report transfection efficiencies as a function of laser power and exposure time for our system. We also show, for the first time, that a continuous wave laser source can be successfully applied to selective gene silencing experiments using small interfering RNA. This work is a major step towards an inexpensive and portable phototransfection system. [DOI: 10.1117/1.3430730]

Keywords: photoporation; phototransfection; gene transfection; gene knockdown; violet diode.

Paper 09428SSR received Sep. 22, 2009; revised manuscript received Dec. 18, 2009; accepted for publication Dec. 29, 2009; published online Jul. 7, 2010.

1 Introduction

Photoporation refers to the use of tightly focused laser light to perforate temporarily the cellular membrane and allow exogenous material to be taken up by the cell.[1] This technique has become increasingly popular due to its simplicity, robustness, and efficiency. Most of its applications have been predominantly, but not limited to, the delivery of nucleic acids such as plasmid DNA[1–3] and messenger RNA[4] to intracellular compartments. In addition, dyes,[2] nanoparticles,[5] and semiconductor nanocrystals[6] can also be injected into the cells, which can be useful for monitoring gene or, potentially, drug activity.

Various laser-based systems have been used for photoporation and ultimately cell transfection. Wavelengths in the ultraviolet[7] (UV), visible[1,6,8–10] (VIS), and infrared[2–4,11] (IR), in both pulsed (nanosecond or femtosecond) and continuous wave (cw) mode, have all been used for cell transfection. The mechanism for poration is dependent on the type of laser used and its pulse duration.[12] Femtosecond cell transfection has currently emerged as the most ubiquitous and consistent method, but this system requires the use of expensive lasers with a typically large footprint (e.g., the ti-sapphire femtosecond laser oscillator). In terms of cw lasers in the VIS light region, the first laser used for cell transfection was the 488-nm output line of an argon-ion laser, which again has a large footprint.[8] In 2005, Paterson et al. used a low-cost cw violet diode laser for cell transfection, which is currently the simplest and most inexpensive method of laser-mediated transfection.[1] They showed that with sufficient control of laser parameters, cw VIS lasers are as effective as their femtosecond IR counterparts. Optical power densities as low as $\sim 1200\ \mathrm{MW/m^2}$ have been successfully used for such cell photoporation.[1] Crucially for the purposes of our discussion, previous studies with the violet diode did not achieve transient transfection but only stable transfection due to the limited material they could deliver to the cell. In stable transfection, only cells that have integrated the plasmid DNA into the cell's genetic genome are selected, and such stable cell lines take many weeks to generate. Transient transfection, as opposed to stable transfection, relies on the transcription and translation of the plasmid DNA itself, and this only takes 24 to 72 h to be achieved; such an inexpensive transient

*Contributed equally to this work.
Address all correspondence to: Maria Leilani Torres-Mapa, University of St. Andrews, Scottish University Physics Alliance (SUPA), School of Physics and Astronomy, North Haugh, St. Andrews, Fife, KY169SS, Scotland, United Kingdom. Tel: 44-1334-461654; Fax: 44-1334-463104; E-mail: mlt9@st-andrews.ac.uk

1083-3668/2010/15(4)/041506/7/$25.00 © 2010 SPIE

method for protein and drug delivery would be of great interest, especially for clinical applications.

Diode lasers are inexpensive and offer a compact footprint, important for miniaturization and automation. Notably, diode lasers at violet-blue wavelengths are already incorporated into most confocal microscope systems and fluorescence-activated cell sorting (FACS) machines. It is thought that the mechanism of photopore generation by cw irradiation relies on the cumulative temperature increase that occurs within a few milliseconds to alter the permeability of the cell.[8,10] An absorptive chemical species in the violet-blue region, such as phenol red dye, is used to aid absorption and local increase in temperature.[8–10] The advantage of using this dye is that it is nontoxic, is easily removed by washing, and is ubiquitously used in cell culture medium.

In this paper, we demonstrate for the first time the successful use of violet diode lasers for transient transfection of mammalian cell lines including the Chinese hamster ovary (CHO-K1) and human embryonic kidney (HEK293) lines. Previously, VIS wavelength cw lasers were shown to transfect CHO-K1,[1,10] NIH3T3 murine fibroblast,[8] and human cardiac cells.[9] Each cell line, due to its differing chemical functions and properties can have diverse reactions to irradiation from a given laser. Here, we show that we can repeatedly and robustly transfect mammalian cell lines using this system with an efficiency of up to ~40%. Additionally, previous reports using a cw 488-nm argon ion laser explored only a single optical power density.[8–10] In contrast, in this study we varied the optical power density and exposure time to determine the optimal parameters for cw transfection. In conjunction with this work, we performed an extensive study on cell viability by varying exposure times for two laser powers to elucidate its effect on cell death and poration. Furthermore, we also propose the use of this violet diode system as an inexpensive tool for specific gene knockdown experiments. To demonstrate this, we phototransfected a modified HEK293 cell line, which expresses the newly identified gene termed willin/FRMD6[13] under the control of an antibiotic inducible promoter, with small interfering RNA (siRNA) against willin; thus specifically blocking the expression of the willin gene product. This represents the first time siRNA has been transfected into mammalian cells using a cw laser source.

2 Materials and Methods

2.1 *Violet Diode Photoporation System*

The laser source was a commercially available 405-nm diode laser (Toptica, IBEAM-405-1V1 with an $M^2 < 1.2$) with maximum power of 40 mW. The beam was magnified by the telescope consisting of lenses L1 and L2 (Fig. 1). A half-wave plate and a polarizing beamsplitter in tandem were used to attenuate the beam power. A dichroic mirror at 45 deg reflected the beam to the rear entrance pupil of a high-numerical-aperture (NA) water immersion, violet corrected microscope objective (Nikon Plan Apo; magnification=63× NA=1.20) with measured transmission of ~84% at 405 nm. The laser was focused to a diffraction-limited spot approximately 0.4 μm in diameter. The power at the sample plane was obtained by taking the power transmission measurements through the optics. The maximum laser power dosages for each cell were first characterized by empirically observing the cell for any signs of granulation, blebbing, or necrosis. A beam shutter (Newport, United Kingdom, model 845 HP-02) placed in front of the laser was used to control the exposure times. An exposure time of 1 s was used to observe the transfection efficiency for each power level employed. Bright-field illumination in Koehler configuration was used to illuminate the sample. The image plane and laser plane were made coincident by changing the positions of lenses L1 and L2 and observing the image and laser focus. An *xyz* stage enabled us to vary the sample position. Finally, a color CCD camera (WATEC 250D) was used to capture the videos of the process.

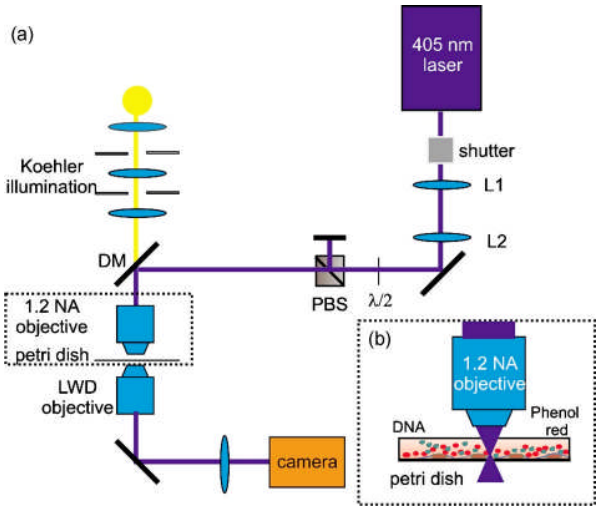

Fig. 1 (a) Schematic of a photoporation system using a 405-nm diode laser: L (L1=50 mm and L2=100 mm), plano-convex lenses; PBS, polarizing beamsplitter; M, mirrors; DM, dichroic mirror; and LWD, long-working-distance objective. The whole system is mounted on a 60×90 cm optical breadboard. (b) Schematic layout of a prepared sample in a petri dish showing the laser beam focused on a cell bathed in DNA and phenol red solution.

2.2 *Cell Culture Procedure*

CHO-K1 cells and HEK293 cells were cultured in T25 flasks at 37 °C and 5% CO_2 in modified Eagle's medium (Sigma, United Kingdom) with 10% fetal calf serum (GlobePharm, University of Surrey, United Kingdom), 20 μg/ml streptomycin (Sigma, United Kingdom), and 20 μg/ml penicillin (Sigma, United Kingdom).

A stable tetracycline inducible system, TRex willin-GFP-HEK, was created using a TRex inducible plasmid pcDNA4/TO/myc-his (Invitrogen, United Kingdom) modified to express willin-GFP, which was then transfected into stable HEK293 cells containing a plasmid expressing a tetracycline repressor, pcDNA6/TR. TRex willin-GFP-HEK cells were cultured in T25 flasks in the presence of Dulbeco modified Eagle's medium (Sigma, United Kingdom) with 10% fetal calf serum (GlobePharm, University of Surrey, United Kingdom), 2 mM L-glutamate, 100 units/ml penicillin and 100 units/ml streptomycin (Sigma, United Kingdom). Stable cells were selected by the addition with 5 μg/ml blasticidin and 250 μg/ml zeocin. Willin-GFP expression was induced with 1 μg/ml tetracycline (Invitrogen, United Kingdom).

Cells were routinely passaged three times a week. CHO-K1 and HEK293 cells were seeded at a density of 2.4×10^4 cells/ml onto 35-mm glass-bottomed culture grade dishes (World Precision Instruments) to achieve 40 to 50% confluency. The cells were incubated at 37 °C for 24 h to allow cell attachment to the bottom of the glass dishes. Meanwhile, TRex willin-GFP-HEK cells were plated 48 h prior to the experiment onto 35-mm culture dishes coated with laminin (Invitrogen, United Kingdom) to improve cells' adherence on the dishes.

2.3 *Targeted DNA Phototransfection*

For each phototransfection experiment, individual CHO-K1 and HEK293 cells were exposed to up to 3.4 mW of laser power for 1 s at the focus. Before exposure, the cell monolayer was washed twice with OptiMEM (Invitrogen, United Kingdom) and then bathed with 30 μl of solution containing 10 μg/ml plasmid encoding for Mito-DsRed (Clontech) and 42.2 μM of phenol red (Sigma) in OptiMEM. Phenol red is a dye commonly used with cell culture media to detect changes in pH. The absorption of the solution used in the photoporation experiments was measured and a molar coefficient cross section of $\sim 1.4 \times 10^4$ cm^{-1} M^{-1} at 405 nm was obtained.

A type 0, 22-mm-diam coverslip was placed on top of the cell monolayer and a region of interest was marked in the center in order to identify the region of dosed cells. On average, 50 healthy looking cells per dish were irradiated on the plasma membrane in a region 1 to 3 μm away from (and not directly above) the nucleus. After dosage, the coverslip was removed with OptiMEM and phenol red solution, and then subsequently washed twice with the same medium. The cells were then further incubated in fresh medium for up to 72 h after photoporation. Control cells were prepared in the same manner but were not exposed to the laser. The photoporated cells were observed under a fluorescent microscope for expression of the Mito-DsRed gene. For each laser power and for each irradiation time, nine experiments were performed, irradiating 50 cells per dish in the process. Therefore in total, for $n=9$ experiments, $\sim$5000 cells were treated, enabling us to accumulate reliable statistics of the process.

2.4 *Cell Viability*

HEK293 cells were plated on 35-mm glass-bottomed dishes and were prepared similarly to transfection experiments except no DNA was added. Cells were exposed to 2.1- and 3.4-mW laser power at exposure times from 80 ms to 5 s. After laser exposure, cells were returned in the incubator for an hour, after which 60 μl of 0.3% trypan blue was added. Trypan blue is an indicator of cell membrane barrier dysfunction. In the state of necrosis, the cell's protective membrane is often compromised, leading to intake of extracellular material. Dead cells stained blue were counted and the viability was calculated by obtaining the percentile ratio of dead cells with irradiated cells. Each data point was an average of three dishes and 50 cells per dish were exposed to the laser.

2.5 *siRNA Chemical Transfection*

Willin knockdown was performed using small interfering RNA (siRNA), to a final concentration of 5 nM, specifically targeting the protein (GACAGAGCAGCAAGAUACUAUUAUU, CACAGACUAUAUGUCGGAAACCAAA, GCCUCUAUAUGAAUCUGCAGCCUGU; Invitrogen) using Gene Eraser (Startagene) according to the manufacture's instructions. Protein expression was analyzed by Western blotting, using anti-GFP (Santa-Cruz) and anti-actin (Sigma) as a loading control.

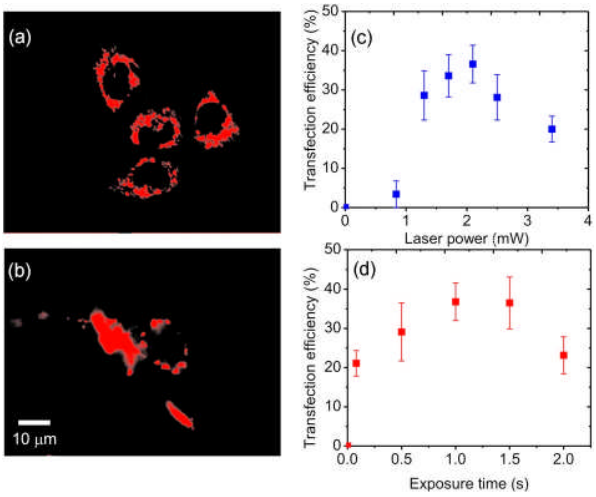

Fig. 2 Fluorescence images of transfected (a) CHO-K1 and (b) HEK293 transfected with Mito-DsRed plasmid, (c) transfection efficiency of HEK293 cells as a function of laser power at the focus using a 1-s exposure time, and (d) transfection efficiency of HEK293 cells as a function of laser exposure time at 2.1 mW. The error bars represent standard deviation, ($n=9$ experiments of 50 dosed cells).

2.6 *Fluorescence Microscopy*

All fluorescence microscopy was performed on a TE2000-E, Nikon microscope. Cells expressing Mito-DsRed were imaged using TRITC HYQ, Nikon Filter cube (excitation, 530 to 560 nm; emission, 590 to 650 nm). Meanwhile, cells induced and expressing willin-GFP were imaged using FITC HYQ Nikon filter cube (excitation, 460 to 500 nm; emission, 510 to 560 nm).

3 Results

3.1 *DNA Phototransfection*

Phototransfection experiments on CHO-K1 and HEK293 cells were performed using a violet diode laser. For the laser parameters used, and under bright-field imaging, no visible reaction from the cell was observed. Successful transient expression was achieved with the Mito-DsRed plasmid for both cell lines, as shown in Figs. 2(a) and 2(b). The transfection efficiency after 72 h as a function of laser power, using a 1-s exposure time for HEK293 cells, is shown in Fig. 2(c). Each power level is significantly different from the control group ($p<0.05$) with the exception of 0.8 mW, as determined by a one-way analysis of variance (ANOVA) followed by Dunnett's statistical test. Overall, a Poisson distribution curve was obtained where the start and tail of the plot were significantly different from each other, as determined from ANOVA followed by Fischer's pairwise test ($p<0.05$). As indicated in Fig. 2(c) an enhancement of transfection efficiency was acquired with an increase in laser power from 0.8 to 1.3 mW

with efficiencies of 3.4 ± 3.4 to $28.6 \pm 6.3\%$, respectively, typifying a power dependence on the probability of cell poration and subsequently transfection. The optimum laser power was found to range from 1.3 to 2.5 mW, which yielded transfection efficiencies between 28.1 ± 5.8 and $36.6 \pm 4.8\%$. Within this range of power levels, the efficiencies were not significantly different from each other but were significantly different from 0.8 and 3.4 mW ($p < 0.05$). Additionally, as the mitochondria were tagged, it was possible to observe their streaming, which is an indicator of the overall health of the treated cells. In comparison, the highest transfection efficiency for CHO-K1 was at $23 \pm 1.5\%$. As established previously,[1] the level of spontaneous transfection was very low and negligible in comparison to the transfection efficiencies we achieved. Spontaneous transfection is defined as cells expressing the protein without exposure to the laser irradiation.

The dependence of transfection efficiency on laser exposure time was also studied for a laser power of 2.1 mW for HEK293 cells. Figure 2(d) shows the transfection efficiency as a function of irradiation time from 80 ms to 2 s. An ANOVA followed by Dunnett's statistical test showed that transfection efficiencies obtained from different exposure times were significantly different compared to the control ($p < 0.05$). Though significant transfection efficiency can already be obtained at a 80-ms exposure, 1.0 and 1.5 s appeared to be optimal for transfection at this laser power. Increasing the exposure time from 1.5 to 2 s resulted in the decline of the average transfection efficiency from 36.5 ± 6.6 to $23 \pm 4.7\%$, respectively, which may be a consequence of a decrease in viability (see in the following).

3.2 *Phototoxicity of Violet Diode Phototransfection*

Careful assessment of the cell viability was performed by exposing the cells to the laser and monitoring any morphological changes in the cells. Cells exposed to 2.1 mW for 6 to 10 s immediately showed signs of necrosis. In a further study, the viability of the cells treated with the laser at shorter exposure times were measured for two laser powers, 2.1 and 3.4 mW, as shown in Fig. 3 (laser exposure ranged from 0.08 to 5 s) in the presence of trypan blue.

In general, viability was observed to decrease with increasing laser exposure time. For a 1-s exposure, viability was measured from 96.4 ± 1.2 and $95.4 \pm 1.2\%$ for laser powers of 2.1 and 3.4 mW, respectively. It marginally decreased from 86.7 ± 1.2 to $65.3 \pm 4.2\%$ at 2 s, respectively. This small increase in laser power from 2.1 to 3.4 mW resulted in a sixfold decline in viability at 3-s exposure times from 72 ± 9.2 to $11.3 \pm 12.1\%$. It was found that viability exponentially decays with exposure time and laser power. LD50, defined as dosage entailing 50% cell viability occurs at an energy density of ~ 6.3 MJ/cm^2.

Notably, with laser exposures beyond the therapeutic dosage for transfection, fluorescence was observed at the targeted site, an indication of single-photon absorption, which might lead to the melting of the plasma membrane. Often when this phenomenon occurred, the cell underwent blebbing, granulation, loss of intracellular material, and necrosis. Neighboring cells, however, were not affected.

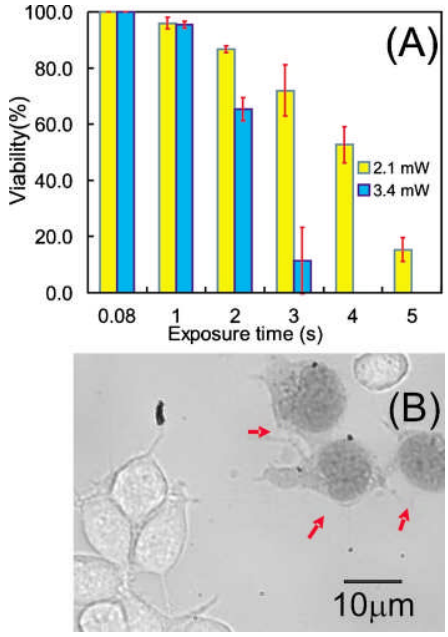

Fig. 3 (a) Viability of HEK293 cells exposed to laser at 2.1 and 3.4 mW at the focus at varying exposure time. Error bars represent ± standard deviation ($n = 3$ experiments of 50 dosed cells). (b) Bright-field image of laser exposed HEK293 cells. Cells pointed to by the red arrows were irradiated with the laser and have taken up the trypan blue dye, a sign of cellular necrosis. (Color online only.)

3.3 *Cell-Specific Gene Knockdown Experiments*

RNA interference (RNAi) is a technology developed by Fire et al.[14] in 1998 that enables the knockdown in expression of a specific gene. siRNA interferes with new protein expression, resulting in silencing of the gene. siRNA is made from a length of 20 to 25 nucleotides that bind specifically to the messenger RNA (mRNA) of the protein of interest. This leads to the formation of a siRNA complex, which results in mRNA cleavage and its subsequent degradation.[15] The applications of this widely used gene silencing technology include studying a gene's function, but also the potential therapeutic modification of gene expression in human diseases. Therefore, for the reasons outlined in the introduction, we explored the possible use of violet diode lasers in cell-specific gene knockdown experiments.

TRex willin-GFP-HEK cells were induced with 1 μg/ml tetracycline to activate willin-GFP expression. After 24 h, 5 nM siRNA manufactured to recognize specifically the willin gene, was chemically transfected into these cells. Willin-GFP protein levels were detected 24, 48, and 72 h after siRNA treatment. Western blot analysis (Fig. 4) shows that willin-GFP expression is significantly reduced after 48 to 72 h of siRNA transfection. Actin was used as a loading control and expression levels remain unchanged throughout siRNA transfection. This, therefore, indicated that the siRNA used were specific and effective in decreasing willin expression.

Therefore, for the photoporation experiments, 5 nM stock of the siRNA duplexes with the Mito-DsRed-encoding plasmid was added to the transfection medium. Initially, 10 μg/ml of Mito-DsRed was also added to identify cells

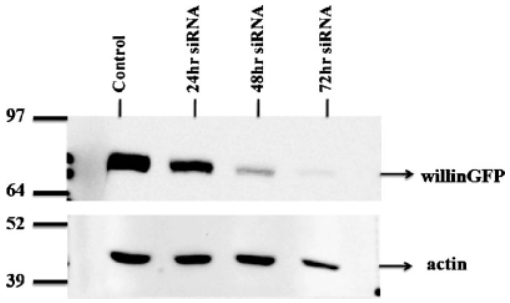

Fig. 4 Western blot analysis showing reduction of willin-GFP expression after 48 h of 5 nM siRNA chemical transfection. TRex willin-GFP cells were induced with 1 μg/ml tetracycline to express willin-GFP 24 h prior to siRNA treatment. Western blots were probed with anti-GFP and anti-actin, with the latter used as a loading control.

that had been successfully transfected. Cells were targeted using a 3.4-mW laser power at the focus and a 1-s exposure time. Control dishes included (1) cells with Mito-DsRed plasmid and the siRNA without laser treatment; (2) cells without the Mito-DsRed plasmid but with siRNA without laser treatment, and (3) cells without both the Mito-DsRed and siRNA with laser treatment. Expression of willin-GFP was then induced by the addition of tetracycline, and cells were monitored for fluorescence over the next 2 days. For all control dishes, spontaneous DNA transfection or knockdown was not observed.

Figure 5 shows images of photoporated TRex willin-GFP-HEK cells in the presence of the willin specific siRNA and the Mito-DsRed plasmid. Figure 5(a) is a successfully transfected TRex willin-GFP-HEK cell, as shown by the expression of mitochondrial targeted red fluorescent protein captured using the TRITC HYQ, Nikon Filter cube. Figure 5(b) is the same field of view but under bright-field imaging. Figure 5(c) shows the same cells, but imaged now using a FITC HYQ Nikon filter cube. As indicated by the blue and red arrows are cells that exhibit clear knocked down of willin-GFP expression, as indicated by the absence of green fluorescence. One cell, indicated by the red arrow point, was also transfected with the Mito-DsRed encoded plasmid. The laser's specificity of action is indicated by the fact that untreated cells have not been knockdowned or transfected with Mito-DsRed, as observed in all control dishes checked under a fluorescence microscope and confirmed by Western blot analysis (data not shown).

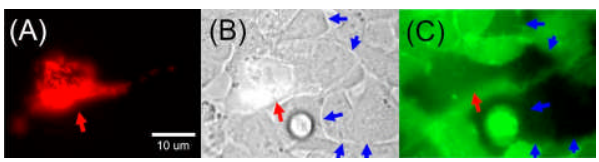

Fig. 5 Gene knockdown using a violet diode system. (a) A TRex-willin-GFP-HEK cell fluorescing red due to the expression of the Mito-DsRed and (b) under bright-field imaging; (c) fluorescence image of the same field of view using a FITC HYQ. The Red arrow points to a cell that has been cotransfected with Mito-DsRed and willin specific siRNA. Blue arrows point to cells that have been transfected with siRNA only. (Color online only.)

3.4 *Temperature Calculations at the Focal Volume*

Based on previous reports using the cw violet laser for transfection, it was conjectured that a melting of the phospholipid bilayer occurs due to the direct absorption of the phenol red in the medium, causing localized thermal effects on the irradiated site.[8,10] To elucidate the mechanistic process of poration, an estimate of the temperature at the beam focus was calculated based on modeling the phenol red as a sphere of radius r immersed in a nonabsorbing medium. Since the absorption and the consequential increase in temperature occur only in close proximity to the focus, one can assume that the laser energy is absorbed only by the phenol red sphere. The radius r of the sphere can be made equivalent to the radius of the beam spot given by $r=0.61\lambda/\mathrm{NA}$, where $\lambda=405$ nm and $\mathrm{NA}=1.2$.

Since most of the incident power of the laser goes through the sphere of radius r, we can assume that the substitution of focused Gaussian beam with a plane wave of incident intensity $I=P/(\pi r^2)\sim 1\times 10^{10}$ W/m^2, where P is the power of the laser at the focal plane going through the geometrical cross section of the sphere, will not introduce any significant error to our estimate. The Mie scattering problem can be solved for the phenol red sphere surrounded by the nonabsorbing medium. The imaginary part of the index of refraction of the phenol red sphere was determined by the equation $\hat{n}=n[1+i(\alpha\lambda/4\pi n)]$, based on the measured absorption coefficient, $\alpha=0.6$ cm^{-1}, noting that the change in the real part of the index of refraction n is negligible. This yielded an expression for the index of refraction given by $\hat{n}=1.33+i(1.93\times 10^{-6})$. The solution provides us the absorption cross section σ of the phenol red sphere, which is $\sigma=2\times 10^{-18}$ m^2. Hence, the heat absorbed Q by the phenol red can be obtained, where $Q=I\sigma\sim 3\times 10^{-8}$ W.

Since, the cw irradiation used for the experiments lasts of the order of milliseconds to seconds and the temperature change saturates immediately after several microseconds,[12] we modeled only the steady state temperature increase, ΔT which is given by $\Delta T=(1/4\pi)(Q/\kappa_0 r)$,[16] where $\kappa_0=0.6$ W/mK is the thermal conductivity of water. We assumed the same thermal conductivity for phenol red. From this, the calculated ΔT is 0.02 K.

4 Discussion

Femtosecond near-IR lasers are generally much more effective tools for cell nanosurgery compared to cw lasers due to the mechanisms of their interaction with biological material.[12] However, since both work with a tightly focused laser beam that is typically an order of magnitude smaller than the cell's diameter ($\sim$10 to 20 μm), they may both be suitable for single-cell transfections studies. In particular, the violet diode laser can be a compact and cost-effective biological transfection tool when compared to the use of a femtosecond pulsed laser.

In contrast to previous work,[8,10] which reported small dark circular spots on the cell that disappeared several minutes after laser irradiation, these dark spots were not observed during our experiments. More conclusively, these dark circular spots repeatedly appear for cells irradiated with laser parameters beyond a therapeutic dosage. No visible reaction, hole,

or cavitation bubble from the cell was observed using the laser and exposure times described in this paper for successful transfection. Whether DNA transfection necessitates a nanosize hole is not yet confirmed, but the increase in membrane permeability may be enough to allow a circular DNA plasmid to enter through the cell membrane. Further studies will be necessary to discover changes within the membrane structure at the site of laser irradiation.

In this work, transient transfection as opposed to stable transfection of CHO-K1 and HEK293 cells were achieved. Selection of cells with integrated DNA in their nuclear genome using an antibiotic called G418 was still also possible and thus enabled us to generate stable colonies from our transiently transfected cell lines. However, the laser energy used in this work was of the order of 2000 μJ, compared to only 12 μJ used by Paterson et al.[1] Successful transient transfection using our cw focused 405-nm laser required an energy density of 1.5 MJ/cm^2, in close agreement with the energy density reported using a focused 488-nm argon-ion laser ($\sim$1 MJ/cm^2).[10]

The cw cell poration was suggested to be mainly due to the large temperature rise in the absorptive medium leading to pore formation on the cell membrane[8,10] however, the temperature calculation at the focus in the phenol red medium reveals that the gradient temperature is very small $\sim$0.02 °C. Our experiments were performed at 25 °C. Hence, the calculated temperature change is insufficient to achieve the reported temperatures of 42 to 45 °C, which are necessary for a membrane phase transition,[17] and is certainly well short of the required temperature rise for microbubble formation.[12] This may imply that a photochemical reaction dominates during irradiation by a focused 405-nm laser related to affecting membrane integrity. Oxidative stress induced by the production of reactive oxygen species (ROS) such as O_2^-, OH*, and H_2O_2 radicals, is known to be elicited by the irradiation of light at this wavelength region,[18–21] which may lead to subsequent lipid peroxidation, closely related to possible impairment of the phospholipid bilayer.[22] At the site of irradiation, localized production of ROS may occur, leading to changes in membrane permeability. The fact that oxidative stress may be involved in this process would agree with our observations that the addition of phenol red enhanced the overall transfection efficiency. Presumably, because it has been previously shown that phenol red can protect against the harmful effects of ROS[23] but its presence in the medium will not inhibit the localized ROS generated at the site of irradiation. Experiments revealed that cell poration was dose dependent, varying as a function of both exposure time and average power. Future extensive experiments will be required to elucidate the exact mechanism for poration events caused by violet diode laser light.

Studies have shown that violet-blue light induces damage through absorption by cellular endogenous photosensitizers,[21,24] which subsequently leads to adverse chemical reactions. Possible cellular chromophores absorbing in the violet-blue region include porphyrin ring structures and flavins.[18–20] In addition, Hockberger et al.[20] reported induced damage by violet light (400 to 410 nm) from a xenon arc mercury lamp on mammalian cells due to stimulated production of H_2O_2 by photoreduction of flavins and/or flavins containing oxidases located within the mitochondria and peroxisomes. ROS production was also equivalently observed using near-IR femtosecond laser pulses, which they attribute to two-photon absorption.[25] Oxidative stress may lead to several structural deformations such as fragmentation and condensation of nuclei, DNA strand breaks, and loss of membrane protective functionality leading to cell apoptosis.[25] Despite this, we have shown that good viability $\sim$90% can still be obtained at optimal parameters with controlled power and exposure time of the focused violet diode laser.

Successful gene knockdown was also achieved using the violet diode laser. Interestingly, there were more occurrences of gene knockdown with the siRNA than with DNA transfection, as shown in Fig. 5(c), where five cells (blue arrows) had knockdown of willin-GFP expression but were not expressing Mito-DsRed. It can be deduced that the efficiency for gene knockdown will be higher compared to DNA transfection as siRNA are much smaller compared to DNA plasmids [i.e., 25 bp (base pairs) versus $\sim$5000 to 6000 bp]. Assuming passive diffusion of DNA or siRNA from an extracellular medium to cytosol during phototransfection, one could compare the rate of diffusion of plasmid DNA and siRNA. The diffusion coefficient could be obtained using the equation $D=(kT/6\pi\eta R_G)$, where k is Boltzmann's constant, η is the viscosity of the medium, and T is the temperature in kelvin.[26] For siRNA, the Flory scaling law could apply, and the radius of gyration R_G is given by $R_G=5.5N^{1/3}$, where N is the number of base pairs.[27] Meanwhile, an estimated relation of R_G based on N for supercoiled DNA plasmids has was derived by Prazeres, where $R_G=0.402\times N$.[28] Based on these relations, we approximated that the 25-bp siRNA diffuses approximately 100× faster than a 5600-bp plasmid DNA, enabling more siRNA molecules to diffuse into the irradiated site than plasmid DNA.

In conclusion, transient transfection of mammalian cells using a violet diode laser was demonstrated. Our studies pave the way for a compact, miniature system utilizing low-power diode systems for cell transfection, which would make it inexpensive and accessible. We also showed that cell-specific gene knockdown experiments are possible with photoporation, opening up new vistas in cell biology. Notably, this is the first technique that would enable the knockdown of a specific gene in a specific cell while it is surrounded by other cells. Such technology would be of particular interest to cell biologists exploring cellular behavior in multicellular tissue.

Acknowledgments

We thank Dr. David Stevenson for useful discussions. We thank the United Kingdom Engineering and Physical Sciences Research Council and Biotechnology and Biological Sciences Research Council for funding. MLT acknowledges the support of a SUPA Prize Studentship. KD is a Royal Society-Wolfson Merit Award Holder. FGM and KD contributed equally to this work.

References

1. L. Paterson, B. Agate, M. Comrie, R. Ferguson, T. K. Lake, J. E. Morris, A. E. Carruthers, C. T. A. Brown, W. Sibbett, P. E. Bryant, F. Gunn-Moore, A. C. Riches, and K. Dholakia, "Photoporation and cell transfection using a violet diode laser," *Opt. Express* **13**(2), 595–600 (2005).

2. D. Stevenson, B. Agate, X. Tsampoula, P. Fischer, C. T. A. Brown, W. Sibbett, A. Riches, F. Gunn-Moore, and K. Dholakia, "Femtosecond optical transfection of cells: viability and efficiency," *Opt. Express* **14**(16), 7125–7133 (2006).
3. X. Tsampoula, V. Garces-Chavez, M. Comrie, D. J. Stevenson, B. Agate, C. T. A. Brown, F. Gunn-Moore, and K. Dholakia, "Femtosecond cellular transfection using a nondiffracting light beam," *Appl. Phys. Lett.* **91**(5), 053902–053903 (2007).
4. L. E. Barrett, J. Y. Sul, H. Takano, E. J. Van Bockstaele, P. G. Haydon, and J. H. Eberwine, "Region-directed phototransfection reveals the functional significance of a dendritically synthesized transcription factor," *Nat. Methods* **3**(6), 455–460 (2006).
5. C. McDougall, D. J. Stevenson, C. T. A. Brown, F. Gunn-Moore, and K. Dholakia, "Targeted optical injection of gold nanoparticles into single mammalian cells," *J. Biophoton.* **2**(12), 736–743 (2009).
6. I. B. Clark, E. G. Hanania, J. Stevens, M. Gallina, A. Fieck, R. Brandes, B. O. Palsson, and M. R. Koller, "Optoinjection for efficient targeted delivery of a broad range of compounds and macromolecules into diverse cell types," *J. Biomed. Opt.* **11**(1), 014034 (2006).
7. W. Tao, J. Wilkinson, E. J. Stanbridge, and M. W. Berns, "Direct gene-transfer into human cultured-cells facilitated by laser micropuncture of the cell-membrane," *Proc. Natl. Acad. Sci. U.S.A.* **84**(12), 4180–4184 (1987).
8. G. Palumbo, M. Caruso, E. Crescenzi, M. F. Tecce, G. Roberti, and A. Colasanti, "Targeted gene transfer in eucaryotic cells by dye-assisted laser optoporation," *J. Photochem. Photobiol., B* **36**(1), 41–46 (1996).
9. A. V. Nikolskaya, V. P. Nikolski, and I. R. Efimov, "Gene printer: laser-scanning targeted transfection of cultured cardiac neonatal rat cells," *Cell Adhes Commun.* **13**(4), 217–222 (2006).
10. H. Schneckenburger, A. Hendinger, R. Sailer, W. S. L. Strauss, and M. Schmidtt, "Laser-assisted optoporation of single cells," *J. Biomed. Opt.* **7**(3), 410–416 (2002).
11. U. K. Tirlapur and K. Konig, "Targeted transfection by femtosecond laser," *Nature* **418**(6895), 290–291 (2002).
12. A. Vogel, J. Noack, G. Huttmann, and G. Paultauf, "Mechanisms of femtosecond laser nanosurgery of cells and tissues," *Appl. Phys. B: Lasers Opt.* **81**, 1015–1047 (2005).
13. F. J. Gunn-Moore, G. I. Welsh, L. R. Herron, F. Brannigan, K. Venkateswarlu, S. Gillespie, M. Brandwein-Gensler, R. Madan, J. M. Tavaré, P. J. Brophy, M. B. Prystowsky, and S. Guild, "A novel 4.1 ezrin radixin moesin (FERM)-containing protein, 'Willin,'" *FEBS Lett.* **579**(22), 5089–5094 (2005).
14. A. Fire, S. Xu, M. K. Montgomery, S. A. Kostas, S. E. Driver, and C. C. Mello, "Potent and specific genetic interference by double-stranded RNA in *Caenorhabditis elegans*," *Nature* **391**(6669), 806–811 (1998).
15. M. T. McManus and P. A. Sharp, "Gene silencing in mammals by small interfering RNAs," *Nat. Rev. Genet.* **3**(10), 737–747 (2002).
16. G. Baffou, R. Quidant, and C. Girard, "Heat generation in plasmonic nanostructures: influence of morphology," *Appl. Phys. Lett.* **94**(15), 153109 (2009).
17. J. R. Dynlacht and M. H. Fox, "Heat-induced changes in the membrane fluidity of Chinese hamster ovary cells measured by flow cytometry," *Radiat. Res.* **130**(1), 48–54 (1992).
18. J. B. Lewis, J. C. Wataha, R. L. W. Messer, G. B. Caughman, T. Yamamoto, and S. D. Hsu, "Blue light differentially alters cellular redox properties," *Gold Bull.* **72B**(2), 223–229 (2005).
19. M. Eichler, R. Lavi, A. Shainberg, and R. Lubart, "Flavins are source of visible-light-induced free radical formation in cells," *Lasers Surg. Med.* **37**(4), 314–319 (2005).
20. P. E. Hockberger, T. A. Skimina, V. E. Centonze, C. Lavin, S. Chu, S. Dadras, J. K. Reddy, and J. G. White, "Activation of flavin-containing oxidases underlies light-induced production of H_2O_2 in mammalian cells," *Proc. Natl. Acad. Sci. U.S.A.* **96**, 6255–6260 (1999).
21. M. L. Cunningham, J. S. Johnson, S. M. Giovanazzi, and M. J. Peak, "Photosensitized production of superoxide anion by monochromatic (290–405 nm) ultraviolet irradiation of NADH and NADPH coenzymes," *Photochem. Photobiol.* **42**(2), 125–128 (1985).
22. P. Morlière, A. Moysan, R. Santus, G. Hüppe, J.-C. Mazière, and L. Dubertret, "UVA-induced lipid peroxidation in cultured human fibroblasts," *Biochim. Biophys. Acta Lipids and Lipid Metab.* **1084**(3), 261–268 (1991).
23. A. Grzelak, B. Rychlik, and G. Bartosz, "Light-dependent generation of reactive oxygen species in cell culture media," *Faraday Symp. Chem. Soc.* **30**(12), 1418–1425 (2001).
24. C. Kielbassa, L. Roza, and B. Epe, "Wavelength dependence of oxidative DNA damage induced by UV and visible light," *Carcinogenesis* **18**(4), 811–816 (1997).
25. U. K. Tirlapur, K. Konig, C. Peuckert, R. Krieg, and K. J. Halbhuber, "Femtosecond near-infrared laser pulses elicit generation of reactive oxygen species in mammalian cells leading to apoptosis-like death," *Exp. Cell Res.* **263**(1), 88–97 (2001).
26. K. Ribbeck and D. Gorlich, "Kinetic analysis of translocation through nuclear pore complexes," *EMBO J.* **20**(6), 1320–1330 (2001).
27. C. Hyeon, R. I. Dima, and D. Thirumalai, "Size, shape, and flexibility of RNA structures," *J. Chem. Phys.* **125**(19), 194905 (2006).
28. D. M. F. Prazeres, "Prediction of diffusion coefficients of plasmids," *Biosens. Bioelectron.* **99**(4), 1040–1044 (2008).

Oncogene (2011) 1–13

www.nature.com/onc

ORIGINAL ARTICLE

Willin/FRMD6 expression activates the Hippo signaling pathway kinases in mammals and antagonizes oncogenic YAP

L Angus[1], S Moleirinho[1,2], L Herron[1], A Sinha[3,4], X Zhang[3,4], M Niestrata[2], K Dholakia[5], MB Prystowsky[6], KF Harvey[3,4], PA Reynolds[2,7] and FJ Gunn-Moore[1,7]

[1]School of Biology, University of St Andrews, St Andrews, UK; [2]School of Medicine, University of St Andrews, St Andrews, UK; [3]Cell Growth and Proliferation Laboratory, Peter MacCallum Cancer Centre, East Melbourne, Victoria, Australia; [4]Department of Pathology, University of Melbourne, Parkville, Victoria, Australia; [5]School of Physics and Astronomy, University of St Andrews, St Andrews, UK and [6]Department of Pathology, Albert Einstein College of Medicine, Bronx, NY, USA